Retrospective Theses and Dissertations

Iowa State University Capstones, Theses and Dissertations

2008

Performance-based seismic analysis and design improvements of two precast concrete structural systems

Mohammad Ataur Rahman

Iowa State University

Performance-based seismic analysis and design improvements of two precast concrete structural systems

by

Mohammad Ataur Rahman

A dissertation submitted to the graduate faculty

in partial fulfillment of the requirements for the degree of

DOCTOR OF PHILOSOPHY

Major: Civil Engineering (Structural Engineering)

Program of Study Committee:

Sri Sritharan, Major Professor
Terry J. Wipf
Fouad S. Fanous
Lester W. Schmerr
Igor Beresnev

Iowa State University

Ames, Iowa

2008

www.manaraa.com

TABLE OF CONTENTS

vii

LIST OF TABLES

LIST OF FIGURES

CHAPTER 3

CHAPTER 6

ABSTARCT

This study focuses on the multiple-level seismic performance in terms of structural and non-structural damages of precast hybrid frame and jointed precast post-tensioned wall systems through dynamic analysis of precast buildings subjected to spectrum compatible ground motions of various intensities. The maximum transient interstory drift, residual interstory drift and floor acceleration are considered as acceptance criteria for evaluating seismic performance of these systems subjected by four levels of ground motions. Interstory drift and floor acceleration are directly related to structural and non-structural damages, respectively. Two dimensional non-linear finite element analytical models for hybrid frames and jointed wall systems used in this study are validated against test results for a five story test building. In designing both precast systems, it is shown that traditional force-based design approach results in significantly higher level of design base shear compared to direct displacement-based design approach. After observing satisfactory performance in the five story model building designed by direct displacement-based approach, similar multiple-level seismic performance is evaluated for five, seven and ten story buildings designed by direct displacement-based method. These low to mid-rise full scale precast hybrid frame and jointed precast post-tensioned wall systems also exhibit the maximum transition interstory drift , residual interstory drift and floor acceleration within the acceptable limits, thus it is recommended that these systems may be utilized as primary lateral load resistant structural systems when designed by the economic approach of direct displacement-based design. Influence of variation of heights of buildings on the performance of these systems is also examined.

CHAPTER 1. GENERAL INTRODUCTION

1.1 INTRODUCTION

Precast concrete structural systems benefit from advantages such as improved quality of construction, efficient use of materials, reduced construction time, and cost efficiency. In addition, precast concrete allows architects and engineers to perform more innovative designs than traditional cast-in-place concrete design. Poor performance [1.1-1.4] of precast structures in past earthquakes has given designers, architects, and contractors a misconception that precast concrete may not a desirable construction technology in seismic regions. This lower level of performance of several precast structures in past earthquakes was either due to the lack of sufficient number of lateral load resisting systems in the structures or a result of using poor connection details between precast elements that contributed to brittle structural behavior [1.5]. Recent advancements in research have introduced efficient precast structural systems (e.g., hybrid frame [1.6] and unbonded jointed precast walls [1.6]) that are capable of maintaining structural integrity as well as providing sufficient energy dissipation under cyclic loading, thus improving the seismic performance of precast structural system. Both the hybrid frame system and unbonded jointed precast wall system use simple concepts. In a hybrid connection, the beam and column are connected through unbonded post-tensioning tendons and mild steel reinforcement across the beam-column interface. In a jointed precast wall system, individual walls are held to foundation by post-tensioning from the top of the wall, and are connected to each other horizontally along the height using special energy dissipating connectors. Despite these huge potential developments for seismic resistance, sufficient analytical research to support their dynamic response under earthquake

loads has not been completed. Such an investigation is expected to elevate the confidence of practicing engineers on using these innovative and economical precast structural systems in seismic regions.

In this study, seismic performance of both hybrid frames and precast jointed walls, suitable for low to mid-rise buildings, will be investigated by conducting dynamic analyses, using various levels of ground motions. Consequently, this study will help predicting the seismic performance of these structural systems. In addition, difference in performance of currently available seismic design methods will be conducted through dynamic analysis of two similar hybrid frames and two similar precast jointed walls.

The remainder of this introductory chapter focuses on the general benefits of precast concrete, description of hybrid frame and unbonded jointed precast wall systems, current seismic design methods, and performance-based seismic evaluation. A short description of previous work on this field will be presented, followed by the scope of research and a thesis layout.

1.2 BENEFITS OF PRECAST CONCRETE

Concrete exhibits high compressive strength and low tensile strength due to its brittleness. Flexural cracks develop in concrete members at early stages of loading as flexural tensile stresses exceed the tensile strength of concrete. Development of undesirable flexural cracking in structures may be delayed or avoided under service conditions by prestressing the concrete. Precast concrete provide the following benefits over the cast-in-place concrete systems.

- **High quality:** Precast concrete products exhibit higher quality and more uniform properties than cast-in-place counterparts because they are produced under controlled environment in a manufacturing plant, where curing conditions such as temperature and humidity are typically controlled and the dependency on craftsmanship is somewhat reduced. Moreover, efficient inspection of precast concrete production enhances the quality of the products [1.7].

- **Use of Advance Technology:** Robotics and computer aided manufacturing is feasible for precast concrete construction, which will lead to more efficient production and erection of components [1.8].

- **Optimum use of materials:** A significant reduction to the concrete volume is achieved in precast concrete element by using high strength concrete and steel. High strength materials help to achieve a longer life cycle [1.9].

- **Reduced construction time:** Construction of precast components requires a significantly reduced amount of formwork and temporary supports in the field compared to cast-in-place concrete construction. Using prefabricated concrete members helps in reducing the construction time of structures in comparison to the cast-in-place concrete construction. Furthermore, time is not wasted due to bad weather conditions or for curing of concrete.

- **Cost efficiency:** Faster erection time and quick factory production lead to reduction in construction and labor costs. Multiple use of the same forms, for constructing standard precast members, also contribute to reducing construction cost [1.8].

1.3 HYBRID FRAME

The hybrid framing concept is used to establish moment-resisting frames from single-bay precast concrete beams and multi-story high precast concrete columns. The beams and column are connected through unbonded post-tensioning tendons and mild steel reinforcement across the beam-column interface, where the unbonded post-tensioning steel is located at the mid-height and mild steel is placed closer to the top and bottom surfaces of the beams (Fig. 1.1). The interfaces and ducts housing the mild steel reinforcement are filled
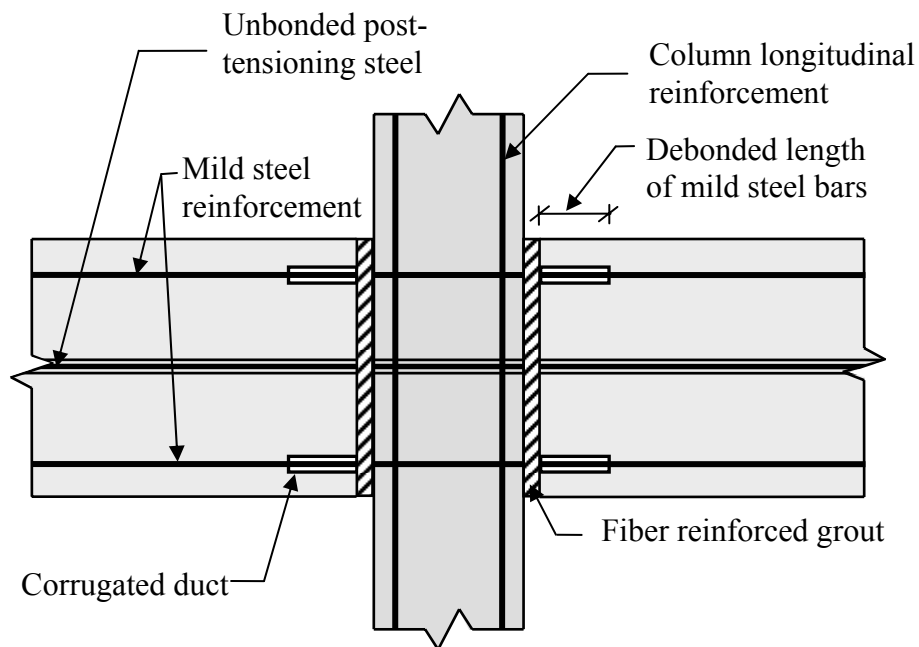
Figure 1.1.   Illustration of the hybrid connection concept

(Joint and transverse reinforcement is not shown for clarity)

with non-shrink cementituous fiber grout prior to post-tensioning. The grout at the interfaces ensures continuity between precast members while grouting the ducts enables the reinforcement to contribute to the stiffness and strength of the hybrid frames. A short length of mild steel reinforcing bars near the interfaces are debonded to control the inelastic strain

accumulation and avoid premature fracture of the reinforcement. Shear transfer across the precast connection interface is relies on a friction mechanism.

When subjected to lateral loads, flexural cracks concentrate at the beam ends in a hybrid frame due to the use of unbonded steel reinforcement at the precast connections. Thus, the beams will undergo minimal structural damage when the hybrid frame is subjected to inelastic lateral deformations. A supplementary advantage of reducing the beam damage along its length is that the frame elongation resulting from the formation of plastic hinges at the beam ends will be smaller than that expected in a monolithic concrete frame. Nonlinear elastic response from the unbonded post-tensioning tendons and hysteretic behavior from the mild steel reinforcement will enable the hybrid frames to dissipate energy and minimize residual displacements. The reduced residual displacements will also make these frames less sensitive to P-Δ effects. The post-tensioning tendons that run across the column width reduces the principal tensile stresses in the beam-to-column joints. The reduction to the principal tensile stress suggests that the amount of joint shear reinforcement could be reduced when compared to the joints in equivalent conventional concrete frames [1.10].

1.4 UNBONDED PRECAST WALL SYSTEMS

Unbonded jointed precast walls can be used as the primary structural system for resisting seismic lateral forces. Individual precast walls are attached to the foundation by unbonded post-tensioning steel running from the top of the wall to the foundation. Two or more of such post-tensioned walls are connected to each other, horizontally along the height, by shear connectors, to form a jointed precast wall system (Fig. 1.2). When detailed with unbonded post-tensioning, a precast concrete wall can provide added benefits such as reduced structural

damage and minimum residual displacements when subjected to seismic lateral forces, due to
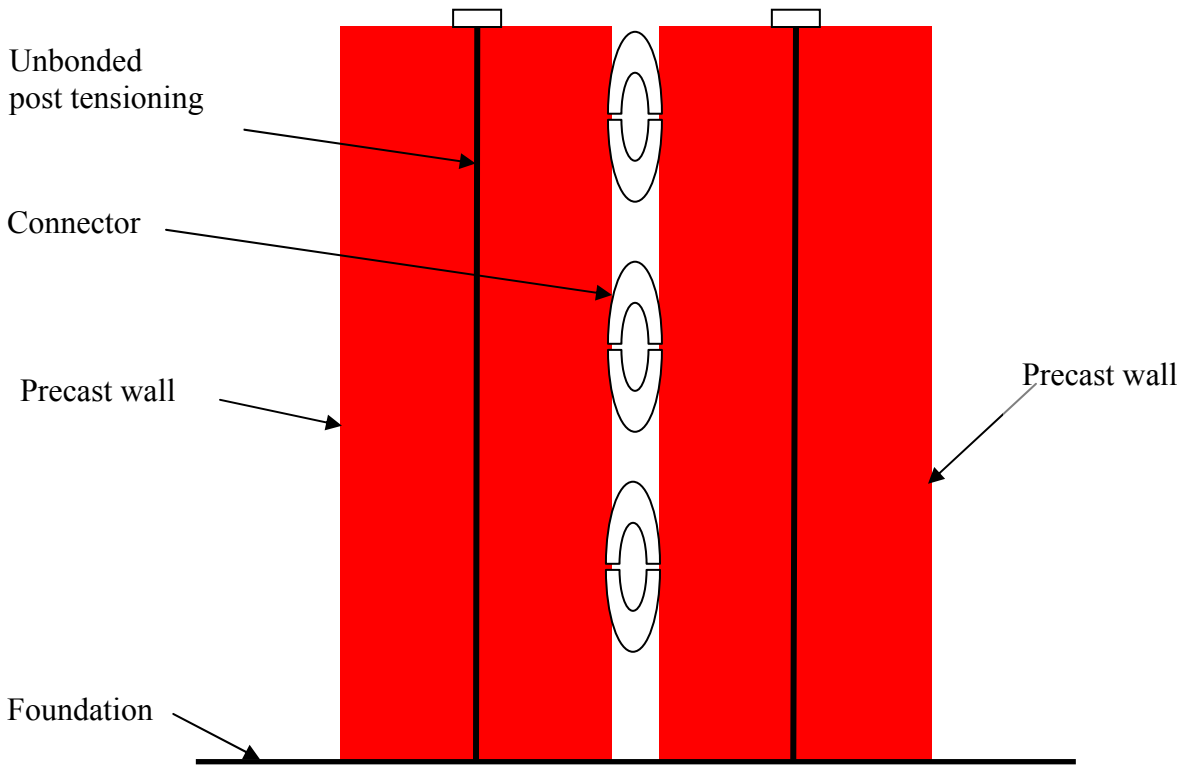
Figure 1.2.   Illustration of a jointed wall system

concentration of flexural cracks and re-centering capability of prestressing tendon [1.11]. The main disadvantage against single unbonded precast walls is the lack of energy dissipating capability, which is eliminated by incorporating shear connectors between the walls in jointed wall systems.

1.5 SEISMIC DESIGN METHODS

Force-Based and Displacement-Based Design

In this thesis, applicability of two seismic design methods is investigated: (1) Force-based design, and (2) Direct displacement-based design. The traditional approach of seismic design

is force-based, which is also widely used in design codes [e.g., 1.12,1.13]. In this approach, the design base shear is obtained from the estimated fundamental period and total mass of the structure, incorporating the influence of seismic intensity in terms of spectral acceleration (Fig. 1.3). It does not involve any target lateral displacement for the building, but the intent is to keep interstory drifts less than or equal to 2% under design level earthquakes.
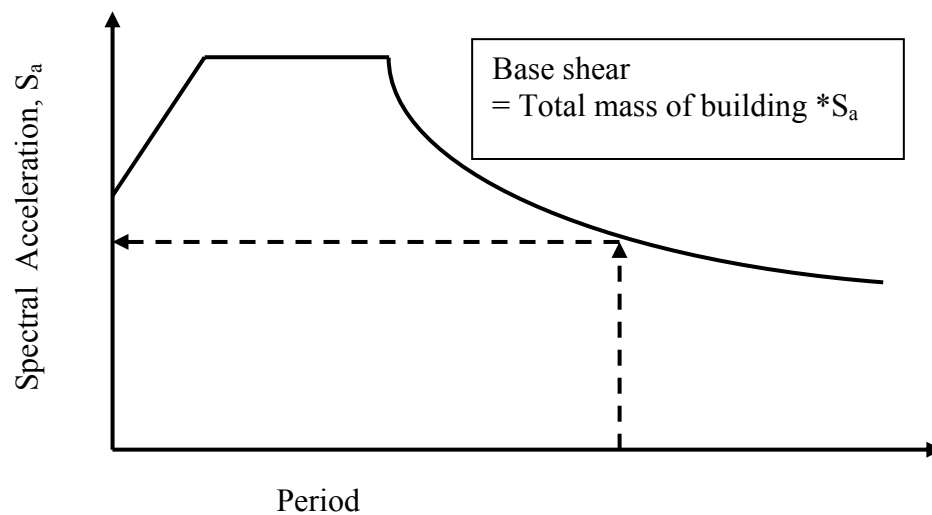
Figure 1.3.   A schematic of a design spectrum acceleration used in estimating design base shear force in force-based design method

In contrast, a target displacement linked to the expected performance of the building is used in direct displacement-based design, which dictates the required effective natural period of an equivalent single-degree-of-freedom system representing the structure, based on the seismic intensity in terms of spectral displacement [1.14]. The total mass of the building, converted to an effective mass for the equivalent single-degree-of-freedom system, and the abovementioned effective period are used to calculate the effective stiffness of the building

[1.14]. Finally, the design base shear is obtained from the product between the target lateral displacement and effective stiffness (Fig. 1.4). Furthermore, it is demonstrated in Ref. [1.14] that the direct displacement-based design approach typically results in smaller design base shear than that obtained from the force-based design approach, thus reducing the cost of the structure.

$$K_e = \frac{4\pi^2 M_e}{T^2_e}$$

K_e = Effective stiffness of an equivalent SDOF system
M_e = Effective mass of an equivalent SDOF system
T_e = Effective period of an equivalent SDOF system

Base shear = K_e *Target Displacement
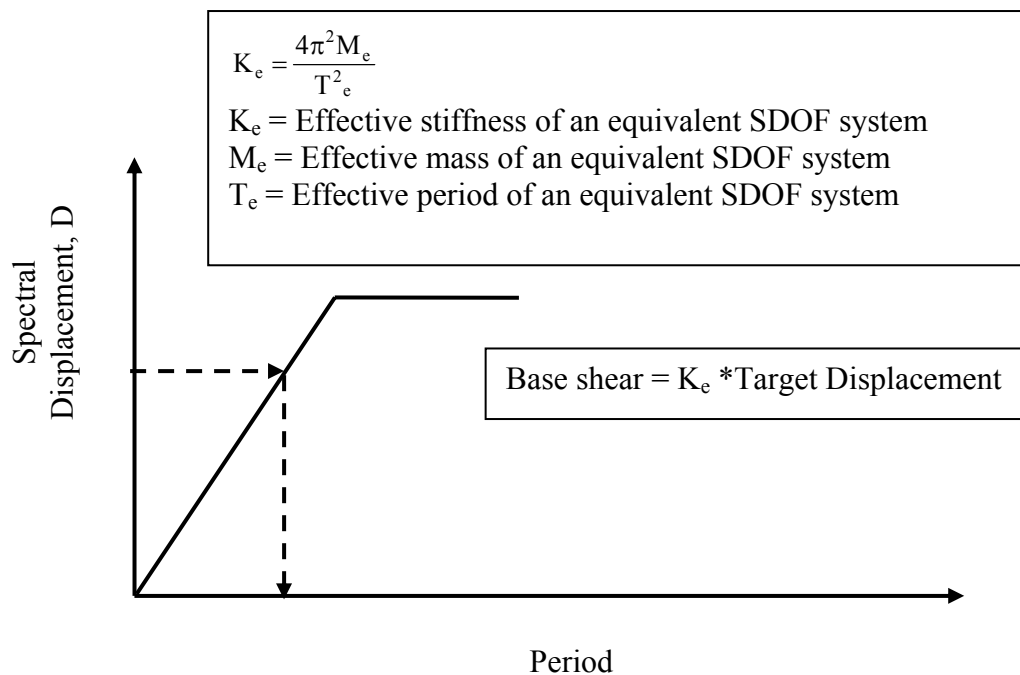
Figure 1.4.   A schematic of a spectrum displacement used in estimating design base shear in direct displacement-based method [1.14]

1.6 MULTIPLE-LEVEL PERFORMANCE-BASED SEISMIC EVALUATION

A multiple-level performance-based seismic evaluation ensures whether a building is capable of fulfilling specified levels of target performances when subjected to earthquakes of different intensities. The philosophy of multiple-level performance-based seismic evaluation should consist of controlling structural and non-structural performance for earthquakes that

may be characterized as frequent, occasional, rare and maximum considered events with mean return periods of 25, 72, 250 to 800, and 800 to 2500 years, respectively. The overall performance of a building, subjected to the aforementioned earthquakes levels, is expected to be operational, life safety, near collapse and collapse, respectively [1.15,1.16].

With the increased interest in performance-based earthquake engineering, the future of force-based design method can be questioned, because of lack of direct connection of this approach with target displacement of the structure when estimating the design base shear. Another obvious disadvantage of this method is higher construction cost compared to the direct displacement-based approach due to the increased design base shear. To compare the performance of similar buildings designed by both approaches, a detailed dynamic analytical investigation is appropriate under different levels of ground motions, representing various earthquake intensity levels. For this process, a multiple-level performance-based evaluation method may be necessary. If it can be shown through this investigation that the direct displacement-based solution can satisfy all acceptance criteria of performance, it will offer a structural design a more economical solution due to the reduced design base shear. Such a rigorous dynamic analytical investigation to realize this economical benefit is not available in present literature. The focus of this thesis is to conduct such study for both hybrid frames and jointed wall systems.

1.7 PREVIOUS WORK

The hybrid frame concept has been studied over the past decade, which included component level [1.17] and structure level [1.6,1.18] testing. More recently, the hybrid frame has been used in a few buildings including a 39-story apartment complex (see Fig. 1.5) in San

Francisco, California [1.19], which proved the practical viability of implementing such an innovative structural concept in real-world applications. This building is not only the tallest concrete structure built in high seismic zone (i.e., Seismic Zone 4) but is also by far the tallest precast, prestressed concrete frame structure built in a region of high seismicity.

Figure 1.5.   A view of 39-story, 420-ft high, Paramount apartment building in San Francisco, California [1.19]

At various stages of investigating and promoting hybrid connections, guidelines for designing hybrid frame systems had been published in Ref. [1.20-1.22]. A design validation and an analysis procedure for precast beam-to-column hybrid connection, referred to as the

modified PRESSS procedure have been presented in Ref. [1.23], by improving the design guidelines proposed in Ref. [1.21]. The computational tool, developed in Ref. [1.23], is capable of producing the monotonic moment-rotation response envelope of a hybrid connection established using unbonded mild steel and post-tensioned reinforcement.

Unbonded jointed wall system has been studied in Ref. [1.24-1.28]. Design procedures and recommendations for unbonded jointed wall system are available in Ref. [1.11,1.21,1.29]. A more detailed presentation of these previous works is presented in literature review in chapter 2.

PREcast SEISMIC STRUCTURAL SYSTEMS (PRESSS) RESEARCH PROGRAM

The PREcast Seismic Structural Systems (PRESSS) research program, sponsored by the National Science Foundation (NSF), Precast/Prestressed Concrete Institute (PCI), and Precast/Prestressed Concrete Manufacturers Association of California (PCMAC) was initiated in the United States in the early 1990s taking into account the exceptional performance of structural walls in past earthquakes, the benefits of precast concrete and the possible design restrictions that must be overcome. This program was initiated as a part of the United States-Japan protocol on large-scale testing for seismic response of precast concrete buildings. Two primary objectives of this program were to: (1) develop comprehensive and rational design recommendations based on fundamental and basic research data which will emphasize the viability of precast construction in the various seismic zones, and (2) develop new materials, concepts and technologies for precast construction in the various seismic zones [1.8].

With a view of obtaining feedback from concrete producers, design engineers and contractors on concept developments and connection classification projects of PRESSS, a concept development workshop was held in April 1991 [1.25]. Following the concept development workshop, and various testing and analytical models in the first two phases of PRESSS program, a five-story precast test building was designed, built and tested under simulated seismic loading at 60 scale, in phase III of the PRESSS program, at the University of California at San Diego [1.18]. This test building, with two bays by two bays, utilized two seismic frames with four different types of jointed moment resisting frames in one direction, while a jointed precast wall system served as lateral load resisting component in the orthogonal direction. Figures 1.6 (a) and (b) show that the hybrid and TCY-gap connections were used in the lower three stories of the two seismic frames whereas pretensioned and TCY connections [1.18] were utilized in the upper two floors. Figure 1.7 illustrates various components of a hybrid connection between precast column and beam. The wall comprised of 4 panels, each of which were 2½ stories tall (18.75-ft) by 9-ft wide and 8-in thick (Figs. 1.8 and 1.9). Two walls, separated by a small gap, were formed by joining the panels vertically. These two walls were secured to the foundation using four unbonded post-tensioning bars, and were connected horizontally by 20 U-shaped flexural plates (UFP connectors, see Fig. 1.10) placed along the vertical joint between the walls (Fig. 1.8). Figure 1.11 represents the 5% damped multiple-level acceleration response spectra, suggested for soil type S_c in high seismic zone as per Ref. [1.15]. In the PRESSS test building, short segment ground motions compatible with acceleration response spectra of 1.5EQ-I, EQ-II and EQ-III shown in Fig. 1.10 were used for seismic testing.
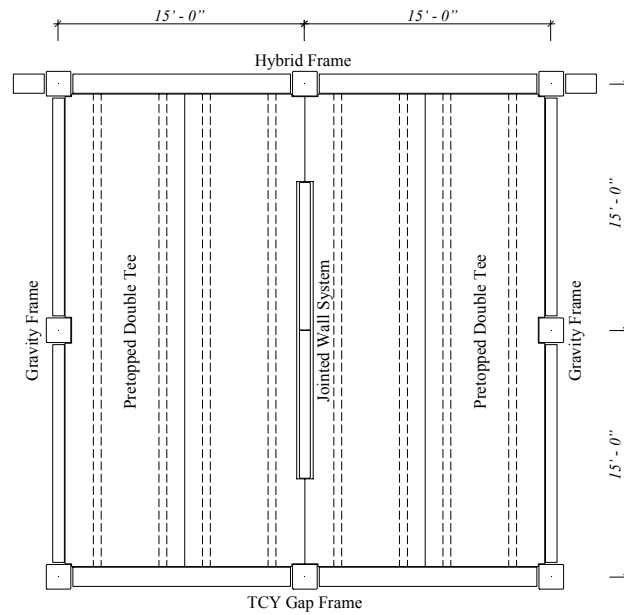
(a) Lower three floors
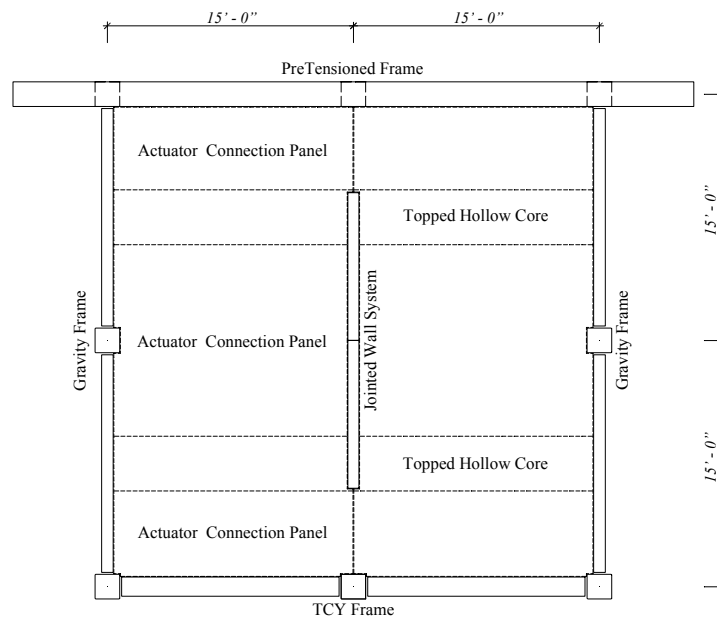
(b) Upper two floors

Figure 1.6.   Floor plans of the PRESSS test building [1.18]
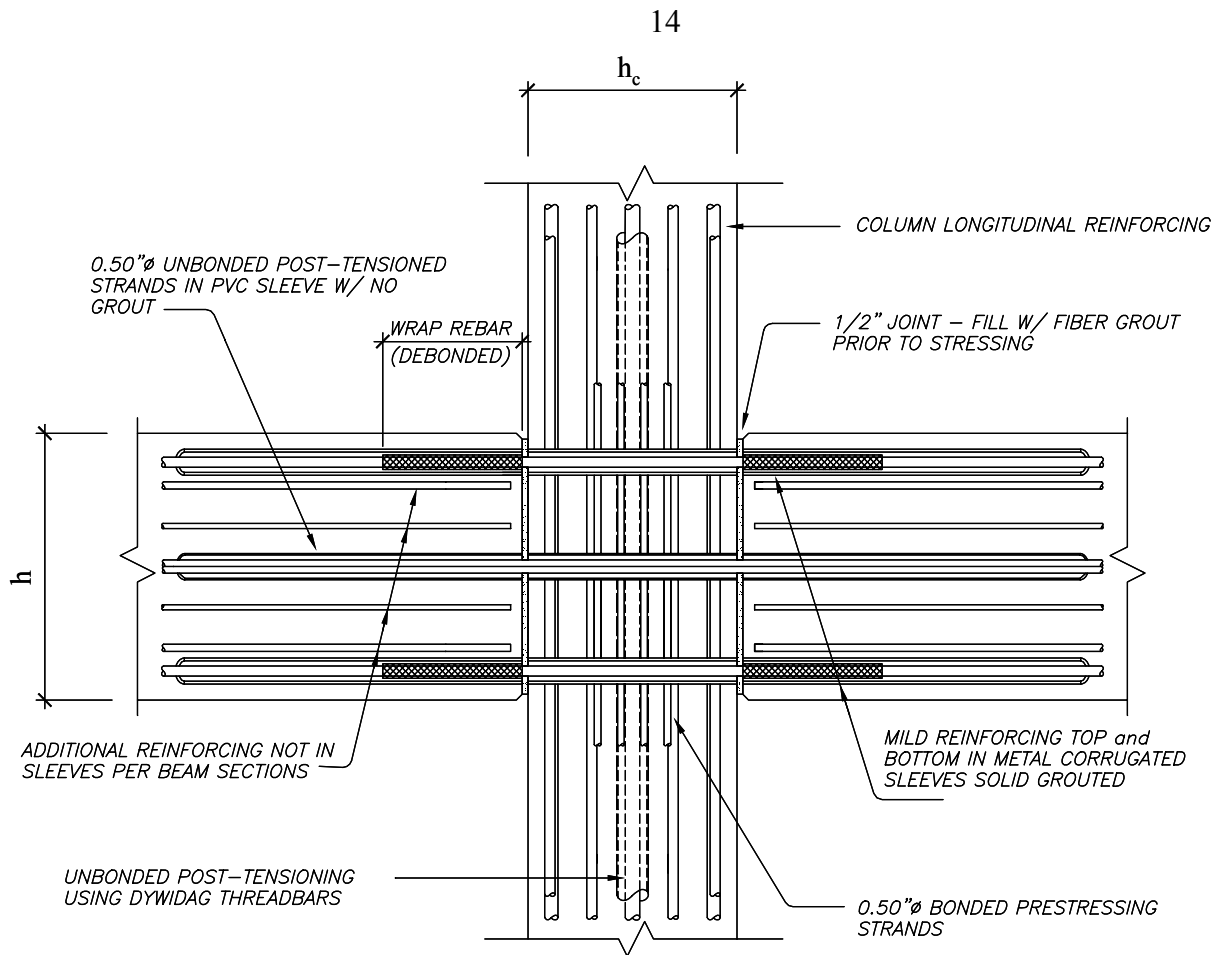
Figure 1.7.   The typical connection details of a precast hybrid frame (transverse reinforcements are omitted for clarity)
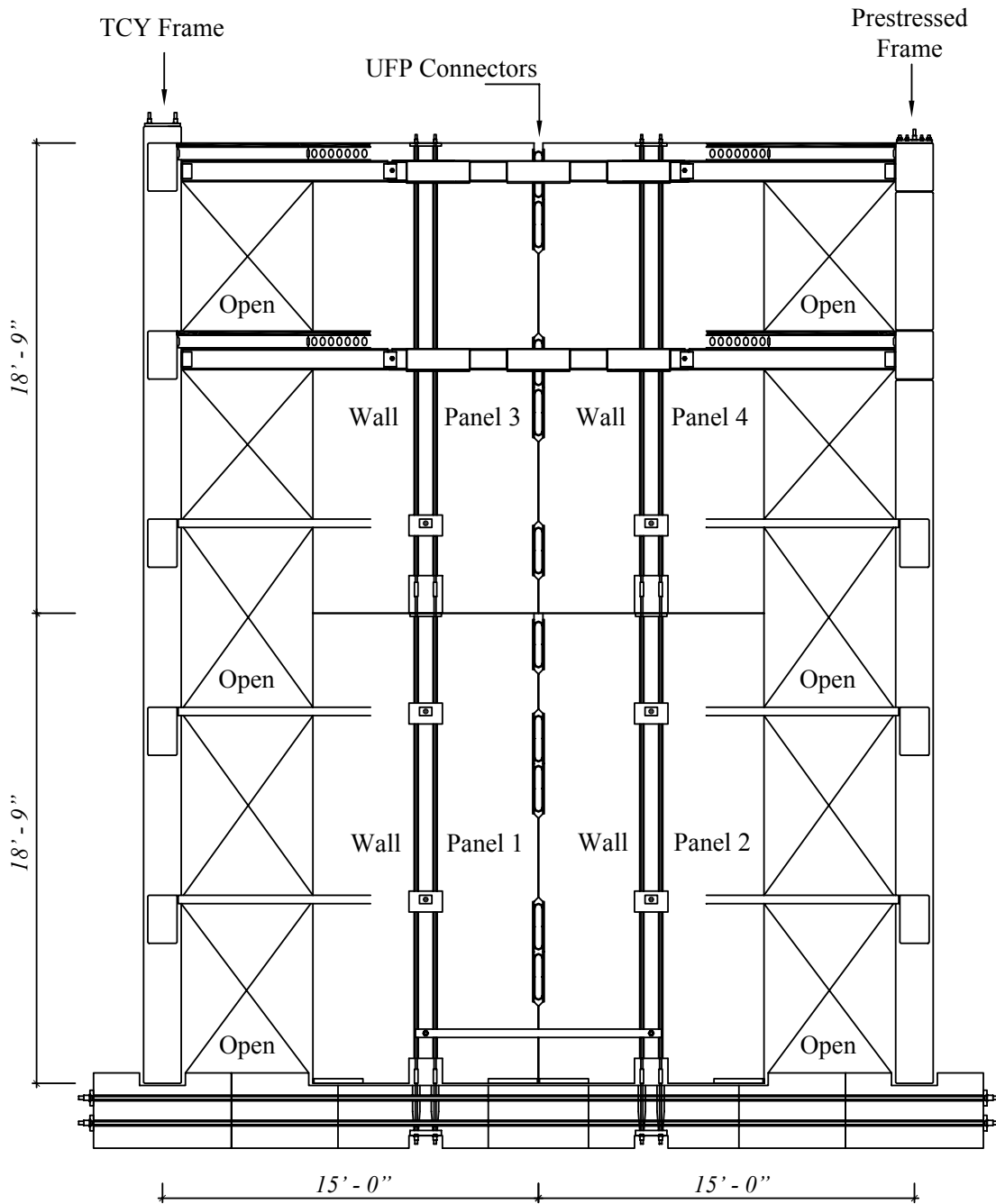
Figure 1.8.   Elevation view of the jointed wall system used in the PRESSS test building [1.18]

Figure 1.9.   The PRESSS building after erecting the wall system [1.18]
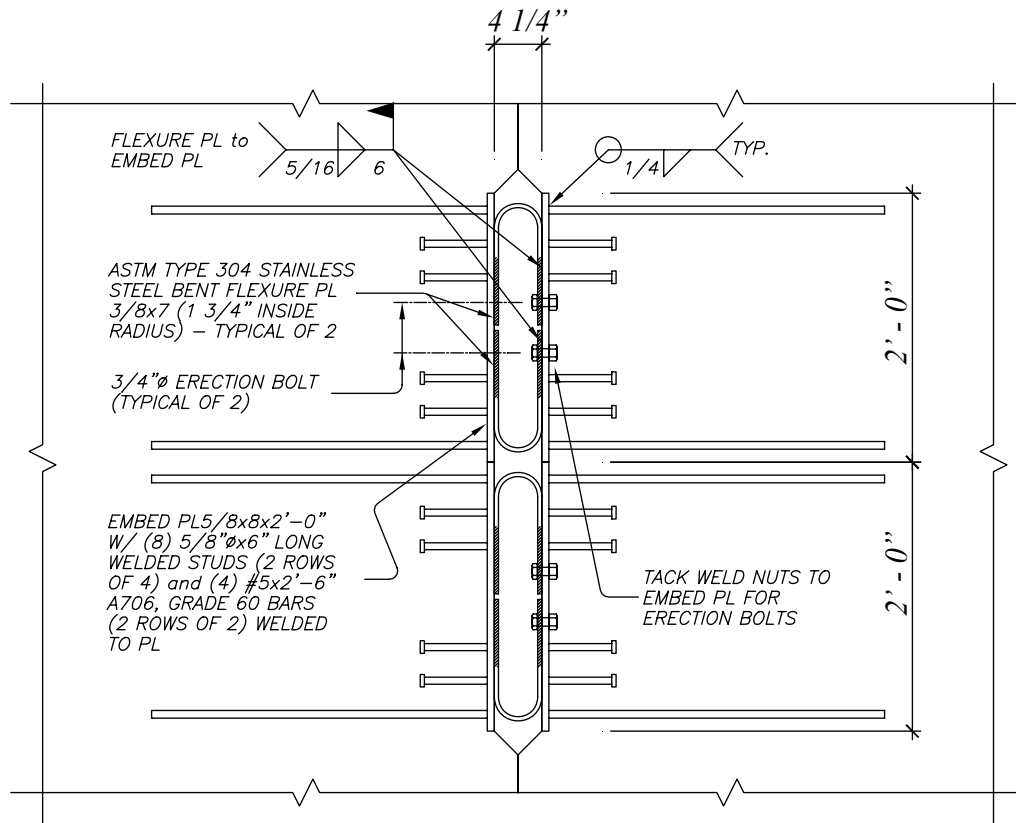
Figure 1.10.Connection details of UFP connectors in the PRESSS building [1.18
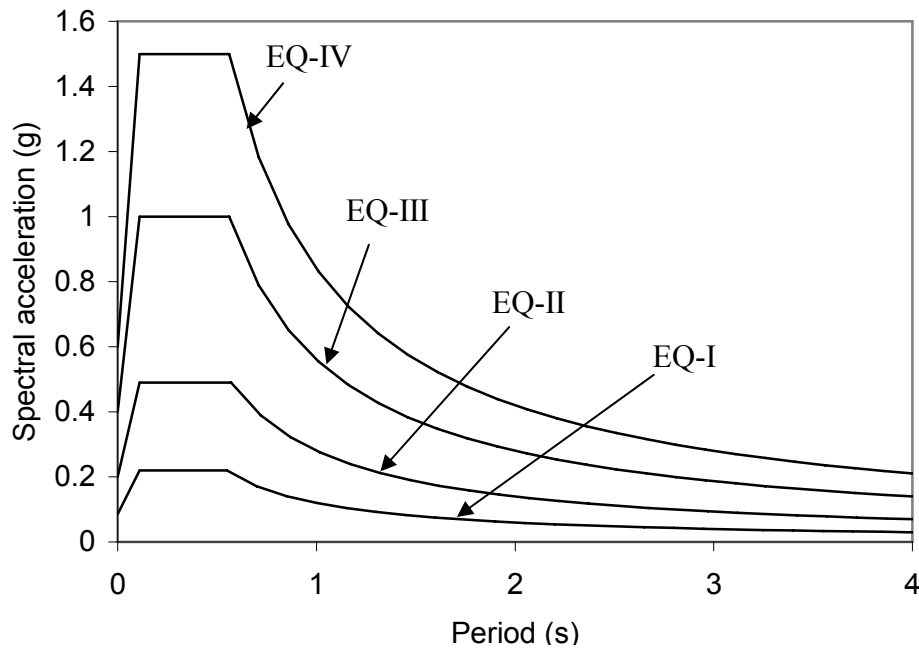
Figure 1.11.   The 5% damped multiple-level acceleration response spectra, suggested for soil type S_c in high seismic zone as per Reference [1.15]

Test results from the PRESSS building is the only available document in the United States, providing information about the seismic performance of the precast structure, comprised of hybrid frame and jointed unbonded precast walls, subjected to various levels of ground motions. However, test results of PRESSS program cannot be used to make a generalized prediction of multiple-level seismic performance of hybrid frame and jointed unbonded precast walls, because these tests were conducted only for a five-storied building subjected by only short-duration ground motions. This study did not explore the effect of varying the height of the building. Performance of the test building under long-duration ground motion was not addressed. Moreover, the jointed walls had only one setup, comprising of two walls, connected by twenty UFP connectors, where incorporation of UFP connectors involved more

cost to the structure. With this one setup of the jointed walls, it was not possible to evaluate the effect of varying the number of UFP connectors on seismic performance of the jointed wall system. In addition, test results could not provide comparison of performance between displacement-based and force-based design, because the only building tested was designed based on direct displacement-based approach.

1.8 SCOPE OF RESEARCH

The overall scope of this research is to evaluate seismic performance of precast concrete buildings designed with hybrid frames or jointed wall systems by subjecting them to earthquakes of different intensities. These buildings are designed using both the direct displacement-based and force-based design methods such that the benefits of the two methods in designing these buildings can be realized. This research scope will be achieved by conducting dynamic analysis of several precast concrete buildings under several earthquake motions as classified in the following tasks:

(1) Using the PRESSS building configuration, a 60% scale five-story building is established as a displacement-based solution. This building will be designed by introducing hybrid frame and jointed unbonded precast walls as lateral load resisting systems in two orthogonal directions. Analysis models for both hybrid frame and wall system will be formulated independently for the two orthogonal directions. Using the input ground motions from the PRESSS building test, it will be ensured that the analytical models can adequately capture the seismic response, which includes time history of top floor displacement, base moment resistance, and displacement of the connectors in case of the jointed wall system.

(2a) A procedure for conducting performance-based evaluation will be developed, using Ref. [1.12,1.13,1.15,1.16] as the basis. Using this procedure, performance-based evaluation of hybrid frame and jointed wall system buildings, designed by both the direct displacement-based and force-based approach, will be conducted. Four combinations of short-duration earthquake motions and eight long-duration ground motions, representing frequent to maximum considered earthquakes, will be used as the input motions. Performance will be evaluated with respect to the maximum transient inter-story drift limits, maximum residual inter-story drift limits, and floor acceleration limits.

(2b) Pushover analysis will be conducted for both of the hybrid frames, designed by displacement-based approach and force-based approach. This will result in direct comparison of base shear vs. roof displacement of the two hybrid frames. In addition, by comparing various responses of the hybrid frames, necessary improvements in the displacement-based design method will be recommended. A similar task will be conducted for the wall system. Moreover, influence of hysteric damping on the performance of the jointed wall system buildings will be investigated by changing the number of wall connectors.

(3) In this task, five**,** seven and ten story high buildings comprised of jointed wall systems will be designed at 100% scale using the direct displacement-based design procedure. Performance-based seismic evaluation of the two buildings will be conducted using the analysis models developed for these buildings.

(4) Five, seven and ten story high buildings comprised of hybrid frames will be designed at 100% scale using the direct displacement-based design procedure with suggested

improvement in task 2b. Analysis models for these buildings will be formulated. Using these analysis models, performance-based seismic evaluation of the three buildings will be conducted.

1.9 THESIS LAYOUT

The thesis will comprise of seven chapters including the general introduction presented in this chapter. The following chapter will contain literature review, which will include past performance of precast concrete frames and walls in seismic regions, and previous investigations on analysis and design of precast concrete frames and precast seismic wall systems. In the third chapter, an analytical model of a 60% scale hybrid frame building will be presented. Following the validation of this analytical model, using the PRESSS test data, a performance-based evaluation will be conducted for two similar buildings, which will represent the direct displacement-based and force-based design solutions for the prototype building at 60% scale. Next, a comparison of multiple-level performance of these two buildings will be conducted. The fourth chapter will formulate an analytical model of a jointed wall system similar to that used in the PRESSS test building. After successful validation of this model, comparison of performance-based evaluation will be done for two similar buildings in the wall direction, designed by using the direct displacement-based and force-based methods, at 60% scale.

In the fifth chapter, five, seven and ten story high full-scale precast jointed post-tensioned wall system buildings will be designed according to the direct displacement-based design method. Multiple level seismic performance of these low to mid-rise buildings will be presented. A similar investigation involving five, seven and ten story high full-scale

buildings comprised of precast hybrid frames designed by using the improved direct displacement-based approach will be presented in chapter six. By using the improved direct displacement-based design method, it will be shown that the performance of the buildings is satisfactorily under collapse level ground motions. This chapter will reveal the difference in performance of hybrid frame buildings as a function of story height which will help with investigating the viability and limitations of using precast hybrid frames in low to mid-rise buildings. The seventh chapter will contain conclusions and recommendations derived from this research, along with recommendations for future research in this topic area.

1.10 REFERENCES

1.1   Fintel, M., "Performance of Buildings with Shear Walls in Earthquakes of the Last Thirty Years", *PCI Journal,* 2002, Vol. 40, No. 3, pp. 62-80.

1.2   *Earthquake Engineering Research Institute*. Northridge Earthquake Reconnaissance Reports, Earthquake Spectra, 1995-1996, Supplement C to Vol. 11.

1.3   Ghosh, S. K., "Observations from the Bhuj Earthquake of January 26, 2001", *PCI Journal,* 2001, Vol. 46, No. 2, pp. 34-42.

1.4   *John A. Martin and Associates, Inc.* Earthquake Images: A Comprehensive Collection of Earthquake Related Slides and Photographs.
        Retrieved from http://www.johnmartin.com/earthquakes/eqshow/index.htm on 20-12-2003.

1.5   Vernu, S., and Sritharan, S., Section, Member and System Level Analysis for Precast Concrete Hybrid Frames, ISU-ERI-Ames Report ERI-04635, Iowa State University, Ames, Iowa, USA, June 2004.

1.6   Priestley, M. J. N., Sritharan, S., Conley, J. R., Pampanin, S., "Preliminary Results and Conclusions From the PRESSS Five-Story Precast Concrete Test Building", *PCI Journal*, 1999, Vol. 44, No. 6, pp. 42-67.

1.7   Park, R., "A Perspective on the Seismic Design of Precast Concrete Structures in New Zealand", *PCI Journal*, 1995, Vol. 40, No. 3, pp. 40-59.

1.8   Priestley, M. J. N., "Overview of PRESSS Research Program", *PCI Journal*, 1991, Vol. 36, No. 4, pp. 50-57.

1.9 Vernu, S., "Connection and Structural Level Analysis of Precast Hybrid Frame Systems", *Master Thesis*, Iowa State University, Ames, Iowa, 2003.

1.10 Sritharan, S., and Rahman, M.A., "Performance-based Seismic Assessment of Two Precast Concrete Hybrid Frame Buildings", *Proceedings of International Workshop on Performance-based Seismic Design, Bled, Slovenia, 2004.*

1.11 Thomas, D. J., and Sritharan, S., An Evaluation of Seismic Design Guidelines Proposed for Precast Jointed Wall Systems, ISU-ERI-Ames Report ERI-04635, Iowa State University, Ames, Iowa, USA, June 2004.

1.12 *Uniform Building Code (UBC)*. International Conference of Building Officials, Whittier, California, USA, 1997, Vol. 2.

1.13 *International Building Code (IBC)*. International Code council, Virginia, USA, 1997.

1.14 Priestley, M. J. N., "Direct Displacement-Based Design of Precast/Prestressed Concrete Buildings", *PCI Journal,* 2002*,* Vol. 47, No. 6, pp. 67-79.

1.15 Performance-Based Seismic Engineering Ad Hoc Subcommittee. SEAOC Blue Book, Revised Interim Guidelines, Performance-Based Seismic Engineering, Structural Engineers Association of California (SEAOC), California, USA, 2003.

1.16 Seismology Committee. Recommended Lateral Force Requirements and Commentary, SEAOC Blue Book, Structural Engineers Association of California (SEAOC), California, USA, 1999.

1.17 Stone, W. C., Cheok, G. S., and Stanton, J. F., "Performance of Hybrid Moment-Resisting Precast Beam-Column Concrete Connections Subjected to Cyclic Loading", *ACI Structural Journal*, 1995, Vol. 92, No. 2, pp. 229-249.

1.18 Sritharan, S., Pampanin, S., and Conley, J. Design Verification, Instrumentation and Test Procedures, PRESSS-3: The Five-Story Precast Test Building, Vol. 3-3. ISU-ERI-Ames Report ERI-03325, Iowa State University, Ames, Iowa, USA, 2002.

1.19 Englekirk, R. E., "Design-Construction of The Paramount – A 39 -Story Precast Concrete Apartment Building", *PCI Journal*, Vol. 47, No. 4, 2002, pp. 56-69.

1.20 Cheok, G. S., Stone, W. C., Nakaki, S. D., "Simplified Design Procedure for Hybrid Precast Concrete Connections", National Institute of Standards and Technology, *SCTR 5765*, 1996.

1.21 Stanton, J. F. and Nakaki, S. D., Design Guidelines For Precast Concrete Seismic Structural Systems, *PRESSS* Report No. 01/03-09, UW Report No. SM 02-02, The University of Washington and The Nakaki Bashaw Group, Inc., 2002.

1.22   ACI Innovative Task Group 1 and Collaborators, Special Hybrid Moment Frames Composed of Discretely Jointed Precast and Post-Tensioned Concrete Members (ACI T1.2-03) and Commentary (T1.2R-03), Michigan, 2003.

1.23   Celik, O., and Sritharan, S., An Evaluation of Seismic Design Guidelines Proposed for Precast Concrete Hybrid Frame Systems. ISU-ERI-Ames Report ERI-04425, Iowa State University, Ames, Iowa, January 2004.

1.24   Nakaki, S. D., Stanton, J. F., and Sritharan, S., "An Overview of the PRESSS Five story Precast Test Building", *PCI Journal*, Special Report, March-April, 1999.

1.25   Nakaki, S.D., Englekirk, R. E., "PRESSS Industry Seismic Workshops: Concept Development", *PCI Journal*, 1991, Vol. 36, No. 5, pp. 54-71.

1.26   Priestley, M. J. N., Sritharan, S., Conley, J. R., Pampanin, S., "Preliminary Results and Conclusions From the PRESSS Five-Story Precast Concrete Test Building", *PCI Journal*, 1999, Vol. 44, No. 6, pp. 42-67.

1.27   Schultz, A. E., and Magna, R. A., "Seismic Behavior of Connections in Precast Concrete Walls", Mete A. Sozen Symposium, Paper No. SP 162-12, American Concrete Institute, Farmington Hills, MI, 1996.

1.28   Conely, J., Sritharan, S., and Priestley, M. J. N., Precast Seismic Structural Systems PRESSS-3: The Five-Story Precast Test Building Vol. 3-1, Wall Direction Response, Report No. SSRP-99/19, Department of Structural Engineering, University of California, San Diego, California, July 2002.

1.29   Pampanin, S., Priestley, M. J. N., and Sritharan, S., "Analytical Modeling of the Seismic Behavior of Precast Concrete Frames Designed with Ductile Connections", *Journal of Earthquake Engineering*, Vol. 5, No. 3, 2001.

CHPATER 2. REVIEW OF LITERATURE

2.1 INTRODUCTION

This chapter describes the past experimental and analytical work of non-emulative precast frame connections and precast post-tensioned wall systems. Recent progress in development of hybrid frame connection will be discussed. Design approaches recommended for these two systems in literature will also be presented.

2.2 Precast Frame Connection Systems

Nakaki, Englekirk, and Plaehn [2.1]

Connection of precast beams and precast columns was achieved by bolting the beams to the column faces, thereby introducing an embedded ductile link. A ductile rod, made up of high quality steel with well-defined strength characteristics and high elongation capacity acted as the key element in this connection. Figure 2.1 illustrates the plan view of the connection.
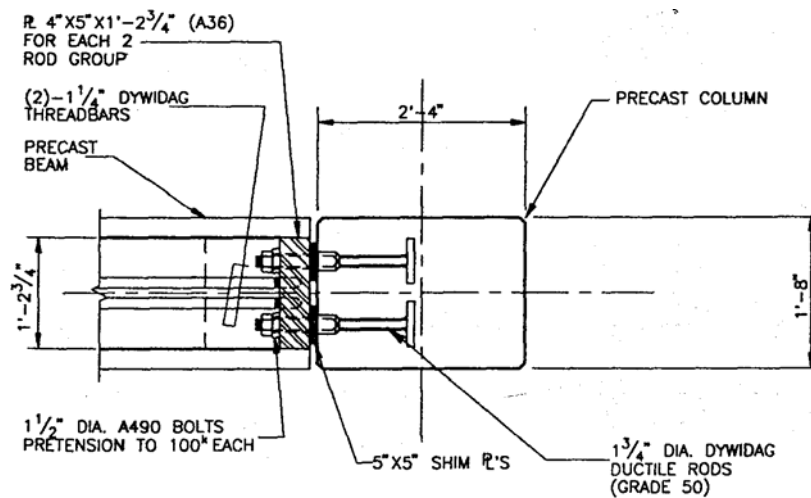
Figure 2.1.   Ductile frame connection details adopted by Nakaki et al. [2.1]

This specimen was tested by imposing cyclic lateral load. The connection rod experienced stress reversals without forming horizontal cracks in the beam-to-column joint region. A significant number of joint diagonal cracks were visible on the test units, which appeared to be more severe than that expected in equivalent monolithic frames. It was concluded that the proposed system provides a satisfactory precast framing concept for applications in seismic regions without significant increase in erection expenses.

Cheok and Lew (NIST) [2.2]

To develop rational design procedures for precast frame connections for seismic regions, an extensive experimental investigation was conducted at NIST on concrete frame sub-assemblages. One-third scale monolithic and precast beam-column frame connections were chosen to test them in three phases under cyclic loading. Four monolithic and two precast specimens were tested in Phase I of the NIST research program. The monolithic connections were designed in accordance with UBC 1985 [2.3], with two specimens suitable for Zone 4 and the remaining two specimens representing the design for Zone 2. The precast specimens with grouted post-tensioning were similar in dimensions to the monolithic specimens designed for Zone 4. Fiber-reinforced grout was used to fill the gap between the precast beams and columns.

Figure 2.2 shows the dimensions and support conditions used in tests of Phase I. Individual specimen was labeled by three letters followed by a numeral. Monolithic and precast were identified by the middle letters M and P, respectively. The last letter Z and numeral stood for seismic zones. For example, Type A frame designed for Zone 4 was represented by B-M-Z4.

27
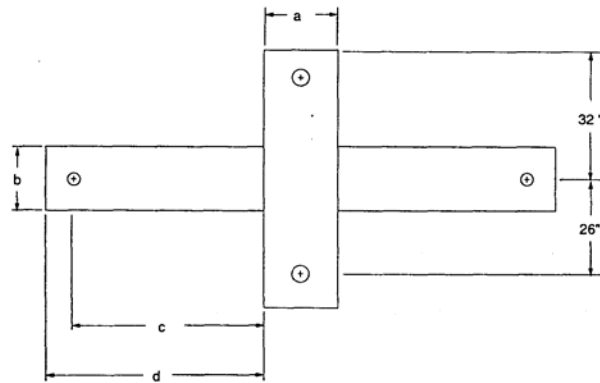
(a) Schematic diagram of a typical specimen

	ZONE 2	ZONE 4	
	A-M-Z2 & B-M-Z2	A-M-Z4 & B-M-Z4	A-P-Z4 & B-P-Z4
a	10"	18"	18"
b	10	16	16
c	40	41-3/4	37
d	46	47-3/4	43

(b) Dimensions of the test Specimens
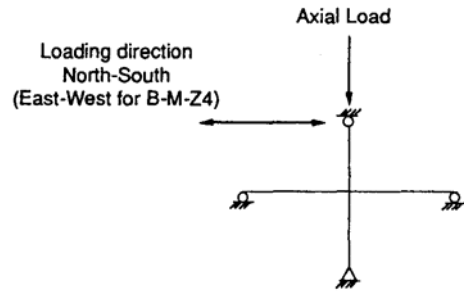
(c) Support conditions

Figure 2.2.   Details of test specimens used in Phase I of the NIST research program [2.2]
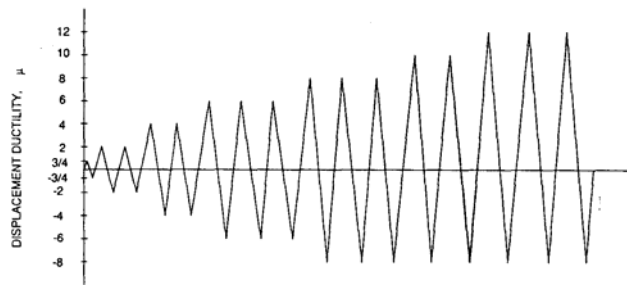
Figure 2.3   Cyclic load sequence used in Phase I of the NIST test program [2.2]

The cyclic load sequence shown in Fig. 2.3 was imposed on these specimens. In terms of strength, ductility, and drift level, the precast specimens generally exhibited behavior equivalent to that of monolithic specimens. Figure 2.4 illustrates lateral force-displacement behavior of one set of monolithic and precast specimens designed for Zone 4. The energy dissipated per load cycle by the precast concrete frames designed for Zone 4 was only 30 percent compared to that of monolithic specimens. Positioning the prestress bars closer to the mid-height of the beam and debonding the prestressing strands were suggested for consideration in Phase II and Phase III testing, respectively, to enhance the energy dissipation capability of the precast frames.

(a) Specimen A-M-Z4

(b) Specimen A-P-Z4
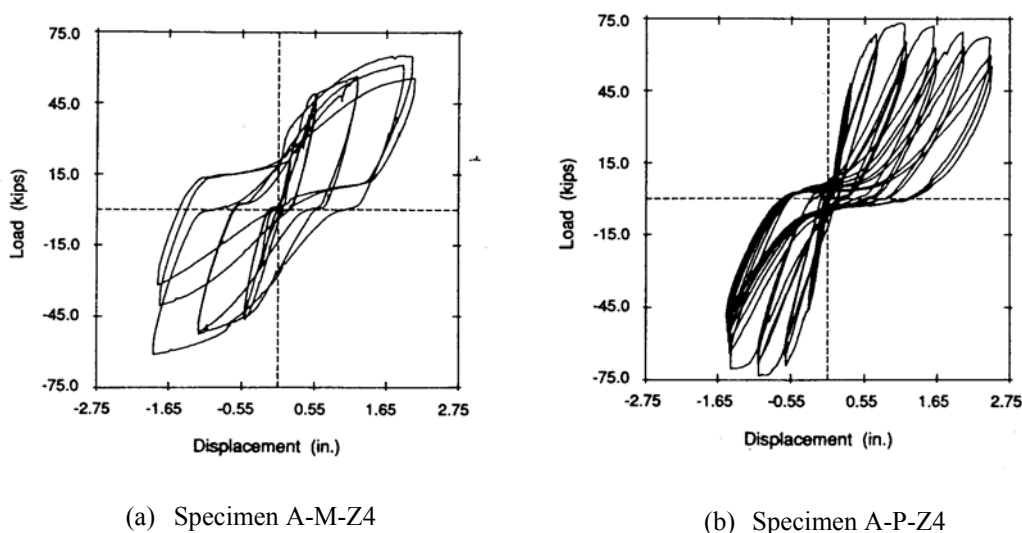
Figure 2.4.   Lateral force-displacement hysteresis behavior of two specimens tested in Phase I of the NIST test program [2.2]

Cheok and Lew (NIST) [2.4]

Six precast specimens, two for Zone 2 and four for Zone 4, were designed and tested under Phase II of the NIST test program. The effect of using the prestressing strands instead of high

strength prestressing bars and changing the location of the prestressing steel was investigated in this phase.

In Phase II, two specimens with partially debonded prestressing strands were tested. The strands were left unbonded in the beam-to-column connection region to avoid zero slopes introduced to the hysteresis loops during load reversals. As shown in Fig 2.4(b), precast frame specimens tested in Phases I and II exhibited hysteresis loops with zero slopes. This observation was believed to be mainly due to the development of inelastic strains in the prestressing strands and associated prestress loss. Use of partially unbonded post-tensioning steel in improving the behavior of prestressed frames was suggested by Priestley and Tao [2.5].

For the precast frame connections tested in Phase III superior performance in terms of strength, ductility and drift capacities was observed compared to those tested in Phase II as well as their monolithic counterparts tested in Phase I. For a particular load cycle in Phase III, the energy dissipated by the precast frames was about 60 percent of the equivalent monolithic frames. In Phase III, precast specimens designed for Zone 4 provided accumulated energy dissipation more than that obtained for the monolithic specimens. The increased crack opening at the precast interface, due to the use of unbonded post-tensioning strands, did not considerably affect the strength of the frame connection.

Figure 2.5 illustrates that the specimens tested in Phase III with partially bonded post-tensioning strands did not result in zero stiffness for the frames during unloading of the lateral load in contrast with a frame response with fully bonded strands. However, the hysteresis loops obtained for the frames with partially bonded strands were narrower than

those produced by specimens having fully bonded prestressing strands. It was recognized that the elastic behavior of the post-tensioning steel limits the energy dissipation of prestressed frames with partially bonded strands. The option of adding mild steel reinforcement as a means of energy dissipating elements in this phase was examined by extending the NIST test program to Phase IV.

(a) F-P-Z4 (Fully bonded strands)   (b) F-P-Z4 (Partially bonded strand)
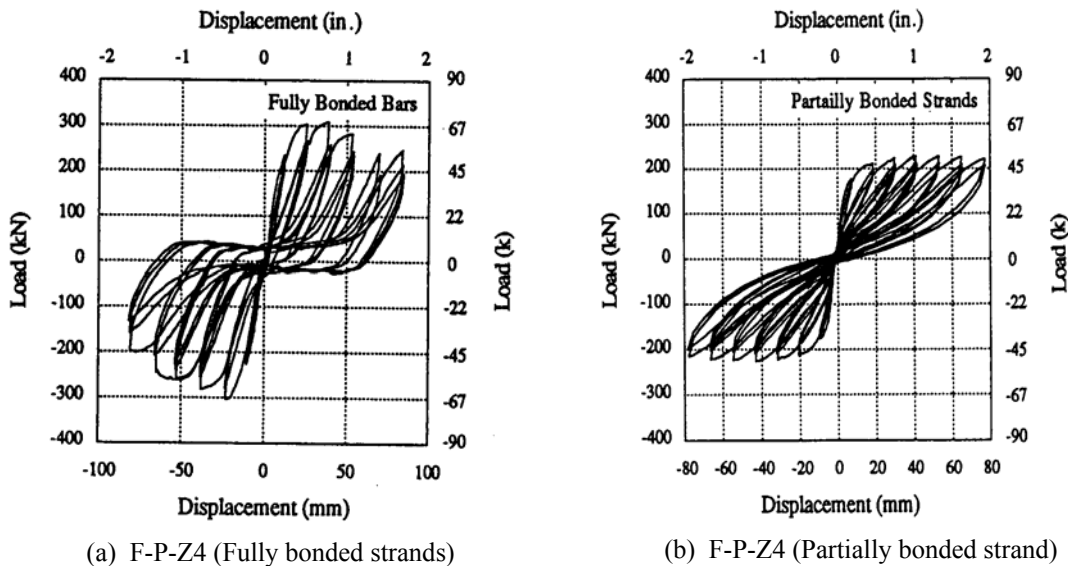
Figure 2.5.   Lateral load-displacement behavior of precast frames with connections utilizing fully and partially bonded prestressing stands [2.4]

Stone, Cheok and Stanton (NIST) [2.6,2.7]

Ten hybrid frame connections consisting of unbonded post-tensioning and mild steel reinforcement were tested in two sub-phases, IV-A and IV-B. In Phase IV-A, cyclic load testing of six specimens with three different connection details were conducted. It was found that placing the post-tensioning steel at the mid-height of the beam was appropriate to provide adequate shear resistance at the precast connection interface. Debonding the mild steel reinforcement in the beam over a short distance on either side of the precast column to

prevent accumulation of inelastic strains and premature fracture of this reinforcement was considered to be appropriate. The lateral load vs. story drift hysteresis responses obtained for two hybrid precast frames (M-P-Z4 and O-P-Z4) are shown in Figure 2.6.

(a) For M-P-Z4   (b) For O-P-Z4
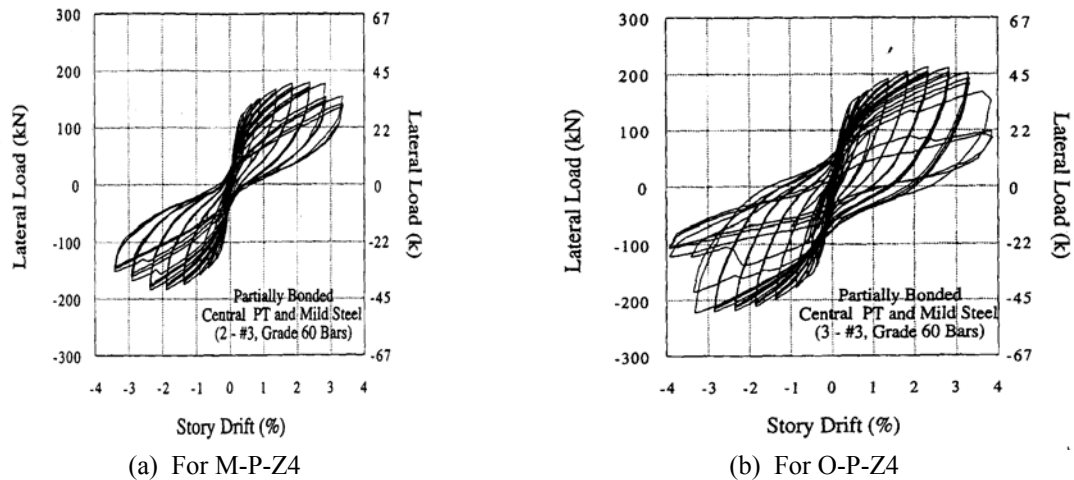
Figure 2.6. Hysteresis responses obtained for two hybrid frame subassemblages tested by Stone et al. [2.6]

Conclusions from the test observations:

- Prior to fracturing of the passive steel reinforcing bars, test specimen did not experience significant strength degradation.

- The hybrid frame has a very large drift capacity. At drift levels of ± 6 percent, the precast frames provided 55 percent of the maximum lateral resistance.

- Hybrid frames dissipated more energy per load cycle than the equivalent monolithic systems up to 1.5 percent story drift. The energy dissipated by the hybrid frames was 75 percent of the energy dissipated by the equivalent monolithic frames at larger drift.

- The hybrid frame exhibited re-centering capability when the lateral load was removed. It showed negligible damage compared to equivalent monolithic frame.

- Shear cracks were not visible on the precast beams after removal of the lateral load in contrast to those observed on the equivalent monolithic frames. Transverse reinforcement in the precast frame remained elastic.

Analytical Studies of Hybrid Frame Connections

A relationship between moment resistance and rotation at the connection interface is required to investigate seismic behavior of hybrid frame buildings using conventional frame analysis methods. Analysis of precast hybrid frames appears to be complicated due to the strain incompatibility between the concrete and unbonded mild steel and prestressing reinforcement. Availability of analytical study in characterizing the behavior of non-emulative precast frame systems is very limited and a summary of literature is provided in the following sections.

Englekirk (1989) [2.8]

For precast concrete frame, the component ductility and system ductility concepts were introduced to evaluate displacements associated with the ultimate load or the ultimate strain for individual members and beam-column subassemblages, respectively. For the cantilever beam, the ultimate displacement was given by: $\Delta_u = [1 - l_p / 2] l_p \Phi_u + \Delta_y$

where, l is the length of the beam, l_p is the plastic hinge length, Φ_u is the plastic curvature, and Δ_y is the beam end displacement at yielding.

Pampanin, Priestley and Sritharan [2.9]

This method, called monolithic beam analogy, makes the section level analysis and creation of continuous moment-rotation envelopes possible for jointed systems by assuming identical

global displacements for members that are connected with both the jointed and monolithic connections, as illustrated in Figure 2.7. This concept enables relationships between neutral axis depth, concrete strain, and steel strains to be established at the jointed connection interface. Conventional means are not capable to establish theses relationship due to the strain incompatibility arising from debonded reinforcing bars and/or unbonded prestressing tendons used in jointed connections.
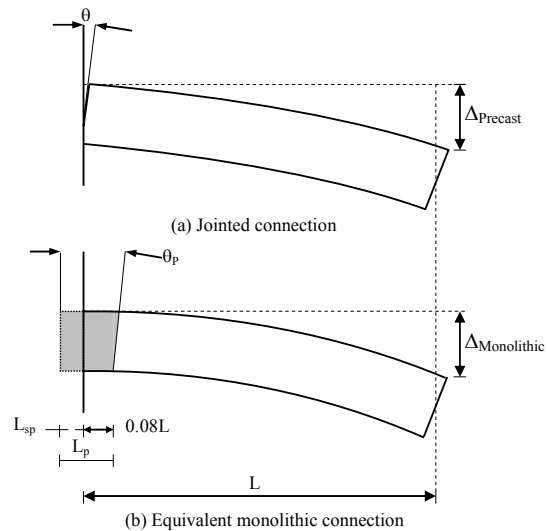
Figure 2.7.   The equivalent monolithic beam analogy concept [2.9]

The precast beams are designed to behave elastically and the beam rotations are concentrated at the connection interfaces in jointed frame system. This mechanism leads to gap opening at the interfaces rather than distributed cracks along the beams. Expressions for extreme fiber concrete strain (ε_c), strain in mild steel tension reinforcement (ε_{st}) and strain in post-tensioning tendon (ε_{ps}) at the beam-column connection interface derived through this analytical study are given below:

$$\varepsilon_c = \left[\frac{\theta}{L_p} + \phi_y \right] c$$

$$\varepsilon_{st} = \frac{(d-c)\theta + \frac{2}{3} L_{sp} \frac{f_{st}}{E_{st}}}{L_{ub} + 2L_{sp}}$$

$$\varepsilon_{ps} = \frac{[h/2 - c]\theta}{L_{ups}} + \varepsilon_{pi}$$

where, L_p is plastic hinge length, θ_p is plastic rotation, ϕ_u is ultimate curvature, ϕ_y is yield curvature, L_{ub} is debonded length of the mild steel reinforcement, L_{ups} is debonded length of post-tensioning steel, ε_{pi} is initial stress of the post-tensioning steel, c is neutral axis depth, and θ is interface rotation. Figure 2.8 was used to calculate the mild steel strain (ε_{st}) in joint interface.

Figure 2.8.   A hybrid connection with imposed interface rotation of θ [2.9]

Utilizing the aforementioned expressions, strains in the extreme concrete compression fiber, mild steel reinforcement and post-tensioning steel may be evaluated at a given rotation θ at the connection interface for an assumed value for the neutral axis depth . From the estimated strain values, stresses in concrete, mild steel reinforcement and prestressing tendons and the corresponding forces can be determined using appropriate stress-strain behavior for the materials. At a given θ, the neutral axis depth is refined iteratively using the force equilibrium condition. After finalizing the neutral axis depth for the selected θ, the corresponding moment resistance can be readily established since the resultant forces and their location are known at the connection interface. A continuous monotonic moment-rotation envelope is established by repeating the procedures for different interface rotations.

Vernue [2.10], Vernu and Sritharan [2.11]

In this study, the authors improved the aforementioned monolithic beam analogy method by modifying the strain penetration term, expressing the stress-strain behavior of the post-tensioning tendons with Mattock's model [2.12] and providing an expression to compute the strain in compression mild steel. Accordingly, for interface rotation θ, following expressions were obtained:

$$\varepsilon_{st} = \frac{(d-c)\cdot\theta + \frac{2}{3}\cdot L_{sp}\frac{f_{st}}{E_s}}{L_{su} + 2\cdot L_{sp}}$$

$$\varepsilon_{pt} = \frac{\left(\frac{h}{2}-c\right)\cdot\theta}{L_{pu}} + \varepsilon_{pi}$$

$$\varepsilon_c = \left[\theta + \phi_e \cdot \left(L_p - \frac{4}{3} \cdot L_{sp} \right) \right] \cdot \frac{c}{L_p}$$

$$\varepsilon_{sc} = \frac{1}{2} \cdot \left[\frac{(c - d')}{c} \cdot \varepsilon_c + \varepsilon_{sy} \cdot \frac{M}{M_y} \right]$$

where, ε_{sc} is strain in compression mild steel, ϕ_e is elastic curvature, d' is distance from the compression mild steel reinforcement to the extreme compression fiber, ε_{sy} is yield strain of the mild steel reinforcement, M is moment resistance in the previous step of iteration procedure, and M_y is yield moment defined when the tension reinforcement reaches ε_{sy}. The rest of the parameters have been defined in the previous article.

By trial and error procedure, the neutral axis depth for a given rotation is established. Based on this neutral axis depth monotonic moment-rotation envelope is produced for a hybrid connection. This method was validated for hybrid connection by comparing with test results for connections samples M-P-Z4 and O-P-Z4, and PRESSS test building (Fig. 2.9).
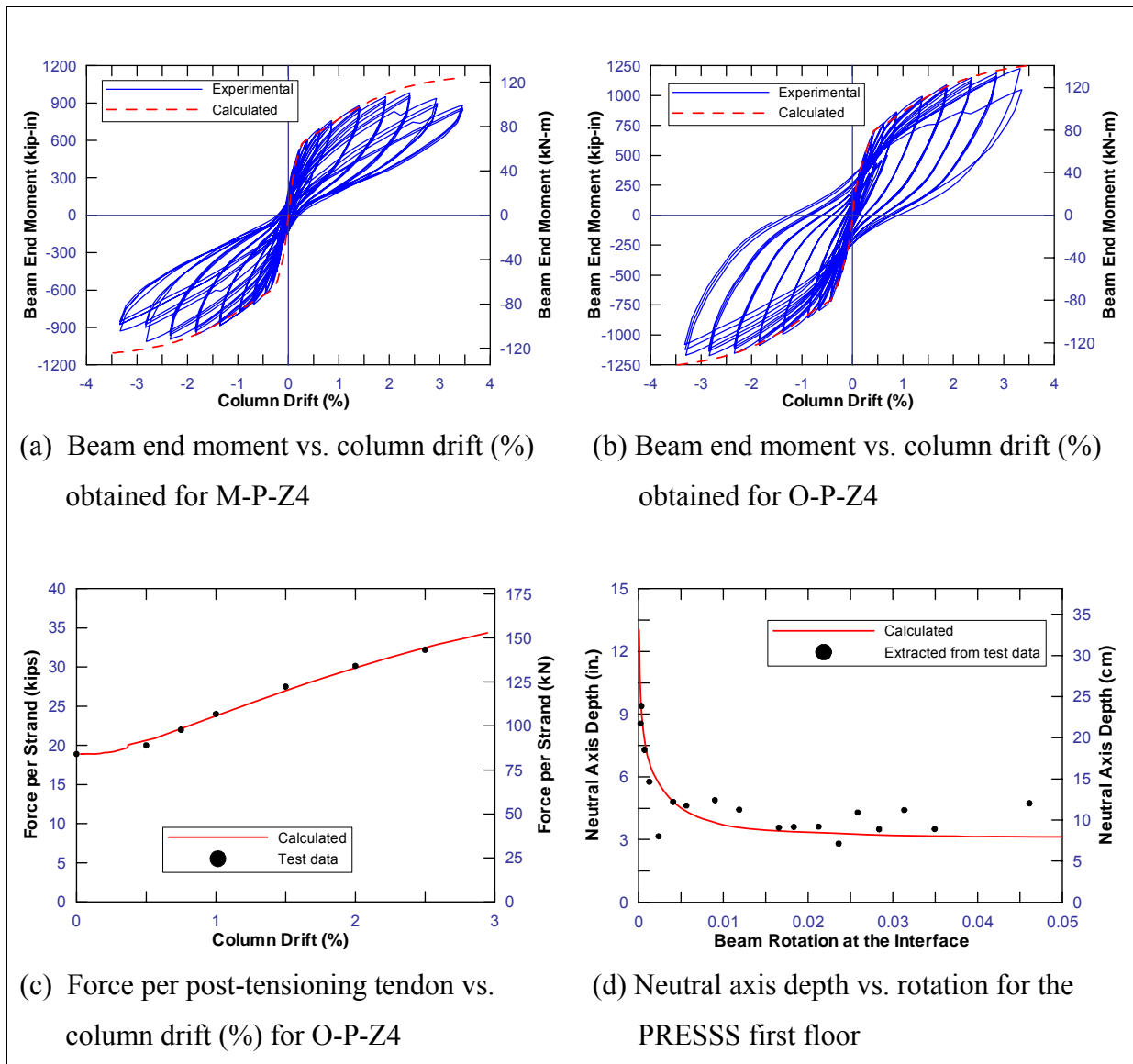
Figure 2.9.   A comparison of MBA analysis results with experimental data presented in Reference [2.11]

PRESSS Design Guidelines (2002) [2.13]

The PRESSS guidelines proposed by Stanton and Nakaki [2.13] provide design procedures

for hybrid beam-column connection for precast concrete structural systems, which were

included in the PRESSS test building. The guidelines use an iterative procedure to determine the neutral axis depth that satisfies the force equilibrium condition at the critical section.

Design Assumptions

The design assumptions considered in the PRESSS guidelines suggested for the unbonded frame systems with damping are as follows:

- The beams have constant cross section.

- The design forces and drifts are known.

- The post-tensioning tendons are totally unbonded over the entire length of the frame and anchored at the exterior faces of the end columns.

- The post-tensioning tendons are located at the mid-height of the beam section, which remain elastic until the frame reached the required design drift.

- The mild steel reinforcement is unbonded over a short distance at the beam-column interface.

- An equal amount of mild steel reinforcement is used at the top and bottom of the beam.

- Fiber reinforced grout pads are used at the interface between the precast concrete columns and beams.

Design Procedure

STEP 1 Establish material properties

The following material properties are established in this step: the beam concrete strength (f_c'), the interface grout strength (f_g'), a suitable value for corresponding β_1, the yield strength (f_{py}) and modulus of elasticity (E_p) of the prestressing steel, the yield strength of

the mild steel reinforcement (f_{sy}), over-strength factors for tension and compression reinforcement at the design limit state ($\lambda_{st,des}$ and $\lambda_{sc,des}$), and the maximum permissible strain in the mild steel reinforcement under cyclic loading ($\varepsilon_{st,\max}$).

STEP 2: Obtain design loads, drifts and required moment capacity of the connection

STEP 3: Estimate beam section dimensions

STEP 4: Calculate the stress change in the post-tensioning tendon between zero interface rotation and design interface rotation (Δf_{pt}) if the beam is rocked about its corner

$$\Delta f_{pt} = 0.5 \cdot E_p \cdot \theta_{des} \cdot \frac{h_g}{l_{pu}}$$

where θ_{des} is the interface rotation at the design limit state.

STEP 5: Estimate moments resisted by the post-tensioning tendons and mild steel reinforcement

The following moment distribution is suggested in the design procedure to maintain the re-centering capability of the frame.

$$M_{pt,des} \approx 0.55 \cdot M_{cap,des}$$

$$M_{st,des} = M_{cap,des} - M_{pt,des}$$

where $M_{pt,des}$ is the moment resistance provided by the post-tensioning tendons at the design drift, $M_{st,des}$ is the corresponding moment resisted by the tension mild steel reinforcement, and $M_{cap,des}$ is the moment capacity of the connection at the design drift.

STEP 6: Calculate area of the post-tensioning tendons (A_{pt})

$$A_{pt} = \frac{M_{pt,des}}{(0.45 \cdot h_g) \cdot f_{py}}$$

STEP 7: Calculate area of the mild steel reinforcement (A_s)

$$A_s = \frac{M_{st,des}}{(0.95 - \zeta) \cdot h_g \cdot \lambda_{st,des} \cdot f_{sy}}$$

where ζ is the distance from the compression mild steel reinforcement to the extreme compression fiber divided by h_g. $\lambda_{st,des}$ is taken as 1.35.

STEP 8: Estimate neutral axis depth

$$\eta_{des} = \frac{0.1}{\beta_1}$$

where η_{des} is the neutral axis depth divided by h_g, β_1 = ratio of depth of equivalent compressive stress block to neutral axis depth

STEP 9: Calculate stress in the tension mild steel reinforcement

$$f_{st,des} = \lambda_{st,des} \cdot f_{sy}$$

STEP 10: Calculate stress in the compression mild steel reinforcement

$$f_{sc,des} = \lambda_{sc,des} \cdot f_{sy}$$

$\lambda_{sc,des}$ is taken as 1.0.

STEP 11: Calculate stress in the post-tensioning tendons at θ_{des}

The stress in the post-tensioning tendons ($f_{pt,des}$) is obtained by considering the greater of the two results found from the following expressions,

$$f_{pt,des} = f_{py}$$

$$f_{pt,des} = f_{pi} + \Delta f_{pt}$$

where, f_{pi} is the initial (jacking) stress in the post-tensioning tendon after losses, Δf_{pt} is the

stress change in the post-tensioning tendon due to elongation as shown in Fig. 2.10.

(a) Displacements **(b)** Forces
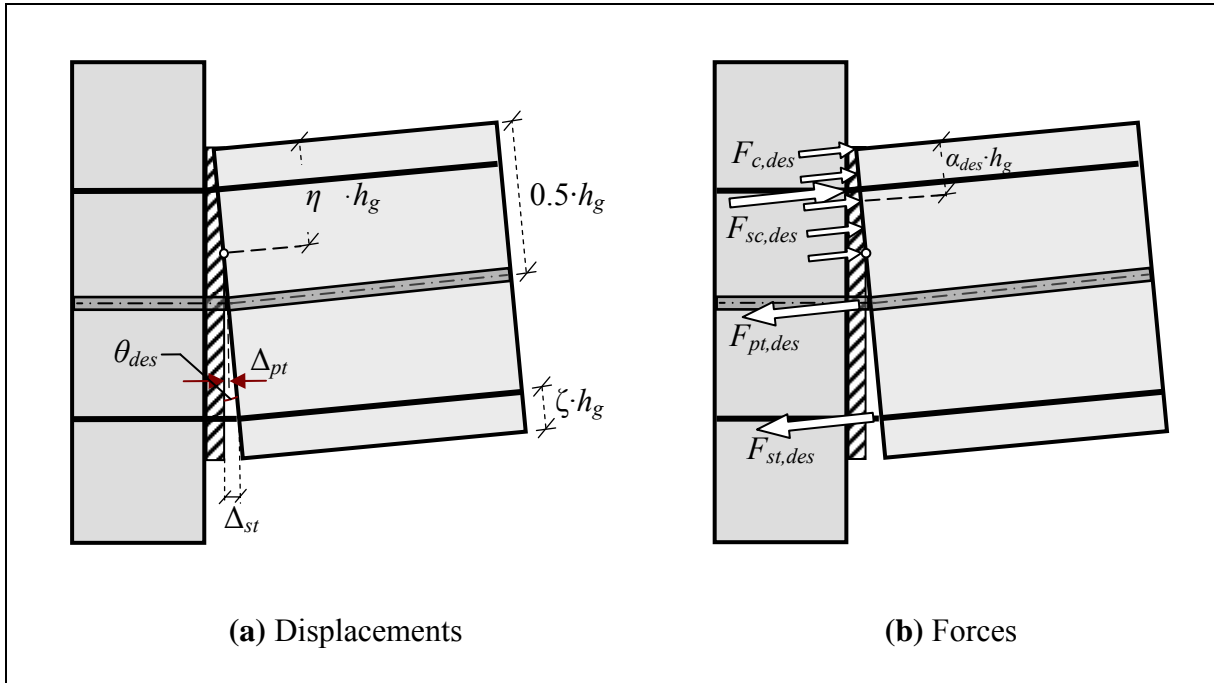
Figure 2.10.   A hybrid frame system at the design limit state [2.13]

STEP 12: Calculate resultant concrete compression force at θ_{des}

The forces in the post-tensioning tendons ($F_{pt,des}$), and the tension and compression mild

steel reinforcement ($F_{st,des}$ and $F_{sc,des}$) are:

$$F_{pt,des} = A_{pt} \cdot f_{pt,des}$$

$$F_{st,des} = A_s \cdot f_{st,des}$$

$$F_{sc,des} = A_s \cdot f_{sc,des}$$

The resultant concrete compression force ($F_{c,des}$) at the beam-column interface can be found using the section equilibrium condition. Hence,

$$F_{c,des} = F_{pt,des} + F_{st,des} - F_{sc,des}$$

STEP 13: Calculate locations of the resultant concrete compression force and the neutral axis depth

The depth of the rectangular stress block (a_{des}) based on Whitney equivalent rectangular stress concept is determined.

$$a_{des} = \frac{F_{c,des}}{0.85 \cdot f'_g \cdot b_g}$$

Therefore, the neutral axis depth is $\eta_{des} \cdot h_g$, where

$$\eta_{des} = \frac{a_{des}}{\beta_1 \cdot h_g}$$

Until the estimated and calculated neutral axis depth values converge, steps 8-13 are repeated.

STEP 14: Calculate moment resistance of the connection

$$M_{pt,des} = F_{pt,des} \cdot (0.5 - \alpha_{des}) \cdot h_g$$

$$M_{st,des} = F_{st,des} \cdot (1 - \alpha_{des} - \zeta) \cdot h_g$$

$$M_{sc,des} = F_{sc,des} \cdot (\alpha_{des} - \zeta) \cdot h_g$$

where α_{des} is the distance from the resultant concrete compression force to the extreme concrete compression fiber divided by h_g at the design drift, and $M_{sc,des}$ is the moment provided by the compression mild steel reinforcement. The total moment strength of the hybrid frame connection is

$$M_{cap,des} = M_{pt,des} + M_{st,des} + M_{sc,des}$$

The aforementioned moment strength must be greater than the moment demand at the design limit state. If this condition is not satisfied, the reinforcement quantities must be increased and the iteration process must be repeated starting from Step 6.

STEP 15: Check restoring properties of the beam

The resisting moments provided by the post-tensioning tendon ($M_{pt,0}$), and the tension and compression mild steel reinforcement ($M_{st,0}$ and $M_{sc,0}$) about the resultant concrete compression force at zero drift are:

$$M_{pt,0} = F_{pt,0} \cdot (0.5 - \alpha_0) \cdot h_g$$

$$M_{st,0} = F_{st,0} \cdot (1 - \alpha_0 - \zeta) \cdot h_g$$

$$M_{sc,0} = F_{sc,0} \cdot (\alpha_0 - \zeta) \cdot h_g$$

At zero drift, the moment provided by the prestressing is required to be greater than the sum of the moments provided by the forces in the tension and compression mild steel reinforcement. Hence, it is required that

$$M_{pt,0} \geq M_{st,0} + M_{sc,0}$$

If this condition is not satisfied, $\dfrac{M_{pt,des}}{M_{cap,des}}$ ratio must be increased in step 5 and the hybrid connection is re-designed to provide the system with an adequate restoring force.

STEP 16: Calculate the debonded length of the mild steel reinforcement

The strain in the mild steel reinforcement must be smaller than the maximum usable strain ($\varepsilon_{st,max}$) at the design drift, which is 0.04 for ASTM 706 bars. From Fig. 2.10,

$$\Delta_{st} = \theta_{des} \cdot \left(1 - \eta_{des} - \zeta\right) \cdot h_g$$

Provide the debonded length for the mild steel reinforcement such that

$$l_{su} \geq \frac{\Delta_{st}}{\varepsilon_{st,max}}$$

STEP 17: Check confinement requirement for the compression region

Following average compression strain over the plastic hinge length is suggested:

$$\varepsilon_c = \frac{\theta_{des} \cdot \left(\eta_{des} \cdot h_g\right)}{l_p} = \frac{\theta_{des}}{k_p}$$

where k_p is the plastic hinge length factor. In the absence of experimental data, k_p is recommended to be taken as 1.0.

Spalling of concrete is expected when the compression strain exceeds the ultimate strain of the unconfined concrete. Under this condition, it is recommended that the compression region should be confined so that concrete can sustain high strains. If spalling of unconfined cover concrete is expected, a reduced beam section equal to the confined core dimensions should be used in the design calculations.

Celik and Sritharan (2004) [2.14]

In this study, the authors improved the design methodology for hybrid beam-column connection in precast concrete structural system recommended by Stanton and Nakaki [2.13] known as PRESSS design guidelines as cited in the previous section. Improvement to the PRESSS design guidelines proposed by Celik and Sritharan [2.14] are presented below:

(i) Stress in Mild steel

In the PRESSS design guideline, stress in mild steel is not expressed as function of beam-column interface rotation θ, which is required for constructing a continuous monotonic moment-rotation envelope. The authors recommended the following expressions to calculate stress in mild steel as a function of beam-column interface rotation:

$$f_{st} = (1000 \cdot \theta) \cdot f_{sy} \qquad \text{for } 0 \leq \theta < 0.001$$

$$f_{st} = f_{sy} \qquad \text{for } 0.001 \leq \theta < 0.005$$

$$f_{st} = (0.84 + 34.4 \cdot \theta - 444.4 \cdot \theta^2) \cdot f_{sy} \qquad \text{for } 0.005 \leq \theta \leq 0.035$$

(ii) Equivalent Rectangular (Whitney) Stress Block

The grout placed at the beam-column interface is assumed to be reinforced with fibers to avoid premature crushing and spalling out of the joint according to the PRESSS guidelines. The fibers also increase the grout strength. Due to lack of adequate models in predicting the inelastic behavior of the grout, including the confinement effects, it is suggested that the grout should be designed to have strength (f'_g) greater than the concrete strength of the adjoining precast members. In addition, the effective concrete compressive strength is taken as $1.6 \cdot f'_c$ at the design drift after considering the confinement effect of concrete. Thus, the depth of the equivalent rectangular stress block in concrete is recommended to modify according to the following expression:

$$a = \frac{F_c}{0.85 \cdot (1.6 \cdot f'_c) \cdot b_g}$$

(iii) Neutral Axis Depth

The authors examined the capability of calculating the neutral axis depth according to PRESSS design guidelines (2002). It was found that this guideline resulted in increase of neutral axis depth with the elevation of beam-column interface rotation indicating the opposite trend observed in PRESSS test building. To alleviate this inconsistency, the authors utilized the analytical investigation conducted by Vernu [2.10] as shown in Fig. 2.11. To simplify the modified procedure, a tri-linear idealization was recommended for expressing neutral axis depth as a function of interface rotation. Figure 2.12 demonstrates this idealization, where point 1 corresponds to the beam height at 0 percent interface rotation, and points 2 and 3 are defined at interface rotations of 0.1 percent and 1.0 percent, respectively.
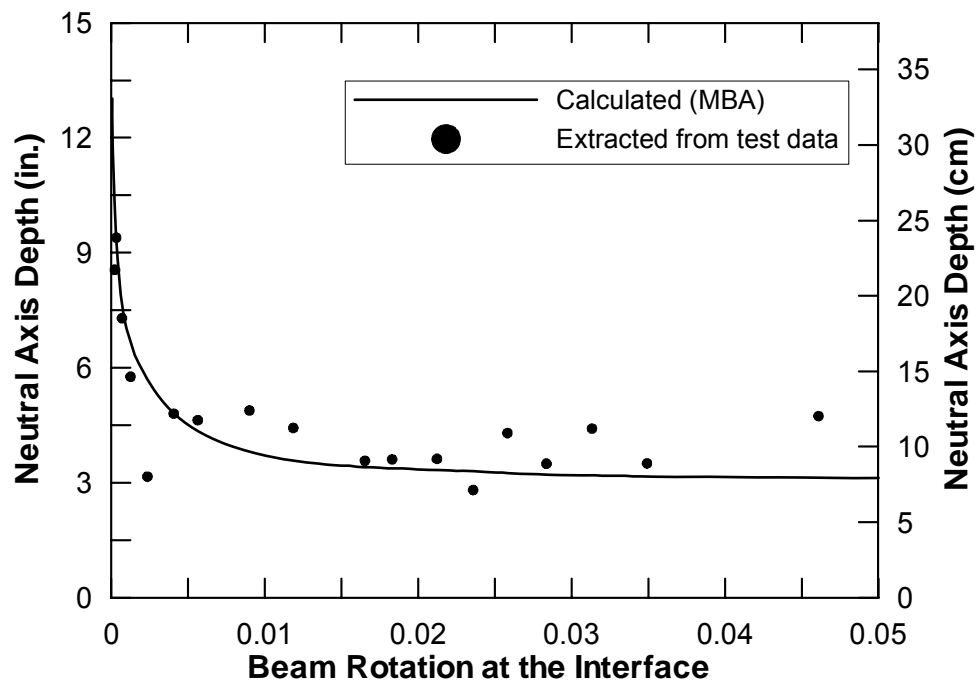
Figure 2.11.   Comparison of the neutral axis depth as a function of the interface rotation for the PRESSS first floor hybrid connection test results and calculated values according to Monolithic Beam Analogy (MBA) method [2.10]
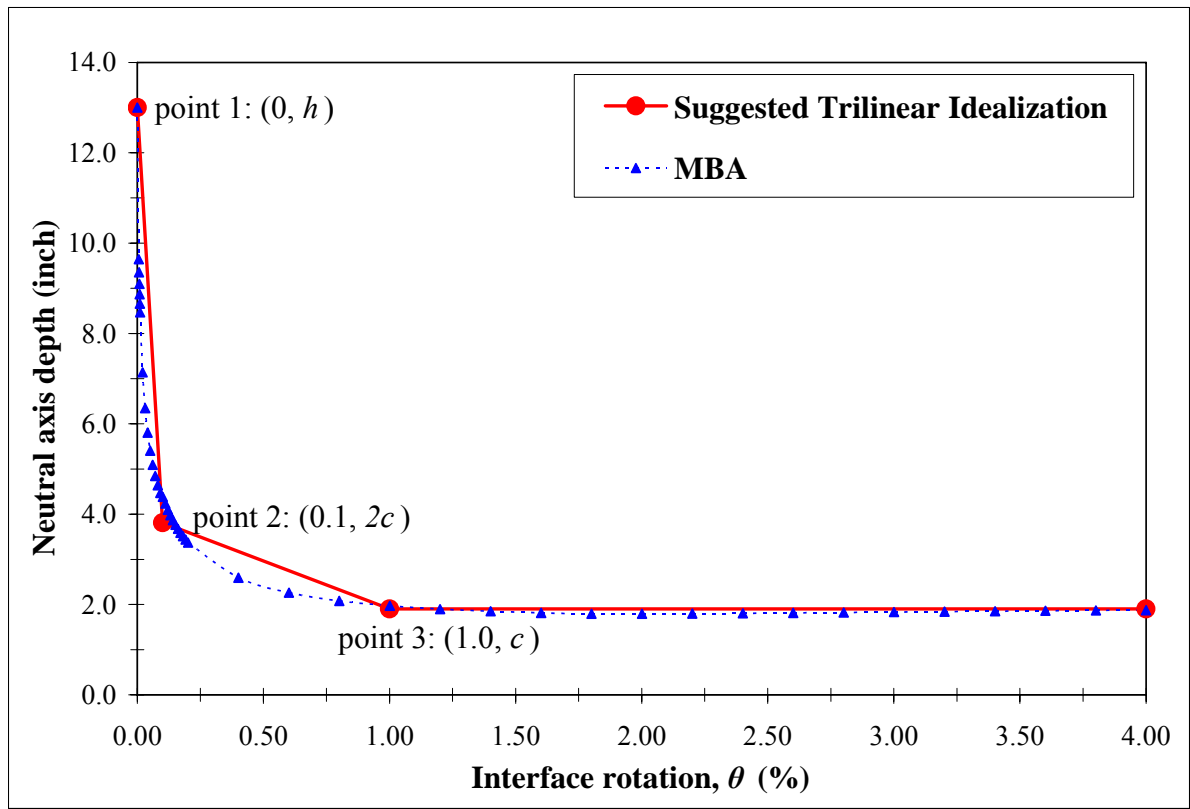
Figure 2.12.   Suggested trilinear idealization to improve the neutral axis depth representation in the modified PRESSS analysis procedure [2.14]

(iv) Stress in Post-Tensioning Tendons

The stress in post-tensioning tendon is calculated as per the following equation recommended in Mattock [2.12] for a given strain in the tendon found from the joint geometry. This modification is introduced to determine the prestressing stress more accurately. Figure 2.13 gives the graphical representation of Mattock's model.

$$f_{pt} = \varepsilon_{pt} \cdot E_p \cdot \left[0.020 + \frac{0.98}{\left[1 + \left(\frac{\varepsilon_{pt} \cdot E_p}{1.04 \cdot f_{py}} \right)^{8.36} \right]^{\frac{1}{8.36}}} \right]$$
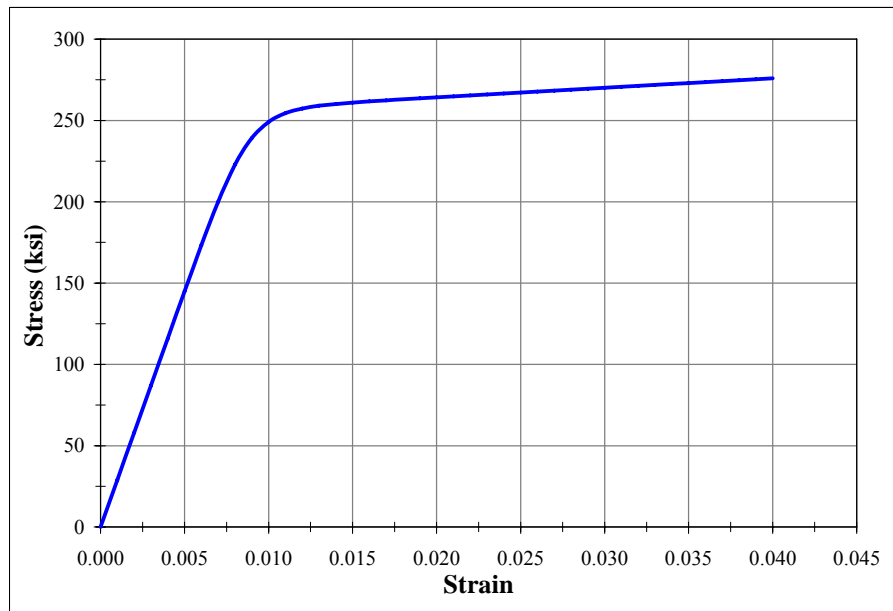
Figure 2.13.   Atheoretical stress-strain curve proposed for Grade 270 prestressing strands by Mattock [2.12]

(v) Decompression Point

The decompression point which defines the beginning of a crack opening at the connection interface and corresponds to the condition when the stress in the extreme concrete compression fiber reaches zero at the beam end adjacent to the column, was introduced in the modified PRESSS guidelines.

The authors also developed a computer program [2.14] capable to design and analyze hybrid beam-column connection in precast concrete structural system incorporating the aforementioned modifications in the PRESSS design guidelines [2.13].

2.3 Unbonded Post-Tensioned Precast Wall Systems

In consideration of the need for a non-emulative precast wall alternative, a concept for an unbonded post-tensioned precast concrete wall system was introduced. This was based on the concept suggested by Priestley and Tao [2.5] for precast building frames with the idea that the post-tensioning would provide an improved restoring force. Kurama et. al. [2.15-2.17] recently investigated this option for precast walls, which consists of separate panels stacked vertically. The behavioral and analytical findings of their study as well as their design recommendations are discussed in this section.

Kurama et al. [2.15-2.17]

Behavior and Analyses

To identify seismic performance, the author specified four states for the lateral force-displacement response of single unbonded post-tensioned precast wall system (Fig. 2.14). The *Decompression State* comes first, which is the point where gap opening is initiated at the horizontal joint between the base of the wall and the foundation. The next state is the *Softening State*. This state is identified by the beginning of a significant reduction in the lateral stiffness of the wall due to gap opening along the horizontal joints and non-linear behavior of the concrete in compression. The *Yielding State* is the third state, the point when the stain in the post-tensioning steel first reaches the limit of proportionality. In the *Failure*

State, flexural failure of the wall occurs, with the triggering of concrete crushing at the toe locations of the walls.

The authors concluded that self centering capability of the wall resulted from elastic behavior of the post-tensioning tendons. The nonlinear displacements occurred primarily due to gap opening along the horizontal joints. They recommended that a tri-linear curve can be used to represent the lateral load-displacement behavior of the unbonded post-tensioned wall by joining various wall states defined above. The unbonded post-tensioned wall exhibited larger displacements under seismic loading compared to normal monolithic concrete wall. An opposite trend was observed for residual displacement (Fig. 2.15).

The non-linear elastic behavior of the wall demonstrated very little inelastic energy dissipation resulting in a "slender" hysteresis (Fig. 2.16). Gap opening between the panels appeared to be smaller with the increase of initial prestressing. The base shear demands attained by analysis were found to be below those estimated by the design procedure. Therefore, the authors recommended that the method of calculating base shear developed for cast-in-place monolithic concrete walls can be applied to unbonded post-tensioned precast walls.
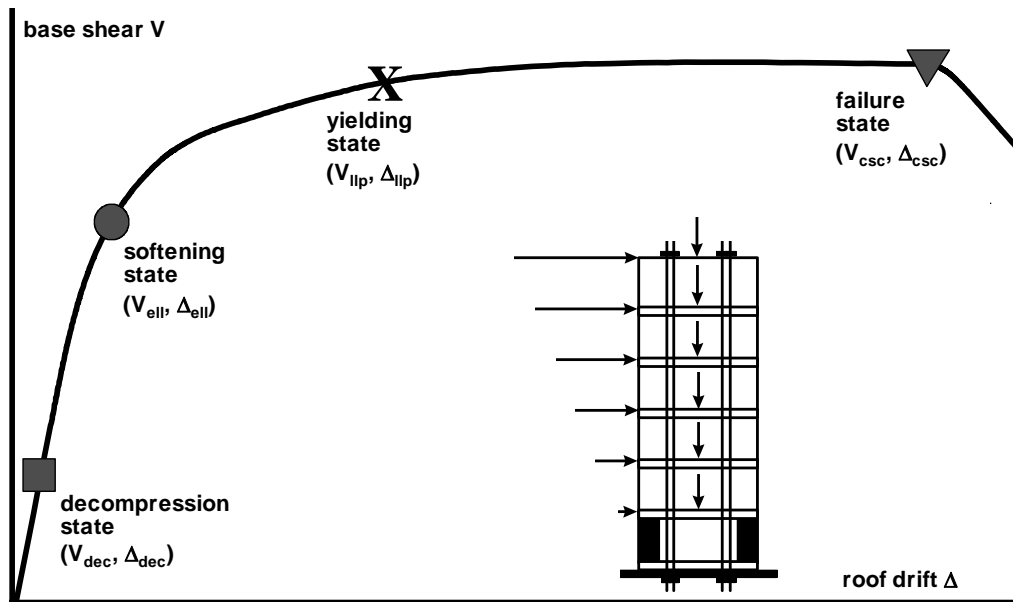
Figure 2.14.   Precast wall base shear-roof drift relationship [2.15,2.16]
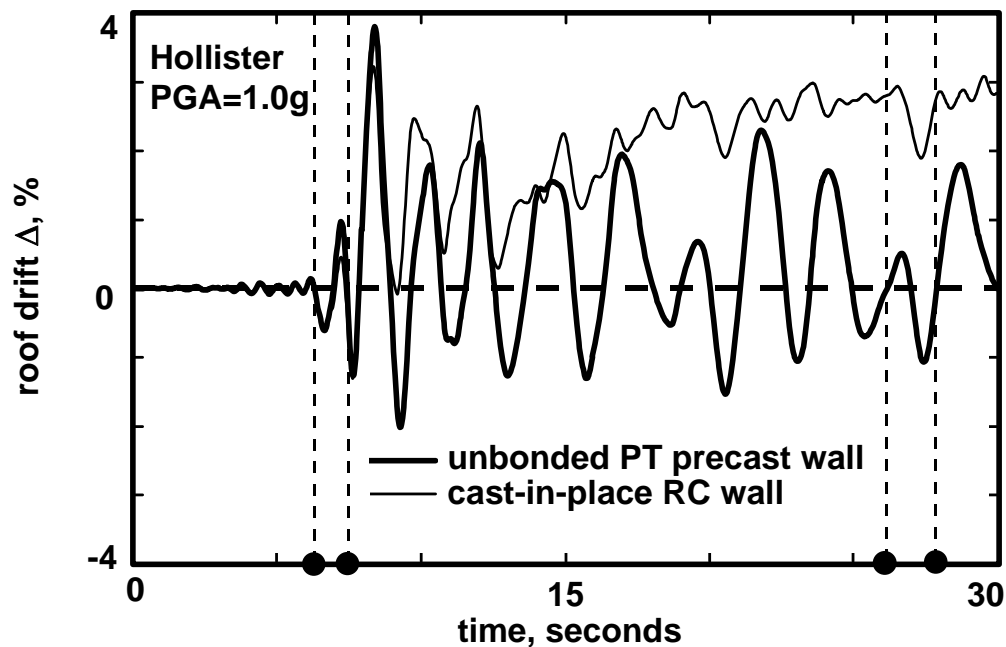
Figure 2.15.   Comparison of roof drifts obtained from dynamic analysis of walls [2.15,2.16]
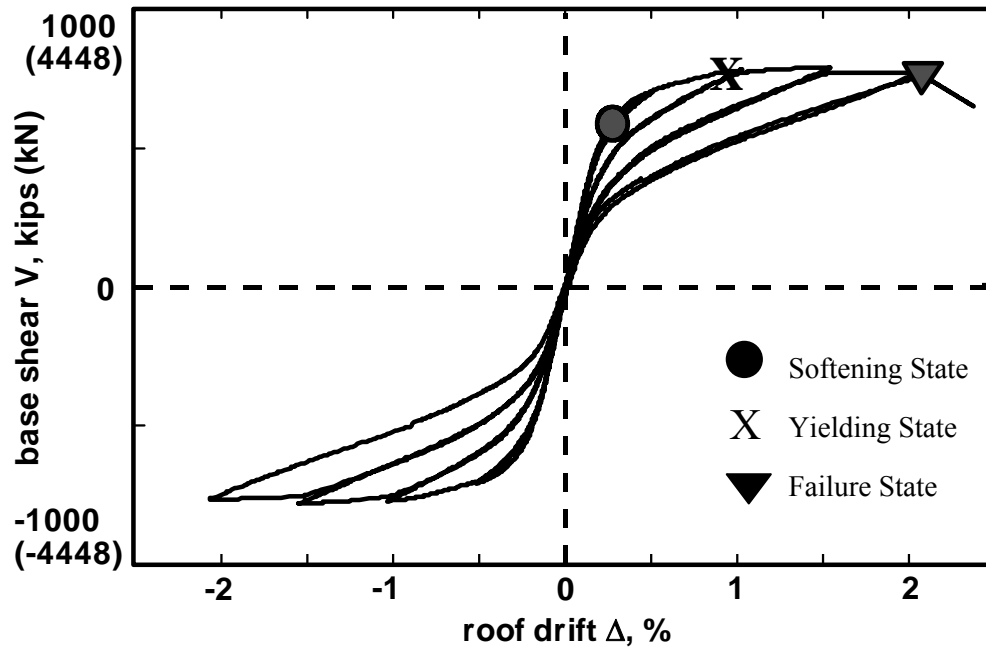
Figure 2.16.   Force displacement response of a precast wall under cyclic loading [2.15,2.16]

Precast Jointed Wall Systems

Researchers have investigated the use of unbonded post-tensioned precast jointed wall systems in buildings as the primary lateral load resisting elements in addition to the single wall systems. The connection between walls is constructed along the height of the wall. Energy dissipation and reduction of lateral drift are expected contribution from wall connectors. Research work on precast jointed wall systems found in literature is presented below.

Priestley et. al. [2.18]

The PRESSS test building included an unbonded post-tensioned precast wall system with UFP connectors along the vertical joint direction. In the wall direction of loading under the

design level earthquake, the wall experienced a peak recorded displacement of 8.3-in, just 8% below the target design displacement of 9-in. The wall experienced a maximum displacement of about 11.5-in. at an event 1.5 times the design level event. The base moment associated with this maximum displacement in the wall direction was approximately 100,000 kip-in with minor spalling in the cover concrete of the walls. During the entire wall direction testing no structural damage was observed.

Thomas and Sritharan [2.19, 2.20]

The authors used the Monolithic Beam Analogy to develop a methodology for analyzing the unbonded post-tensioned jointed precast wall system. A relation between extreme concrete fiber strain and the neutral axis depth (c), the base rotation (θ) has been established by setting the total displacement of jointed precast wall equal to the total displacement of equivalent monolithic wall.

$$\theta = (\phi_u - \phi_e)L_p = \left(\frac{\varepsilon_{c,ext}}{c} - \phi_e\right)L_p$$

where $\varepsilon_{c,ext}$ is the extreme fiber concrete strain and L_p is the plastic hinge length.

The authors found that the plastic hinge length (L_p) of $0.06h_w$ gave good prediction of the observed base moment vs. lateral displacement response for the PRESSS test building. Thus, the following expression was obtained,

$$\varepsilon_{c,ext} = c\left(\frac{\theta}{0.06h_w} + \phi_e\right) \qquad \text{where } \phi_e = \frac{M}{E_c I_{eff}}.$$

The analysis procedure suggested by the authors is summarized below.

Step 1: Define wall dimensions and material properties including yield strength of post-tensioning steel (f_{py}), concrete strength (f_c'), concrete density (γ_c), modulus of elasticity for

post-tensioning steel (E_p), area of post-tensioning steel (A_p), initial post-tensioning force (P_0), height of wall (h_w), length of wall panel (l_w), thickness of wall (t_w), connector force-displacement relationship, and number of panels (n).

Stpe 2: Calculate wall moment capacity at the decompression point: $M_{decomp} = \dfrac{(P_0 + W)I}{0.5 t_w l_w l_w}$

where *I* is the gross moment of inertia of the wall.

Step 3: Select base rotation (θ).

Step 4: Assume a neutral axis depth (c) for the selected rotation.

Step 5: Determine the forces at the base rotation (θ) and neutral axis depth (c) ensuring that equilibrium is met.

- Find the tendon elongation: $\Delta_p = \left(\dfrac{l_w}{2} - c\right)\theta$

- Find the increase in tendon stress: $\Delta f_p = E_p \dfrac{\Delta_p}{h_w}$

- Find the total post-tensioning force (P) and the total tension force (N) under the current base rotation and assumed neutral axis depth:

$$P = \Delta f_p A_p + P_0$$

$$N = P + W$$

Step 6: Using a force versus vertical displacement curve determine the force contribution of the connectors (F_{sco}). The compressive force (C) can be determined from the equilibrium condition of the wall panel in the vertical direction:

$C = N + F_{sc}$, for leading wall

$C = N - F_{sc}$, for trailing wall

$F_{sc} = N_{con} F_{sco}$, where N_{con} is total number of connectors in a vertical joint

Step 7: Determine the extreme fiber concrete strain for the assumed neutral axis depth (c):

$$\varepsilon_{c,ext} = c\left(\frac{\theta}{0.06h_w} + \frac{M}{E_c I_{eff}}\right)$$

where, *M* is the base moment resistance of the wall panel, E_c is the modulus of elasticity of concrete and I_{eff} is the effective moment of inertia of the wall.

Step 8: Calculate the compression force and its location utilizing the confinement model suggested by Mander et al. [2.21]. If the confined compressive force (C_{conf}) is not equal to the compressive force established by equilibrium (C), then the neutral axis depth is increased and steps 5 through 7 must be repeated until the two forces converge.

Step 9: Calculate the resisting moment of the wall panel by taking moment about the corner of the each wall panel utilizing the distance (y) from the edge of the wall to the resultant compression force.

$$M_{cap,panal1} = C(l_w - y) - 0.5Nl_w$$

$$M_{cap,panal1} = -C(y) + 0.5Nl_w$$

Step 10: compute the total moment capacity of wall system:

$$M_{cap,wall} = M_{cap,panal1} + M_{cap,panal2}$$

Sritharan et al. [2.22] and Aaleti [2.23]

The authors developed a simplified procedure for seismic design and monotonic analysis of precast post-tensioned jointed walls. The following assumptions, consistent with suggestions of Stanton and Nakaki [2.13], were considered for the design of jointed precast wall systems:

- The wall will undergo in-plane deformations only. Torsion and out-of-plane deformations are prevented by providing adequate out-of-plane bracing.

- All individual walls are assumed to have identical dimensions, reinforcement details, and the initial prestressing force.

- All the vertical joints contain an equal number of identical connectors, and a dependable force vs. displacement response envelope is available for the connector.

- All walls undergo the same lateral displacement at the floor and roof levels due to the rigid floor assumption.

- The post-tensioning steel is located at the center of each wall.

- The strength of fiber grout that is typically placed between the wall base and foundation is greater than the strength of concrete in the walls.

- The post-tensioning steel reaches the yield strain at the design drift. The corresponding rotation at the wall base is assumed to be θ_{design}, which may be taken as 2%.

The following seven steps are recommended for the design of the jointed wall systems.

Step 1: Material Properties and Wall Dimensions

- Establish the following material properties

  Prestressing steel: Modulus of elasticity (E_p) and yield strength (f_{py}).

  Concrete: Unconfined concrete strength (f_c'), elastic modulus of concrete (E_c), and appropriate coefficient of friction between the precast wall base and foundation (μ).

  Connector: Force vs. displacement response envelope.

- Establish the wall dimensions

Select the total length of the wall system (L_s) or length of a single wall (L_w), wall height (H_w), wall thickness (t_w), and the number of walls (n).

When deciding the number of walls in each system, use the smallest possible value for n with a suitable H_w/L_w ratio. Stanton and Nakaki (2002) suggest that H_w/L_w should be more than 2.0 to ensure flexural dominant behavior for the wall. If the length of each wall or the total length of the wall system is known, the other variable can be determined with following expression.

$$L_w = \frac{L_s}{n}$$

Guidance to determine an initial value for the wall thickness:

1. Select a value in the range of $h_{story}/16$ to $h_{story}/25$, where h_{story} is the story height [2.24].

2. The wall thickness should be sufficient to limit the shear stress in the wall to the permissible limit specified in code (e.g., ACI 318-05 2005).

3. The wall thickness should be sufficient to accommodate the required confinement reinforcement at the wall ends.

Step 2: Design Moment Resistance

Establish the base moment resistance for the wall system (M_{design}). Hence, the precast wall system should be designed such that $\phi M_n \geq M_{design}$

where ϕ is the flexural strength reduction factor and M_n is the nominal moment capacity of the wall system at the design drift.

Step 3: Force Resisted by the Connector

- Estimate the force in the connector (F_{con}) at the design drift from the force-displacement envelope curve available for the connector with an assumption that vertical relative displacement between the walls is $0.9L_w\theta_{design}$.

- The number of connectors should be determined such that a desired level of equivalent damping is incorporated in the wall system. For UFP connectors, the required number of connectors may be established as given below, to ensure that the wall system would have a desired level equivalent damping [2.25].

$$N_{con} = \frac{\pi\zeta_{eq}M_n}{1.25(n-1)F_{con}L_w}$$

where N_{con} is the number of connectors in each vertical joint between the precast walls and ζ_{eq} is the required level of equivalent viscous damping.

Step4: Calculate Area of the Post-tensioning Steel

- The design moment for the wall that would provide the largest moment resistance can be determined with the following expressions.

$$M_{design,wall} = \Omega\frac{M_{design}}{n\phi} \; ; \quad \Omega = 1 + \frac{\lambda\phi N_{con}F_{con}L_w}{M_{design}}$$

where Ω is the moment contribution factor and λ is a constant. When $n = 2$, $\lambda = 0.9$ and $M_{design,wall}$ will correspond to the moment demand in the leading wall (i.e., $M_{design,lead}$). When $n \geq 3$, $\lambda = 1.04$ and the $M_{design,wall}$ will correspond to the moment in an intermediate wall (i.e., $M_{design,inter}$).

- Find the area of the post-tensioning steel (A_p) in a jointed wall system of two walls using the expression developed based on moment equilibrium of forces acting on the base of the leading wall as given below (Fig. 2.17).
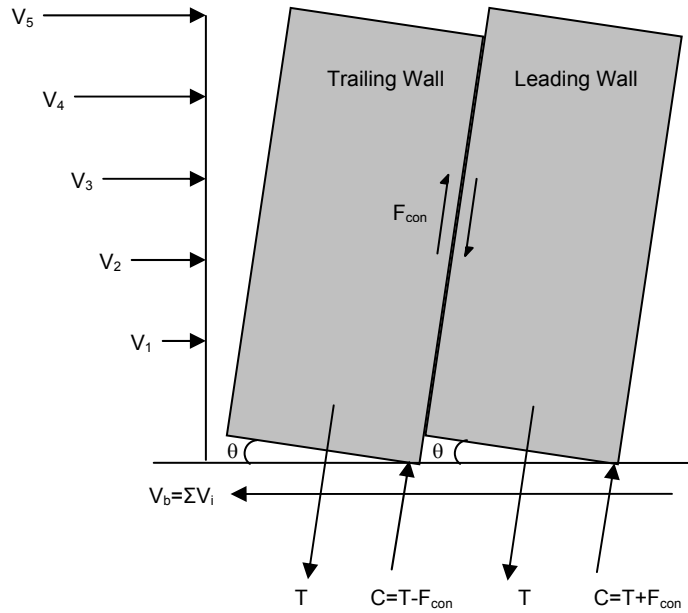
Figure 2.17.　　Forces acting on a jointed two-wall system at base rotation θ (C = resultant compressive force and T = P_D + force in the prestressing tendon) [2.22, 2.23]

$$M_{design,lead} = \left(P_D + 0.95f_{py}A_p\right) * \left(\frac{L_w}{2} - \frac{P_D + 0.95f_{py}A_p + N_{con}F_{con}}{2*(\alpha.f_{cc}^{'})t_w}\right)$$
$$+ N_{con}F_{con} * \left(L_w - \frac{P_D + 0.95f_{py}A_p + N_{con}F_{con}}{2*(\alpha.f_{cc}^{'})t_w}\right)$$

where P_D, the summation of the wall self weight and superimposed live load, is equated to ($\gamma_c L_w t_w H_w + W_{floor} L_w$), γ_c is the unit weight of concrete, W_{floor} is the distributed superimposed live load at the base of wall from all floors, $0.95f_{py}$ represents the expected stress in the post-tensioning steel in the critical wall at the design drift, and $\alpha.f_{cc}^{'}$ approximates the expected confined concrete strength of the equivalent rectangular stress block with $f_{cc}^{'}$ representing the strength of the confined concrete. The value of α may be obtained as follows.

$$\alpha = \frac{2*r*\left(0.98 - 0.0022 * f_c^{'}\right)}{r - 1 + 2^r}$$

where $\qquad r = 1.24 + 0.01*\left(\dfrac{f_c^{'} - 4.0}{0.25}\right)$
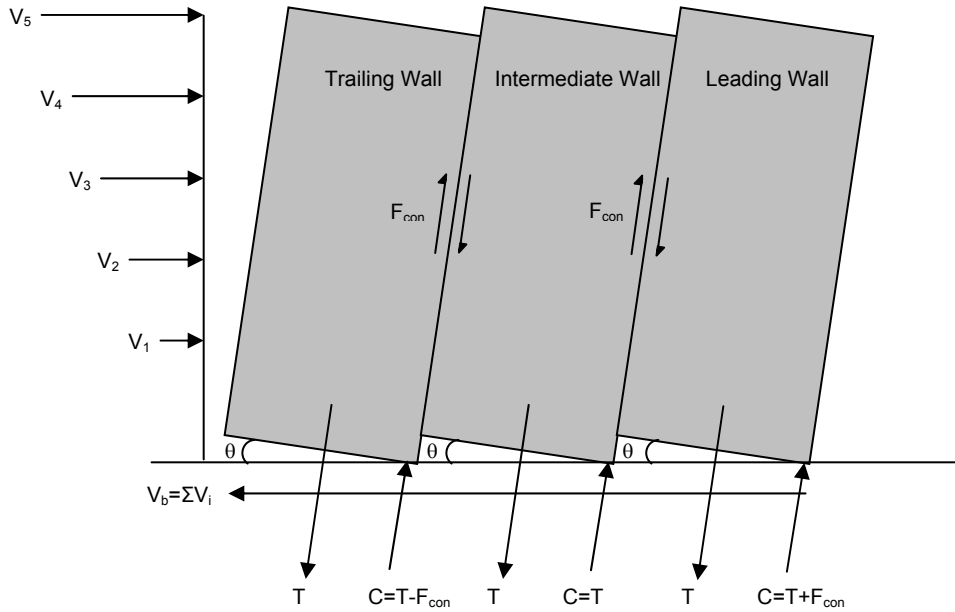
Figure 2.18.   Forces acting on a jointed three-wall system at base rotation θ (C = resultant compressive force and $T = P_D +$ force in the prestressing tendon) [2.22, 2.23]

- For a multi-wall system with $n \geq 3$ (Fig. 2.18), the required area of the post-tensioning steel is established using the moment equilibrium of the forces acting at the base of an intermediate wall,

$$M_{design,inter} = \left(P_D + 0.95 f_{py} A_p\right)*\left(\frac{L_w}{2} - \frac{P_D + 0.95 f_{py} A_p}{2*(\alpha.f_{cc}^{'})t_w}\right) + N_{con}F_{con}L_w$$

The connector forces acting on both sides of an intermediate wall are assumed to be the same.

Step 5: Design the Initial Stress for the Post-tensioning Steel

- Estimate the neutral axis depth at the base of the trailing wall at the design drift.

$$c_{design,trail} = \frac{P_D + f_{py} A_p - N_{con} F_{con}}{\beta * (\alpha . f_{cc}^{'}) t_w}$$

where the value of β can be approximated to 0.96.

- Assuming that the post-tensioning steel reaches the yield limit state in the trailing wall at the design drift, the initial stress in the post-tensioning steel is established,

$$f_{pi} = f_{py} - \frac{(0.5 L_w - c_{design,trail}) \theta_{design} E_p}{H_w}$$

Step 6: Estimate the Moment Capacity

The connector details, area of the post-tensioning steel and initial prestress designed in the previous steps may be used in all walls in the jointed system instead of designing the walls individually. With the help of a suitable analysis procedure [e.g., 2.19, 2.22 and 2.23] calculate the total base moment resistance of the jointed wall system to verify that $\phi M_n \geq M_{design}$ condition is fulfilled. The proposed design method is expected to adequately satisfy $\phi M_n \geq M_{design}$. However, wall dimensions may be modified in order to satisfy the condition $\phi M_n \geq M_{design}$.

Step 7: Design of Confinement Reinforcement

By observing the test results of the PRESSS building and identifying that the leading wall would face the maximum resultant compressive force at the base, the following expression has been suggested for estimating the maximum concrete strain demand in the compressive regions of the wall toes [2.21].

$$\varepsilon_{conc} = c_{max,lead} \left(\frac{M_{max,lead}}{E_c I_{gross}} + \frac{\theta_{max}}{0.06 H_w} \right)$$

where $M_{max,lead}$ is the base moment resistance of the leading wall at the maximum expected drift, the corresponding base rotation is θ_{max}, which may be taken as $1.5*\theta_{design}$, I_{gross} is the gross moment of inertia of the wall and is equal to $\dfrac{t_w L_w^3}{12}$, and $c_{max,lead}$ is the neutral axis depth at the base of the leading wall at θ_{max}. The value of $c_{max,lead}$ may be established as part of the analysis of the wall system in Step 6. Following an estimate for ε_{conc}, quantify the required amount of confinement reinforcement in the wall toes using an appropriate confinement model [26].

The shear resistance at the base of the wall should be ensured using a shear friction mechanism. If an interface material such as grout is placed between the precast walls and foundation, this should be reflected in the value of μ. Since the stress in the post-tensioning steel and the connector force increase with drift, it will be necessary to perform this check at both θ_{design} and θ_{max}.

2.4 REFERENCES

2.1   Nakaki, S. D., Englekirk, R. E., and Plaehn, J. L.,"Ductile Connectors for Precast Concrete Frame," *PCI Journal*, 1994, Vol. 39, No. 5, pp. 46-59.

2.2   Cheok, G. S., and Lew, H. S., "Performance of Precast Concrete Beam-to-Column Connections Subject to Cyclic Loading," *PCI Journal,* 1991, Vol. 36, No. 3, pp. 56-67.

2.3   *International Conference of Building Officials*. Uniform Building Code, Whittier, CA, 1985.

2.4   Cheok, G. S., and Lew, H. S., "Model Precast Concrete Beam-to-Column Connections Subject to Cyclic Loading," *PCI Journal*, 1993, Vol. 38, No. 3, pp. 80-92.

2.5   Priestley, M. J. N., and Tao, J. T., "Seismic Response of Precast Prestressed Concrete Frames with Partially Debonded Tendons," *PCI Journal*, 1993, Vol. 38, No. 1, pp. 58-69.

2.6   Stone, W. C., Cheok, G. S., and Stanton, J. F., "Performance of Hybrid Moment-Resisting Precast Beam-Column Concrete Connections Subjected to Cyclic Loading," *ACI Structural Journal*, 1995, Vol. 92, No. 2., pp. 229-249.

2.7   Stanton, J., Stone, W. C., and Cheok, G. S., "A Hybrid Reinforced Precast Frame for Seismic Regions," *PCI Journal*, 1997, Vol. 42, No. 2, pp. 20-32.

2.8   Englekirk, R. E., "An Analytical Approach to Establishing the Seismic Resistance Available in Precast Concrete Frame Structures," *PCI Journal*, 1989, Vol. 34, No. 1, pp. 92-101

2.9   Pampanin, S., Priestley, M. J. N., and Sritharan, S., "Analytical Modeling of Seismic Behavior of Precast Concrete ductile Frame Connection," *Journal of Earthquake Engineering*, 2001, Vol. 5, No. 3, pp. 329-367.

2.10 Vernu, S., "Connection and structural level analysis of precast hybrid frame systems," *M.S. Thesis,* Iowa State University, Ames, Iowa, 2003.

2.11 Sritharan, S., and Vernu, S., "Analysis and Design of Precast Hybrid Frames," *Proceedings of the Pacific Conference on Earthquake Engineering*, Paper No. 024, Christchurch, New Zealand, 2003.

2.12 Mattock, A. H., "Flexural Strength of Prestressed Concrete Sections by Programmable Calculator," *PCI Journal*, Vol. 24, No. 1, 1979, pp. 26-37.

2.13 Stanton, J. F. and Nakaki, S. D., "Design Guidelines For Precast Concrete Seismic Structural Systems," *PRESSS Report No. 01/03-09, UW Report No. SM 02-02*, The University of Washington and The Nakaki Bashaw Group, Inc., 2002.

2.14 Celik, O., and Sritharan, S., "An Evaluation of Seismic Design Guidelines Proposed for Precast Hybrid Frame Systems," ISU-ERI-Ames Report ERI-04425, Iowa State University, Ames, Iowa, USA, 2004.

2.15 Kurama, Y., Pessiki, S., Sause, R., and Lu, L., "Seismic Behavior and Design of Unbonded Post-Tensioned Precast Concrete Walls," *PCI Journal*, 1999, Vol. 44, No. 3.

2.16 Kurama, Y., Pessiki, S., Sause, R., and Lu, L., "Lateral Load Behavior and Seismic Design of Unbonded Post-Tensioned Precast Concrete Walls, *ACI Structural Journal,* July-Aug. 1999, Vol. 96, No. 4, pp. 622-632.

2.17 Kurama, Y., Pessiki, S., Sause, R., and Lu, L., "Seismic Response Evaluation of Unbonded Post-Tensioned Precast Walls," *ACI Structural Journal,* September-October 2002, Vol. 99, No. 5, pp. 641-651.

2.18 Priestley, M. J. N., Sritharan, S., Conley, J.R., and Pampanin, S., Preliminary Results and Conclusions from the PRESSS Five-Story Precast Concrete Test Building, *PCI Journal,* Nov-Dec. 1999.

2.19 Thomas, D., J., Analysis and Validation of a Seismic Design Method Proposed for Precast Jointed Wall Systems, *M.S. Thesis*, Department of Civil, Construction and Environmental Engineering, Iowa State University, Ames, Iowa, USA, 2003.

2.20 Thomas, D., J., and Sritharan, S., An Evaluation of Seismic Design Guidelines Proposed for Precast Jointed Wall Systems, ISU-ERI-Ames Report ERI-04635, Iowa State University, Ames, Iowa, USA, June 2004.

2.21 Mander, J. B., Priestly, M. J. N., and Park, R., "Theoretical Stress-Strain Model for Confined Concrete," *Journal of Structural Engineering*, August 1998, Vol. 114, No. 8.

2.22 Sritharan, S., Aaleti, D., and Thomas, D. J., Seismic Analysis and Design of Precast Concrete Jointed Wall Systems, ISU-ERI-Ames Report ERI-04643, Iowa State University, Ames, Iowa, USA, October 2006 (submitted to PCI).

2.23 Aaleti, S., Design and analysis of unbonded post-tensioned precast wall systems, *M.S. Thesis,* Department of Civil, Construction and Environmental Engineering, Iowa State University, Ames, Iowa, USA, 2005.

2.24 Englekirk, R. E., Seismic Design of Reinforced and Precast Concrete Buildings, John Wiley and Sons, Inc., New Jersey, USA, 2003.

2.25 Galusha, J.G., Precast, Post-Tensioned Concrete Walls Designed to Rock, M.Sc. Thesis, Department of Civil Engineering, University of Washington, 1999.

CHAPTER 3. A PERFORMANCE-BASED SEISMIC EVALUATION OF TWO FIVE-STORY PRECAST CONCRETE HYBRID FRAME BUILDINGS

A paper accepted in *ASCE Structure Journal*

M. Ataur Rahman[1] and Sri Sritharan[2]

ABSTRACT

The unique features of the hybrid frame, which include minimum structural damage when subjected to earthquake loading and the re-centering capability, are the result of using a combination of mild steel reinforcement and unbonded prestressing to establish connections between precast beams and precast columns. Using acceptance criteria defined in terms of inter-story frame drift and floor acceleration, this paper presents a multiple-level performance-based seismic evaluation for two five-story precast concrete hybrid frame buildings. The design and analysis of these two buildings, established as the displacement-based and force-based design solutions for a prototype building used in the PREcast Seismic Structural System (PRESSS) program, were conducted at 60 percent scale so that the analysis models could be validated using the PRESSS test data. Despite a difference of 40 percent in the design base shear, the two buildings satisfied the acceptance criteria when subjected to input motions with intensities less than or equal to that of the design-level earthquake. For

[1]PhD Candidate, Department of Civil, Construction and Environmental Engineering, e-mail: ataur70@iastate.edu, Iowa State University, Ames, IA 50011, USA
[2]Associate Professor, Department of Civil, Construction and Environmental Engineering, e-mail: sri@iastate.edu, tel.: 515-294-5238, fax: 515-294-7424, Iowa State University, Ames, IA 50011, USA

input motions, equal to 150 percent of the design-level earthquake, the building designed using the displacement-based principles did not satisfy the inter-story drift limit, whereas the force-based solution provided acceptable performance.

3.1 INTRODUCTION

3.1.1 Framing Concept

The hybrid framing concept is used to construct moment-resisting frames from single-bay precast concrete beams and multi-story high precast concrete columns. Figure 3.1(a) shows typical details of a hybrid frame, in which the beams and column are connected using unbonded post-tensioning tendons (PT) and mild steel (MS) reinforcement across the precast interfaces at the mid-height and closer to the top and bottom surfaces of the beams, respectively. Prior to post-tensioning, the spaces between the edge of precast beam and column surfaces along the vertical plane in the beam column connection regions called precast interfaces, and ducts housing the mild steel reinforcement are filled with non-shrink cementituous fiber grout. The grout at the above mentioned interfaces ensures continuity between precast members while grouting of the ducts enables the reinforcement to contribute to the stiffness, strength and hysteretic energy dissipation of the hybrid frames. The mild steel reinforcing bars are debonded over a short length near the interfaces to reduce the inelastic strain accumulation and avoid premature fracture of the reinforcement. A friction mechanism is relied upon for shear transfer across the precast connection interface. The combination of using mild steel and prestressing steel to provide moment resistance at the precast connections reduces the hysteresis energy dissipating ability of the hybrid frame when compared to a monolithic concrete frame connection designed to resist the same moment (Stone et al. 1995; Stanton et al. 1997).

The hybrid frame studies during the past decade include experimental verification using component (Stone et al. 1995; Stanton et al. 1997) and structure level testing (Priestley et al. 1999; Pampanin et al. 2000; Sritharan 2002). More recently, the hybrid frame has been implemented in a few buildings, including a 39-story apartment complex in San Francisco, California (Englekirk 2002).

3.1.2 Benefits

The use of unbonded steel reinforcement at the interfaces between columns and beams assist with concentrating most of the flexural and inelastic actions at the beam ends. Consequently, the beams undergo minimal structural damage and experience only limited cracking when the hybrid frame is subjected to inelastic lateral deformations, which has been witnessed experimentally (Stone et al. 1995; Stanton et al. 1997; Priestley et al. 1999; Sritharan 2002). Furthermore, nonlinear elastic response from the unbonded post-tensioning tendons and hysteretic behavior from the mild steel reinforcement will enable the hybrid frames to dissipate energy and minimize residual displacements. The post-tensioning tendons that run across the column width reduce the principal tensile stresses in the beam-to-column joints. The reduction to the principal tensile stress suggests that the amount of joint shear reinforcement could be reduced when compared to the joints in equivalent monolithic concrete frames (Sritharan and Ingham 2003).

3.2 HYBRID FRAME BUILDINGS

Two precast hybrid frame buildings were chosen for the analytical investigation reported in this paper, with an objective of examining the consequences of using force-based and direct displacement-based design methods for the design of low-rise hybrid frame within a

performance-based framework. The two hybrid frame buildings represented 50% of the prototype building, shown in Fig. 3.1(b), at 60 percent scale. Therefore, only two of the four bays in the prototype seismic frames were included in the hybrid frame buildings. These modifications to the prototype building configuration were consistent with the procedures used to create the PRESSS test building that was subjected to rigorous seismic testing (Nakaki et al. 1999; Priestley et al. 1999; Sritharan 2002). With these changes, the ratios of member dimension, member force, base shear, mass, stress, acceleration and time were taken as 0.6, 0.6^2, 0.5×0.6^2, 0.5×0.6^3, 1.0, 0.6^{-1} and 0.6 between the building models and the prototype structure (Collins 1999; Conley et al. 2002; Sritharan et al. 2002).

Figure 3.2 shows the typical floor plan and elevation view of the hybrid frame in the two hybrid buildings, which consisted of two identical seismic frames in one direction and a precast wall system in the orthogonal direction as the primary lateral load resisting systems. The analytical investigation was performed for these buildings in the frame direction of response. The PRESSS building used the same configuration, but with four different precast frame connections including hybrid connections in the lower three floors and pretensioned connections in the upper two floors of a seismic frame.

The first hybrid frame building, referred to as HFB1, was dimensioned and detailed using a direct displacement-based design (DBD) method that was adopted in the design of the PRESSS building (Collins 1999; Priestley 2002; Sritharan et al. 2002). In the DBD method, the buildings are designed for a target displacement using effective periods of their fundamental mode of response. By representing the hysteretic action in terms of equivalent viscous damping, the effective periods are established using appropriate displacement design

spectra. The effective mass for the fundamental mode, which is determined by assuming a displacement profile, and the effective period are used to determine the effective stiffnesses of the buildings. Finally, the design base shear is calculated by multiplying the equivalent target displacement and effective stiffness. More detailed presentation of the DBD method is available elsewhere (Priestley 2002). Using the design experience with the PRESSS building, the design base shear was calculated 587 kN for each seismic frame in HFB1. This was based on an equivalent viscous damping of 14.5% (Priestley 2002) and a target inter-story design drift of 2.5% as per Seismology Committee (1999) and Performance-Based Seismic Engineering Ad Hoc Subcommittee (2003) of the Structural Engineers Association of California (SEAOC). Because this base shear is comparable to that used for the seismic frames in the PRESSS test building, the dimensions of the precast beams and columns and the hybrid frame connection details in the lower three floors in HFB1 were taken the same as those used in the hybrid frame of the PRESSS test building. The pretensioned connections were used in the upper two floors of the seismic frame in the PRESSS test building, which were replaced with equivalent hybrid connections in HFB1.

The second building, referred to as HFB2, was established using a force-based design method (FBD) in accordance with the design codes used in current practice (e.g., Uniform Building Code (UBC) 1997; International Building Code (IBC) 2000). The design base shear for each seismic frame in HFB2 was 979 kN, which was from a base shear of 10849 kN for the prototype building that was obtained using a period of 0.44 s and R-factor of 8. Hence, HFB1 and HFB2 should be considered as two contrasting solutions for the design of the prototype building shown in Fig. 3.1(b), with the base shear of HFB1 being 40% lower than

that of HFB2. It should be noted that the design base shear in HFB2 was restricted by the code upper limit on the seismic coefficient. Without this limitation, the code-based design base shear of HFB2 was 1232 kN, which was not given further consideration because it violated the recommended design practice. However, the base shear calculated based on the first mode period found by dynamic analysis was 769 kN for each seismic frame in HFB2. Thus, the design base shear of HFB1 became 24% lower than base of HFB2, due to removal of code period limit in force-based approach. For the design of both buildings, the soil condition was assumed to be very dense soil or soft rock, with the shear wave velocity in the range of 366 m/s to 762 m/s, which is identified as Soil Profile Type S_C in (UBC 1997) and Site Class C in (IBC 2000).

Tables 3.1 and 3.2 summarize the member dimensions, material properties and connection details derived for the two hybrid frame buildings. The beams and columns in HFB1 and HFB2 were dimensioned such that they would experience similar shear stresses in the interior beam-to-column joints when subjected to the maximum moments at the beam ends. The design of the hybrid connections in HFB1 and HFB2 followed the recommendations of Stanton and Nakaki (2002) and Celik and Sritharan (2004), which include a requirement that the design moment contribution ratio between those provided by the mild steel reinforcement and post-tensioning steel should be taken as 0.45:0.55. This requirement ensures a certain level of restoring force in the connection, thereby enabling recentering of the hybrid buildings after undergoing an earthquake excitation. The specified material properties were used in the design of the two buildings. However, the measured material properties from the hybrid frame in the PRESSS building were used in the analysis of the two buildings so that

the concept used for modeling the hybrid connections could be validated using the PRESSS test data. As with the PRESSS test building, the two hybrid buildings were designed with 16 X-shaped steel plate connections between each floor and the beams in the seismic frames (see Fig. 3.3), and hybrid connections between the columns and footings (Collins 1999). The inertia force introduced by horizontal ground acceleration at the floors was intended to be transferred through the flexible X-plate connection with the possibility of additional energy dissipation through this connection. However, as demonstrated in (Vernu and Sritharan 2004), the stiffness and strength of X-plates were sufficiently high and thus, they did not experience any significant inelastic action nor markedly influence the response of the PRESSS building.

3.3 ANALYTICAL MODELS

For the analysis of both buildings, 2-D models were developed using the computer program RUAUMOKO (Carr 2003) and only one seismic frame was included in each model. In series with the seismic frame, a pin-based fictitious column was also modeled (see Fig. 3.4(a)). By lumping the seismic mass at the floor levels of the fictitious column and modeling the floor connections with bi-linear inelastic axial springs between the column and seismic frame, the influence of the floor connections was included in the analyses. The force-deformation response of these spring elements was established analytically by subjecting an X-plate to monotonically increasing lateral deformation in the in-plane response direction of the seismic frames. Key properties of the spring elements are included in Table 3.1. The lateral load resistance from the gravity columns and out-of-plane bending of the precast wall system was neglected in the analytical models, except for the validation portion of the study. For the

validation study, two rotational springs connected in parallel were used at the base of the fictitious column to model the moment-response of a gravity column and one-half of the wall system subjected to out-of-plane bending (see spring properties in Table 3.1).

As demonstrated previously (Pampanin et al. 2001), the beams and columns in the RUAUMOKO models were represented by beam-column elements while two rotational springs per nodal location modeled the hybrid connections at the beam-to-column and column-to-footing interfaces (see Fig. 3.4(b)). The use of two springs to model each hybrid connection was to represent the moment contributions of the mild steel reinforcement and prestressing steel separately. The moment–rotation response envelopes of the springs were derived using the procedure reported in (Celik and Sritharan 2004). In this procedure, the moment resistance of a hybrid connection is determined at a given interface rotation by accounting for the stress-strain behavior of the reinforcing steel, elongation of the post-tensioning tendon due to gap opening, and enhancement in concrete strength due to the confinement effect.

The modified Takeda hysteresis and bi-linear elastic models (Carr 2003) were used to define the cyclic behavior of the rotational springs representing the mild steel (MS) reinforcement and post-tensioning tendons (PT), respectively. The combination of using two cyclic models for the precast connections was to capture both the hysteretic energy dissipation and re-centering capability of the hybrid frames. To account for the influence of flexural cracking, the moment of inertia for the beam-column elements was taken as a fraction of that corresponded to the uncracked concrete gross section (I_g). Based on the test observations reported for the PRESSS building (Priestley et al. 1999) and recommendations by (Paulay

and Priestley 1992), $0.6I_g$, I_g, and $0.5I_g$ were used for the columns in the first story, all other columns, and beams, respectively. Figure 3.5(a) shows the monotonic moment-rotation envelopes at the beam ends as modeled in the first floor of HFB1, while Fig. 3.5(b) illustrates the assumed responses for the aforementioned two types of rotational springs. Furthermore, Fig. 3.5(c) shows the lateral load behavior of the HFB1 model, including its recentering capability, by presenting the recorded base shear forces when the model was subjected to cyclic roof drifts of ±0.5%, ±1.5% and ±2.5%. The equivalent viscous damping calculated for the drift cycles at ±2.5% was 15.5%, which is comparable to that assumed for the design calculations.

The satisfactory behavior of the hybrid frame models described above confirms that that the effects of gap opening were adequately modeled at the precast interface. However, the limitations of the models should also be realized. As with the frequently used beam-column elements to model concrete and steel frame structures, the hybrid frame models also does not account for the frame elongations. Furthermore, the adopted analysis approach does not directly quantify the stress and strains in the critical connection regions.

3.4 PERFORMANCE-BASED EVALUATION

Seismic performance of the two hybrid frame buildings was evaluated under earthquake input motions corresponding to four intensity levels. At each intensity level, the damage state in the buildings was quantified using the maximum transient inter-story drift, maximum residual inter-story drift, the maximum floor acceleration and maximum plastic rotation, where inter-story drift is defined as the relative floor displacement divided by story height. The acceptable performance of the buildings was arbitrated by comparing the maximum

values of the inter-story drift and floor acceleration against the limiting values that are established below. The seismic hazard corresponding to the four intensity levels and the limiting values for the transient inter-story drifts were defined in accordance with the recommendations of (Seismology Committee 1999). However, the acceptable floor accelerations were defined using an IBC (2000) recommendation for the design of non-structural components. More details on the seismic hazard, the corresponding input ground motions and the limiting values for the inter-story drift and floor acceleration are given below.

3.4.1 Seismic Hazard

Consistent with the Appendices G and I of the SEAOC Seismology Committee (1999) and the revisions proposed for Appendix I in by the SEAOC Performance-Based Seismic Engineering Ad Hoc Subcommittee (2003), the four earthquake intensity levels were identified as EQ-I, EQ-II, EQ-III and EQ-IV (see Fig. 3.6). These four intensities, respectively, correspond to 22%, 50%, 100% and 150% of a design-level earthquake that is expected in a high seismic zone for soil type S_C without the influence of near source effects. The four levels of earthquakes are characterized as frequent, occasional, rare and maximum considered events and have mean return periods of 25, 72, 250 to 800, and 800 to 2500 years, respectively. According to the performance-based seismic design concept presented by the SEAOC Seismology Committee (1999), the buildings with conventional structural systems when subjected to ground motions compatible with EQ-I, EQ-II, EQ-III and EQ-IV may be expected to produce operational, occupiable, life safety and near collapse performances for

both structural and non-structural components. At the minimum, the hybrid frame buildings were considered to meet the same performance levels under the four earthquake levels.

3.4.2 Input Ground Motions

Two sets of earthquake input motions were used to evaluate the seismic performance of the HFB1 and HFB2 buildings. The first set consisted of four combinations of short duration spectrum compatible earthquake motions, while the second set consisted of eight scaled input motions recorded in past earthquakes. The motivation for the use of the first set of input motions was that it followed the procedure adopted for the pseudodynamic testing of the PRESSS building (Sritharan et al. 1999) and provided an opportunity to examine the validity of using short-duration input motions in performance-based seismic testing of structural systems.

Using the strong segments of recorded input motions from small to large earthquakes, short-duration earthquake ground motions compatible with the 1.5EQ-I, EQ-II, EQ-III and EQ-IV spectra were previously developed as part of the PRESSS test program (Sritharan et al. 1999; Sritharan et al. 2002,). The reason for using 1.5EQ-I as the target spectrum was that this spectrum was previously considered to be equal to EQ-I according to the SEAOC Seismology Committee (1999), which has been later scaled down by a factor of 2/3 in revised guidelines proposed by the Performance-Based Seismic Engineering Ad Hoc Subcommittee (2003) to produce the new EQ-I spectrum as shown in Fig. 3.6. Unless otherwise mentioned, the new and old target spectra are referred to as EQ-I and 1.5EQ-I, respectively, throughout this paper. Figure 3.7 shows spectrum compatible short-duration

ground motions derived in reference (Sritharan et al. 1999) for 1.5EQ-I, EQ-II, EQ-III and EQ-IV. There were two ground motions reported for EQ-IV and were referred to as EQ-IVa and EQ-IVb. The original motions used to create the short-duration ground motions of 1.5EQ-I, EQ-II, EQ-III, EQ-IVa and EQ-IVb were recorded at stations with soil profile type S_C in the 1974 Hollister, 1971 San Fernando, 1940 Imperial Valley, 1993 Northridge and 1978 Tabas earthquakes, respectively. Using a short segment of the strong portion of the recorded motion, each of the spectrum compatible motion was established by multiplying the Fourier amplitudes of the original motion by the spectral ratio found between the target acceleration response spectrum and acceleration spectrum of the original motion. The computer program SHAPE was used for this purpose (Earth Mechanics 1998). More descriptions of the input records and the process used for creating the short-duration input motions may be found in Refs. (Sritharan et al. 1999; Sritharan et al. 2002).

Table 3.3 lists different combinations of the short-duration ground motions used in the analyses of the hybrid frame buildings. As shown in Fig. 3.7, the analyses were performed using each combination of records as one sequence with zero accelerations for about 13.30 s of duration between the records. This procedure enabled the free vibration response of the buildings to be examined after subjecting them to each earthquake segment. Furthermore, by capturing the damage in a progressive manner, the use of the records as a continuous sequence provided realistic estimate of the building damage at the end of each earthquake segment despite using the short-duration records (Pampanin et al. 2001).

Table 3.4 provides details of the eight scaled long-duration input motions used for evaluating the performance of the hybrid frame buildings. The original records of these input motions

were obtained typically from stations with soil profile type S_C as defined in (UBC 1997). The soil type classification for the stations that recorded the original motions of IM-d and IM-f was not available. These sites, which are described to have deep alluvial soil, may be classified to have soil profile type S_D. However, the use of these records in the precast building analyses was justified due to the resemblance of the spectra obtained for these motions with the EQ-III and EQ-IV spectral shapes shown in Fig. 3.6.

As detailed in Table 3.4, the original recorded motions were scaled such that their spectra would be comparable to the target spectra within a dominant period range. Figure 3.8 (a) illustrates the procedure that determined the suitable period range and the scale factor for IM-c to make the original input motion representative of an EQ-III earthquake. As shown in this figure, the scale factor was chosen such that the 5% damped acceleration response spectrum of the scaled input motion would have spectral ordinates greater than or equal to 70% of the EQ-III ordinates within the dominant period range for the buildings. The 70% limit on the spectral ordinates was imposed consistent with the recommendation suggested by the SEAOC Seismology Committee (1999) for choosing site-specific ground motions for dynamic analyses, while the dominant period range for the buildings was defined using the elastic and effective periods calculated for the buildings using the pushover analysis results presented in the next section. Given that the elastic period of HFB2 was lower than that of HFB1, the lower limit of the dominant period range was taken as that corresponding to the elastic fundamental period of HFB2. The effective period of HFB1 controlled the upper limit of the dominant period range, where the effective period of the building was calculated using the secant stiffness as per Eq. 1 (also see insert in Fig.3.8 (a)). In each case, the secant

stiffness was defined by taking the roof drift (i.e., average inter-story frame drift), defined by the roof displacement divided by the building height, to be equal to the acceptable drift.

$$T_{effective} = T_{elastic} \sqrt{\frac{K_{elastic}}{K_{secant}}} \qquad (1)$$

where $T_{elastic}$ = elastic fundamental period of the building,

$K_{elastic}$ = elastic stiffness of the building estimated from the pushover results, and

K_{secant} = secant stiffness of the building estimated from the pushover results at the acceptable drift limit.

Note that during the dynamic analyses, the maximum transient drifts seldom exceeded the acceptable drifts limits presented below. Hence, the average drift was equated to the acceptable drift when determining K_{secant} For the EQ-III intensity used in Fig. 3.8 (a), the dominant period range was found to be 1.18 to 3.77 s for the buildings at 100% scale. Figures 3.8 (a) and 3.8 (b) depict acceleration response spectra for all modified long-duration ground motions listed in Table 3.4. Because the analyses of the hybrid buildings were conducted at 60 percent scale, the time step and accelerations of all input motions listed in Tables 3.3 and 3.4 were modified by scale factors of 0.6 and 1.67, respectively. These modifications were made when performing the analyses of the buildings.

3.4.3 Inter-story Drift Limits

The following inter-story drift limits were used as acceptable limits to evaluate the building performances at the four earthquake intensity levels: maximum transient drifts of 0.5% (EQ-I), 1.5% (EQ-II), 2.5% (EQ-III) and 3.8% (EQ-IV); and maximum residual drifts of 0.1% (EQ-I), 0.3% (EQ-II), 0.5% (EQ-III) and 0.75% (EQ-IV). These limits were chosen based on

the guidance given in the SEAOC Blue Book (Seismology Committee 1999) and considering the re-centering nature of the hybrid frames. Although it is unnecessary to set a stringent residual drift limit for an earthquake that is expected to cause near collapse response of the buildings, imposing restrictive limits on residual drifts at all earthquake levels was considered necessary since the objective of the investigation was to compare seismic responses of two hybrid frame buildings.

3.4.4 Floor Acceleration Limits

To limit damage to non-structural elements that may be anchored to the floors during seismic response of the precast buildings, a set of floor acceleration limits were imposed. These limits were derived using the recommendations of (Tong et al. 2004) and the (IBC 2000) provision for estimating design forces required to anchor different types of non-structural elements under seismic condition.

According to (IBC 2000), the design seismic force, for anchoring a non-structural element, is determined from Eq. 2:

$$F_p = \frac{0.4 a_p S_{DS} W_p (1 + 2\frac{z}{h})}{\frac{R_p}{I_p}} \qquad (2)$$

where F_p = seismic design force at the center of gravity of the non-structural element,

a_p = non-structural element amplification factor varying from 1.0 to 2.50,

S_{DS} = design spectral response at short period,

W_p = weight of the non-structural element,

z = height in structure at point of attachment of the non-structural element,

h = roof height of the structure relative to the base,

R_p = non-structural element response modification factor varying from 1.0 to 5.0,

and

I_p = non-structural element importance factor which is either 1.0 or 1.5.

By separating the influence of non-structural element related parameters including that accounts for nonlinear response (i.e., $R_p = 1$, $I_p = 1$, $a_p = 1$), a simplified form of Eq. 2 was introduced by Tong et al. (2004) to establish an allowable floor acceleration. In the present study, this simplified form was represented by Eq. 3, after incorporating a variable to account for the scale factor (used for the structural member dimensions):

$$A_f = [0.4\ S_{DS}\ (1+2\ z\ /\ h)]/S \qquad (3)$$

where A_f = permissible floor acceleration, and

S = scale factor, which is 0.60 for HFB1 and HFB2.

Anticipating dominant response from the first mode, Eq. 3 increases the acceptable floor acceleration as the height of floor increases, yielding the maximum acceptable floor acceleration at the roof level of the building. Due to the influence of higher modes, it is possible for the lower floors to experience accelerations as high as those recorded at the roof level of the building, which was witnessed during the PRESSS building test (Priestley et al. 1999). Consequently, the acceptable acceleration at any floor was taken as that determined for the roof level of the buildings from Eq. 3, which should be recognized in the design of nonstructural elements.

The floor acceleration limits for the four levels of earthquakes were defined using Eq. 3, which assumes elastic response for the nonstructural elements. The values of S_{DS} for EQ-I, EQ-II, EQ-III and EQ-IV as per the recommendations of the SEAOC Performance-Based Seismic Engineering Ad Hoc Subcommittee (2003) are 2.16 m/s^2, 4.80 m/s^2, 9.81 m/s^2 and 14.72 m/s^2. Including the scale factor of 0.6, the permissible fifth floor accelerations are 4.33 m/s^2 (EQ-I), 9.61 m/s^2 (EQ-II), 19.65 m/s^2 (EQ-III) and 29.47 m/s^2 (EQ-IV). For full-scale building analyses, these values should be taken as 2.60 m/s^2, 5.77 m/s^2, 11.79 m/s^2 and 17.68 m/s^2, respectively.

3.5 RESULTS

By comparing the analysis results from the frame model developed for HFB1 with pseudodynamic test data obtained for the PRESSS building, the modeling procedure described above was validated. Using the input motions and the mass and viscous damping parameters from the PRESSS building test, Figs. 3.9(a) and 3.9(b) compare the measured lateral displacement at the third floor of the hybrid frame and base moment of this frame in the PRESSS building with those obtained analytically from the HFB1 model. It is noted that the pseudodynamic testing of the PRESSS building was conducted using 0.75EQ-I (i.e., old 0.5EQ-I), 1.5EQ-I (i.e., old EQ-I), EQ-II and EQ-III-M, which is a modified form of EQ-III (Priestley et al. 1999, Sritharan et al. 2002). Good agreement seen between the experimental and analytical results in Figs. 3.9(a) and 3.9(b) confirmed that the procedure used for establishing the HFB1 and HFB2 models was satisfactory. Validation of the hybrid model at the connection level may be found in Celik and Sritharan (2004).

As the first step in characterizing the lateral load behavior, both hybrid building models were subjected to pushover analyses. Figure 3.10 compares the responses obtained for the two models using the base shear normalized by the building weight and the roof displacement normalized by the building height (i.e., roof drift or average inter-storey drift). The increased stiffness and strength of HFB2 are apparent in this figure. Due to the increased stiffness, the fundamental period of the HFB2 was 0.25 seconds less than that obtained for HFB1 (see Table 3.1). An interesting observation from the pushover responses of the two buildings began to respond nonlinearly approximately at the same displacement of 3.8 mm despite using different methods to design the hybrid buildings. In addition, the selected inter-story drift limits are included in Fig. 3.10 to show the different base shear demands expected on both buildings for the four earthquake levels.

The key results obtained by subjecting the two building models to all combinations of short-duration earthquake motions are summarized in Figs. 3.11 and 3.12. Generally, the maximum transient inter-story drifts of HFB1 were higher than those of HFB2 by as much as 100% (Fig. 3.11), presumably due to the increased flexibility of HFB1. For up to the EQ-III level motions, Fig. 3.11 shows that both buildings exhibited acceptable performances in terms of the maximum transient inter-story drift, which was typically governed by the first floor lateral displacement. The maximum transient inter-story drifts of the HFB1 building were very close to the acceptable limit of 0.5% for the EQ-I intensity motions, whereas the maximum transient inter-story drifts of HFB2 were noticeably lower than the acceptable limit. For the EQ-II intensity motions, both buildings exhibited maximum drifts lower than the acceptable value. For the next earthquake level (EQ-III), the maximum transient drifts of

HFB1 were again higher and closer to the limit than those observed for HFB2, but never exceeded the limit of 2.5% which was the target design drift. At EQ-IV, the HFB2 building produced transient inter-story drifts lower than the acceptable limit of 3.8%. However, for the same short-duration ground motions, HFB1 exhibited transient drifts of up to 4.62%, which is about 22 percent greater than the acceptable limit. In response to observing such a high maximum drift, it is worth noting that the hybrid frame in the PRESSS building was subjected to a maximum inter-story drift of 4.5% (Priestley et al. 1999, Sritharan 2002). At this stage of testing, it was reported that fracture of a few mild steel reinforcing bars occurred in the hybrid connections, which caused some insignificant loss in the lateral load resistance of the frame, but there was no indication that the frame would collapse at this drift level.

The residual drifts of the two buildings after subjected to all short-duration earthquake segments were found to be negligible and were well below the acceptable limits. The re-centering property of the hybrid frame systems was believed to be responsible for minimizing the residual drifts in the two buildings.

Figure 3.12 illustrates that the maximum floor accelerations of the two buildings were appreciably below the acceptable limits for all short-duration ground motions. Due to the increased flexibility, the HFB1 building generally produced lower maximum floor accelerations than the HFB2 building. However, the EQ-IV level ground motion in combination-1 and the EQ-I level ground motion in combination-4 induced larger floor accelerations in HFB1 than in HFB2, indicating the dependency of the building responses on the frequency contents of the input motions.

Figure 3.13 compares the maximum transient inter-story drifts obtained for the two buildings when subjected to the long-duration ground motions (from IM-a to IM-h representing the four earthquake intensity levels). As previously witnessed for the short-duration motions, both buildings produced acceptable performances in terms of the inter-story drift up to the EQ-III level motions. At the EQ-IV level motions, the maximum transient inter-story drift of HFB1 obtained for IM-f and IM-g motions were 5.75% and 5.46%, respectively. These values, which are significantly greater than the acceptable limit of 3.8% and the maximum frame drifts observed for the short-duration motions, raise concerns on the satisfactory performance of HFB1 to EQ-IV level motions. For all EQ-IV level motions, the maximum transient inter-story drifts of the HFB2 building were equal or below the acceptable drift limit.

The dependency of the building responses on the frequency contents of the input earthquakes was also emphasized by the analysis results in Fig. 3.13. For example, at EQ-IV level, the response to IM-f produced the largest inter-story drift demand in HFB1 and the smallest inter-story drift demand in HFB2, whereas the maximum inter-story drifts in both buildings were similar and equal to the acceptable limit when they were subjected to the IM-h motion. It is possible for both buildings to exceed the acceptable inter-story drift limit at EQ-IV, but the likelihood of this occurring for the force-based design building HFB2 with a larger base shear is relatively low.

Figure 3.14 shows that the maximum floor accelerations generated by the two building models under all long-duration input motions representing the EQ-I to EQ-IV level earthquakes and the acceptable limits. As previously seen in Fig. 3.12 for short-duration

motions, the HFB1 building generally produced the lower maximum floor accelerations than the HFB2 building and both buildings satisfied the acceptance criteria set for the floor acceleration. However, the floor accelerations obtained from the analyses were typically higher and closer to the limits than those observed under short-duration motions. The lower floor accelerations obtained under short-duration motions are believed to be due to the reduced content of high-frequency cycles in them.

To illustrate the differences in the responses of the two buildings, Table 3.5 compares the maximum plastic rotations experienced under the long-duration ground motions at the first floor level beam ends as well as at the column bases (i.e., at locations A through G identified in Fig 3.2(b)). When a connection responded only in the linear range at a particular location, the corresponding plastic rotation was recorded as zero. Overall, the maximum plastic rotations recorded at the column bases were greater than those obtained at the beam ends. Averaging the values obtained for different earthquakes showed the maximum column plastic rotation to be about 15% greater the average plastic rotation found at the first-floor beam ends. Furthermore, the maximum plastic rotations recorded in HFB2 were generally lower than those recorded in HFB1. Although the maximum plastic rotation recorded at any location in HFB2 was in the 50 to 100 percentage range of the corresponding value in HFB1, the maximum plastic rotation in HFB2 on average was 70% of that recorded in HFB1.

Due to the reduced design base shear, it was anticipated that the HFB1 building would experience larger cumulative damage than HFB2. Measures that can reflect the cumulative damage using parameters such as plastic rotation at the beam-to-column connection interface or plastic strain in the mild steel reinforcement should also be included in the performance-

based evaluation of buildings. Because of insufficient knowledge on this topic especially for hybrid connections, only the maximum inter-story drifts and maximum floor accelerations were primarily used to compare the performances of the two precast buildings in this paper. Nonetheless, the accumulated plastic rotations occurred to the exterior frame connections at the first floor of the buildings were examined for the two buildings using the responses obtained for the EQ-IV motions IM-f and IM-h. These accumulated rotations were found to be 2.96 and 0.85 radians for the HFB1 building and 0.68 and 0.60 radians for the HFB2 building, which confirmed the expected lower cumulative damage to the precast connections in HFB2. It is important to note that the frequency content of the input motion significantly influenced the accumulated plastic rotations in the buildings. For IM-f, the accumulated plastic rotations of the two buildings differed by more than a factor of 4, while the IM-h input motion produced comparable accumulated rotations in both buildings.

3.6 CONCLUSIONS

Seismic performances of two hybrid frame buildings representing a 5-story prototype building at 60% scale were analytically studied in this paper. The first building was derived using a direct displacement-based design method while the second building was established from a force-based method in accordance with the current design practice. The design base shear of the first building was 40% lower than that of the second building and thus the lateral strength and stiffness of the two buildings were significantly different.

Following validation of the analytical modeling procedure, both buildings were subjected to several short- and long-duration earthquake input motions which were comparable with

acceleration response spectra corresponding to four levels of earthquake intensities. Using the analysis results, the following conclusions were drawn:

1. The seismic performance of the two buildings satisfied the performance limits under earthquake input motions with intensities similar to or below that of the design-level earthquake. Hence, the force-based methods described in design codes for monolithic concrete special moment frames and the direct displacement-design described in (Priestley 2002) are acceptable procedures for the design of the prototype five-story precast hybrid frame building to produce acceptable performance at design-level earthquakes.

2. At EQ-IV, the building based on the force-based method produced acceptable performance. However, the building designed according to the displacement-based method was unsatisfactory as it resulted in significantly higher maximum transient inter-story drifts than the acceptable limit of 3.8% assumed in this study. The performance of the building based on the displacement-based design could be improved by designing for the EQ-IV spectrum at a target drift of 3.8%.

3. The combination of hysteretic energy dissipation and re-centering capabilities of the hybrid connections produced negligible residual drifts for all earthquake motions, and thus satisfying the maximum residual inter-story drift was not a problem.

4. The maximum floor accelerations determined for both buildings were below the acceptable limits for all input motions. Based on the responses of the buildings, it appears that the floor acceleration limits introduced in this paper for the four levels of earthquakes are satisfactory.

5. Overall the hybrid building designed to the displacement-based method experienced the largest plastic rotation. When these values obtained at the column bases and the end of first floor beams were compared, the largest plastic rotations experienced by the building designed to the force-based method on average was about 70% of those recorded in the building designed to the displacement-base method.

6. The short-duration earthquake motions generally produced the expected trends of the building behavior satisfactorily. The noticeable difference in the responses of the buildings to short- and long-duration motions was that the floor accelerations found under the short-duration motions were significantly smaller than those found for the long-duration motions.

7. The design base shear of HFB1 was lower than the base shear of HFB2 by 24% when the first mode period found from dynamic analysis, instead of period limited by code, was used to calculate the base shear of HFB2 according to force-based approach.

8. For the two EQ-IV level motions investigated, the plastic accumulated rotations for the exterior hybrid frame connection at the first floor were found to be higher for HFB1 than for the HFB2 building. Future research should focus on quantifying the acceptable cumulative damage parameters such as the plastic rotation so that these parameters can also be included in the performance-based seismic evaluation of hybrid frame buildings.

It is acknowledged that the emphasis of this paper is on establishing satisfactory analytical models for precast hybrid frame buildings, formulating a methodology for comparing responses of hybrid frame buildings designed using the DBD and FBD methods, and

demonstrating the expected performance of low-rise hybrid frame buildings designed to a lower base shear than required by the current code of practice. As such, the earthquake ground motion was used as the main variable. To generalize the conclusions presented above, similar studies involving variables such as building height and soil type may be necessary.

3.7 ACKNOWLEDGEMENTS

3.8 APPENDIX I. REFERENCES

Carr. A. J. (2003). RUAUMOKO - Inelastic Dynamic Analysis Program. University of Canterbury, Christchurch, New Zealand.

Celik, O., and Sritharan, S. (2004). An Evaluation of Seismic Design Guidelines Proposed for Precast Concrete Hybrid Frame Systems. ISU-ERI-Ames Report ERI-04425, Iowa State University, Ames, Iowa, USA, 83-198.

Collins, R. H. (1999). Design of a Precast Concrete Building for Seismic Loading. Thesis of M.Sc., University of Washington, USA, 37-235.

Conley, J., Sritharan, S., and Priestley, M. J. N. (2002). Precast Seismic Structural Systems PRESSS-3: The Five-Story Precast Test Building, Vol. 3-1: Wall Direction Response, Report Number: SSRP-99/19, University of California, San Diego, California, USA.

Earth Mechanics, Computer Program (1998): SHAPE, Fountain Valley California, USA.

Englekirk, R. E. (2002). "Design-Construction of The Paramount – A 39-story Precast Prestressed Concrete Apartment Building." *PCI Journal,* 47(4), 56-71.

International Building Code (IBC). (2000). International Code council, Virginia, USA, 331-377.

Nakaki, S. D., Stanton J. F., and Sritharan, S. (1999). "An Overview of the PRESSS Five-story Precast Test Building." *PCI Journal*, 44(2), 26-39.

Pampanin, S., Priestley, M. J. N., and Sritharan, S. (2000). The Five-Story Precast Test building, PRESSS phase-3, Vol. 3-4, Frame Direction Response, Report Number: SSRP-2000/08, University of California, San Diego, California, USA.

Pampanin, S., Priestley, M. J. N., and Sritharan, S. (2001). "Analytical Modeling of Seismic Behavior of Precast Concrete Ductile Frame Connection." *Journal of Earthquake Engineering*, 5(3), 329-367.

Paulay, T., and Priestly, M. J. N. (1992). Seismic Design of Reinforced Concrete and Masonry Buildings, John Wiley and Sons, Inc., New York, USA, 142, 163.

Performance-Based Seismic Engineering Ad Hoc Subcommittee. (2003). Revised Interim Guidelines: Performance-Based Seismic Engineering for the SEAOC Blue Book, Structural Engineers Association of California, California, USA, 128-132.

Priestley, M. J. N., Sritharan, S., Conley, J. R., and Pampanin, S. (1999) "Preliminary Results and Conclusions from the PRESSS Five-Story Precast Concrete Test Building." *PCI Journal*, 44(6), 42-67.

Priestley, M. J. N. (2002). "Direct Displacement-Based Design of Precast/Prestressed Concrete Buildings." *PCI Journal*, 47(6): 67-79.

Seismology Committee. (1999). Recommended Lateral Force Requirements and Commentary (Blue Book). Structural Engineers Association of California (SEAOC), California, USA, 327-421.

Sritharan, S. (2002). "Performance of Four Jointed Precast Frame Systems under Simulated Seismic Loading." *Proceedings of the Seventh National Conference on Earthquake Engineering*; Paper No. 264, Boston, USA.

Sritharan, S., and Ingham J. M. (2003). "Application of Strut-And-Tie Concepts to Concrete Bridge Joints in Seismic Regions." *PCI Journal*, 48 (4), 66–89.

Sritharan, S., Pampanin, S. and Conley, J. (2002). Design Verification, Instrumentation and Test

Procedures, PRESSS-3: The Five-Story Precast Test Building, Vol. 3-3. ISU-ERI-Ames Report ERI-03325, Iowa State University, Ames, Iowa, USA, 14-68.

Sritharan, S., Igarashi, A., Priestley, M. J. N., and Seible, F. (1999). "Test Design of the PRESSS Five-Story Precast Concrete Building." *Proceedings of the 68th SEAOC Annual Convention*, Santa Barbara, California, USA, 255-261.

Sritharan, S., and Rahman, M.A. (2004). "Performance-based Seismic Assessment of Two Precast Concrete Hybrid Frame Buildings." *Proceedings of International Workshop on Performance-based Seismic Design,* Bled, Slovenia.

Stanton, J. F., Stone, W. C., and Cheok, G. S. (1997). "A Hybrid Reinforced Precast Frame for Seismic Regions." *PCI Journl,* 42(2), 20-32.

Stanton, J. F., and Nakaki, S. D. (2002). Design Guidelines for Precast Concrete Seismic Structural Systems, PRESSS Report Number-01/03-09, University of Washington Report Number-SM 02-02, University of Washington, Seattle, USA.

Stone, W. C., Cheok, G. S., and Stanton, J. F. (1995). "Performance of Hybrid Moment-Resisting Precast Beam-Column Concrete Connections Subjected to Cyclic Loading." *ACI Structural Journal,* 91(2), 229-249.

Uniform Building Code (UBC). (1997). International Conference of Building Officials, Whittier, California, USA, 2, 13-38.

Vernu, S., and Sritharan, S. (2004). Section, Member and System Level Analyses for Precast Concrete Hybrid Frames. ISU-ERI-Ames Report ERI-04635, Iowa State University, Ames, Iowa, USA, 107-147.

APPENDIX II. NOTATION

A_f = floor acceleration;

F_p = seismic design force at the center of gravity of the non-structural element;

I_p = non-structural element importance factor which is either 1.0 or 1.5;

$K_{elastic}$ = elastic stiffness of the building estimated from the pushover results;

$K_{sec\,ant}$ = secant stiffness of the building estimated from the pushover results at the acceptable drift limit;

L_p = plastic hinge length;

R_p = non-structural element response modification factor varying from 1.0 to 5.0, and;

S = scale factor;

S_{DS} = design spectral response at short period;

$T_{elastic}$ = elastic fundamental period of the building;

W_p = weight of the non-structural element;

a_p = non-structural element amplification factor varying from 1.0 to 2.50;

f_c' = unconfined concrete strength;

h = roof height of the structure relative to the base;

z = height in structure at point of attachment of the non-structural element;

f_{pi} = initial stress of post tensioning tendon after losses;

f_{py} = yield strength of post tensioning tendon;

f_{su} = ultimate strength of mild steel reinforcement;

f_{sy} = yield strength of mild steel reinforcement;

θ = interface rotation;

Table 3.1.   A summary of various building parameters

Parameter	HFB1 (DBD)	HFB2 (FBD)
Column (width x depth)	457 mm x 457 mm	508 mm x 508 mm
Beam (width x depth)	355 mm x 584 mm	406 mm x 686 mm
Unconfined concrete strength, $f_c^?$	60.60 MPa[*] (34 MPa[†])	34 MPa[†]
__Mild steel reinforcement__		
Yield strength, f_{sy}	413 MPa[†] (468.5 MPa[*])	413 MPa[†]
Ultimate strength, f_{su}	675 MPa[*]	675 MPa[*]
__Post-tensioning tendon__		
Yield strength, f_{py}	1757 MPa[*]	1757 MPa[*]
Initial stress after losses, f_{pi}	820 MPa[†]	820MPa[†]
Grout strength	69 MPa[†] (64 MPa[*])	69 MPa[†]
__X-plate contribution per floor__		
Yield strength	389.46 kN	650.41 kN
Elastic stiffness	1.72×10^6 kN/mm	2.87×10^6 kN/mm
Hardening ratio	0.00157	0.00157
__Properties of spring modeling wall contribution__		
Yield moment	74.93 kN-m	-----
Elastic rotational stiffness	74.93×10^3 kN-m/radian	-----
Hardening ratio	0.00544	-----
__Properties of spring modeling gravity column contribution__		
Yield moment	207.75 kN-m	-----
Elastic rotational stiffness	97.09×10^3 kN-m/radian	-----
Hardening ratio	0.0269	-----
__Dynamic property__		
Fundamental period	0.96 s	0.71 s

[†]specified properties in design; [*]measured properties.

95

Table 3.2.   A summary of hybrid frame connection details

	HFB1 (DBD)		HFB2 (FBD)	
Location	A_s (mm^2)	A_{pt} (mm^2)	A_s (mm^2)	A_{pt} (mm^2)
Floor 1	567.7	592.3	800.0	691.0
Floor 2	400.0	493.6	600.0	592.3
Floor 3	400.0	493.6	567.7	592.3
Floor 4	348.4	342.6	400.0	394.8
Floor 5	348.4	342.6	400.0	394.8
Exterior column base	567.7	1612.9	800.0	1612.9
Interior column base	567.7	1612.9	800.0	1612.9

Table 3.3.   Different combinations of short-duration ground motions used in the analysis

	Earthquake Intensity Level			
Combinations	EQ-I	EQ-II	EQ-III	EQ-IV
Combination-1	EQ-I	EQ-II	EQ-III	EQ-IVa
Combination-2	EQ-I	EQ-II	EQ-III	EQ-IVb
Combination-3	0.22EQ-III	(-) 0.50EQ-III	EQ-III	(-) 1.5EQ-III
Combination-4	0.15EQ-IVb	(-) 0.33EQ-IVb	0.67EQ-IVb	EQ-IVb

Table 3.4.   List of ground motions selected for the analysis

Identification of the Input Motion	Earthquake Intensity	Earthquake Name (Year) and Station	Magnitude	Direction of Component	Scale Factor	PGA after multiplying by the Scale Factor (g)
IM-a	EQ-I	Morgan Hill (1984); Station: Gilory # 6, San Ysidro Microwave Site	6.1 (M_s)	East-West	0.65	0.19
IM-b	EQ-II	Loma Prieta (1989); Station: Saratoga Aloha Avenue	7.1 (M_s)	North-South	0.64	0.32
IM-c	EQ-III	Northridge (1994); Station: Castaic Old Ridge Route	6.8 (M_s)	East-West	1.68	0.86
IM-d	EQ-III	Imperial valley (1940); Station: Elcentro	7.2 (M_s)	North-South	1.50	0.48
IM-e	EQ-III	Kobe-Japan (1995); Station: KJM	6.9 (M_w)	East-West	1.10	0.66
IM-f	EQ-IV	Tabas-Iran (1978)	7.4 (M_s)	344 degrees from North	1.00	0.93
IM-g	EQ-IV	Chi-Chi-Taiwan (1999); Station: CHY	7.6 (M_s)	80 degrees from North	1.47	1.33
IM-h	EQ-IV	Kobe-Japan (1995); Station: KJM	6.9 (M_w)	North-South	1.77	1.46

PGA = Peak Ground Acceleration, M_s = Surface Wave Magnitude, M_w = Moment Magnitude

Table 3.5.   Plastic rotation at the first floor level beam-to-column connections, and at column-to-base

connections at locations A, B, C, D, E, F and G as shown in Fig. 3.2(b)

Input motion	Location-A		Location-B		Location-C		Location-D		Location-E		Location-F		Location-G	
	HFB1	HFB2	HFB1	HFB2	HFB1	HFB2	HFB1	HFB2	HFB1	HFB2	HFB1	HFB2	HFB1	HFB2
IM-a	0.0000	0.0000	0.0000	0.0000	0.0000	0.0000	0.0000	0.0000	0.0016	0.0010	0.0017	0.0016	0.0015	0.0010
IM-b	0.0095	0.0050	0.0088	0.0042	0.0088	0.0042	0.0096	0.0051	0.0121	0.0063	0.0121	0.0070	0.0121	0.0063
IM-c	0.0198	0.0194	0.0188	0.0184	0.0188	0.0184	0.0198	0.0194	0.0213	0.0184	0.0217	0.0193	0.0212	0.0184
IM-d	0.0148	0.0070	0.0140	0.0061	0.0140	0.0061	0.0148	0.0070	0.0160	0.0087	0.0163	0.0095	0.0160	0.0088
IM-e	0.0141	0.0110	0.0132	0.0101	0.0132	0.0101	0.0141	0.0110	0.0185	0.0119	0.0190	0.0126	0.0186	0.0119
IM-f	0.0549	0.0271	0.0536	0.0189	0.0536	0.0189	0.0549	0.0200	0.0552	0.0214	0.0556	0.0222	0.0552	0.0213
IM-g	0.0409	0.0332	0.0397	0.0321	0.0397	0.0321	0.0410	0.0333	0.0432	0.0358	0.0436	0.0368	0.0431	0.0358
IM-h	0.0341	0.0348	0.0329	0.0336	0.0329	0.0336	0.0341	0.0348	0.0364	0.0361	0.0366	0.0371	0.0363	0.0362
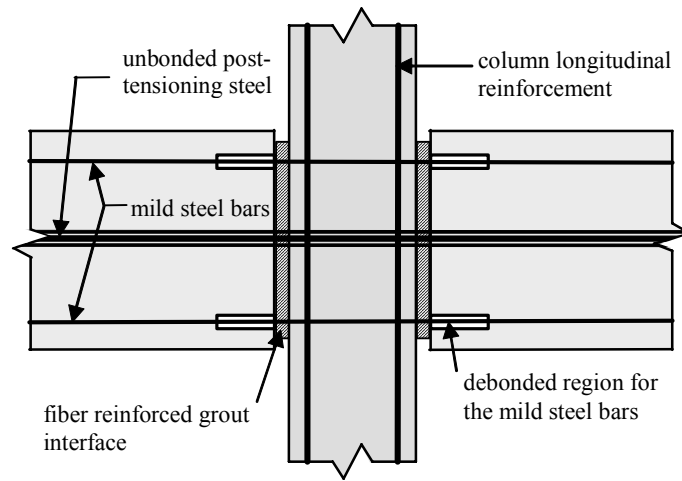
Figure 3.1(a).   The typical connection details of a precast hybrid frame (transverse reinforcements are omitted for clarity)
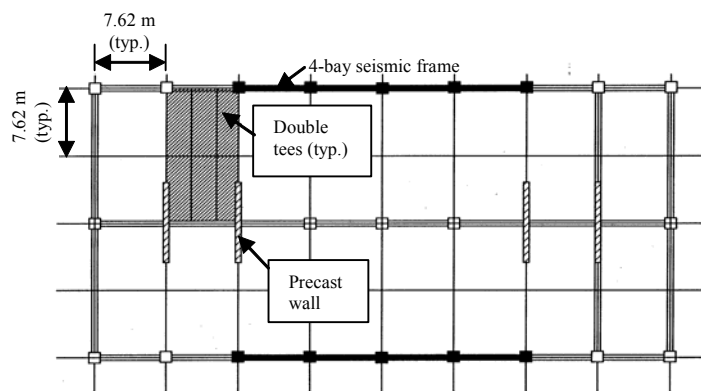
Figure 3.1(b).   Plan view of the precast concrete prototype building (Nakaki et al. 1999)
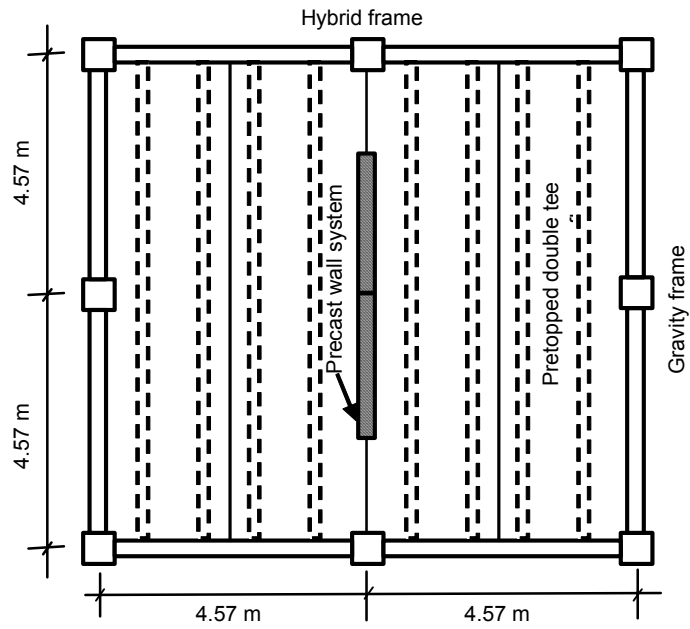
Figure 3.2(a).   Plan view of the scaled hybrid frame building
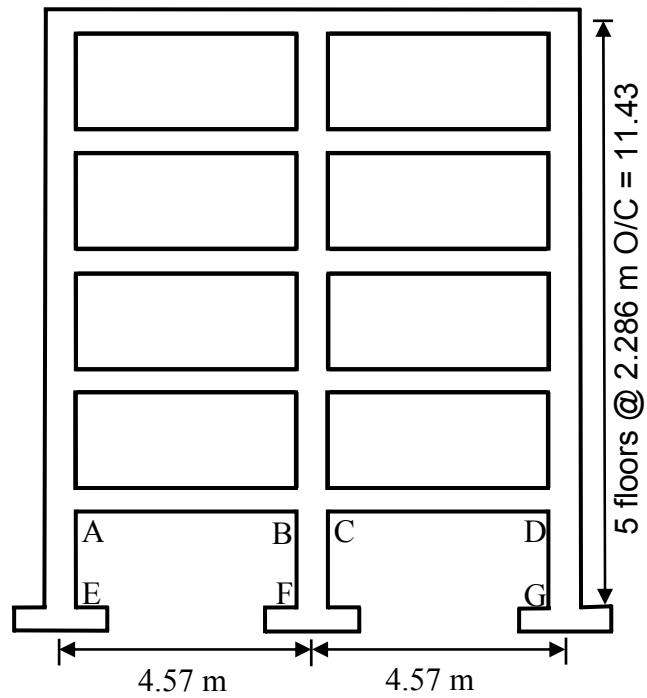
Figure 3.2(b).   Elevation view of the scaled hybrid frame building
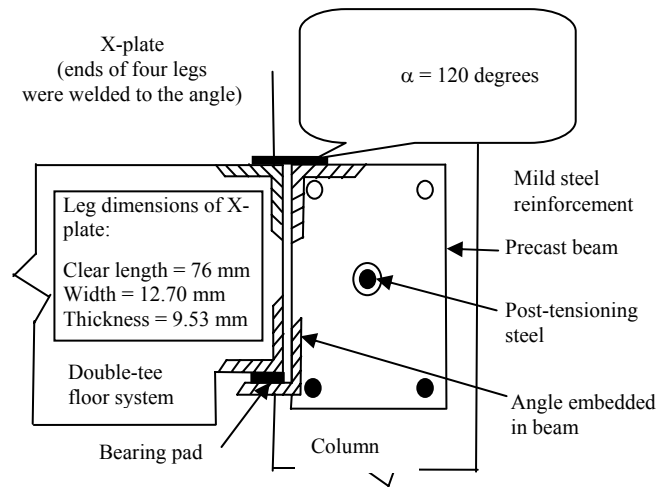
Figure 3.3.   Illustration of connection between floor system and hybrid frame through X-plate

(not to scale)
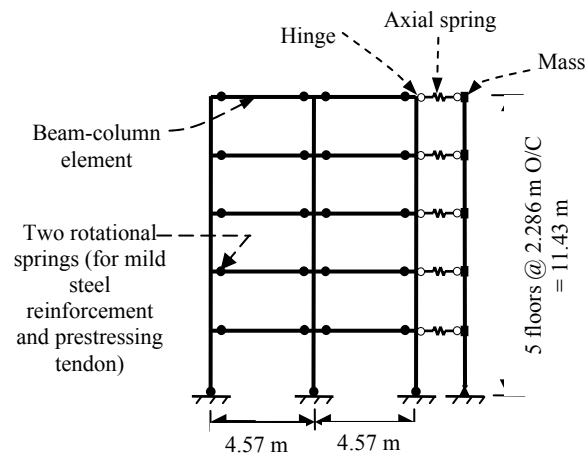
Figure 3.4(a).   A schematic view of the 2-D model used for the analysis of hybrid

frame buildings
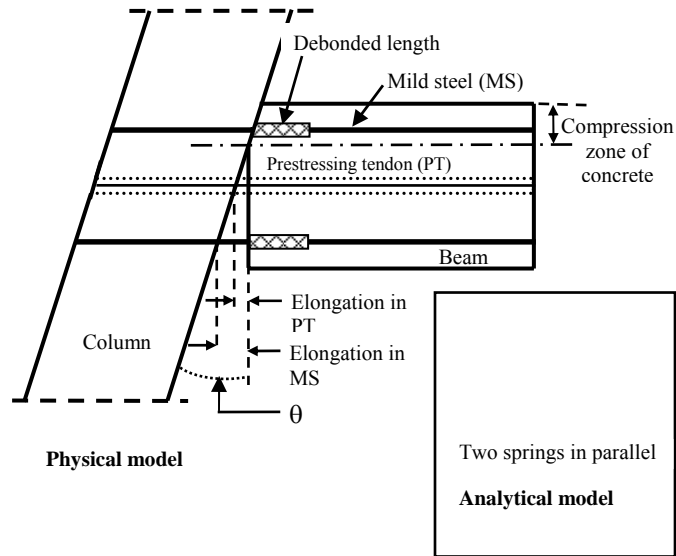
Figure 3.4(b).   Details of a typical hybrid connection are shown at interface rotation θ
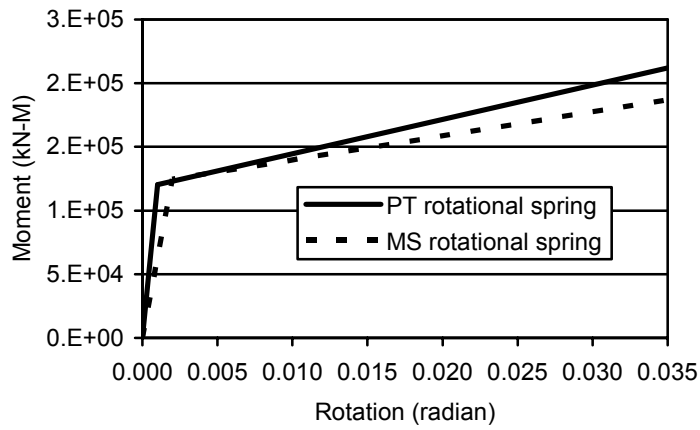
Figure 3.5(a).   Monotonic moment-rotation envelopes of PT and MS rotational

springs at the first floor beam ends
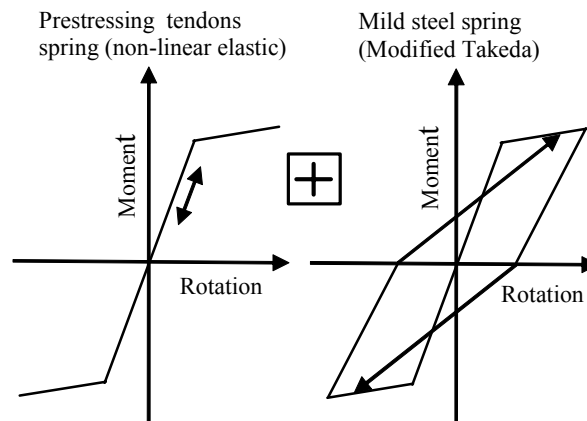
Figure 3.5(b).   Illustration of typical moment rotation responses of PT and MS

rotational springs
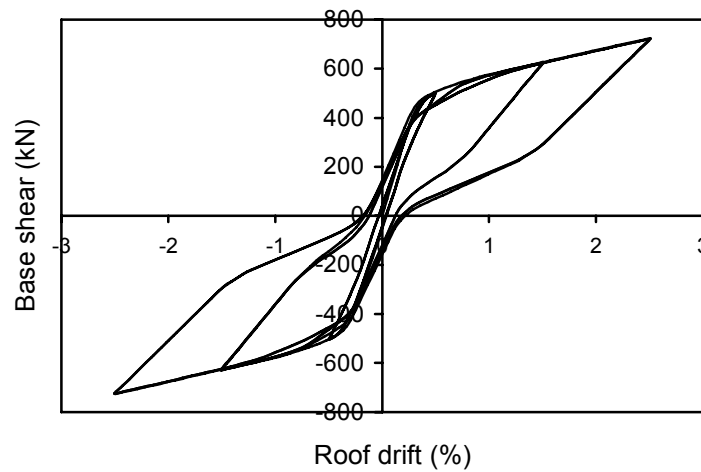
Figure 3.5(c).   Cyclic pushover response of HFB1
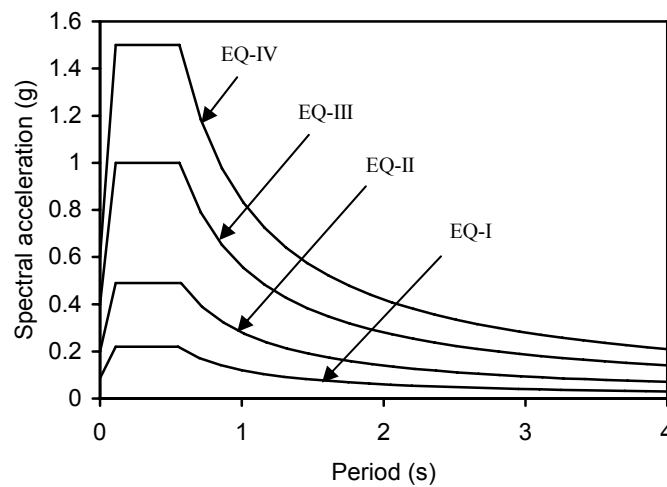
Figure 3.6.   The 5% damped multiple-level acceleration response spectra, suggested for soil

type S_C in high seismic zone as per the Performance-Based Seismic Engineering

Ad Hoc Subcommittee (2003) of SEAOC.
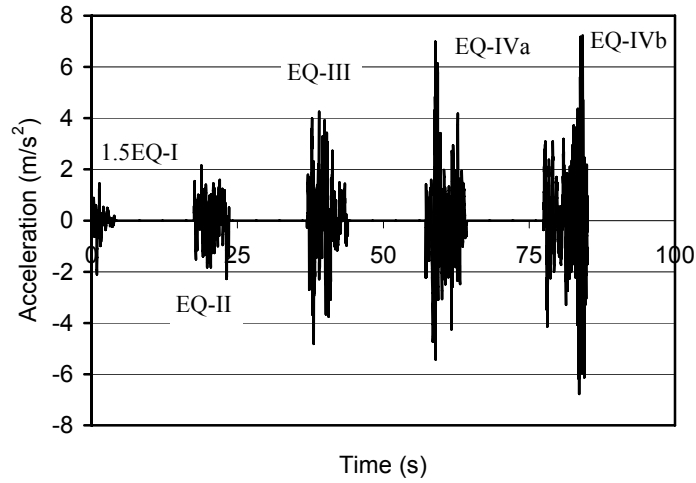
Figure 3.7.   Short duration earthquake input motions
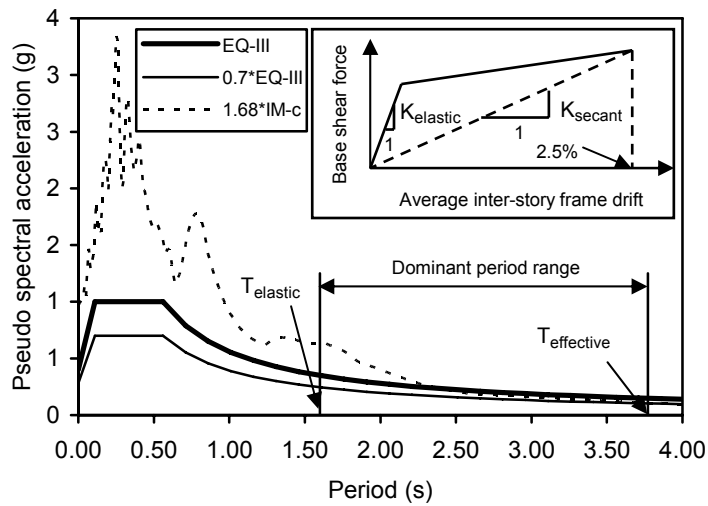
Figure 3.8(a).   Illustration of the procedure used to scale an input ground motion to make it

representative of an EQ-III level earthquake.

105
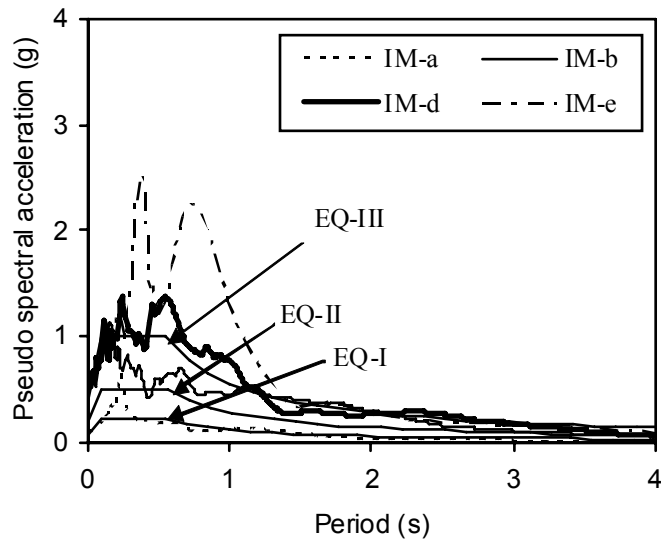
Figure 3.8(b).   Pseudo spectral acceleration of EQ-I, EQ-II and EQ-III levels of ground motions

listed in Table 3.4, scaled by following the procedure demonstrated in Fig. 3.8(a)
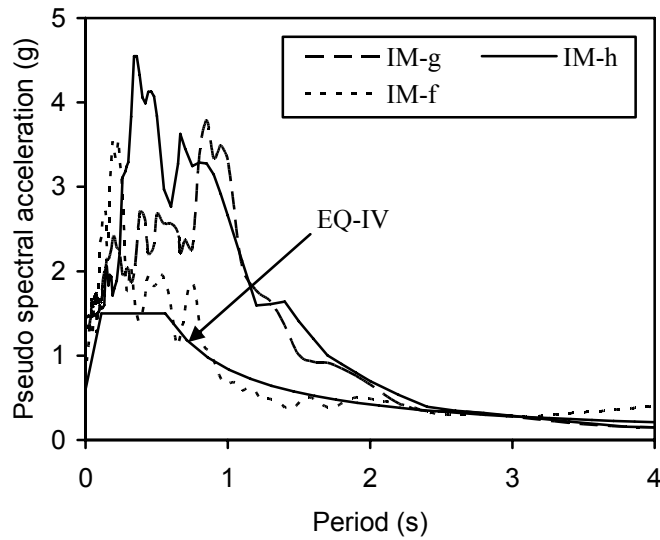
Figure 3.8(c).   Pseudo spectral acceleration of EQ-IV level ground motions listed in Table

3.4, scaled by following the procedure demonstrated in Fig. 3.8(a)
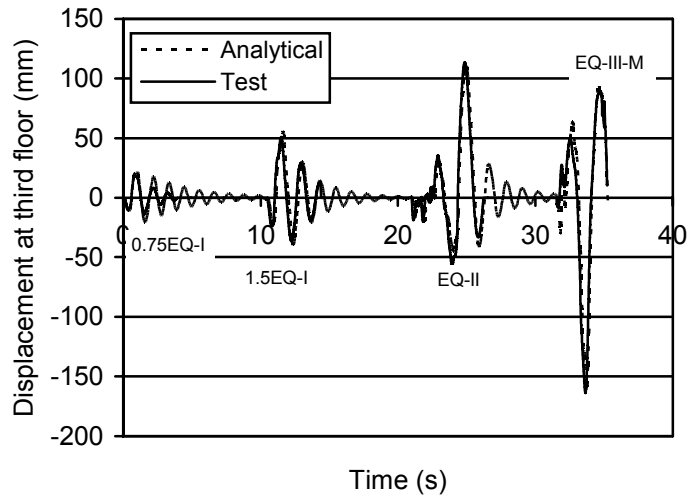
Figure 3.9(a).   Comparison of the third floor displacements from the HFB1 (DBD) analysis and
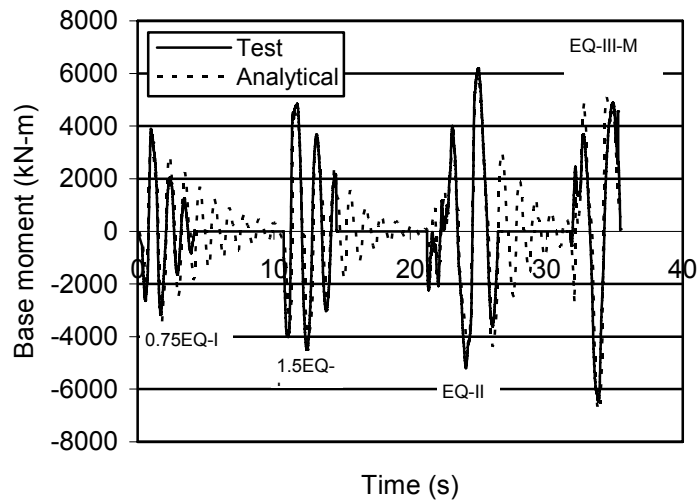
PRESSS test data

Figure 3.9(b).   Comparison of the base moment obtained from the HFB1 (DBD) analysis and

PRESSS test data
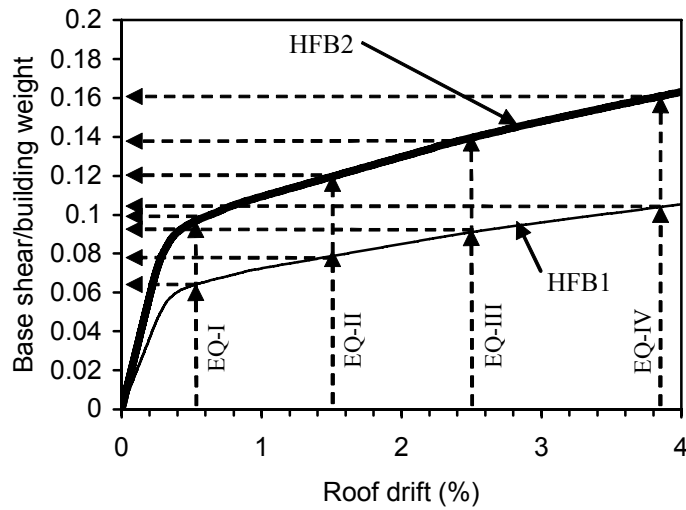
Figure 3.10.   Pushover analysis results for the HFB1 (DBD) and HFB2 (FBD) building models
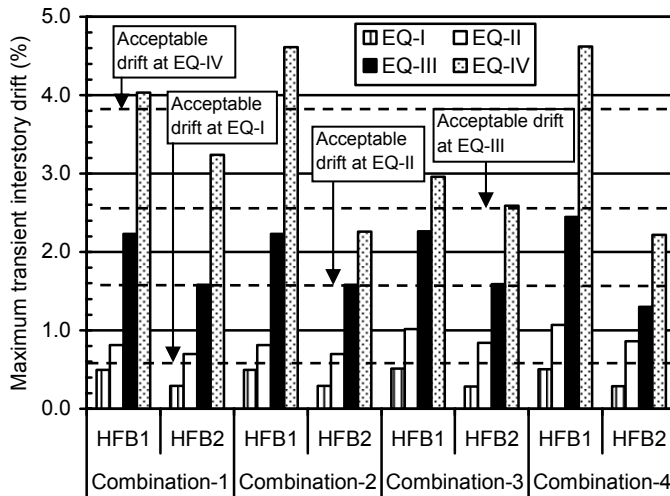
Figure 3.11.   The maximum transient inter-story drifts obtained for HFB1 (DBD) and HFB2 (FBD) when subjected to various combinations of short-duration ground motions summarized in Table 3.3
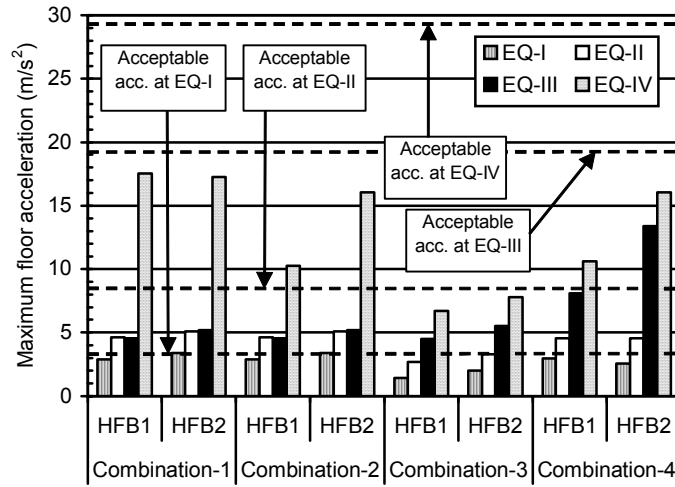
Figure 3.12.   The maximum floor accelerations obtained for HFB1 (DBD) and HFB2 (FBD) when subjected to various combinations of short-duration ground motions summarized in Table 3.3
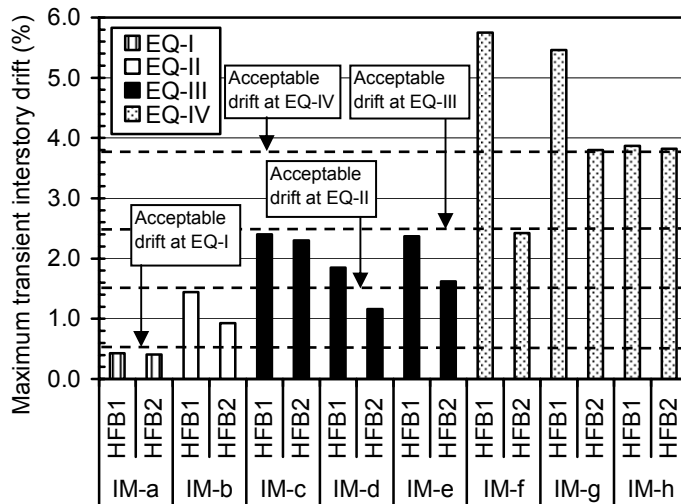
Figure 3.13.   The maximum transient inter-story drifts obtained for HFB1 (DBD) and HFB2 (FBD) when subjected to various long-duration ground motions summarized in Table 3.4
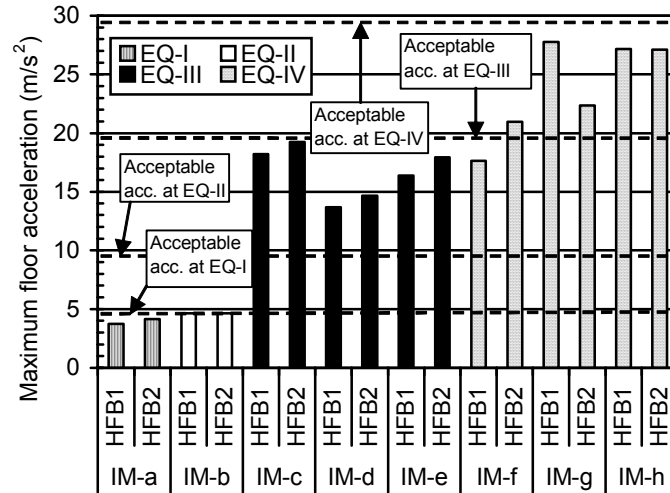
Figure 3.14.   The maximum floor accelerations obtained for HFB1 (DBD) and HFB2 (FBD) when subjected to various long-duration ground motions summarized in Table 3.4

CHAPTER 4. AN EVALUATION OF FORCE-BASED DESIGN VS. DIRECT DISPLACEMENT-BASED DESIGN OF JOINTED PRECAST POST-TENSIONED WALL SYSTEMS

A paper accepted in *Earthquake Engineering and Engineering Vibration Journal*

M. Ataur Rahman[1] and Sri Sritharan [2]

Abstract

The unique features of jointed post-tensioned wall systems, which include minimum structural damage and re-centering capability when subjected to earthquake lateral loads, are the result of using unbonded post-tensioning to attach the walls to the foundation, along with employing energy dissipating shear connectors between the walls. Using acceptance criteria defined in terms of inter-story drift, residual drift, and floor acceleration, this study presents a multiple-level performance-based seismic evaluation of two five-story unbonded post-tensioned jointed precast wall systems. The design and analyses of these two wall systems, established as the direct displacement-based and force-based solutions for a prototype building used in the PREcast Seismic Structural Systems (PRESSS) program, were performed at 60% scale so that the analyses model could be validated using the PRESSS test data. Both buildings satisfied the performance criteria at four levels of earthquake motions although the design base shear of the direct displacement-based jointed wall system was 50% of that demanded by the force-based design method. The study also investigated the feasibility of controlling the maximum transient inter-story drift in a jointed wall system by increasing the number of energy dissipating shear connectors between the walls without significantly affecting its re-centering capability.

[1]PhD Candidate, Department of Civil, Construction and Environmental Engineering, Iowa State University, Ames, IA 50011, USA
[2]Associate Professor, Department of Civil, Construction and Environmental Engineering, e-mail: sri@iastate.edu, tel.: 515-294-5238, fax: 515-294-7424, Iowa State University, Ames, IA 50011, USA

4.1 Introduction

Jointed precast wall systems with unbonded post-tensioning can be used as the primary structural system for resisting earthquake lateral forces in high seismic regions. In these systems, individual precast wall is secured to the foundation using unbonded prestress tendons running from the top of the wall to the foundation. Two or more of such post-tensioned walls are connected horizontally to each other using shear connectors, which are distributed along the wall height, to form a jointed precast wall system (Fig. 4.1). The basic concept of this wall system is to allow the walls to rock individually at the base when subjected to a ground excitation of significant magnitude and return to its original vertical position after the event has concluded (Priestley et al. 1999; Thomas and Sritharan 2004). The vertical post-tensioning contributes to overturning moment resistance and ensures transfer of shear forces between the walls and foundation through a friction mechanism. The shear connectors between the walls contribute to both moment overturning moment resistance as well as hysteretic energy dissipation.

When designed with unbonded post-tensioning, a precast concrete wall provides additional benefits under seismic loading condition, which include reduced damage due to concentration of flexural cracking at the base and negligible residual displacements as a result of its re-centering capability. Instead of joining the walls, researchers have also investigated the possibility of using single precast walls connected to the foundation using unbonded post-tensioning. A significant drawback of these walls is that they have limited energy dissipation capacity and thus they can experience significantly large transient inter-story drifts (Conley et al. 2002; Kurama et al. 1999a; Kurama et al. 1999b; Kurama et al.

2002).

In seismic regions, design base shear of jointed precast wall system may be established using two methods. The traditional approach is to follow the force-based design (FBD) approach as recommended in refs. (Uiniform Building Code (UBC) 1997; International Building Code (IBC) 2000). In this approach, design base shear is obtained from the estimated fundamental period and total mass of the structure, incorporating the influence of seismic intensity in terms of a design spectral acceleration. In this method, the target level lateral displacement of the building is not directly used to quantify the design base shear. In contrast, the direct displacement-based design (DDBD) method uses the target displacement that is selected to match the expected performance of the building to establish the design base shear. In this approach, the base shear is determined using an effective period for the fundamental mode and seismic intensity in terms of a design spectral displacement (Priestley 2002). By representing the hysteretic action with equivalent viscous damping, the effective period is established using an effective mass for the fundamental mode of the building, which is determined by assuming a suitable displacement profile for this mode. The effective period is used to determine the effective stiffness of the building. Finally, the design base shear is calculated by multiplying the equivalent target displacement and effective stiffness. More detailed presentation of the DDBD method is available elsewhere (Priestley 2002).

Using acceptance criteria defined in terms of inter-story drift, residual drift, and floor acceleration, this paper presents a multiple-level performance-based seismic evaluation of FBD and DDBD solutions for a five-story precast unbonded post-tensioned jointed wall system. The significance of studying the two approaches to design a five-story jointed wall

system is that they lead to drastically different design base shear forces, and thus a systematic seismic evaluation of the systems based on the two design forces have economical implications for the design of jointed precast walls.

4.2 Unbonded post tensioning precast jointed wall systems

Figure 4.2 shows the plan view of a five-story precast concrete building chosen for the investigation reported in this paper. The building primarily uses four jointed walls to resist lateral forces in the transverse direction of the building. As with the PRESSS test building (see Fig. 4.4) (Nakaki et al. 1999; Priestley et al. 1999; Sritharan 2002), the consequences of using the FBD and DDBD to design the jointed wall systems was conducted on 25% of the building at 60% scale (see Fig 4.3 for the plan view of the reduced building). This approach was necessary to ensure satisfactory modeling of jointed wall system using the PRESSS test data

In model scale building shown in Figs. 4.3 and 4.4, one jointed wall system consisting of two precast walls is used. Each wall is secured to the foundation using unbonded post-tensioning bars located at the centroid of the wall. The walls are connected horizontally using U-shaped stainless steel flexural plates (also known as UFP connectors). Construction details and expected behavior of the UFP connectors may be found elsewhere (Nakaki et al. 1999; Thomas and Sritharan 2004). The combination of modeling a portion of the building and the use of reduced scale lead to the ratios of 0.6, 0.6^2, 0.25×0.6^2, 0.25×0.6^3, 1.0, 0.6^{-1} and 0.6, respectively, for the member dimension, member force, base shear, mass, stress, acceleration and time between the building model and the prototype structure.

The first jointed wall system, referred to as JWS1, was designed for the building Fig. 4.3 using DDBD as adopted for the design of the PRESSS building (Collins 1999, Galusha 1999, Priestley 2002; Sritharan et al. 2002). Using an equivalent viscous damping of 18% and a target inter-story design drift of 2% (as per ITG 5.1-XX (2006), Seismology Committee (1999) and Performance-Based Seismic Engineering Ad Hoc Subcommittee (2003) of the Structural Engineers Association of California (SEAOC)), the design base shear of 867.4 kN was found for JWS1. Because this design base shear is similar to that used for the jointed wall system in the PRESSS test building, the dimensions of the precast walls and details of unbonded post tensioning tendons and UFP connectors for JWS1 were taken the same as those used for the jointed wall in the PRESSS test building.

Base shear for the second building, referred to as JWS2, was calculated to be 1734.7 kN using FBD in accordance with the design codes used in current practice (e.g., UBC 1997; IBC 2000). This base shear was derived from the design base shear calculated for the prototype building with the code-based estimate for the fundamental period of 0.44 sec. Consequently, JWS1 and JWS2 should be considered as two contrasting solutions for the design of the jointed walls in Figs. 4.2 and 4.3, with the base shear of JWS1 being 50% less than that of JWS2. It should be noted that the design base shear in JWS2 was restricted by the code upper limit on the seismic coefficient. Without this limitation, the design base shear of JWS2 was 2185.13 kN, which was not given further consideration because it violated the recommended design practice. For calculating the values of design base shear of both JWS1 and JWS2, the soil condition was assumed to be very dense soil or soft rock, with the shear wave velocity in the range of 366 m/s to 762 m/s, which is identified as Soil Profile Type S_C

in UBC (1997) and Site Class C in IBC (2000). Because the design base shear forces differed by a factor of two between JWS2 and JWS1, it was decided that the FBD solution (i.e., JWS2) could be modeled using two JWS1 systems for evaluating the seismic performance. In other words, seismic analysis of both buildings could be evaluated using a single dynamic model with appropriate modifications to the seismic mass.

4.3 Analytical model

For the analysis of the jointed wall system, a 2-D analytical model was developed using the finite element computer program RAUMOKO (Carr 2003). Figure 4.5 includes the model of the jointed wall system comprised of two unbonded post-tensioned precast walls, in which each unbonded post-tensioned wall is represented using an elastic beam-column element positioned at the wall centerline. The rotational capacity of each unbonded post-tensioned wall is represented by a non-linear rotational spring at the base of the beam-column element. Although there are twenty UFP connectors positioned between the two unbonded walls, their combined effect is modeled equally at each floor level, resulting in five non-linear inelastic vertical direction springs with each modeling four UFPs. These springs are connected to rigid beam-column elements extending from the centerline of each wall towards the centerline of the jointed wall system as seen in Fig. 4.5.

In the PRESSS test building, the lateral load resistance in the wall direction was assisted by two gravity columns and the framing action resulting from out-of-plane response of the two seismic frames and precast floor at the lower three floor levels (Thomas and Sritharan 2004). Including these contributions in the analytical model was considered essential for validation of the analysis model; however they were excluded during the performance-based evaluation

of JWS1 and JWS2. A one bay frame, rigidly connected in series to the left side of the jointed wall model, represents the framing action resulting from the seismic frames and precast floors. Similarly, a beam-column element is added to the right side of the jointed wall model to account for the effect of the two gravity columns (see Fig. 4.5). Seismic mass of the building, lumped at five floor levels, was assigned to the five nodes of the element modeling the gravity columns (Fig. 4.5). Properties of various elements used in Fig. 4.5 for modeling the building are presented in the subsequent sections.

With the description of the jointed wall model described above, it should be realized that the distance between the wall elements is fixed at L_w, which is the length of each wall. Consequently, it is assumed that the distance between the centers of rotation at the wall bases remains unchanged as depicted in Figure 4.6. In reality, the compression ends of the wall bases cannot significantly deform beyond the rigid foundation, causing overestimation of the UFP connectors. For a given rotation at the wall bases, the value of the UFP deformation calculated for the model, the UFP deformation expected in the structure and the ratio between these two deformations are given by equations (1), (2) and (3), respectively:

$$d_m = \left(\frac{L_w}{2} \times \theta\right) \times 2 = L_w \times \theta \qquad (1)$$

$$d_a = (L_w - N) \times \theta \qquad (2)$$

$$F = \frac{d_a}{d_m} = \frac{L_w - N}{L_w} \qquad (3)$$

where,

d_m = UFP deformation calculated for the model

d_a = UFP deformation expected in the actual structure

L_w = length of one unbonded wall

θ = rotation in base of wall

N = neutral axis depth at the wall base

F = ratio of between the UFP deformations in the actual and model wall systems

To compensate for the error in the UFP deformation in the model, the elastic and inelastic stiffnesses of the UFP springs were modified by multiplying them by factor F determined from Eq. 3. The test data from the PRESSS building confirmed that the floor displacement and UFP deformation were approximately linearly correlated. Similar trend was found in the analytical results of the present model because of utilizing the rigid links between the walls and the UFP springs.

4.4 Characteristics of elements used in the analytical model

Properties of various elements, used in the analytical model, were derived based on their material properties and geometric dimensions, which are included in Table 4.1. The material properties were taken identical to those established for the PRESSS test building. Since each wall in the jointed system was expected to undergo negligible damage with inelastic actions concentrated at the wall base, the walls in the analytical model were represented by elastic beam-column elements with their stiffness based on their gross section properties. Each wall

element was connected to the foundation using an elastic bi-linear rotational spring to model the flexural resistance of the wall at the base and the corresponding concentrated crack opening at this location. Moment-rotation behavior of the rotational springs, which were found by analyzing the wall behavior using the procedure recommended in (Aaleti 2005), are reported in Table 4.1.

Each of the two columns, included in the one bay seismic frame model (see Fig. 4.5), represented three seismic columns shown in the plan view of the structure shown in Fig. 3. These columns were modeled as linear elastic beam-column elements with the effective moment of inertia equal to 70% of the gross moment of inertia of the column section in the first story and 100% of the gross moment of inertia in the upper stories. This approach was followed to capture the effect of observed flexural cracking on the seismic columns during the wall direction testing of the PRESSS test building (Priestley et al. 1999).

The beams in the one bay seismic frame model (Fig. 4.5) represented the floor systems at the five floor levels. These beams were modeled using linear elastic beam-column elements. The beams in the first three floor levels included elasto-plastic rotational springs at the ends, whereas the beams at the fourth and fifth floor levels were connected to the columns using pin connections. Such rotational springs and pin connections were incorporated in the model to adequately capture the behavior of actual connections between the floor and seismic frames as used in the PRESSS test building as well as the expected framing action resulting from the seismic frames and flooring systems. More descriptions of these connections and their expected behavior may be found in Thomas and Sritharan (2004). The effects of two gravity columns seen in Fig. 4.3 were modeled using a single gravity column, which was

placed in series with the jointed wall system model as shown in Fig. 4.5. Uncracked section properties were used to model these columns using an elastic beam-column element. The base of this element was attached to the foundation using a non-linear rotational spring with the Modified Takeda hysteretic rule available in RAUMOKO (Carr 2003), which was to satisfactorily capture the moment-rotation behavior of the gravity column at this location. The moment-rotation properties of this spring were obtained from ref. (Thomas 2003) and are included in Table 4.1.

Based on the force-displacement test results reported for UFP connectors by Thomas (2003), equivalent bi-linear inelastic axial springs modeled the contribution of UFPs. These springs (Fig. 4.5), whose properties are summarized in Table 4.1, were mainly responsible for the hysteretic energy dissipation of the jointed wall systems. Rayleigh damping model (Carr 2003) was used to introduce viscous damping in dynamic analysis. The percentage of critical damping at the first and fifth modes were given as input parameters to define the damping matrix as a function of mass and stiffness matrices.

The elastic modulus, moment of inertia, and cross sectional area values of a wall member were multiplied by 10^3, 10^4, and 10^8, respectively, to establish the properties of rigid beam-column elements, which linked wall elements to the UFP springs. These high values for the element properties ensured adequate behavior for the rigid elements. As previously noted, the lateral load resistance of the seismic frame and gravity columns was included to adequately validate the analytical model. However, for comparing multiple level performance of the two unbonded post-tensioned jointed precast wall systems (i.e., JWS1 and JWS2), these contributions were not included.

4.5 Model validation

In the wall direction, the PRESSS test building was subjected to five levels of short-duration ground motions as shown in Fig. 4.7, and they were referred as 0.75EQ-I, 1.5EQ-I, EQ-II, EQ-III and -1.5EQ-III. EQ-I, EQ-II, EQ-III and EQ-IV represent four levels of seismic hazard expressed in terms of spectral accelerations (see Fig. 4.8), and were established by the Performance-Based Seismic Engineering Ad Hoc Subcommittee (2003) of the Structural Engineers Association of California (SEAOC). Of these different seismic hazard levels, EQ-III represents the design-level earthquake ground motions, while EQ-IV, which is equivalent to 1.5 times EQ-III, correspond to the maximum considered earthquakes. For these four levels of seismic hazard, Sritharan et al. (1999 and 2002) created spectrum compatible short-duration ground motions. Three of these grounds motions, multiplied by different scale factors, were used for the wall direction test of the PRESSS building. Details for using different scale factors for the PRESSS building test may be found in Rahman and Sritharan (2006). The analytical model of the PRESSS building with the jointed wall described in Section 4 (see Fig. 4.5) was also subjected to these five levels of short-duration ground motions in Fig. 4.7. Figures 4.9 and 4.10 show that the comparison between the experiment and analytical results for the top floor displacement and base moment as a function of time. Good agreements between the analytical and experimental results are seen, which confirm the satisfactory representation of the analytical model. Furthermore, as shown in Fig. 4.11, the analytical model also satisfactorily captured the deformation of the UFP connectors as a function of time. All of these validations suggest that the jointed wall model incorporated in

Fig. 4.5 can be used to satisfactorily evaluate the seismic performance of jointed wall systems JWS1 and JWS2.

4.6 Performance-based seismic evaluation

Seismic performance of JWS1 and JWS2 designed using DDBD and FBD was evaluated at EQ-1, EQ-II, EQ-III and EQ-IV using the maximum transient inter-story drift, maximum residual inter-story drift, and the maximum floor acceleration, where the inter-story drift is defined as the relative floor displacement divided by story height. According to the performance-based seismic design concept presented by the SEAOC Seismology Committee (1999), ordinary buildings with conventional structural systems when subjected to ground motions compatible with EQ-I, EQ-II, EQ-III and EQ-IV may be expected to produce operational, occupiable, life safety and near collapse performances for both structural and non-structural components. At the minimum, the precast jointed wall systems were expected to meet the same performance levels under the four earthquake levels.

The acceptable performance of the joined walls was arbitrated by comparing the maximum values of the inter-story drift, residual drift and floor acceleration against the limiting values. The limiting values for the transient inter-story drifts and residual drifts were defined in accordance with the recommendations of Seismology Committee (1999) and ITG 5.1-XX (2006.). However, the acceptable floor accelerations were defined using an IBC (2000) recommendation for the design of non-structural components. More details on multiple levels input ground motions and the limiting values for the inter-story drifts and floor acceleration are given below.

4.6.1 Input ground motions

Two sets of earthquake input motions were used to evaluate the seismic performance of the jointed wall systems JWS1 and JWS2. The first set consisted of four combinations of short-duration spectrum compatible earthquake motions, while the second set consisted of eight scaled input motions recorded in past earthquakes. The motivation for using the first set of input motions was that it followed the procedure adopted for the pseudodynamic testing of the PRESSS building (Sritharan et al. 1999) and provided an opportunity to examine the validity of using short-duration input motions in performance-based seismic testing of structural systems.

Table 2 lists different combinations of the short-duration ground motions used in the seismic evaluation of the jointed wall systems, which were performed using each combination of records as one sequence with zero accelerations for about 13.3 s of duration between the records. This procedure enabled the free vibration response of the jointed walls to be examined after subjecting them to each earthquake segment. The original motions used to create the short-duration ground motions of 1.5EQ-I, EQ-II, EQ-III, EQ-IVa and EQ-IVb were recorded at stations with soil profile type S_C in the 1974 Hollister, 1971 San Fernando, 1940 Imperial Valley, 1993 Northridge and 1978 Tabas earthquakes, respectively. More descriptions of the input records and the process used for creating the short-duration input motions may be found in refs. (Sritharan et al. 1999; Sritharan et al. 2002; Rahman and Sritharan 2006).

Table 4.3 provides details of the eight scaled long-duration input motions used for evaluating the performance of the jointed wall systems. The original records of these input motions were

obtained typically from stations with soil profile type S_C as defined in (UBC 1997). As detailed in Table 4.3, the original recorded motions were scaled such that their spectra would be comparable to the target spectra within a dominant period range, following the procedure developed in (Rahman and Sritharan 2006). Figures 4.12 (a) and (b) depict the acceleration response spectra for all modified long-duration ground motions listed in Table 4.3. Because the analyses of the jointed wall systems were conducted at 60 percent scale, the time step and accelerations of all input motions listed in Tables 4.2 and 4.3 were modified by scale factors of 0.6 and 1.67, respectively. These modifications were made when performing the analyses of the buildings.

4.6.2 Inter-story drift limits

The following inter-story drift limits were used as acceptable limits to evaluate the joined wall system performances at the four earthquake intensity levels: maximum transient drifts of 0.4% (EQ-I), 1.2% (EQ-II), 2.0% (EQ-III) and 3.0% (EQ-IV); and maximum residual drifts of 0.1% (EQ-I), 0.3% (EQ-II), 0.5% (EQ-III) and 0.75% (EQ-IV). These limits were chosen based on the guidance given in the SEAOC Blue Book (Seismology Committee 1999), ITG 5.1-XX (2006) and considering the re-centering nature of the jointed wall systems.

4.6.3 Floor acceleration limits

To limit damage to non-structural elements that may be anchored to the floors during seismic response of the precast buildings, a set of floor acceleration limits were imposed. These limits were derived in Rahman and Sritharan (2006) using the recommendations of Tong et al. (2004) and the IBC (2000) provision for estimating design forces required to anchor

different types of non-structural elements to building floors under seismic condition. A controlling parameter of these floor acceleration limits is the spectral acceleration corresponding to a short period that is used to define the design response acceleration spectrum (IBC 2000). For the design spectra recommended by the SEAOC Performance-Based Seismic Engineering Ad Hoc Subcommittee (2003), the values of the sort-period spectral acceleration ordinates are 2.16 m/s^2, 4.80 m/s^2, 9.81 m/s^2 and 14.72 m/s^2 for EQ-I, EQ-II, EQ-III and EQ-IV, respectively (Rahman and Sritharan 2006). The corresponding limiting floor accelerations are 2.60 m/s^2, 5.77 m/s^2, 11.79 m/s^2 and 17.68 m/s^2. Including the scale factor of 0.6, the following limits are used in this study: 4.33 m/s^2 (EQ-I), 9.61 m/s^2 (EQ-II), 19.65 m/s^2 (EQ-III) and 29.47 m/s^2 (EQ-IV).

4.7 Results from earthquake analysis of jointed wall systems

Figures 4.13 and 4.14 summarize the key results obtained by subjecting the two jointed wall systems, JWS1 and JWS2, to all combinations of short-duration earthquake motions. As expected due to the increased flexibility, the maximum transient inter-story drifts of JWS1 were higher than those obtained for JWS2 for all levels of ground motions (Fig. 4.13). The utmost difference between the maximum transient inter-story drifts of JWS1 and JWS2 were 112%, 132%, 191% and 245%, for EQ-I, EQ-II, EQ-III and EQ-IV level motions, respectively. This observation indicates that the highest difference between the maximum transient inter-story drifts of the two jointed walls increases as intensity of the ground motion increases. However, a similar trend is not observed for the smallest difference in the maximum transient inter-story drifts of JWS1 and JWS2, which were found to be 29%, 43%, 8% and 23%, for EQ-I, EQ-II, EQ-III and EQ-IV level motions, respectively. Furthermore,

Figure 4.13 illustrates that both jointed walls exhibited acceptable performances in terms of the maximum transient inter-story drift for the four levels of short-duration ground motions. For EQ-I and EQ-II level motions, the maximum transient inter-story drifts of JWS1 and JWS2 were noticeably lower than the acceptable limits. When the two wall systems were subjected to the EQ-III level short-duration motions, the maximum transient inter-story drift recorded for JWS1 was 1.15%, which is 58% of the acceptable limit of 2% established for EQ-III level motions. Similarly, when all EQ-IV level motions were considered, JWS1 exhibited the maximum transient inter-story drift of 2.81%, which is 94% of the acceptable limit. In comparison, the highest level of the maximum transient inter-story drifts obtained for JWS2 were 0.82% (41% of acceptable limit) and 2.02% (67% of acceptable limit) for EQ-III and EQ-IV level motions, respectively. Such low values for the maximum transient inter-story drifts for JWS2 under EQ-III and EQ-IV level motions suggest that the stiffness of JWS2 may be unnecessarily high and that JWS1 provides a more economical solution.

Figure 4.14 represents the maximum floor accelerations of JWS1 and JWS2 when subjected to short-duration ground motions. Generally, the maximum floor accelerations in JWS2 building were higher than those obtained for JWS1 by as much as 78%, 33%, 20% and 34% for EQ-I, EQ-II, EQ-III and EQ-IV level motions, respectively. However, for the EQ-III level motions in combination-1, combination-2 and combination-3 as well as for the EQ-IV level motion in combination-3, the maximum floor accelerations obtained for JWS2 were lower than those of JWS1, indicating the dependency of the jointed wall responses on the frequency contents of the input motions. The maximum floor accelerations in JWS1 for all levels of ground motions were appreciably below the acceptable limits. A similar trend was

demonstrated by JWS2, except for the EQ-I level ground motions in combinations 1 and 2, for which the acceptable limit of the maximum floor acceleration was exceeded by 2%.

Figure 4.15 compares the maximum transient inter-story drifts obtained for the two jointed wall models when subjected to the long-duration ground motions, listed in Table 4.3. As previously witnessed for the short-duration motions, both buildings produced acceptable seismic performances in terms of the maximum inter-story drifts, with sufficient margin of safety for all levels of ground motions represented by IM-a through IM-h. This observation suggests that the jointed wall systems established using both the DDBD and FBD are acceptable design solutions. The maximum inter-story drifts of JWS1 were generally higher than those of JWS2 and they differ by as much as 109% (see data corresponding to IM-b in Fig. 4.15), indicating that the DDBD solution is more economical than the FBD solution. The highest values of the maximum transient inter-story drifts exhibited by JWS1 were 30%, 54%, 85% and 76% of the acceptable maximum transient inter-story drift limits for EQ-I, EQ-II, EQ-III and EQ-IV level ground motions, respectively. In contrast, JWS2 achieved 25%, 26%, 68% and 71% of the respective acceptable limits of the transient inter-story drifts. Unlike it was observed for short duration input motions, the difference between the maximum transient inter-story drifts of the two jointed walls, which is generally small, does not seem to increase as the intensity of the ground motion increases.

The dependency of the building responses on frequency contents of the input earthquake was also emphasized by the analyses results in Fig. 4.15. For example, at EQ-IV level, the responses of JWS1 and JWS2 to IM-g led to only 7% difference in the maximum transient inter-story drifts, whereas the corresponding difference was 76% for IM-f, although IM-f and

IM-g ground motions were chosen to represent EQ-IV level input motions. Moreover, when the two jointed walls were subjected to IM-e, JWS2 produced larger transient inter-story drift than JWS1. Although not typical, such occurrence is expected because, among other parameters, the inelastic displacement excursion occurring in the opposite direction also influences the maximum transient drift especially in building systems that can re-center. It is to be noted that similar results were observed in Rahman and Sritharan (2006) for precast hybrid frames designed to re-center after subjected to earthquake lateral loading.

Figure 4.16 illustrates the maximum floor accelerations observed for the two jointed wall systems when subjected to all long-duration ground motions of Table 4.3 representing the EQ-I to EQ-IV level earthquakes. Generally, the maximum floor accelerations in JWS2 were higher than those observed for JWS1 because of the increased lateral stiffness. The largest difference between the maximum floor accelerations of JWS2 and JWS1 were 50%, 4%, 29% and 24%, respectively, for EQ-I, EQ-II, EQ-III and EQ-IV level earthquake motions.

The maximum floor accelerations of JWS1 were satisfactory and were 72% to 85% of the associated acceptable limits for all levels of earthquake motions. In contrast, the response of JWS2 produced floor accelerations somewhat greater than the acceptable limits for three input motions: 17%, 2.6% and 0.9% higher than the associated acceptable limits for input ground motions IM-a (EQ-I), IM-c (EQ-III) and IM-h (EQ-IV), respectively. Since the jointed wall designed using the FBD method violates the designated acceptable limits for the maximum floor acceleration for three levels of earthquakes, it appears that excessive floor accelerations could result in excessive damage to non-structural components in the building containing JWS2.

The re-centering capability of the unbonded post-tensioning tendon enabled both jointed wall systems to produce insignificant residual inter-story drifts at the end of short- as well as long-duration ground motions. The maximum residual inter-story drifts observed for two jointed wall systems were less than 0.004%, which is much lower than the acceptable limits. The increase in transient inter-story drift exhibited by JWS1 did not cause any concerns with the re-centering ability of this wall system.

To investigate the influence of energy dissipating UFP connectors on the response of jointed wall systems, the response of JWS1 model was examined under IM-c and IM-d by changing the number of connectors. First, the sensitivity of energy dissipating mechanism on the maximum transient inter-story drift and the maximum residual inter-story drift was examined under design-level earthquake motion IM-d. As expected, Figures 4.17 (a) and (b) show that the maximum transient inter-story drift decreased with increased number of energy dissipating UFP connectors, but the maximum inter-story residual drift also increased. Increase in the residual drift was expected because there was no change in the post-tensioning force that provided the elastic restoring force needed for recentering the wall system. However, in all cases, the residual inter-story drift was within acceptable limit. Similar trends were observed when JWS1 was subjected to IM-c with various numbers of UFPs as shown in Figs. 4.18 (a) and (b).

4.8 Conclusions

Seismic performances of two jointed wall systems representing a 5-story prototype building at 60% scale were analytically studied in this paper. The first jointed wall system was derived using the direct displacement-based design approach while the second jointed wall system

was established from the traditional force-based approach. The design base shear of the first building was 50% lower than that of the second building. Following the validation of the analytical modeling procedure, both jointed wall systems were subjected to short- and long-duration earthquake input motions, which were comparable with acceleration response spectra corresponding to four levels of earthquake intensities. Using the analysis results, the following conclusions were drawn:

1. The seismic performance of the two jointed wall systems satisfied the performance limits of the maximum transient inter-story drift, residual inter-story drifts and maximum floor acceleration for all levels of short-duration ground motions.

2. The maximum transient inter-story drifts observed in jointed wall designed using the direct displacement-based design was generally more than those of the force-based jointed wall system, when subjected to long-and short-duration ground motions. An opposite trend was observed for the maximum floor acceleration.

3. Both jointed wall systems produced the maximum transient inter-story drifts lower than the acceptable limits when subjected to all levels of long-duration ground motions. For the same set of ground motions, the displacement-based jointed wall system (JWS1) also satisfied the floor acceleration limits, whereas the force-based jointed wall system (JWS2) failed to satisfy the acceleration limits established for EQ-I, EQ-III and EQ-IV level ground motions.

4. Due to the re-centering capability that stems from the unbonded post-tensioned tendons, both jointed wall systems showed residual inter-story drifts lower than the acceptable limits under both short- and long-duration input motions.

5. The transient inter-story drift in precast jointed wall systems can be controlled by increasing the hysteretic damping in the jointed wall system by adding more number of energy dissipating shear connectors. Although, increasing the number of shear connectors increases the residual inter-story drifts of the jointed walls, they are not expected to exceed the limiting values established for the residual inter-story drifts.

6. Based on the satisfactory performance of the jointed wall system designed using the direct displacement-based design that led to a lower design base shear force, it appears that this design method would lead to a more economical design than the force-based design method for jointed wall systems in low-rise buildings. However, analysis similar to that presented above for JWS1 should be repeated for several other low-rise buildings to generalize this conclusion.

4.9 Acknowledgements

4.10 References

Aaleti, S (2005), Design and Analysis of Unbonded Post-Tensioned Precast Wall Systems, M.S. Thesis, Department of Civil, Construction and Environmental Engineering, Iowa State University, Ames, Iowa, USA.

Carr AJ (2003). RUAUMOKO - Inelastic Dynamic Analysis Program. University of Canterbury, Christchurch, New Zealand.

Collins RH (1999), Design of a Precast Concrete Building for Seismic Loading. Thesis of M.Sc., University of Washington, USA, 37-235.

Conley J, Sritharan S and Priestley MJN (2002), Precast Seismic Structural Systems PRESSS-3: The Five-Story Precast Test Building, Vol. 3-1: Wall Direction Response, Report Number: SSRP-99/19, University of California, San Diego, California, USA.

Galusha JG (1999), Precast, Post-tensioned Concrete Walls Designed to Rock, M.S. Thesis, Department of Civil Engineering, University of Washington, Seattle, Washington, USA.

International Building Code (IBC) (2000), International Code council, Virginia, USA, 331-377.

ITG 5.1-XX (2006), "Acceptance Criteria for Special Unbonded Post-Tensioned Structural Walls Based on Validation Testing," American Concrete Institute.

Kurama Y, Pessiki S, Sause R and Lu L (1999), "Lateral Load Behavior and Seismic Design of Unbonded Post-Tensioned Precast Concrete Walls," ACI Structural Journal, July-August, Vol. 96, No. 4, 622-632

Kurama Y, Pessiki S, Sause, R and Lu L (1999), "Seismic Behavior and Design of Unbonded Post-Tensioned Precast Concrete Walls," PCI Journal, Vol. 44, No. 3, May-June, 72-88.

Nakaki SD, Stanton JF and Sritharan S (1999), "An Overview of the PRESSS Five-story Precast Test Building," PCI Journal, 44(2), 26-39.

Performance-Based Seismic Engineering Ad Hoc Subcommittee (2003), Revised Interim Guidelines: Performance-Based Seismic Engineering for the SEAOC Blue Book, Structural Engineers Association of California, California, USA, 128-132.

Priestley MJN (2002), "Direct Displacement-Based Design of Precast/Prestressed Concrete Buildings," PCI Journal Vol. 47, No. 6, 67-79.

Priestley MJN, Sritharan S, Conley JR and Pampanin S (1999), "Preliminary Results and Conclusions From the PRESSS Five-Story Precast Concrete Test Building," PCI Journal, Vol. 44, No. 6, 42-67.

Rahman MA and Sritharan S (2006), "A Performance-Based Seismic Evaluation Of Two Five-Story Precast Concrete Hybrid Frame Buildings," submitted to ASCE Structural Journal (under review).

Seismology Committee. (1999), Recommended Lateral Force Requirements and Commentary (Blue Book). Structural Engineers Association of California (SEAOC),

California, USA, 327-421.

Sritharan S and Rahman MA (2004), "Performance-based Seismic Assessment of Two Precast Concrete Hybrid Frame Buildings," Proceedings of International Workshop on Performance-based Seismic Design, Bled, Slovenia.

Sritharan S (2002), "Performance of Four Jointed Precast Frame Systems under Simulated Seismic Loading," Proceedings of the Seventh National Conference on Earthquake Engineering; Paper No. 264, Boston, USA.

Sritharan S, Pampanin S and Conley J (2002), Design Verification, Instrumentation and Test Procedures, PRESSS-3: The Five-Story Precast Test Building, Vol. 3-3. ISU-ERI-Ames Report ERI-03325, Iowa State University, Ames, Iowa, USA.

Thomas DJ and Sritharan S (2004), An Evaluation of Seismic Design Guidelines Proposed for Precast Jointed Wall Systems, ISU-ERI-Ames Report ERI-04635, Iowa State University, Ames, Iowa, USA, June.

Thomas DJ (2003), Analysis and Validation of a Seismic Design Method Proposed for Precast Jointed Wall Systems, M.Sc. Thesis, Department of Civil, Construction and Environmental Engineering, Iowa State University, Ames, Iowa, USA.

Tong M, Lee G, Rzhevsky V, Qi J and Shinozuka M (2004), A Comparison of Seismic Risk of Non-structural Systems in a Hospital Before and After a Major Structural Retrofit, ATC-29-2 Seminar on Seismic Design, Retrofit, and Performance of Non-structural Components in Critical Situations <http://shingo8.eng.uci.edu/ATC-29-2.htm, date-11-17-2004>

Uniform Building Code (UBC) (1997), International Conference of Building Officials, Whittier, California, USA, 2, 13-38.

Table 4.1.   Dimensions of the jointed wall JWS1 and the properties of the analytical model shown

in Fig. 4.5

Parameter	Value
Wall height	11.43 m
Wall length	2.7432 m
Wall thickness	203.2 mm
Initial post-tensioning force	765.95 kN
Area of post-tensioning tendons	2193.54 mm^2
Yield strength of post-tensioning tendons	827.40 MPa
Elastic modulus of post-tensioning tendons	200 GPa
Wall concrete strength	52.64 MPa
Properties of spring modeling moment resistance of a wall at base	
Yield moment	15.49 x 10^2 kN-m
Elastic rotational stiffness	12.38 x 10^5 kN-m/rad
Hardening ratio	0.043
Properties of spring modeling UFPs at each floor level	
Yield strength	129.35 kN
Elastic stiffness	105.08 kN/mm
Hardening ratio	0.035
Properties of spring modeling_seismic column contribution	
Yield moment	327.61 kN-m
Elastic rotational stiffness	140.41 x 10^3 kN-m/rad
Hardening ratio	0.0356
Properties of spring modeling_gravity column contribution	
Yield moment	406.70 kN-m
Elastic rotational stiffness	203.35 x 10^3 kN-m/rad
Hardening ratio	0.0278
Fundamental period	JWS1 = 0.4592 sec
	JWS2 = 0.3251sec

Table 4.2. Different combinations of short-duration ground motions used for the performance based seismic evaluation of precast jointed wall systems

	Earthquake Intensity Level			
Combinations	EQ-I	EQ-II	EQ-III	EQ-IV
Combination-1	EQ-I	EQ-II	EQ-III	EQ-IVa
Combination-2	EQ-I	EQ-II	EQ-III	EQ-IVb
Combination-3	0.22EQ-III	(-) 0.50EQ-III	EQ-III	(-) 1.5EQ-III
Combination-4	0.15EQ-IVb	(-) 0.33EQ-IVb	0.67EQ-IVb	EQ-IVb

Table 4.3. List of ground motions selected for the performance-based seismic evaluation of precast jointed wall systems

Identification of the Input Motion	Earthquake Intensity	Earthquake Name (Year) and Station	Magnitude	Direction of Component	Scale Factor	PGA after multiplying by the Scale Factor (g)
IM-a	EQ-I	Morgan Hill (1984); Station: Gilory # 6, San Ysidro Microwave	6.1 (M_s)	East-West	0.65	0.19
IM-b	EQ-II	Loma Prieta (1989); Station: Saratoga Aloha Avenue	7.1 (M_s)	North-South	0.64	0.32
IM-c	EQ-III	Northridge (1994); Station: Castaic Old Ridge Route	6.8 (M_s)	East-West	1.30	0.67
IM-d	EQ-III	Imperial valley (1940); Station: Elcentro	7.2 (M_s)	North-South	1.50	0.48
IM-e	EQ-III	Kobe-Japan (1995); Station: KJM	6.9 (M_w)	East-West	1.10	0.66
IM-f	EQ-IV	Tabas-Iran (1978)	7.4 (M_s)	344 degrees from North	1.00	0.93
IM-g	EQ-IV	Chi-Chi-Taiwan (1999); Station: CHY	7.6 (M_s)	80 degrees from North	0.95	0.86
IM-h	EQ-IV	Kobe-Japan (1995); Station: KJM	6.9 (M_w)	North-South	1.18	0.97

PGA = Peak Ground Acceleration, M_s = Surface Wave Magnitude, M_w = Moment Magnitude
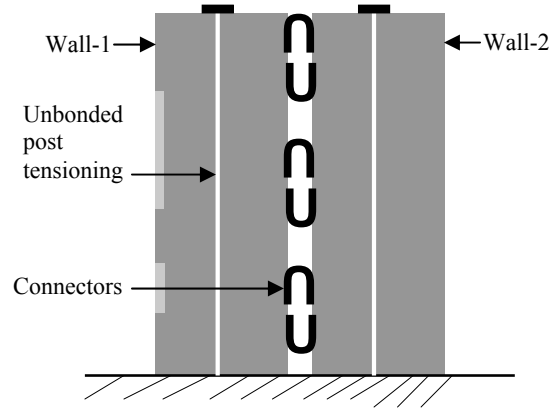
Figure 4.1.   Illustration of an unbonded post tensioning jointed wall system
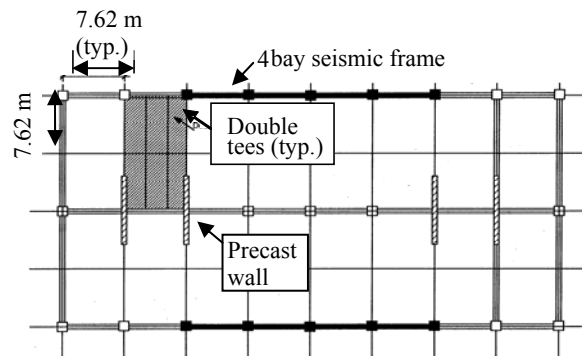
Figure 4.2.   Plan view of the precast concrete prototype building (Nakaki et al. 1999)
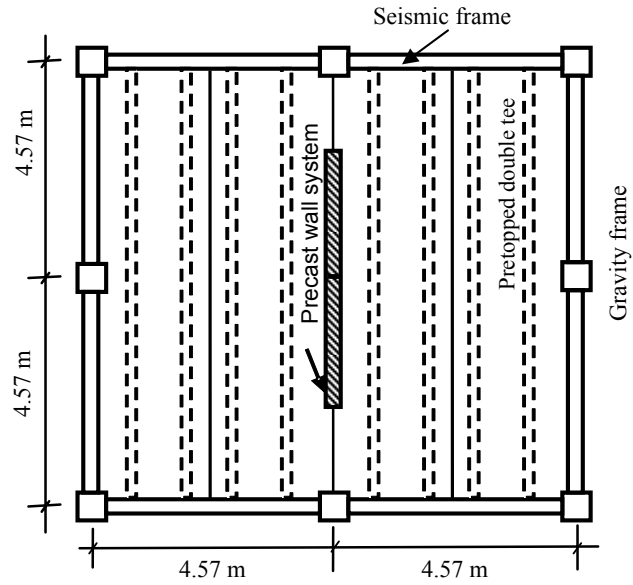
Figure 4.3.   Plan view of the scaled post-tensioned precast wall system building

Figure 4.4.   The PRESSS test building after erecting the jointed wall system
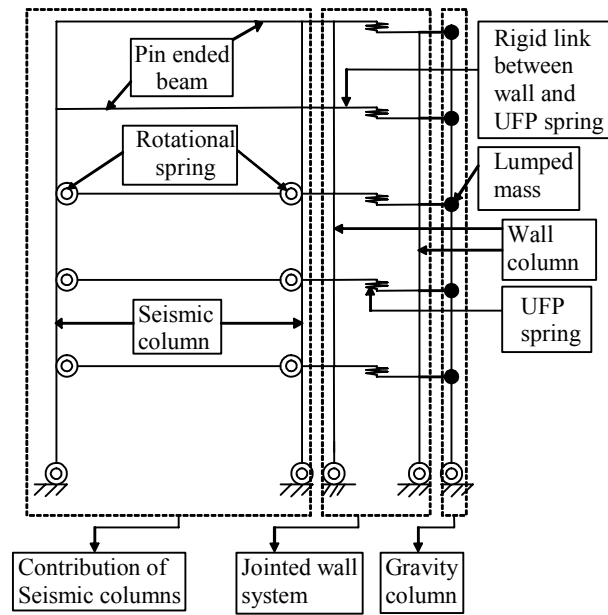
Figure 4.5.   Proposed analytical model for the building with the jointed wall system shown in Fig. 4.3
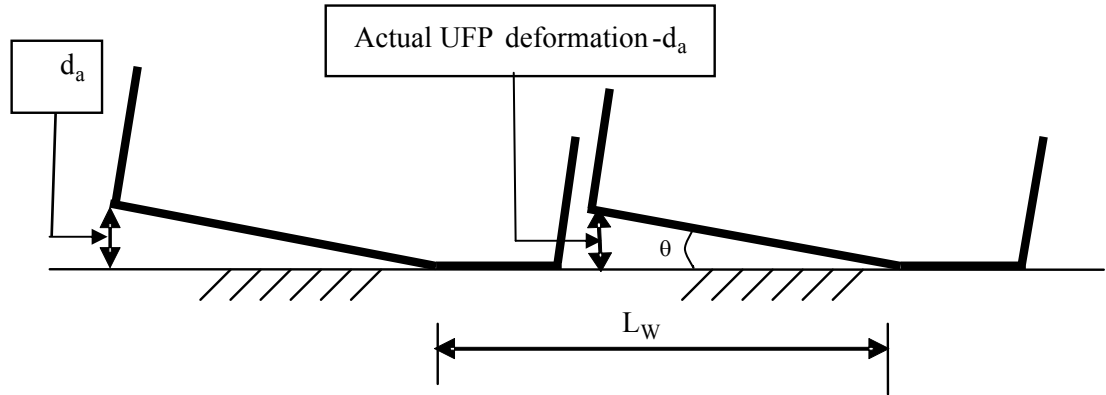
Figure 4.6.　Illustration of rotations of walls and the corresponding UFP deformation at a base rotation of θ
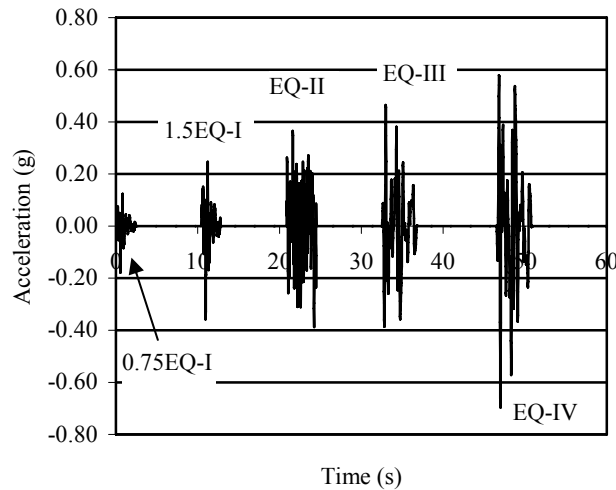
Figure 4.7.　Short-duration earthquake ground motions used for testing of the PRESSS building in the jointed wall direction
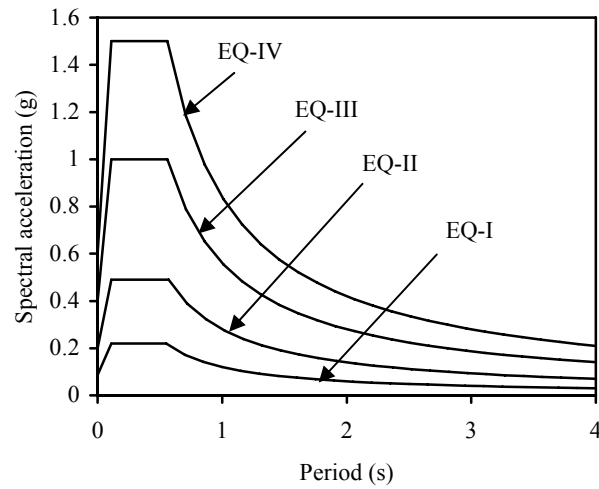
Figure 4.8. The 5% damped multiple-level acceleration response spectra suggested for soil type Sc in high seismic zone as per the Performance-Based Seismic Engineering Ad Hoc Subcommittee (2003) of SEAOC
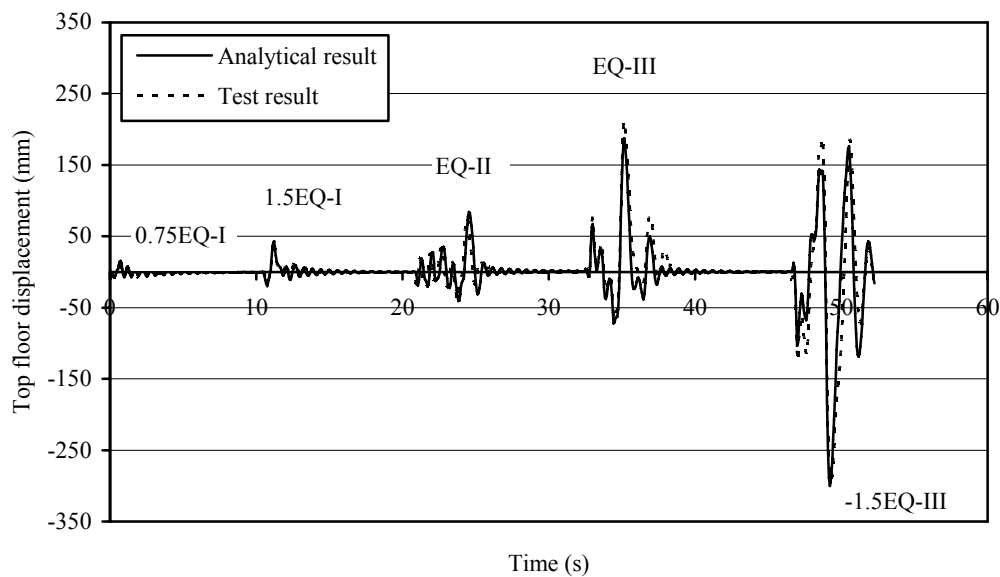
Figure 4.9. Comparison between the analytical and experimental lateral displacement at the fifth floor of the PRESSS test building in the jointed wall direction
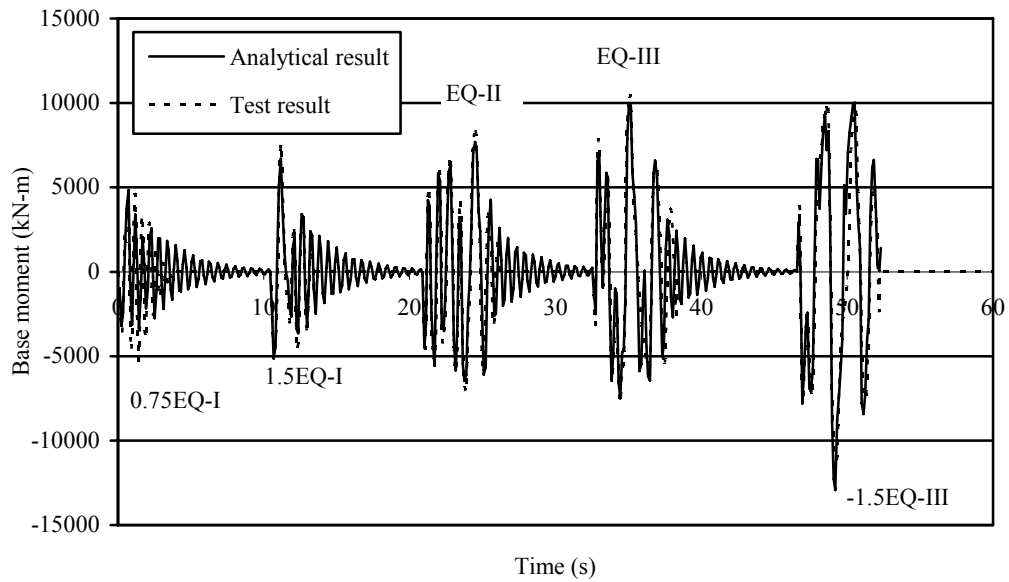
Figure 4.10.   Comparison between the analytical and experimental base moment of the PRESSS

test building in the jointed wall direction
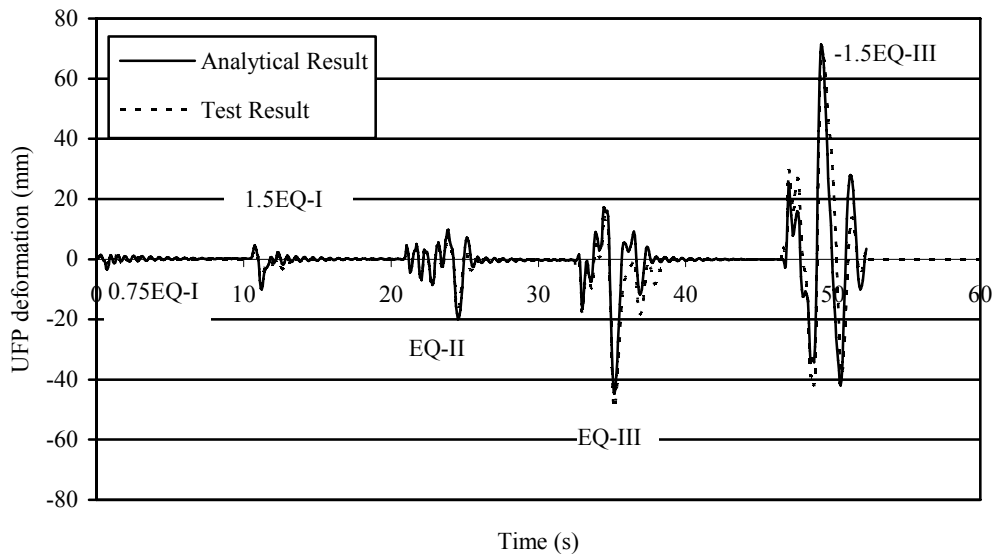
Figure 4.11.   Comparison between the analytical and experimental UFP deformatin at the fifth

floor of the PRESSS test building in the jointed wall direction

144
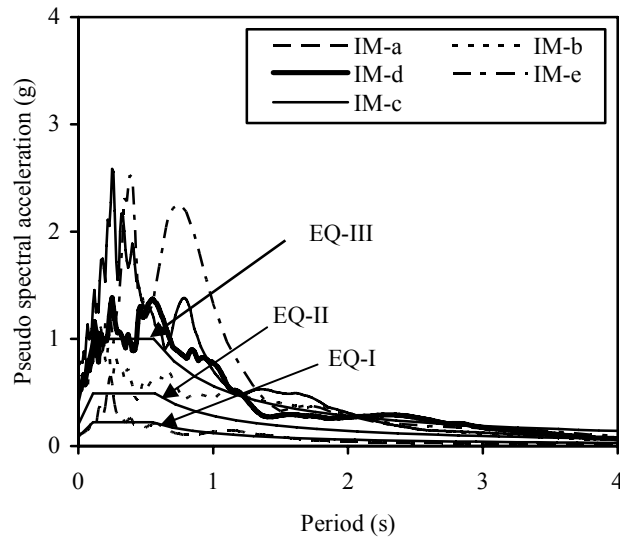
Figure 4.12 (a).　The 5% damped acceleration response spectra of EQ-I, EQ-II and EQ-III with those produced for scaled ground motions IM-a through IM-e listed in Table 4.3
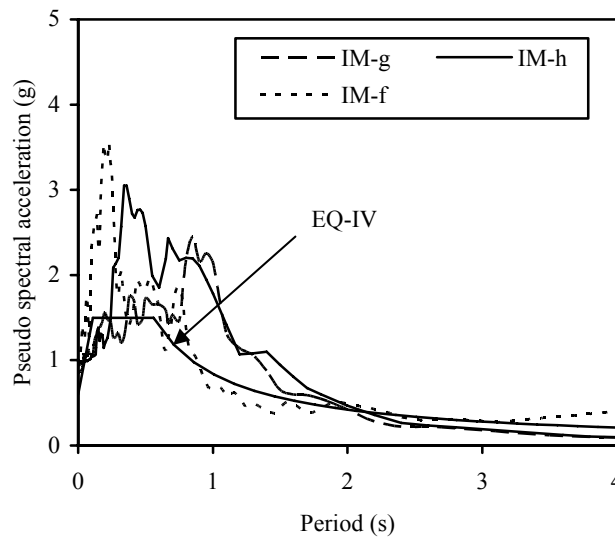
Figure 4.12 (b).　The 5% damped acceleration response spectra of EQ-IV with those produced for scaled ground motions IM-f through IM-h listed in Table 4.3
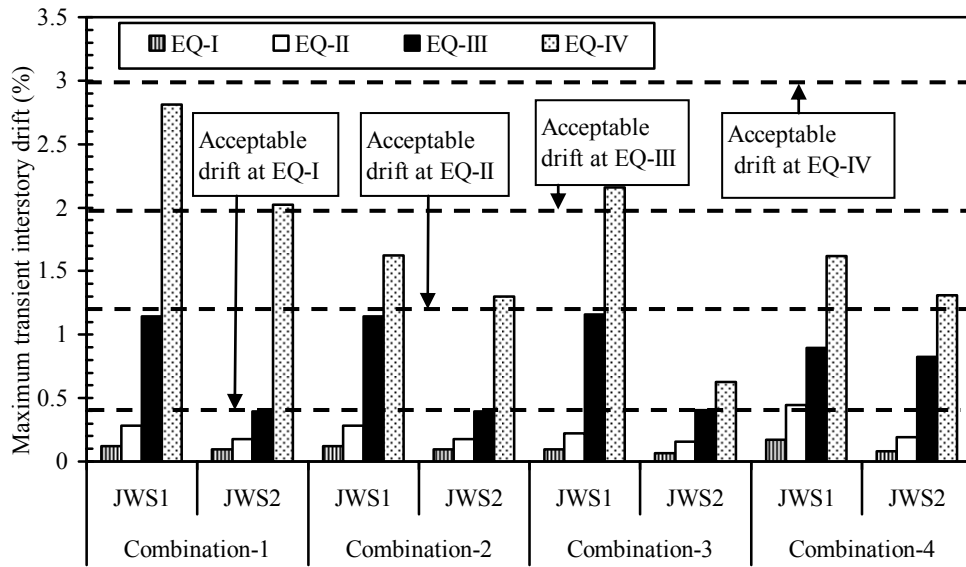
Figure 4.13.   The maximum transient interstory drifts obtained for JWS1 (DDBD) and JWS2 (FBD) when subjected to various combinations of short-duration ground motions summarized in Table 4.2
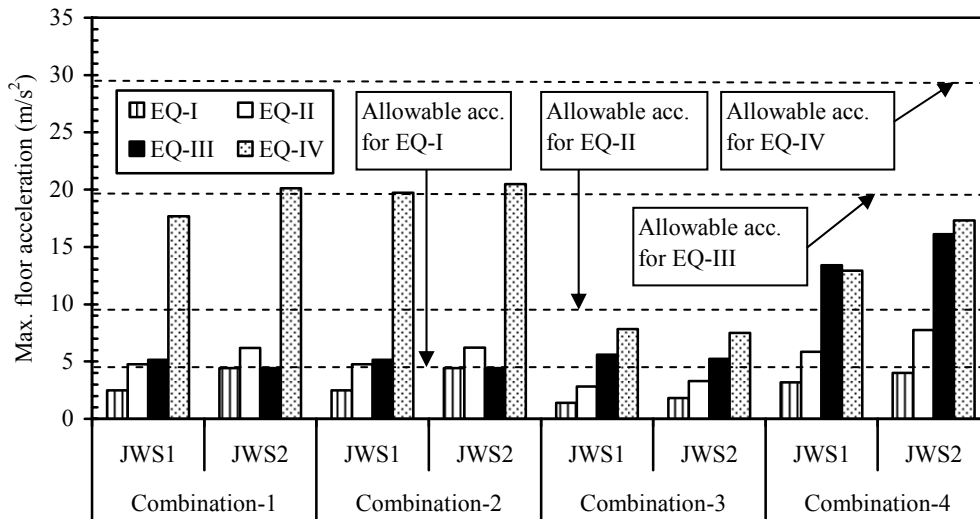
Figure 4.14.   The maximum floor accelerations obtained for JW1 (DDBD) and JW2 (FBD) when subjected to various combinations of short-duration ground motions summarized in Table 4.2
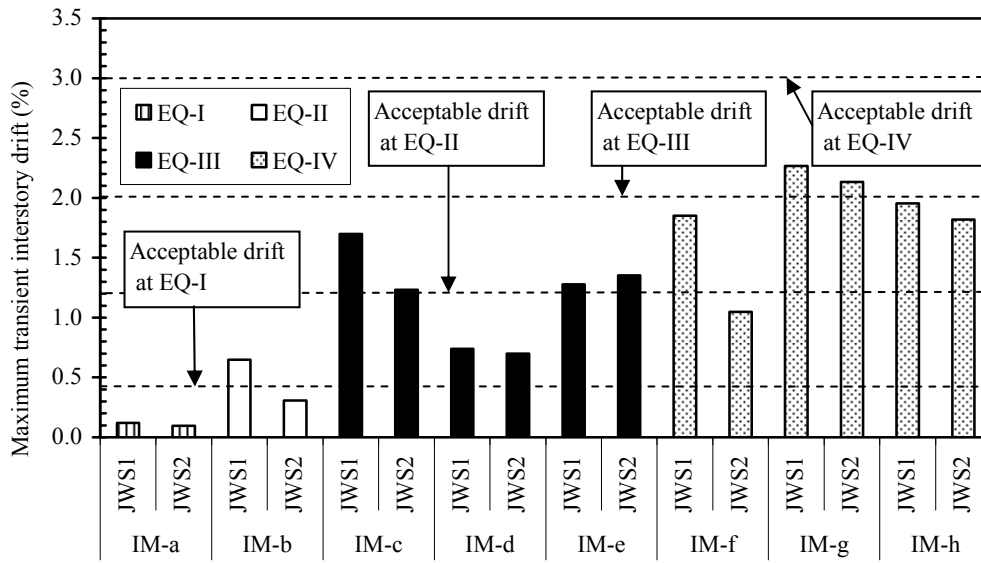
Figure 4.15.   The maximum transient interstory drifts obtained for JWS1 (DDBD) and JWS2 (FBD) when subjected to various long-duration ground motions summarized in Table 4.3
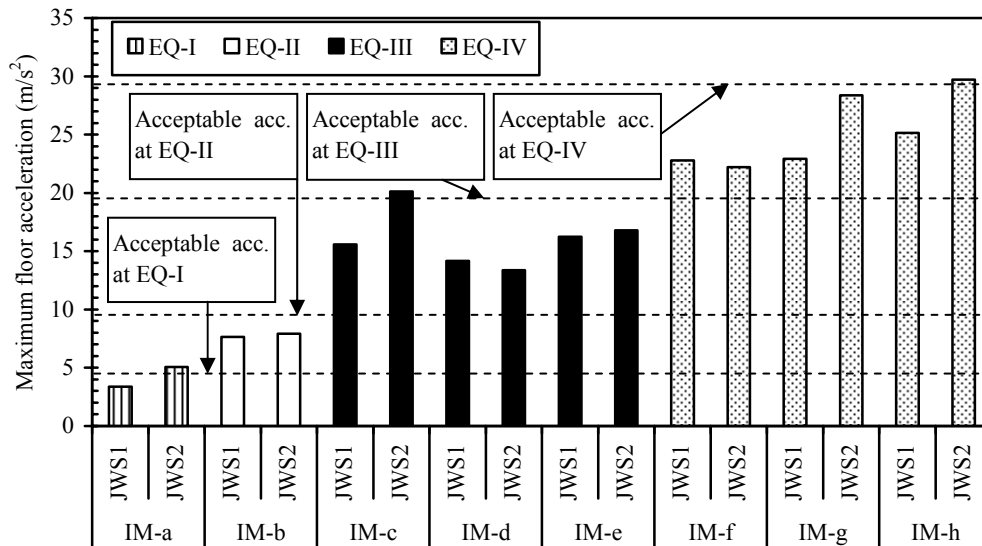
Figure 4.16.   The maximum floor accelerations obtained for JWS1 (DDBD) and JWS2 (FBD) when subjected to various long-duration ground motions summarized in Table 4.3
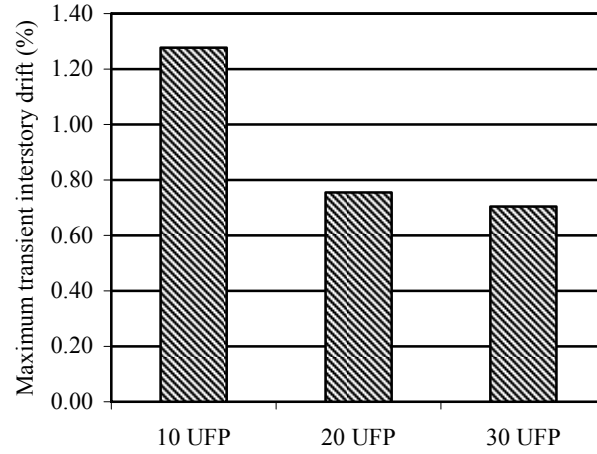
Figure 4.17 (a).   Illustration of the influence of the number of UFP connectors on the maximum transient interstory drift of JWS1 using input motion IM-d
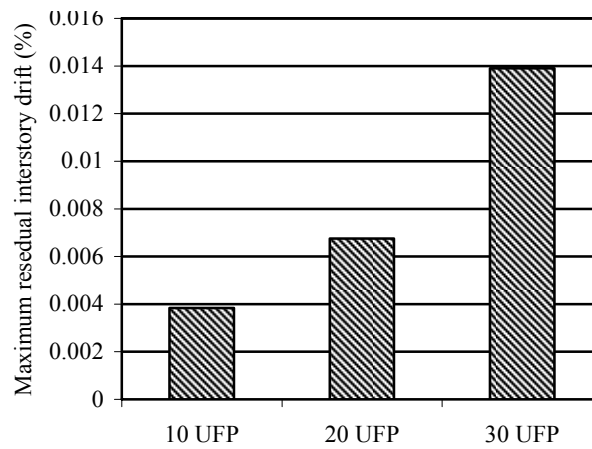
Figure 4.17 (b).   Illustration of the influence of the number of UFP connectors on the maximum residual interstory drift of JWS1 using input motion IM-d
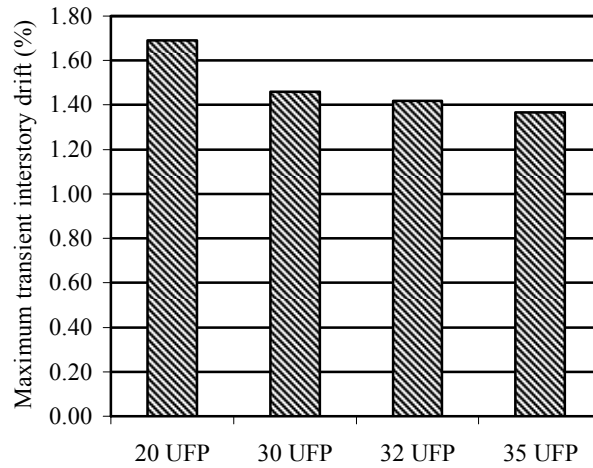
Figure 4.18 (a).   Illustration of the influence of the number of UFP connectors on the maximum
transient interstory drift of JWS1 using input motion IM-c
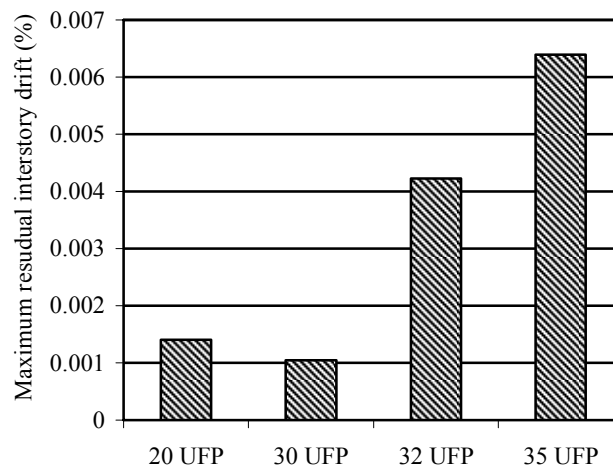
Figure 4.18 (b).   Illustration of the influence of the number of UFP connectors on the maximum
residual interstory drift of JWS1 using input motion IM-c

CHAPTER 5. SEISMIC RESPONSE OF PRECAST POST-TENSIONED JOINTED WALL SYSTEMS DESIGN FOR LOW TO MID-RISE BUILDINGS USING THE DIRECT DISPLACEMENT-BASED APPROACH

M. Ataur Rahman[1] and Sri Sritharan[2]

ABSTRACT

This paper presents an investigation on the seismic performance of precast post-tensioned jointed wall systems designed for a five, seven and ten story building using the direct displacement-based design approach. Using earthquake motions of different intensities, the performance of the buildings was evaluated using response parameters such as the maximum transient interstory drift, floor acceleration and residual interstory drift. The three buildings performed satisfactorily in terms of the maximum transient interstory drift and residual interstory drift. The maximum floor accelerations exceeded the acceptable limits in some analysis of the seven and ten story buildings and thus a strategy to control floor accelerations in these buildings is suggested by modifying the wall dimensions. It was identified that low-rise building achieved transient interstory drifts closer to the acceptable limits compared to the taller building. An opposite trend was observed regarding floor acceleration. In taller jointed wall systems, the average interstory drift of the building was less sensitive to the increase in the maximum interstory drift compared to that in a low-rise jointed wall system.

[1]PhD Candidate, Department of Civil, Construction and Environmental Engineering, e-mail: ataur70@iastate.edu, Iowa State University, Ames, IA 50011, USA
[2]Associate Professor, Department of Civil, Construction and Environmental Engineering, e-mail: sri@iastate.edu, tel.: 515-294-5238, fax:515-294-7424, Iowa State University, Ames, IA 50011, USA

5.1 INTRODUCTION

Precast concrete wall systems have shown to be an excellent choice for designing earthquake resistant buildings, which benefits from the quality and cost-efficiency of prefabrication. A concept for a precast unbonded post-tensioned concrete wall system has been investigated in consideration of its potential benefits over an emulative precast concrete wall for seismic applications (Priestley et al. 1999; Thomas 2003; Thomas and Sritharan 2004). In this jointed wall system, individual precast walls are secured to the foundation using unbonded prestress tendons running from the top of the wall to the foundation. Shear connectors distributed vertically along the height connects two or more walls together horizontally as shown in Fig. 5.1. The use of unbonded post-tensioning allows the walls to rock individually at the base and minimizes the residual displacements of the wall system when subjected to earthquake lateral loading by providing a restoring force (Priestley et al. 1999; Thomas and Sritharan 2004). In addition, the prestress contributes to the overturning moment resistance and transfer of shear forces at the wall bases, where the shear transfer is ensured based on a friction mechanism. Hysteretic energy dissipation for the wall system is primarily provided by the connectors placed between the walls.

Design base shear of jointed precast wall systems may be established by using two different methods. The first approach is the traditional force-based design (FBD) method as recommended in design codes such as the Uiniform Building Code (UBC) (1997) and the International Building Code (IBC) (2000). In this approach, the design base shear is obtained from the estimated fundamental period of the structure in the elastic region and the total seismic mass, while incorporating the influence of seismic intensity in terms of a design

spectral acceleration. The target lateral displacement of the building is not used in quantifying the design base shear. The second approach is the direct displacement-based design (DDBD) method, which uses a target displacement that is selected to ensure the expected performance of the building when establishing the design base shear. In this approach, the base shear is determined using an effective period for the fundamental mode and seismic intensity in terms of a design spectral displacement representing design-level earthquakes (Priestley 2002). By representing the expected hysteretic energy dissipation with equivalent viscous damping, the effective period is established using an effective mass for the fundamental mode of the building, which is determined based on an assumed displacement profile for this mode. The effective period is used to determine the effective stiffness of the building. Finally, the design base shear is calculated by multiplying the equivalent target displacement and effective stiffness. More detailed presentation of the DDBD method proposed specifically for prestressed structural systems may be found in Priestley (2002).

Using acceptance criteria defined in terms of interstory drift, residual drift, and floor acceleration, a multiple-level performance-based seismic evaluation was conducted on a FBD and DDBD solution for a five-story precast unbonded post-tensioned jointed wall system (Rahman and Sritharan 2006). This study was motivated to exploit the economical benefit of the DDBD for the design of jointed precast wall systems because the design base shear derived for the wall system using DDBD was 50% less than that obtained from the FBD method, although the jointed wall systems designed by both FBD and DDBD methods exhibited acceptable seismic performance. The economical benefit of DDBD method for

designing post-tensioned jointed wall systems is the motivation for the research of the present paper.

The objective of the study presented herein is to evaluate the seismic performance of jointed precast post-tensioned wall systems designed for low to mid-rise buildings using the DDBD approach. For practical construction constraints and in accordance with the current precast industry practice, the height of building is limited to ten stories. Consequently, the focus of the study was on five, seven and ten story jointed wall systems and their performance evaluation under multiple level earthquakes in terms of the maximum transient interstory drift, floor acceleration and residual interstory drift

5.2 UNBONDED POST TENSIONING PRECAST WALL SYSTEMS IN FIVE, SEVEN AND TEN STORY BUILDINGS

The plan view of the three prototype precast concrete buildings is shown in Figure 5.2. A 60% scale model of the five-story building was designed, built and tested in the PRESSS program to verify the conceptual viability of using unbonded post tensioning precast wall systems under multiple levels short-duration seismic input motions (Nakaki et al. 1999; Priestley et al. 1999; Sritharan 2002). Thus the chosen plan view ensured manifestation of constructible precast concrete buildings.

As identified in Fig. 5.2, four jointed wall systems are used to resist lateral seismic forces in the transverse direction of each building. Each wall system is comprised of two precast walls that are secured to the foundation using unbonded post-tensioning bars located at the centroidal axis. The walls are connected horizontally by U-shaped stainless steel flexural plates known as UFP connectors. Expected structural responses and construction details of

UFP connectors may be found elsewhere (Galusha 1999; Nakaki et al. 1999; Thomas and Sritharan et al. 2007). The jointed wall systems for five, seven and ten story buildings were designed by following the design methodology presented in (Aaleti 2005) for a target inter story design drift of 2% to satisfy the specifications of ITG 5.1-XX (2006), Seismology Committee (1999) and Performance-Based Seismic Engineering Ad Hoc Subcommittee (2003) of the Structural Engineers Association of California (SEAOC)). Design base shear forces for the three buildings were calculated using DDBD method for high seismic zone defined by the Performance-Based Seismic Engineering Ad Hoc Subcommittee (2003) of SEAOC, assuming very dense soil or rock with shear wave velocity in the range of 366 m/s to 762 m/s identified as Site Class C in IBC (2000).

Table 5.1 shows design base shear force calculated by FBD and DDBD methods. Design base shear force calculated by FBD method (IBC 2000) for one jointed wall system in five and ten story buildings were 4819 kN and 7089 kN, respectively. In contrast, DDBD method resulted in significantly lower amount of design base shear i.e., 2409 kN and 4565 kN for the five and ten story buildings, respectively. It appears that the design base shear force was reduced by 50% and 36% for the five and ten story buildings, respectively, by choosing DDBD method instead of FBD method. Such substantial reduction in base shear force obtained by using DDBD method will result in an economical solution for constructing the structures.

5.3 DYNAMIC ANALYSIS MODELS

In an earlier study (Rahman and Sritharan 2006), a 2-D analysis model for a jointed precast wall system was developed for the wall system of the PRESSS test building using the non-

linear finite element computer program RAUMOKO (Carr 2003). The adequacy of the model was validated using the PRESSS test data. Therefore, a similar procedure was followed to establish the analysis models of the five, seven and ten story jointed wall systems.

Figure 5.3 illustrates the analytical model of the jointed wall system for the ten-story building, where each wall system comprised of two unbonded post-tensioned precast walls. These walls were represented in the model using elastic beam-column elements positioned at the wall centerlines. The moment-rotation behavior of each unbonded post-tensioned wall was represented by a non-linear elastic rotational spring at the base of the beam-column element. Although there were fifty three UFP connectors positioned between the two unbonded walls, their combined effect was concentrated at the floor level using ten identical non-linear inelastic shear springs along the height of the walls. These springs were connected to rigid beam-column elements extending from the centerline of each wall towards the centerline of the jointed wall system as seen in Figure 5.3. Figure 5.4 illustrates idealized non-linear elastic moment-rotation and non-linear inelastic force-displacement hysteric behavior of rotational and axial springs representing rotational and displacement resistance capacities of post-tensioned walls and UFP shear connectors, respectively. A beam-column element per floor was added to the right side of the jointed wall system model to account for the effect of the gravity columns (see Figure 5.3). Seismic mass of the building, lumped at all ten floor levels, was assigned to the nodes of the elements modeling the gravity columns. A similar procedure was followed to develop the analytical models for the five and seven story jointed wall system buildings.

Properties of various elements, used in the analytical model, were derived based on their material properties and geometric dimensions, which are included in Table 5.2. Since each wall in the jointed system was expected to undergo negligible damage with inelastic actions concentrated at the wall base, the walls in the analytical model were represented by elastic beam-column elements with their stiffness based on their gross section properties. Each wall element was connected to the foundation using an elastic bi-linear rotational spring to model the flexural resistance of the wall at the base and the corresponding concentrated crack opening at this location. Moment-rotation behavior of the rotational springs, which were found by analyzing the individual response of the walls under monotonic loading using the procedure recommended in (Aaleti 2005), are reported in Table 5.2. This procedure is indentical to that used for an earlier model and validated using experimental data in Rahman and Sritharan (2006).

5.4 PERFORMANCE-BASED SEISMIC EVALUATION

Seismic performance of the five, seven and ten-story jointed wall system buildings designed using DDBD was evaluated using four levels of earthquake intensities, namely EQ-1, EQ-II, EQ-III and EQ-IV (see Fig. 5.5). These intensity levels representing different earthquake hazard were proposed by the Performance-Based Seismic Engineering Ad Hoc Subcommittee (2003) of the Structural Engineers Association of California (SEAOC) such that EQ-III represents the design-level earthquake ground motions, whereas EQ-IV, which is equivalent to 1.5 times EQ-III, corresponds to the maximum considered earthquakes. According to the performance-based seismic design concept presented by the SEAOC Seismology Committee (1999), ordinary buildings with conventional structural systems when

subjected to ground motions compatible with EQ-I, EQ-II, EQ-III and EQ-IV may be expected to produce operational, occupiable, life safety and near collapse performances for both structural and non-structural components. The precast jointed wall systems were expected to meet the same performance levels at the minimum.

The acceptable performance of the joined wall systems was determined by comparing the maximum values of the transient interstory drift, residual interstory drift and floor acceleration against the permissible values. The permissible values for the transient interstory drifts and residual interstory drifts were defined in accordance with the recommendations of Seismology Committee (1999) and ITG 5.1-XX (2006.), whereas the acceptable floor accelerations were defined using an IBC (2000) recommendation for the design of non-structural components. Details of the earthquake input ground motions and the permissible values of the parameters defining the building performance are presented below.

5.5 INPUT GROUND MOTIONS

The five, seven and ten story jointed wall system buildings were evaluated by using two sets of earthquake input motions. The first set consisted of eight long-duration scaled input motions recorded in past earthquakes, while the second set consisted of four combinations of short-duration spectrum compatible earthquake motions. The motivation for using the second set of input motions was that it followed the procedure adopted for the pseudodynamic testing of the PRESSS building (Sritharan et al. 1999) and provided an opportunity to examine the validity of using short-duration input motions in performance-based seismic testing of structural systems.

Table 5.3 provides details of eight scaled long-duration input motions used for evaluating the performance of the jointed wall systems. The originals of these input motions were recorded at free field stations of soil profile type S_C as defined in UBC 1997. All original recorded motions were scaled as detailed in Table 5.3 such that their spectra would be comparable to the target spectra following the procedure presented in (Rahman and Sritharan 2007). More detail information about these ground motions along with the depiction of the acceleration response spectra for all modified long-duration ground motions may be found in (Rahman and Sritharan 2007).

Table 5.4 lists different combinations of short-duration ground motions used in the seismic evaluation of the jointed wall systems, which were performed using each combination of records as one sequence with zero accelerations for a duration of twenty five seconds between the records. This procedure enabled the free vibration response of the jointed wall systems to be examined after subjecting them to each earthquake segment. The original motions used to create the short-duration spectrum compatible ground motions of 1.5EQ-I, EQ-II, EQ-III, EQ-IVa and EQ-IVb were recorded at stations with soil profile type S_C in the 1974 Hollister, 1971 San Fernando, 1940 Imperial Valley, 1993 Northridge and 1978 Tabas earthquakes, respectively. More descriptions of the input records and the process used for creating the short-duration input motions may be found in refs. (Sritharan et al. 1999; Sritharan et al. 2002; Rahman and Sritharan 2007).

5.6 INTER STORY DRIFT LIMITS

To evaluate the joined wall system performance at the four earthquake intensity levels, the following inter story drift limits were used as permissible limits: maximum transient

interstory drifts of 0.4% (EQ-I), 1.2% (EQ-II), 2.0% (EQ-III) and 3.0% (EQ-IV); and maximum residual interstory drifts of 0.1% (EQ-I), 0.3% (EQ-II), 0.5% (EQ-III) and 0.75% (EQ-IV). These limits were those recommended by Rahman and Sritharan (2006) based on the guidance given in the SEAOC Blue Book (Seismology Committee 1999), ITG 5.1-XX (2006) and considering the re-centering nature of the jointed wall systems.

5.7 FLOOR ACCELERATION LIMITS

The permissible floor accelerations for the jointed wall system buildings were established to limit earthquake damage to non-structural elements, which may be anchored to the floors. These limits were derived in Rahman and Sritharan (2007) using the recommendations of Tong et al. (2004) and the IBC (2000) provision for estimating design forces required to anchor different types of non-structural elements to building floors under seismic condition. A controlling parameter of these floor acceleration limits is the spectral acceleration corresponding to a short period that is used to define the design response acceleration spectrum (IBC 2000). Accordingly, the permissible limits of the floor accelerations are 2.60 m/s^2 (EQ-I), 5.77 m/s^2 (EQ-II), 11.79 m/s^2 (EQ-III) and 17.68 m/s^2 (EQ-IV).

5.8 ANALYSIS RESULTS

Figures 5.6(a), (b) and (c) depict the deflected shapes of the five, seven and ten story jointed wall systems for the long-duration earthquake motions that produced the maximum interstory drift in each intensity level. The five story wall system shows a linear increase in floor displacement as the floor height increases for all four levels of ground motions. This trend changes to a nonlinear variation as the number of story in the wall system increases. For example, the ten story wall system exhibits a linear increase in lateral floor displacement

with height for the EQ-I ground motion. However, this trend changes to a nonlinear shape, increasing the interstory drift with story height for EQ-II through EQ-IV ground motions. Although less pronounced, observations similar to those observed for the ten-story wall system can be seen in the response of the seven story wall system. Two conclusions drawn from these figures are that: 1) the fundamental mode of response controlled the maximum floor displacements in all three buildings, and 2) the contribution of the flexural response of the walls in the jointed system increased with respect to the lateral displacement induced by the rotation at the base of walls as the number of story in the wall system increased.

As the earthquake intensity increased from EQ-I to EQ-II, from EQ-II to EQ-III, and from EQ-III to EQ-IV, displacements at all floors were amplified by 186%, 200% and 10% in the seven story building, by 305%, 160% and 13% in the five story building, respectively (see Figs. 5.6(a) and (b)). Due to the aforementioned elevation of earthquake intensity, the ten story building experienced the amplifications of floor displacements by 201%, 171% and 64% (see Fig. 5.6(c)). The five and seven story buildings experienced as much as 12-20 times higher levels of rate of increase in floor displacement due to elevation of ground motion from EQ-II to EQ-III compared to that as a consequence of elevation of ground motion in the range of EQ-III - EQ-IV. In contrast, the ten story building demonstrated only 2.67 times higher level of rate of increase in floor displacement due to elevation of ground motion from EQ-II to EQ-III compared to elevation of ground motion in the range of EQ-III - EQ-IV. It seems that abruptness of difference in floor displacement due to increase of ground motion in the range of EQ-II to EQ-III and EQ-III to EQ-IV depletes in buildings having higher heights like ten stories. In addition, for a common floor level in all of the three buildings, taller

building demonstrated lower floor displacement consistently for all four levels of ground motions EQ-I through EQ-IV.

Figure 5.7 shows correlations between average drift and the maximum interstory drift for the five, seven and ten story buildings. These correlations were established based on lateral floor displacements of the three buildings obtained by using eight long-duration ground motions. In all cases, it is seen that the relationship between the maximum interstory drift and average drift can be characterized using a linear function. Furthermore, both the average and the maximum interstory drifts are less for the ten story wall system than the five and seven story wall systems . For a given value of the maximum interstory drift, the average interstory drift reduces with increasing height of the wall system. It also appears that in taller jointed wall systems, the average interstory drift of the building is less sensitive to the increase in the maximum interstory drift compared to that in a low-rise jointed wall system. The correlation between the maximum interstory drift and average drift will be helpful for designing jointed wall system by providing a trend to obtain the maximum interstory drift for an average interstory drift.

Figures 5.8(a), (b) and (c) represent the maximum interstory drifts obtained for the five, seven and ten story jointed wall system buildings when subjected to the long-duration ground motions. In each case, the building interstory drifts were less than the acceptable limits for all four levels of earthquakes. Furthermore, it was found that as the building height increased, the ratio between the maximum transient drift to the acceptable limit generally reduced. These observations suggest that a) the design base shear established for the low to mid-rise

jointed wall systems buildings based on DDBD is adequate, and b) further reduction to the design base shear is possible for the mid-rise buildings.

The differences in the maximum transient interstory drifts obtained between buildings for the same event were more pronounced at large earthquake intensities. For the design level ground motions (i.e., for EQ-III events), the five story building produced the maximum transient interstory drift in the range of 0.74% – 1.7%, whereas the ten story building exhibited the maximum transient interstory drift in the range of 0.37% – 0.85%. These drift ratios indicate that the five story jointed wall system building experienced about twice the maximum transient drifts experienced by the ten-story building. At EQ-IV events, the corresponding ranges for the maximum transient drifts were 1.85% – 2.27% and 0.62% – 0.76%, respectively, exhibiting a factor of almost three between the two building responses. However, for EQ-I and EQ-II input motions, the ten story building experienced the maximum transient interstory drifts of 0.11% and 0.34%, which compared 0.12% and 0.65% for the five story jointed wall system building.

Tables 5.5 presents the maximum residual interstory drifts achieved by all three jointed wall system buildings. The re-centering capability provided by unbonded post-tensioning enabled the buildings to produce insignificant amount of residual interstory drifts after subjecting to earthquakes of all intensities.

Figures 5.9(a), (b) and (c) depict the maximum floor accelerations obtained for the five, seven and ten story jointed wall system buildings when subjected to the long-duration ground motions. The maximum floor accelerations obtained for the five story building were within the permissible limits, ensuring safety of non structural components of the building at all four

levels of earthquakes. For the seven story building, the floor acceleration limits satisfied for all ground motions except for IM-c and IM-a. A similar trend was observed for the ten story building with an additional violation of the acceptable limit for the IM-h ground motion representing an EQ-IV event. These observations, which suggest that taller jointed wall systems designed based on DDBD has a higher tendency to violate the acceptable limits of floor accelerations, are consistent with an earlier finding that the design base shear obtained for the seven and ten story building could be reduced so that they can produce larger transient drifts and smaller floor accelerations.

Due to the design level ground motions of earthquake level EQ-III, the five story building showed the maximum floor acceleration in the range of 8.50 m/s^2 - 9.76 m/s^2, whereas the ten story building exhibited the maximum floor acceleration in the range of 10.56 m/s^2 - 17.06 m/s^2. Thus, the moderately high building, comprised of ten stories, experienced as much as 74.80% and as low as 24.23% higher value of the maximum floor acceleration compared to the low rise building, comprised of five stories, under design level ground motions. However, for EQ-I, EQ-II and EQ-IV, the moderately high (ten story) building showed the maximum floor acceleration of 2.85 m/s^2, 5.31 m/s^2 and 15.36 m/s^2 - 19.87 m/s^2 and the low rise (five story) building demonstrated the maximum floor acceleration of 2.03 m/s^2, 4.56 m/s^2 and 13.67 m/s^2 - 15.10 m/s^2, respectively. It shows that the moderately high building exhibited 40.40%, 16 .45% and 12.36% - 31.60% higher level of the maximum floor acceleration compared to the low rise building when subjected to long-duration ground motions of earthquake levels EQ-I, EQ-II and EQ-IV. In addition, the dependency of the building responses on frequency continents of the input earthquake was also emphasized by the analyses results. For example, at EQ-III level, the difference in responses of the ten and five

story buildings for the maximum floor acceleration subjected by IM-c was 82.26%, whereas the corresponding difference was only 24.23% for IM-d, although both of these ground motions were chosen to represent EQ-III level ground motions.

Traditionally, short duration ground motions are used in experimental research. Therefore, the present study also investigated the performance of the jointed wall system buildings under short-duration spectrum compatible ground motions representing EQ-I to EQ-IV events. Figures 5.10(a), (b) and (c) depict the maximum transient interstory drift of the five, seven and ten story jointed wall system buildings when subjected to the four combinations of short-duration ground motions. All three buildings showed satisfactory performance in terms of the maximum transient interstory drift with sufficient margin of safety with respect to their permissible limits. Short-duration ground motions from combination-2 were chosen to compare the transient interstory drift and floor acceleration performance of the buildings under short and long-duration ground motions. Generally, short-duration ground motions resulted lower values of the maximum transient interstory drift compared to long duration motions for all of the three buildings except for the EQ-I level short-duration ground motion in the seven and five story buildings where both short and long-duration ground motions created identical transient interstory drift. The largest differences between the maximum transient interstory drift due to long and short-duration motions were 116.77%, 173.31% and 2.62% for the ten story building; 48.79%, 91.71% and 135.89% for the seven story building; 129.80%, 48.47% and 39.65% for the five story building when subjected to EQ-II, EQ-III and EQ-IV level ground motions, respectively. It shows that this difference was increased consistently with taller building for design level ground motion.

Figures 5.11(a), (b) (c) show the maximum floor accelerations resulted from for the five, seven and ten story jointed wall system buildings under the short-duration ground motions. The floor accelerations obtained for all three buildings were satisfactory. Comparing Figs. 5.11(a), (b) and (c) with Figs. 5.9(a), (b) and (c) revealed that long-duration ground motions resulted in higher floor accelerations than the short-duration ground motions. The largest differences in the maximum floor accelerations obtained between the long and short-duration ground motions were 43.5%, 22.4%, 274% and 40.5% for the ten story building; 13.4%, 40.7% and 166.3% and 22% for the seven story building; 35.6%, 59.7%, 215.2% and 27.7% for the five story building when subjected by EQ-I, EQ-II, EQ-III and EQ-IV level ground motions, respectively, with the largest different being for the EQ-III level earthquakes. Therefore, it appears that subjecting the building to realistic long duration motions are necessary to obtain the maximum transient interstory drifts and floor accelerations and that use of short-duration ground motions may underestimate these parameters sometimes by a significant amount.

Figures 5.12 shows the maximum transient interstory drift at four levels of long-duration ground motions normalized by the respective allowable limits of interstory drift, in the five, seven and ten story buildings. The largest achievement in transient interstory drifts were 30%, 54%, 85% and 76% of the associated acceptable limit for the five story building when subjected by EQ-I, EQ-II, EQ-III and EQ-IV level ground motions, respectively. These achievements were 34%, 34%, 59% and 77% for the seven story building, and 27%, 29%, 43% and 25% for the ten story building. Figure 5.13 represents the maximum floor acceleration at four levels of long-duration ground motions, normalized by the respective allowable limits of floor acceleration, in the three buildings. The largest attainment in floor

acceleration were recorded as 78%, 79%, 83% and 85% of the associated acceptable limit for the five story building when subjected by EQ-I, EQ-II, EQ-III and EQ-IV level ground motions, respectively. However, the achievements in floor acceleration were 129%, 91%, 90% - 112% and 80% - 99% for the seven story building, and 110%, 92%, 90% - 145% and 87% - 112% for the ten story building.

To ensure the protection against damage to nonstructural elements in jointed wall system building, keeping the floor acceleration within the acceptable limit is essential. To address this issue, the highest level of violation of the maximum floor acceleration limit which was observed in the ten story building, was chosen to resolve by decreasing the moment of inertia of the walls through decreasing the thickness of the walls resulting in a more flexible structure. Figures 5.14 and 5.15 show that the maximum floor acceleration was consistently reduced due to the reduction of moment of inertia of the walls in the ten story building subjected to ground motions IM-h and IM-c. Figure 5.14 shows that reduction in moment of inertia of walls by 10% helped the building to achieve the maximum floor acceleration lower than the acceptable limit under ground motion IM-h. Similarly, for IM-c, reduction of moment of inertia of walls by 40% led the building to satisfy acceptable limit of floor acceleration (see Fig. 5.15). The maximum transient interstory drifts and residual interstory drifts were also within the acceptable limits after the aforementioned modification of the walls.

5.9 CONCLUSIONS

Seismic performances of low to mid-rise post-tensioned jointed wall system buildings designed by the direct displacement-based design approach were analytically investigated in

this paper. Using a validated analytical modeling procedure, the five, seven and ten story post-tensioned jointed wall system buildings with an identical plan view were subjected to long and short-duration earthquake input motions having acceleration response spectra representative of four levels of earthquake intensities. Using the analysis results the following conclusions were drawn:

(1) All three jointed wall systems designed for low to mid-rise buildings deflected predominantly by the fundamental mode. For a common floor level, taller building exhibited less floor displacement compared to low-rise building.

(2) The sensitivity of the average drift to the increase of the maximum interstory drift was reduced in jointed wall systems as the number of story in the building increased. For a given value of the maximum transient interstory drift, taller building exhibited lower average drift.

(3) Irrespective of the height, all of the three buildings demonstrated satisfactory performance in terms of the maximum transient interstory drift when subjected to both short and long-duration ground motions representing the four levels of earthquake intensities.

(4) The maximum transient interstory drift was reduced for taller buildings. The difference in capacity, to resist interstory drift, between the tallest (ten story) and smallest (five story) buildings increased with the elevation of intensity of ground motions.

(5)   The re-centering capacity of the unbonded post-tensioning bars enabled the buildings to produce negligible amount of residual interstory drifts after subjecting them to both the long and short-duration ground motions.

(6)   For all long-duration ground motions, the five-story building showed lower values of the maximum floor accelerations compared to the respective acceptable limits for four levels of earthquakes. But, the seven and ten-story buildings violated the limits for few ground motions. Generally, the values of the maximum floor acceleration increased for taller buildings.

(7)   Short-duration ground motions generated smaller values of the maximum transient interstory drift and floor accelerations compared to long-duration ground motions. It appears that it is necessary to use actual-long duration ground motions for analyzing the real full scale buildings to avoid the possibility of under estimating transient interstory drift and floor acceleration.

(8)   For short-duration ground motions, all three buildings performed satisfactorily in terms of allowable floor acceleration.

(9)   Low-rise building tends to achieve the maximum transient interstory drifts closer to the acceptable limits compared to the taller building. Taller building has stronger tendency to approach and exceed unity of normalized floor acceleration compared to low-rise building.

(10)   By making necessary modification in the precast wall dimension of jointed wall system as recommended in this paper, the maximum floor acceleration of taller buildings may be brought to acceptable limit.

(11)   Based on the satisfactory performance of the jointed wall systems designed by direct displacement-based design that led to lower base shear (Rahman and Sritharan 2006; Rahman and Sritharan 2007), it appears that this design method would result in a more economical design than the traditional force-based design method.

5.10 ACKNOWLEDGEMENTS

5.11 REFERENCES

Aaleti, S., 2005. Design and analysis of unbonded post-tensioned precast wall systems, M.S. Thesis, Department of Civil, Construction and Environmental Engineering, Iowa State University, Ames, Iowa, USA.

Carr, A. J., 2003. *RUAUMOKO - Inelastic Dynamic Analysis Program*. University of Canterbury, Christchurch, New Zealand.

Conley, J., Sritharan, S., and Priestley, M. J. N., 2002. Precast Seismic Structural Systems PRESSS-3: The Five-Story Precast Test Building, Vol. 3-1: Wall Direction Response, Report Number: SSRP-99/19, University of California, San Diego, California, USA.

Galusha, J. G., 1999. Precast, Post-tensioned Concrete Walls Designed to Rock, M.S. Thesis, Department of Civil Engineering, University of Washington, Seattle, Washington, USA.

International Building Code (IBC), 2000. *International Code Council*, Virginia, USA, 331-377.

ITG 5.1-XX, 2006. Acceptance criteria for special unbonded post-tensioned structural walls based on validation testing, *American Concrete Institute*.

Kurama, Y., Sause, R., Pessiki, S., and Lu, L., 2002. Seismic response evaluation of unbonded post-tensioned precast walls, *ACI Structural Journal*, September-October, **99 (5),** 641-651.

Kurama, Y., Pessiki, S., Sause, R., and Lu, L., 1999a. Lateral load behavior and seismic design of unbonded post-tensioned precast concrete walls, *ACI Structural Journal*, July-August, **96 (4),** 622-632.

Kurama, Y., Pessiki, S., Sause, R., and Lu, L., 1999b. Seismic behavior and design of unbonded post-tensioned precast concrete walls, *PCI Journal*, May-June, **44 (3),** 72-88.

Nakaki, S. D., Stanton, J. F., and Sritharan, S., 1999. An overview of the PRESSS five-story precast test building, *PCI Journal*, **44(2),** 26-39.

Performance-Based Seismic Engineering Ad Hoc Subcommittee, 2003. Revised Interim Guidelines: Performance-Based Seismic Engineering for the SEAOC Blue Book, Structural Engineers Association of California, California, USA, 128-132.

Priestley, M. J. N., 2002. Direct displacement-based design of precast/prestressed concrete buildings, *PCI Journal,* **47 (6),** 67-79.

Priestley, M. J. N., Sritharan, S., Conley, J., R., and Pampanin, S., 1999. Preliminary results and conclusions from the PRESSS five-story precast concrete test building, *PCI Journal*, **44 (6),** 42-67.

Priestley, M. J. N., Tao, J. R, 1993. Seismic response of prestressed concrete frames with partially debonded tendons, *PCI Journal*, Jan-Feb.

Rahman, M., A., and Sritharan, S., 2007, A performance-based seismic evaluation of two five-story precast concrete hybrid frame buildings, accepted in *ASCE Structural Journal* (in print).

Rahman, M., A., and Sritharan, S., 2006, An evaluation of force-based design vs. direct displacement-based design of jointed precast post-tensioned wall systems, *Earthquake Engineering and Engineering Vibration* **5(2)**, 285-296.

Seismology Committee, 1999. Recommended Lateral Force Requirements and Commentary (Blue Book). Structural Engineers Association of California (SEAOC), California, USA, 327-421.

Sritharan, S., 2002. Performance of four jointed precast frame systems under simulated seismic loading, *Proceedings of the Seventh National Conference on Earthquake Engineering,* Paper No. 264, Boston, USA.

Sritharan, S., Pampanin, S., and Conley, J., 2002. Design Verification, Instrumentation and Test Procedures, PRESSS-3: The Five-Story Precast Test Building, Vol. 3-3. ISU-ERI-Ames Report ERI-03325, Iowa State University, Ames, Iowa, USA.

Thomas, D., J., and Sritharan, S., 2004. An Evaluation of Seismic Design Guidelines Proposed for Precast Jointed Wall Systems, ISU-ERI-Ames Report ERI-04635, Iowa State University, Ames, Iowa, USA, June.

Thomas, D., J., 2003. Analysis and Validation of a Seismic Design Method Proposed for Precast Jointed Wall Systems, M.Sc. Thesis, Department of Civil, Construction and Environmental Engineering, Iowa State University, Ames, Iowa, USA.

Tong, M., Lee, G., Rzhevsky, V., Qi, J., and Shinozuka, M., 2004. A comparison of seismic risk of non-structural systems in a hospital before and after a major structural retrofit,

ATC-29-2 Seminar on Seismic Design, Retrofit, and Performance of Non-structural Components in Critical Situations, <http://shingo8.eng.uci.edu/ATC-29-2.htm, date-11-17-2004>

Uniform Building Code (UBC), 1997. *International Conference of Building Officials*, Whittier, California, USA, **2**, 13-38.

Table 5.1.   Design base shear force calculated by force-based and direct displacement-based methods for low and mid-rise buildings

Story of Buildings	Force-based Design Method (kN)	Direct Displacement-based Design Method (kN)
Five-story	4819	2384
Ten-story	7089	4565

Table 5.2.   Dimensions of the jointed wall systems and the properties of the analytical models shown in Fig. 3 for the five, seven and ten story buildings

Parameter	Value		
	Five-story	**Seven-story**	**Ten-story**
Wall height	19.05 m	26.67 m	38.01 m
Wall length	4.57 m	4.57 m	6.10 m
Wall thickness	337 mm	381mm	381mm
Initial post-tensioning force	1530 kN	2892.54 kN	9096.04 kN
Area of post-tensioning tendons	3838.70 mm^2	5483.86 mm^2	15903.20 mm^2
Yield strength of post-tensioning tendons	827.40 MPa	827.40 MPa	827.40 MPa
Elastic modulus of post-tensioning tendons	200 GPa	200 GPa	200 GPa
Wall concrete strength	41.37 MPa	41.37 MPa	41.37 MPa
Properties of spring modeling moment resistance of a wall at base			
Yield moment	80.50×10^2 kN-m	129.67×102 kN-m	378.22×10^2 kN-m
Elastic rotational stiffness	6.85×10^6 kN-m/rad	11.12×106 kN-m/rad	35.93×10^6 kN-m/rad
Hardening ratio	0.0200	0.0012	0.0095
Properties of spring modeling UFPs at each floor level			
Yield strength	464.55 kN	448.29 kN	615.54 kN
Elastic stiffness	39.42 kN/mm	38.04 kN/mm	52.24 kN/mm
Hardening ratio	0.035	0.035	0.035

Table 5.3.   List of long-duration ground motions selected for the performance-based evaluation of the ten, seven and five story precast jointed wall system buildings

Identification of the Input Motion	Earthquake Intensity	Earthquake Name (Year)	Magnitude	Scale Factor	PGA after multiplying by the Scale Factor (g)
IM-a	EQ-I	Morgan Hill (1984)	6.1 (M_s)	0.65	0.19
IM-b	EQ-II	Loma Prieta (1989)	7.1 (M_s)	0.64	0.32
IM-c	EQ-III	Northridge (1994)	6.8 (M_s)	1.30	0.67
IM-d	EQ-III	Imperial valley (1940)	7.2 (M_s)	1.50	0.48
IM-e	EQ-III	Kobe-Japan (1995)	6.9 (M_w)	1.10	0.66
IM-f	EQ-IV	Tabas-Iran (1978)	7.4 (M_s)	1.00	0.93
IM-g	EQ-IV	Chi-Chi-Taiwan (1999)	7.6 (M_s)	0.95	0.86
IM-h	EQ-IV	Kobe-Japan (1995)	6.9 (M_w)	1.18	0.97

PGA = Peak Ground Acceleration, M_s = Surface Wave Magnitude, M_w = Moment Magnitude

Table 5.4.   List of combinations of short-duration ground motions used for the performance-based evaluation of the ten, seven and five story precast jointed wall system buildings

Idendification of Combinations	Earthquake Intensity			
	Earthquake Level-I	Earthquake Level-II	Earthquake Level-III	Earthquake Level-IV
Combination-1	EQ-I	EQ-II	EQ-III	EQ-IVa
Combination-2	EQ-I	EQ-II	EQ-III	EQ-IVb
Combination-3	0.22EQ-III	(-) 0.50EQ-III	EQ-III	(-) 1.5EQ-III
Combination-4	0.15EQ-IVb	(-) 0.33EQ-IVb	0.67EQ-IVb	EQ-IVb

Table 5.5.   Maximum residual interstory drift of the seven and ten story buildings under long-
duration motions

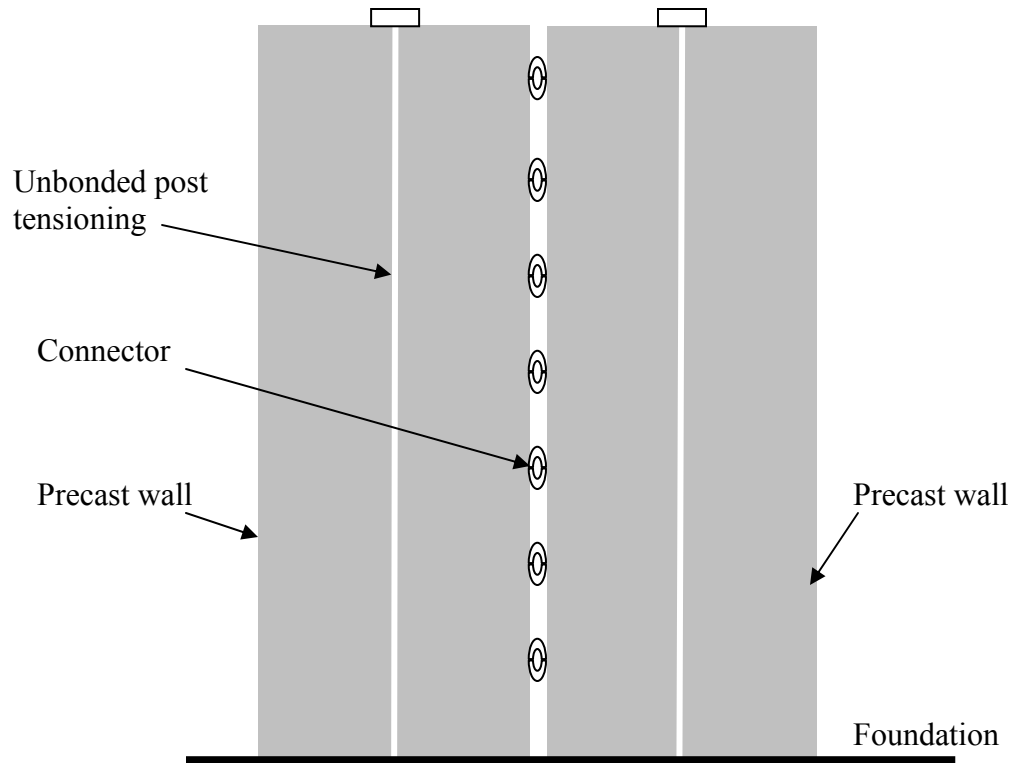| Identification of the Input Motion	Earthquake Intensity	Maximum resedual interstory drift (%)		Acceptable resedual interstory drift (%)
		Ten story	Seven story	
IM-a	EQ-I	0.0113	0.0051	0.10
IM-b	EQ-II	0.0156	0.0083	0.30
IM-c	EQ-III	0.0049	0.0093	0.50
IM-d	EQ-III	0.0236	0.0438	0.50
IM-e	EQ-III	0.0205	0.0197	0.50
IM-f	EQ-IV	0.0237	0.0089	0.75
IM-g	EQ-IV	0.0044	0.0016	0.75
IM-h	EQ-IV	0.0095	0.0021	0.75

Figure 5.1.   Illustration of a unbonded prcast post tensioned jointed wall system
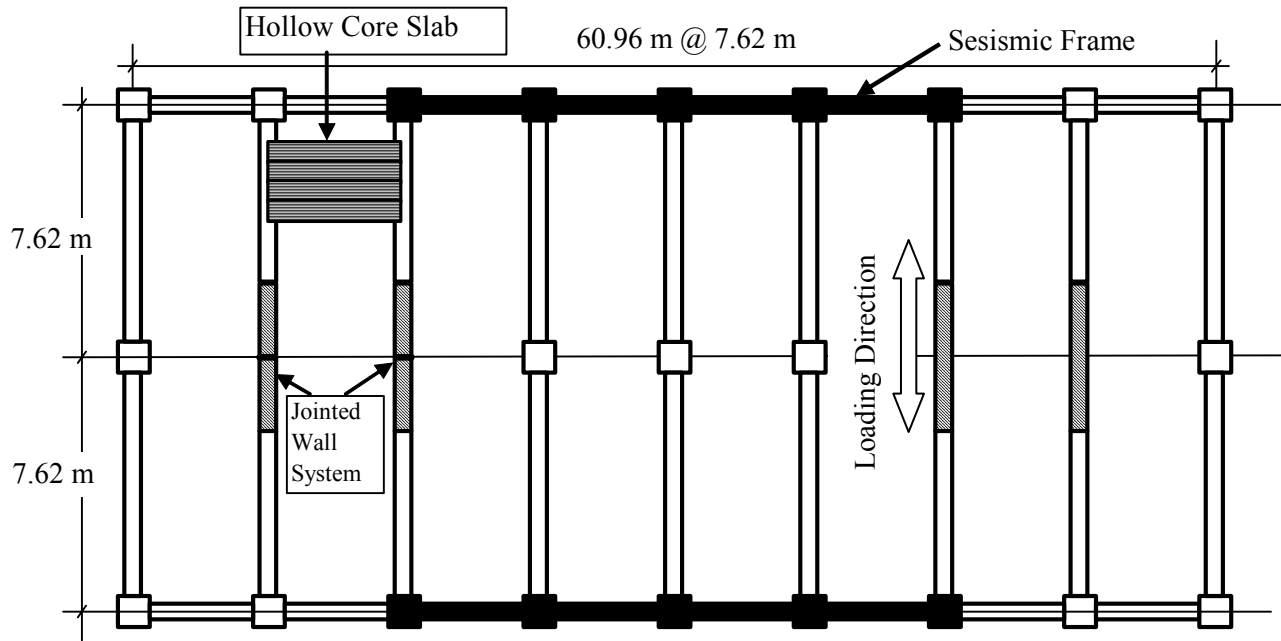
Figure 5.2.   Plan view of the five, seven and ten story prototype buildings
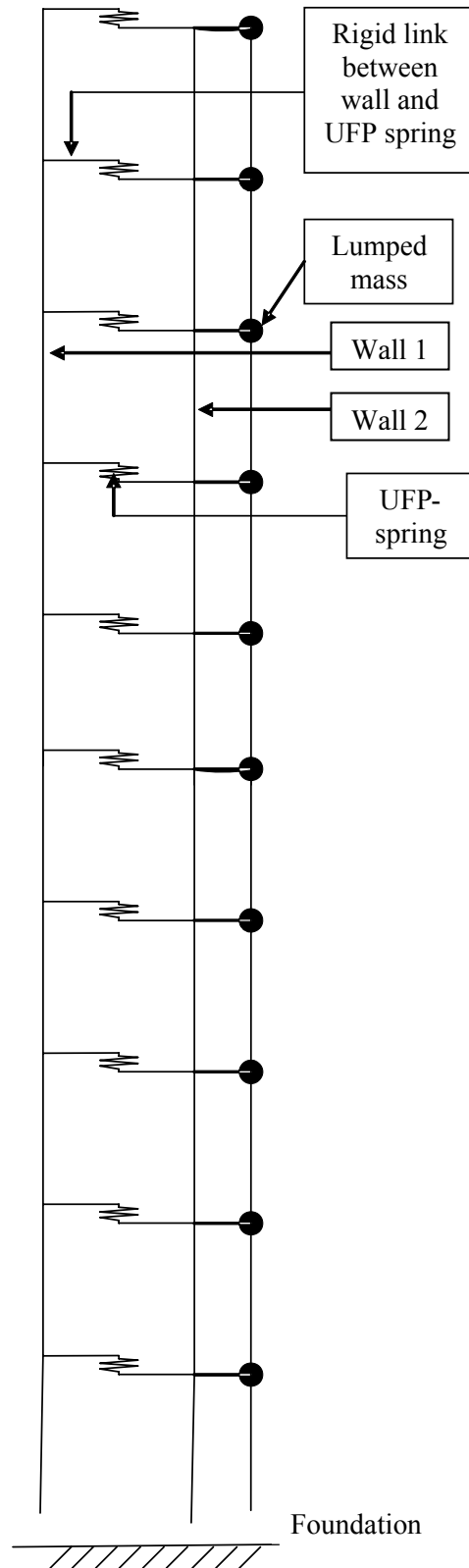
Figure 5.3.   Analytical model of the wall system in the ten story building
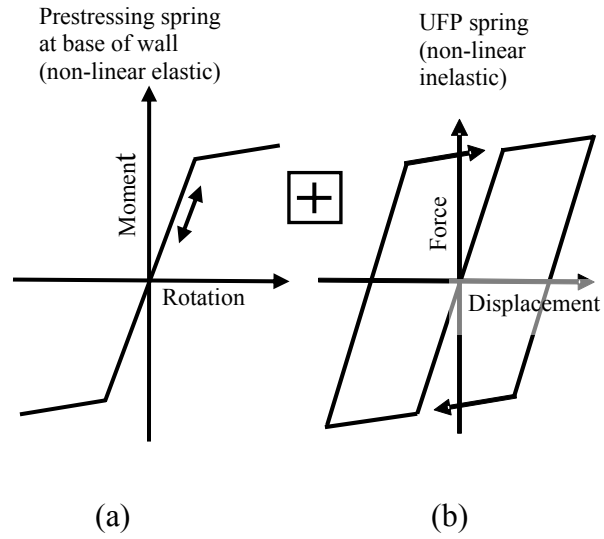
Figure 5.4.   Illustration of typical moment-rotation response of post-tensioning spring located at each

wall base and force-displacement response of UFP spring placed between two walls
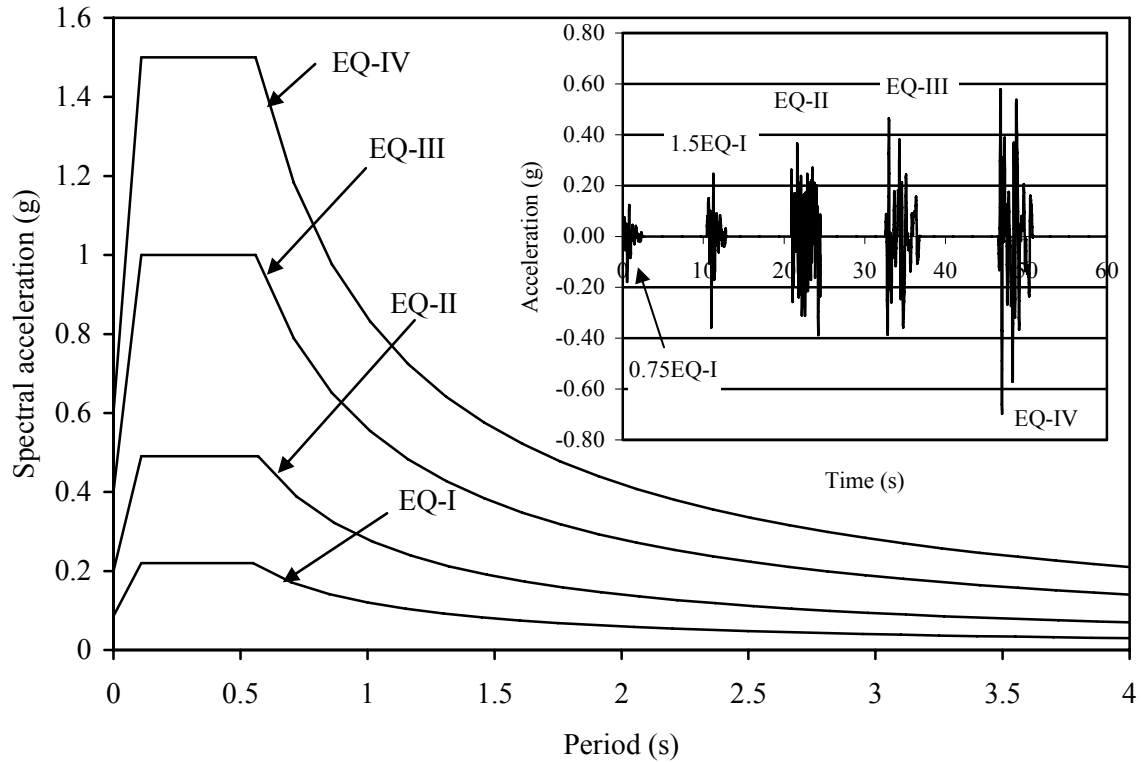
Figure 5.5. The 5% damped multiple-level acceleration response spectra suggested for soil type Sc in high seismic zone as per the Performance-Based Seismic Engineering Ad Hoc Subcommittee (2003) of SEAOC. (The insert in the figure shows short-duration earthquake ground motions used for testing of the PRESSS building in the jointed wall direction.)
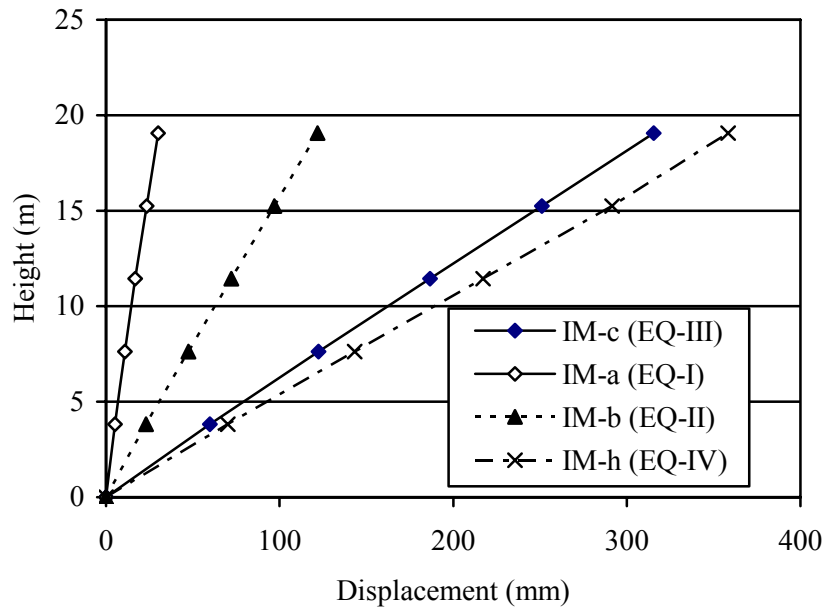
182

Figure 5.6(a).   Deflected shape of the five story building when achieving at the maximum interstory

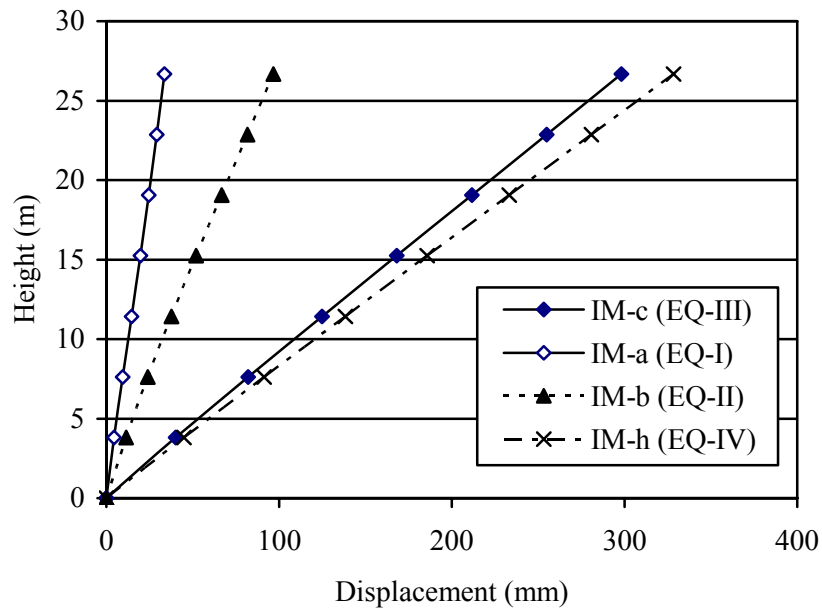drifts imposed by the four levels of ground motions

Figure 5.6(b).   Deflected shape of the seven story building when achieving at the maximum interstory

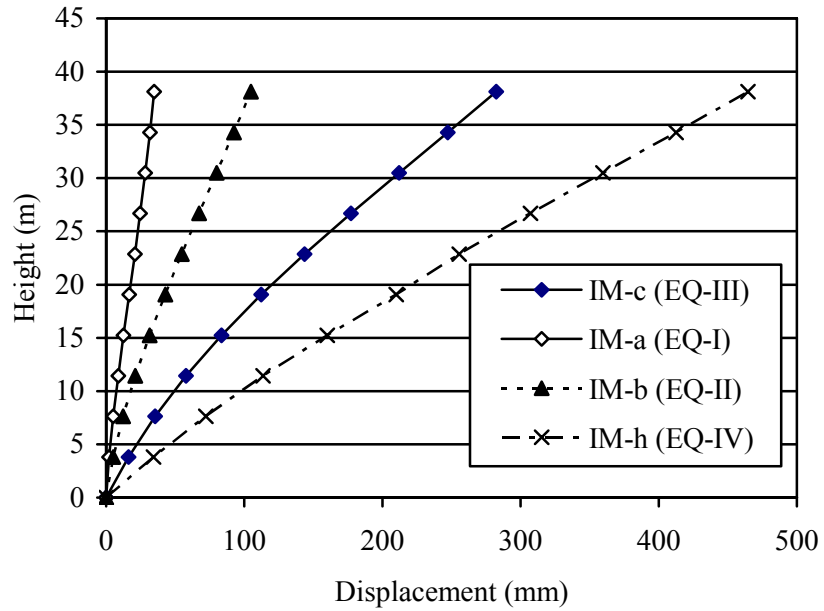drifts imposed by the four levels of ground motions

Figure 5.6(c).   Deflected shape of the ten story building when achieving at the maximum interstory drifts imposed by the four levels of ground motions
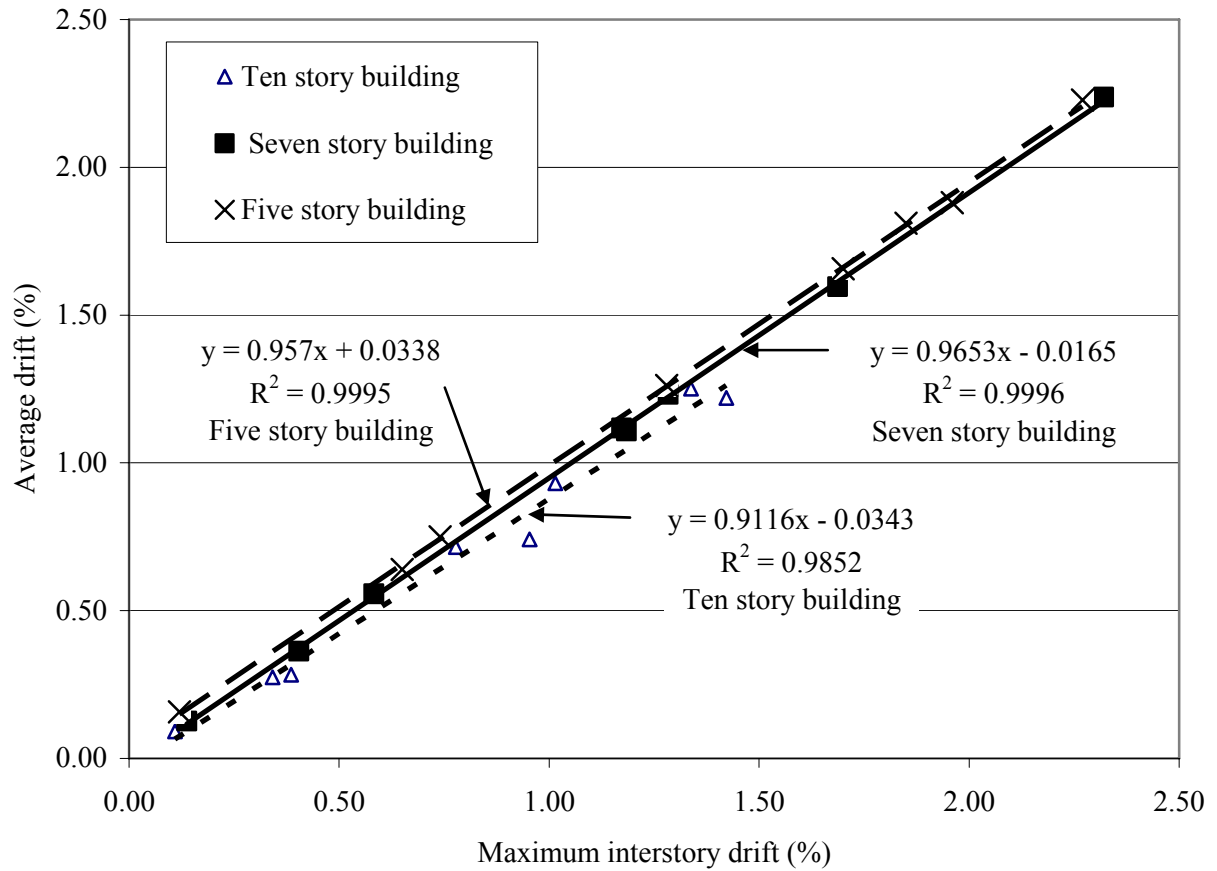
Figure 5.7. Correlation between the average and maximum interstory drifts obtained for the five, seven and ten story post-tensioned jointed wall system based on the responses to long-duration ground motions

Figure 5.8(a). Maximum transient interstory drift obtained for the five story jointed wall system building subjected to the long-duration ground motions

Figure 5.8(b).   Maximum transient interstory drift obtained for the seven story jointed wall system building subjected to the long-duration ground motions

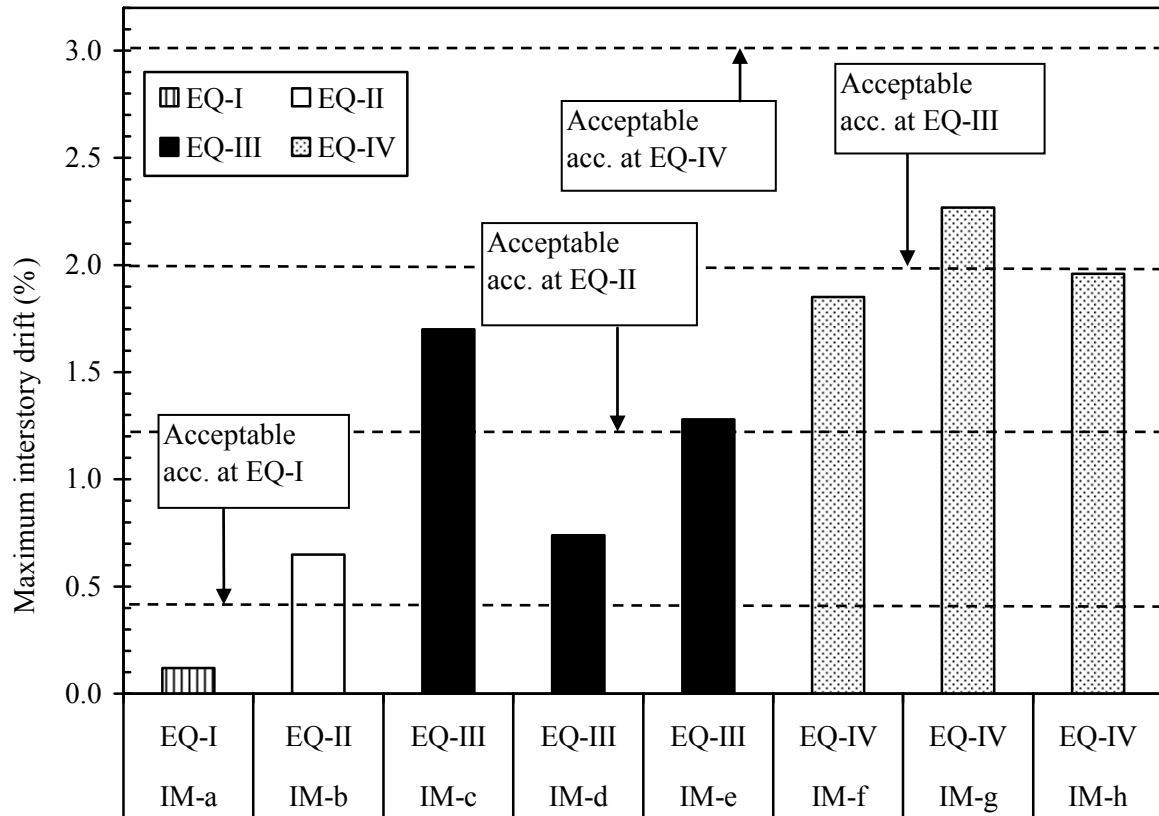Figure 5.8(c).   Maximum transient interstory drift obtained for the ten story jointed wall system building subjected to long-duration ground motions

Figure 5.9(a).   Maximum floor acceleration obtained for the five story jointed wall system building subjected to the long-duration ground motions
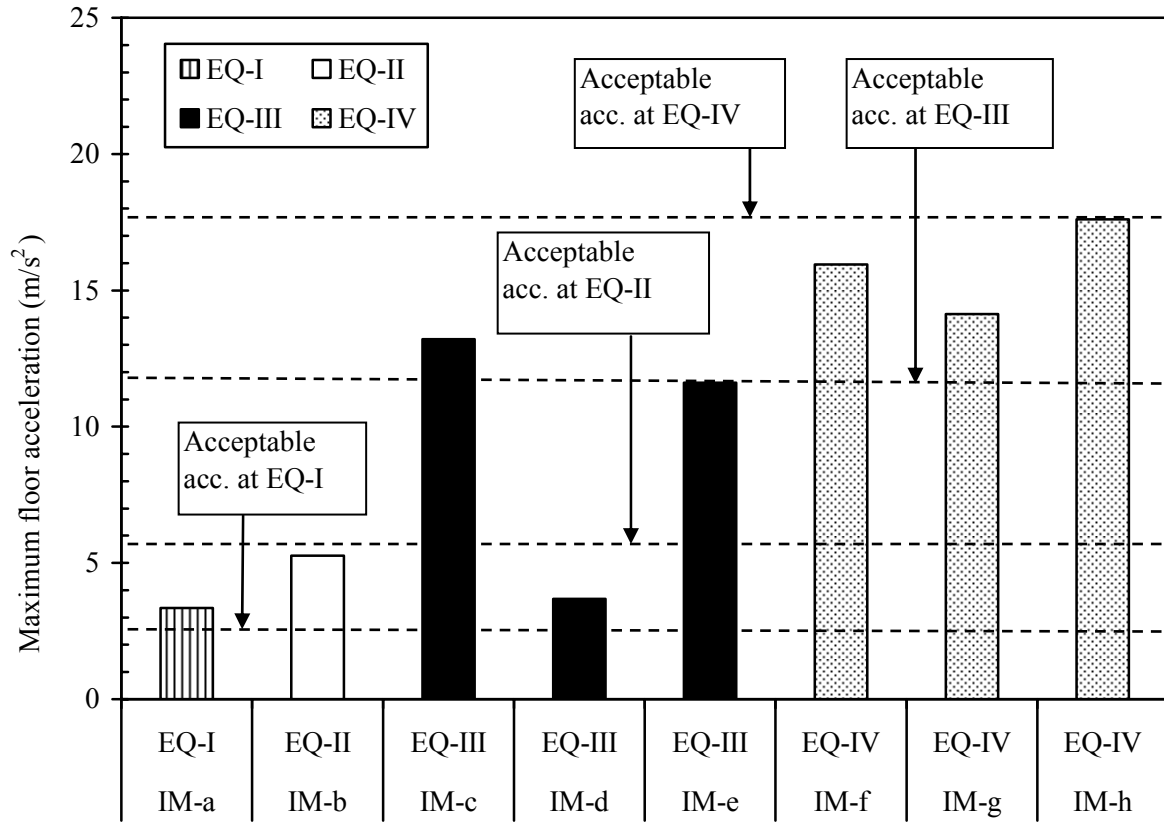
Figure 5.9(b).   Maximum floor acceleration obtained for the seven story jointed wall system building subjected to the long-duration ground motions
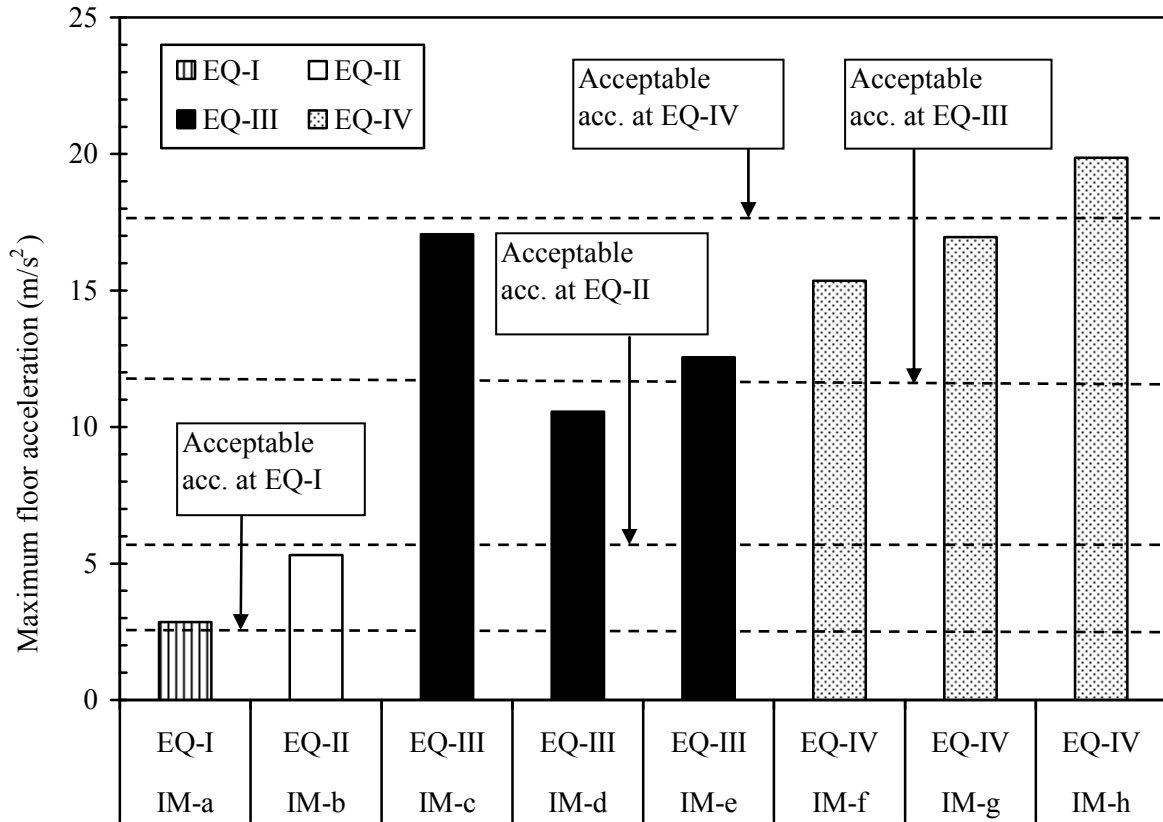
Figure 5.9(c).   Maximum floor acceleration obtained for the ten story jointed wall system building subjected to the long-duration ground motions
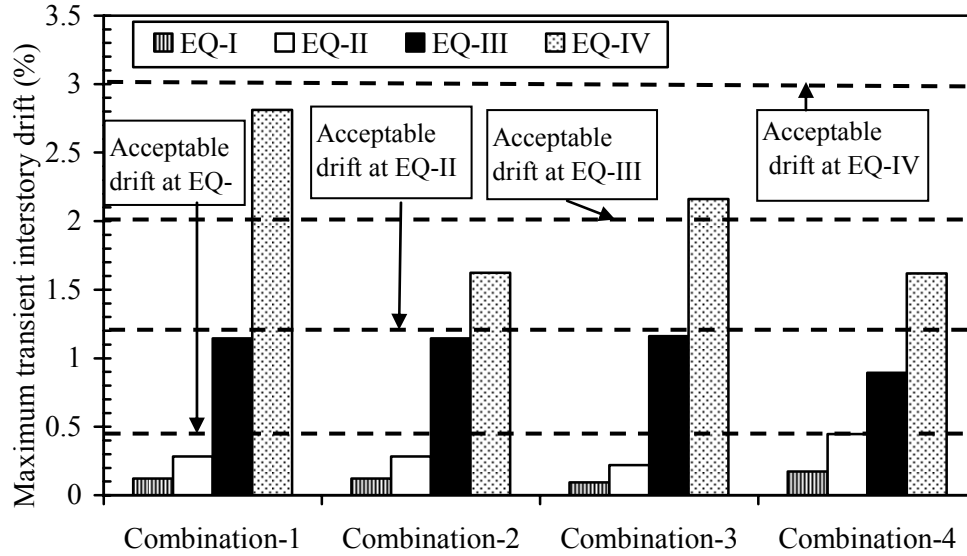
Figure 5.10(a).   Maximum transient interstory drift obtained for the five story building when subjected to short-duration ground motions
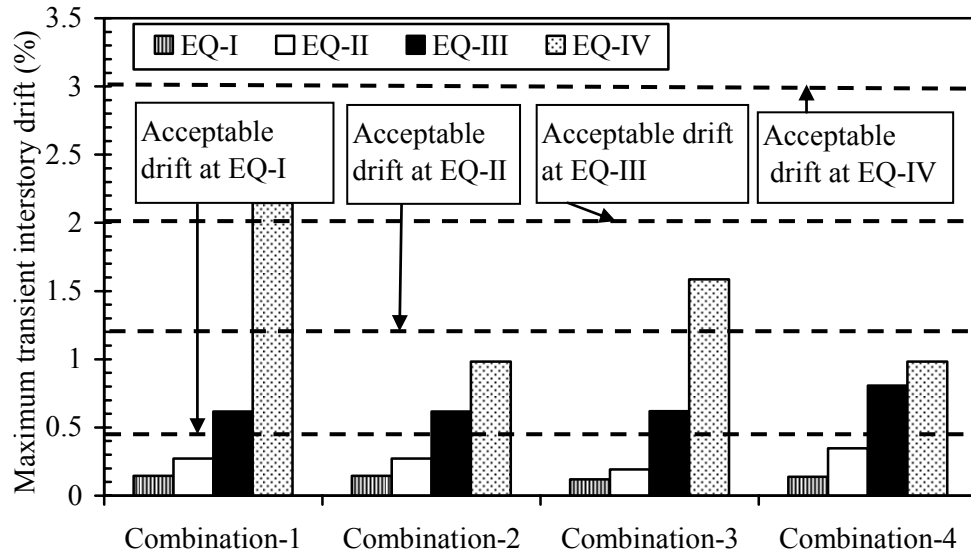
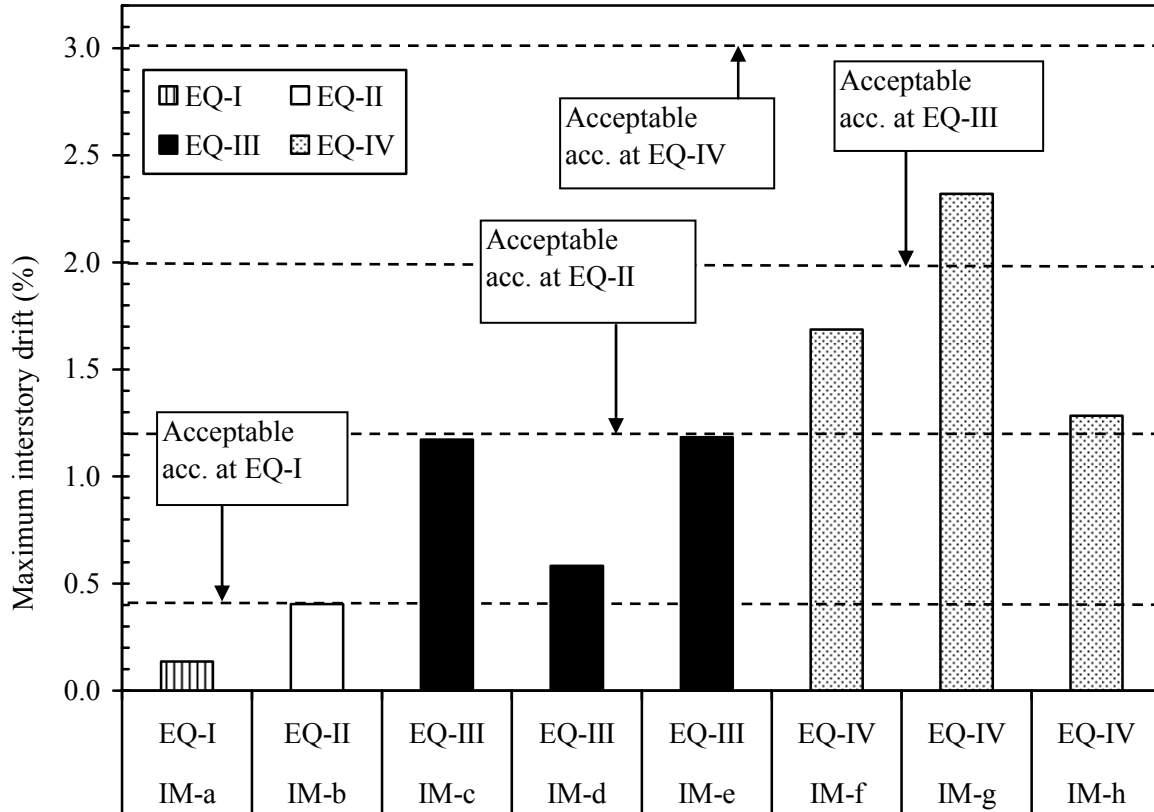Figure 5.10(b).   Maximum transient interstory drift obtained for the seven story building when subjected to short-duration ground motions
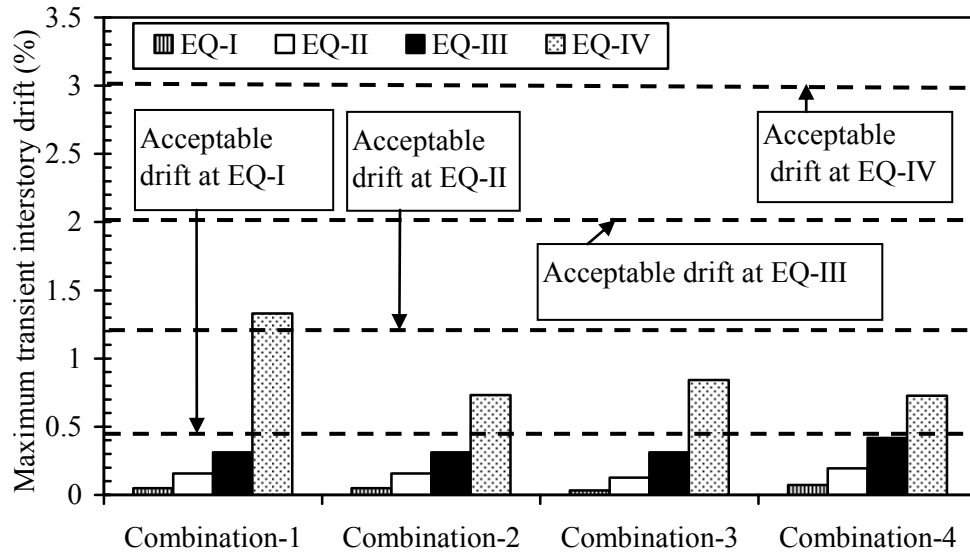
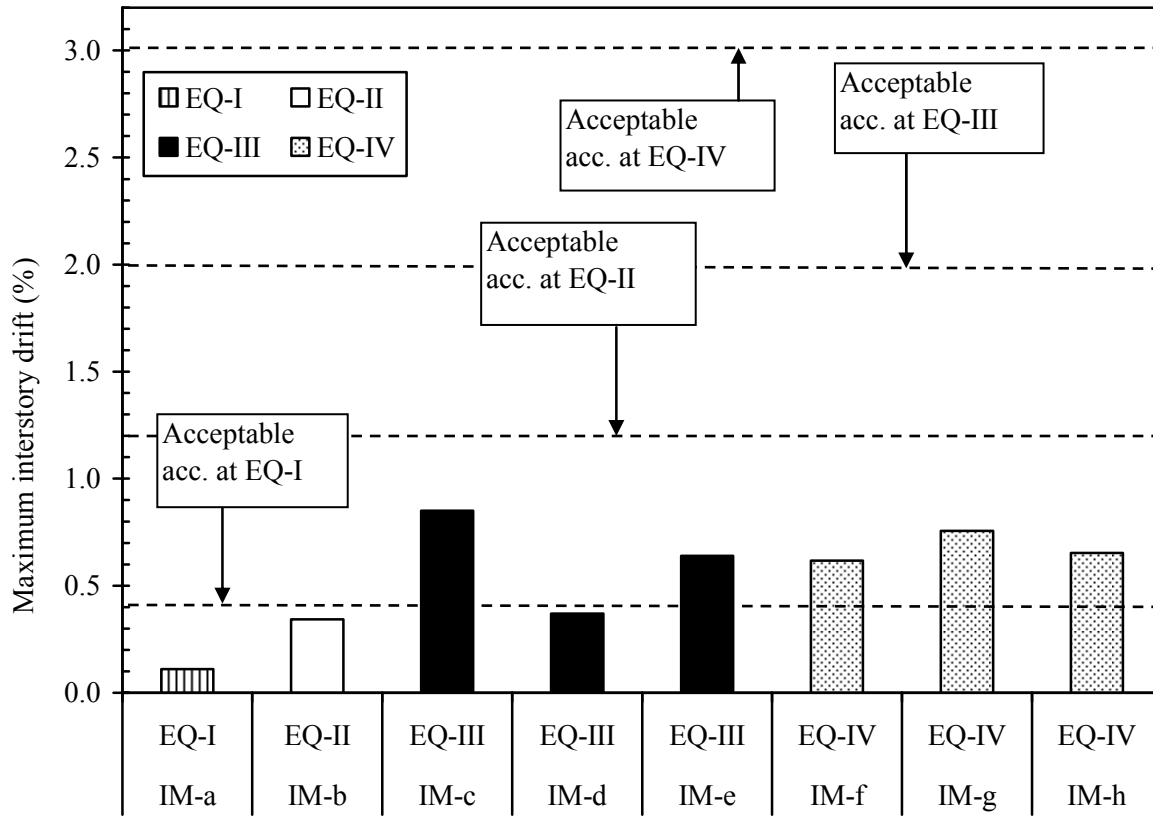Figure 5.10(c). Maximum transient interstory drift obtained for the ten story building when subjected to short-duration ground motions

194

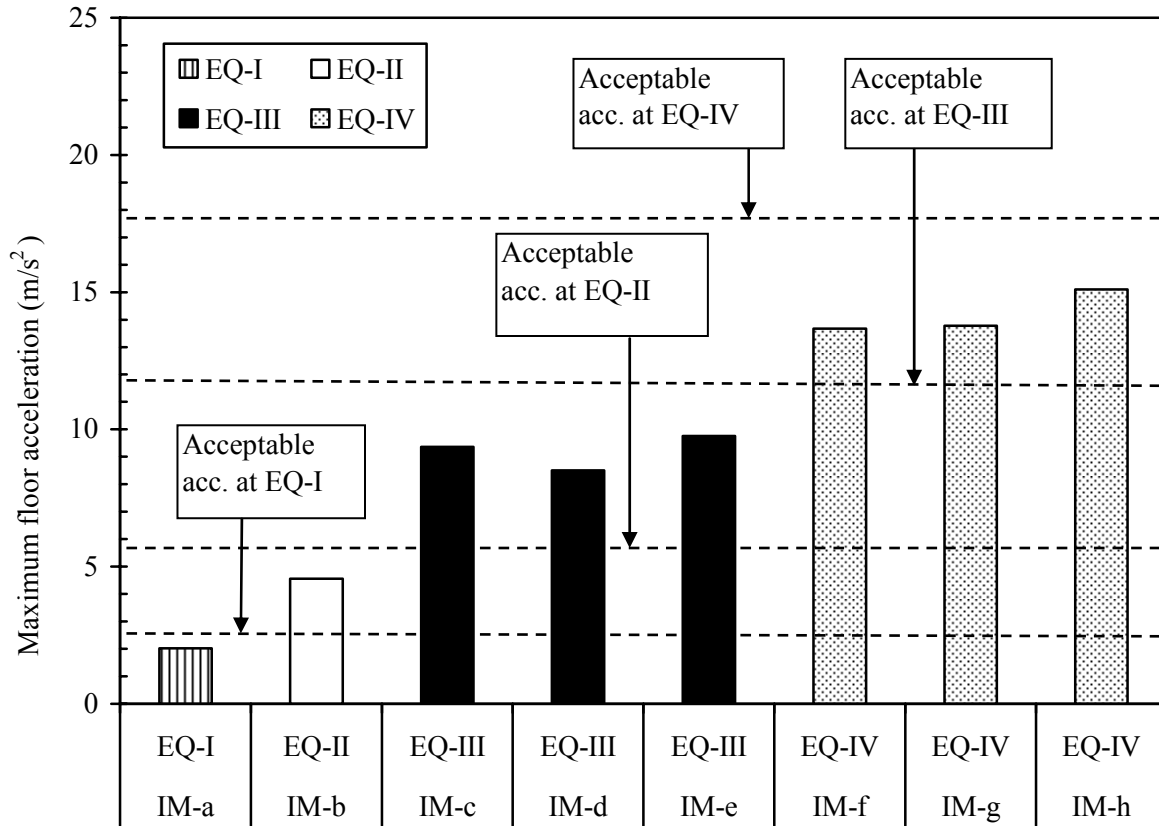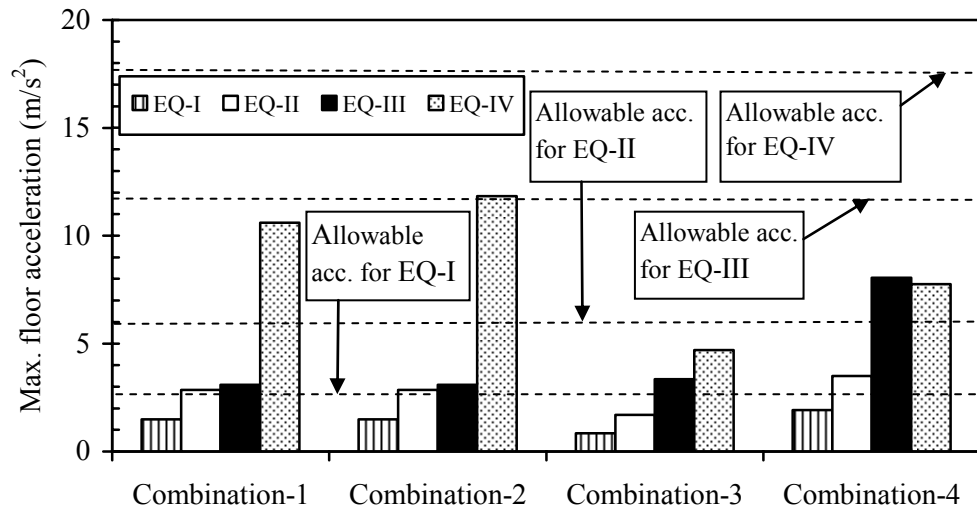Figure 5.11(a). Maximum floor acceleration obtained for the five story building when subjected to short-duration ground motions
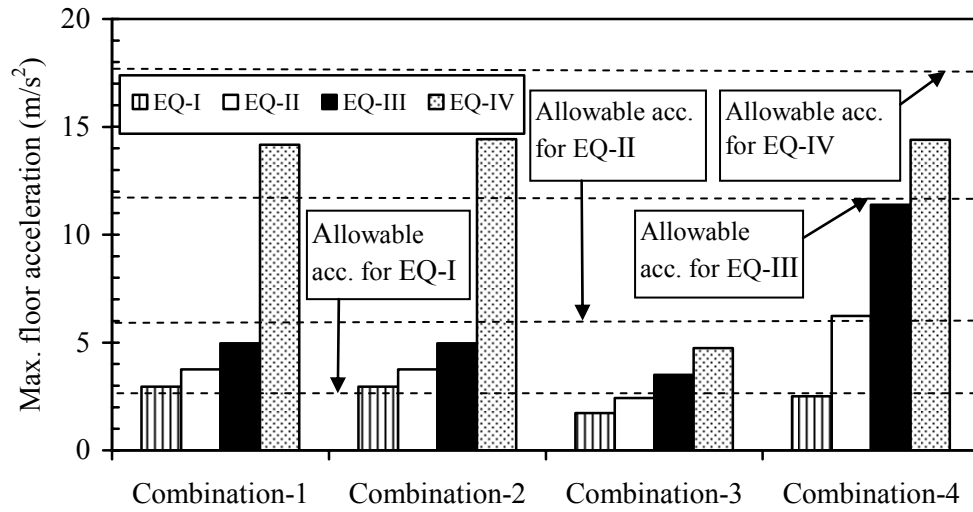
Figure 5.11(b).   Maximum floor acceleration obtained for the seven story building when subjected to short-duration ground motions

196
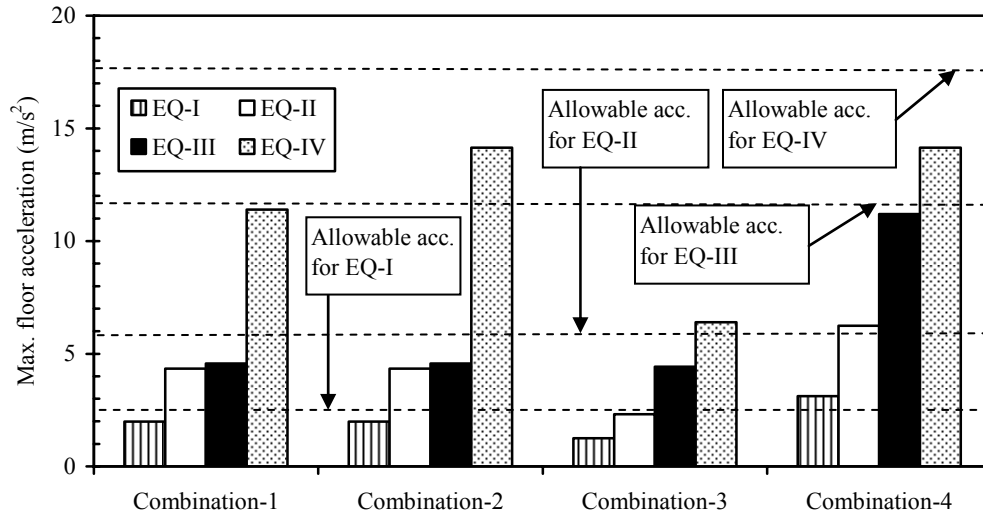
Figure 5.11(c).   Maximum floor acceleration obtained for the ten story building when
subjected to short-duration ground motions
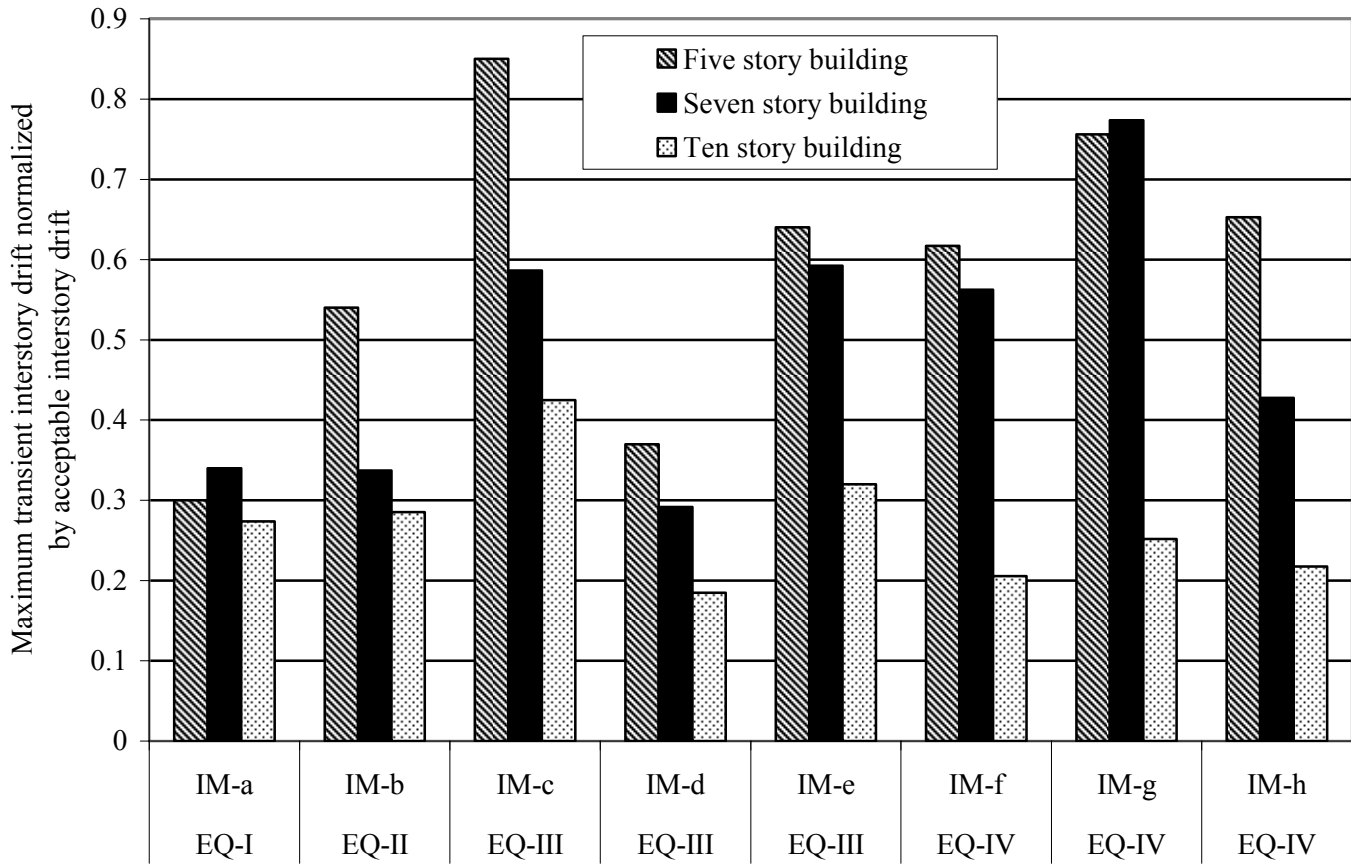
Figure 5.12.   The maximum transient interstory drift normalized by the acceptable interstory drift
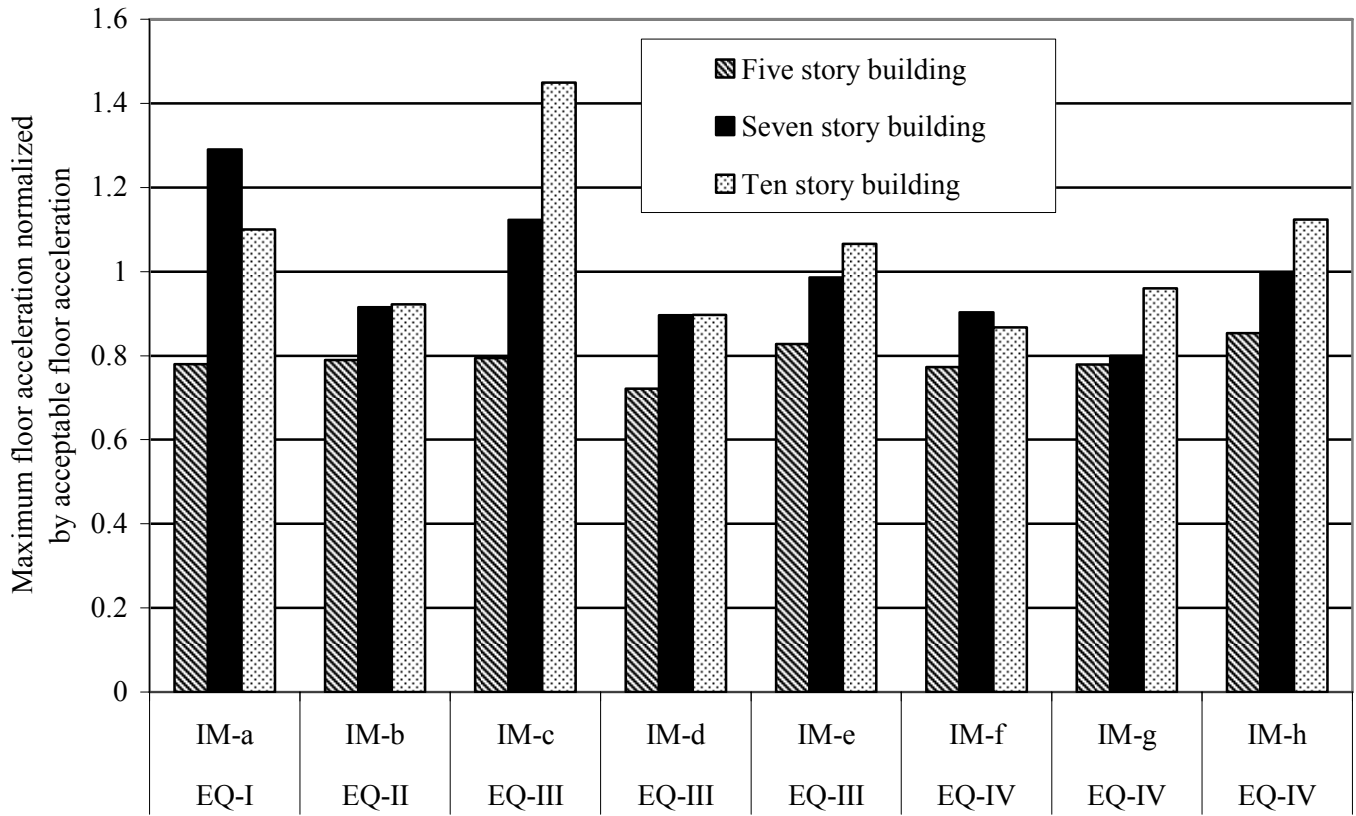
Figure 5.13.   The maximum floor acceleration normalized by the acceptable floor acceleration
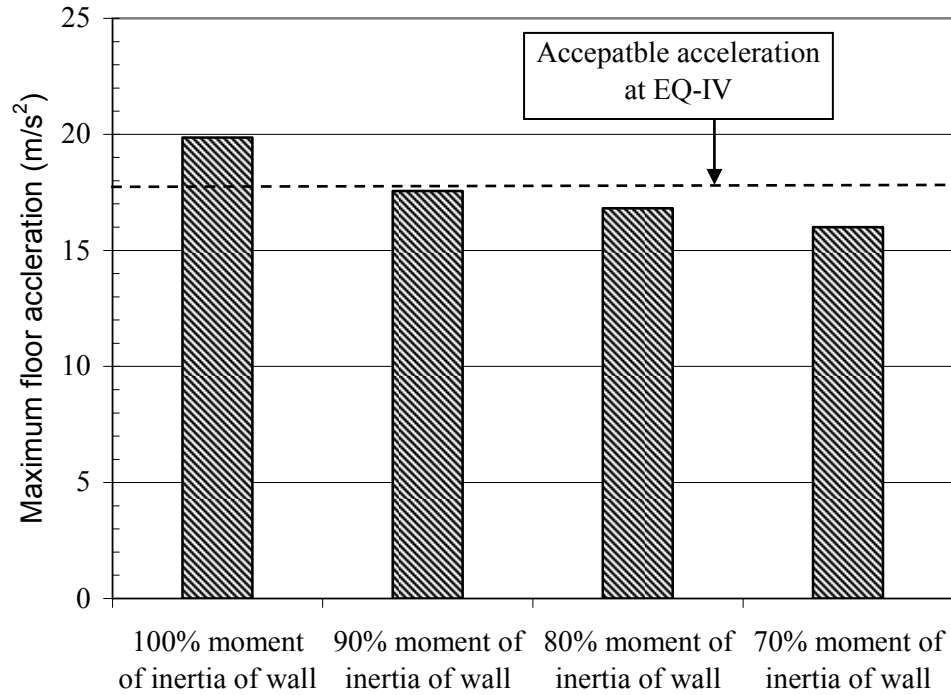
Figure 5.14. Effect of moment of inertia of wall in controlling the maximum floor acceleration when

the ten story building was subjected to ground motion IM-h
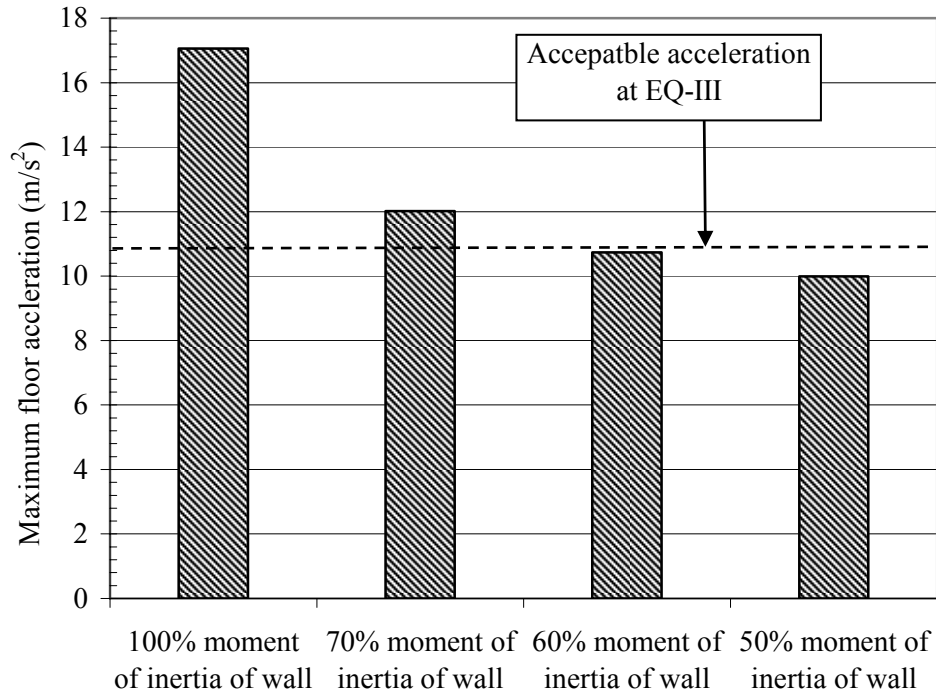
Figure 5.15.   Effect of moment of inertia of wall in controlling the maximum floor acceleration when

the ten story building was subjected to ground motion IM-c

CHAPTER 6. PERFORMANCE-BASED SEISMIC EVALUATION OF HYBRID FRAME SYSTEMS FOR LOW TO MID-RISE BUILDINGS DESIGNED BY IMPROVED DIRECT DISPLACEMENT-BASED APPROACH

A paper to be submitted *in Earthquake Spectra Journal*

M. Ataur Rahman[1] and Sri Sritharan[2]

ABSTRACT

This paper evaluates the multiple levels seismic performance of the ten, seven and five story precast hybrid frame systems designed by improved direct displacement-based design approach. The maximum transient interstory drift, floor acceleration and residual interstory drift were used as acceptance criteria for evaluating the seismic performance. The three buildings performed satisfactorily in terms of the maximum transient interstory drift, maximum floor acceleration and residual interstory drift. This study suggested the use of an improved direct displacement based design method utilizing the inelastic displacement spectrum to ensure satisfactory multiple-level seismic performance of hybrid frame buildings instead of using elastic displacement spectrum presently recommended in literature. The maximum transient interstory drift and maximum floor acceleration achieved in the three buildings normalized by the respective allowable values were also presented to examine the optimization of seismic performance of these structures with various heights. The sensitivity of average drift toward the maximum transient interstory drift depleted when the heights of hybrid frame buildings were raised.

[1]PhD Candidate, Department of Civil, Construction and Environmental Engineering, Iowa State University, Ames, IA 50011, USA
[2]Associate Professor, Department of Civil, Construction and Environmental Engineering, e-mail: sri@iastate.edu, tel.: 515-294-5238, fax: 515-294-7424, Iowa State University, Ames, IA 50011, USA

6.1 INTRODUCTION

Precast hybrid frame system could be a good choice for designing earthquake resistant buildings with the added benefits of prefabrication. This framing concept is used to construct moment-resisting frames from single-bay precast concrete beams and multi-story high precast concrete columns. Figure 6.1(a) illustrates typical details of a hybrid frame. In hybrid frame, the beams and column are connected using unbonded post-tensioning tendons (PT) and mild steel (MS) reinforcement across the precast interfaces at the mid-height and closer to the top and bottom surfaces of the beams, respectively. The interfaces and ducts housing the mild steel reinforcement are filled with non-shrink cementituous fiber grout prior to post-tensioning. The grout at the interfaces ensures continuity between precast members while grouting of the ducts enables the reinforcement to contribute to the stiffness, strength and hysteretic energy dissipation of the hybrid frames. To reduce the inelastic strain accumulation and avoid premature fracture of the reinforcement, the mild steel reinforcing bars are debonded over a short length near the interfaces. A friction mechanism is relied upon for shear transfer across the precast connection interface. The use of prestressing steel along with mild steel to develop moment resistance at the precast connections reduces the hysteresis energy dissipating ability of the hybrid frame when compared to a monolithic concrete frame connection designed to resist the same moment (Stone et al. 1995; Stanton et al. 1997).

The application of unbonded steel reinforcement at the precast interfaces between columns and beams assist with concentrating most of the flexural and inelastic actions at the beam ends. Thus, the beams go through minimal structural damage and experience only limited

cracking when the hybrid frame is subjected to inelastic lateral deformations, which has been witnessed experimentally (Stone et al. 1995; Stanton et al. 1997; Priestley et al. 1999; Sritharan 2002). Moreover, nonlinear elastic response from the unbonded post-tensioning tendons and hysteretic behavior from the mild steel reinforcement will enable the hybrid frames to dissipate energy and minimize residual displacements. The post-tensioning tendons running across the column width reduce the principal tensile stresses in the beam-to-column joints. Such reduction in the principal tensile stress suggests that the amount of joint shear reinforcement could be reduced when compared to the joints in equivalent monolithic concrete frames (Sritharan and Ingham 2003).

The insight of precast hybrid frame was suggested by Priestley and Tao (1993) with the inspiration that the unbonded post-tensioning would provide an improved restoring force to the lateral load resisting systems. The hybrid frame studies during the past decade include experimental verification using component (Stone et al. 1995; Stanton et al. 1997) and structure level testing (Priestley et al. 1999; Pampanin et al. 2000; Sritharan 2002). The hybrid frame has been implemented in a few buildings, including a 39-story apartment complex in San Francisco, California (Englekirk 2002). More recently multiple levels seismic performance of hybrid frame building at 60% scale for a five story building was investigated by Rahman and Sritharan (2007).

6.1.1 Design Philosophy

Design base shear of hybrid frame system may be established by using two methods. The traditional approach is to follow the force-based design (FBD) approach as recommended in refs. (Uiniform Building Code (UBC) 1997; International Building Code (IBC) 2000). In this

approach, design base shear is obtained from the estimated fundamental period and total mass of the structure, incorporating the influence of seismic intensity in terms of a design spectral acceleration. In this method, the target level lateral displacement of the building is not directly used to quantify the design base shear. In contrast, the direct displacement-based design (DDBD) method uses the target displacement calculated to match with the expected performance of the building in establishing the design base shear (Priestley 2002). In this method, the buildings are designed for a target displacement using an effective period of their fundamental mode of response. By representing the hysteretic action in terms of equivalent viscous damping, the effective period is established using design level displacement spectra. The effective mass for the fundamental mode, which is determined by assuming a displacement profile, and the effective period are used to determine the effective stiffnesses of the buildings. Finally, the design base shear is calculated by multiplying the equivalent target displacement and effective stiffness. More detailed description of the DDBD method is available elsewhere (Priestley 2002).

Using acceptance criteria defined in terms of interstory drift, residual drift, and floor acceleration, a multiple-level performance-based seismic evaluation of FBD and DDBD solutions for a five-story hybrid frame building at 60% scale was presented in (Rahman and Sritharan 2007). A systematic seismic evaluation of the systems had economical implications because the design base shear derived from DDBD method was 60% of that derived from DDBD method, although both of the hybrid frame buildings designed by FBD and DDBD methods performed satisfactorily up to design level earthquake. However, the DDBD building did not satisfy the interstory drift limits when subjected by input motions, equal to

150 percent of the design-level earthquake

The objective of the present study is to evaluate the performance of hybrid frames in low to mid-rise buildings imposed by multiple levels of seismic loads when designed by an improved DDBD approach. Through performance evaluation in terms of the maximum transient interstory drift, floor acceleration and residual interstory drift of the full scale five, seven and ten story buildings, viability of using hybrid farme system for such low to mid-rise systems designed by DDBD method will be investigated.

6.2 PROPOSED IMPROVED DIRECT DISPLACEMENT-BASED DESIGN METHOD

The DDBD method described above is according to the recommendation reported in (Priestley 2002). In this existing methodology of DDBD, effective period of the equivalent single degree of freedom system is calculated from the elastic displacement spectra at design level earthquake. The elastic spectrum for 5% viscous damping at design level earthquake is modified for the equivalent viscous damping coming from the hybrid frame while calculating effective period of the equivalent single degree of freedom system. But, the hybrid frames designed based on this approach could not satisfy the performance limit of the interstory drift at earthquakes with 1.5 times intensity compared to that of the design level earthquake. To address this deficiency of the existing DDBD method, this study recommends introducing inelastic displacement spectrum of ground motion with 1.5 times intensity compared to that of the design level earthquake at 5% viscous damping to calculate the effective period for an appropriate ductility. Base shear calculated based on this inelastic spectrum is normalized by a factor of 1.5 to find the design base at design level earthquake. This design base shear is

then compared with that obtained from the existing DDBD method involving elastic displacement spectrum and the higher one is taken as final design base shear.

6.3 HYBRID FRAME SYSTEMS IN FIVE, SEVEN AND TEN STORY BUILDINGS

Figure 6.1(b) shows the plan view of the five, seven and ten story hybrid frame buildings investigated in this study. A model five-story building at 60% scale was designed, built and tested using the identical plan as prototype to verify the conceptual viability of using hybrid frame building under multiple levels short-duration seismic loads (Nakaki et al. 1999; Priestley et al. 1999; Sritharan 2002; Sritharan et al. 2002). Thus, the chosen plan view ensured manifestation of realistically constructable precast concrete hybrid frame buildings.

In Fig. 6.1(b), two identical seismic hybrid frames resisted lateral loads in the longitudinal direction of the five, seven and ten story buildings. Lateral load in the transverse direction was resisted by four jointed precast post-tensioned wall system. Figures 6.2(a) and (b) show the typical elevation views of the five and ten story hybrid frames. The five, seven and ten story hybrid frame systems were designed for the base shear force calculated by following the proposed improved DDBD method for a target displacement of 2.5% as per Seismology Committee (1999) and Performance-Based Seismic Engineering Ad Hoc Subcommittee (2003) of the Structural Engineers Association of California (SEAOC)). Design base shear forces for the three buildings were calculated using DDBD method for high seismic zone defined by the Performance-Based Seismic Engineering Ad Hoc Subcommittee (2003) of SEAOC, assuming very dense soil or rock with shear wave velocity in the range of 366 m/s to 762 m/s identified as Soil Profile Type S_c in UBC (1997) and Site Class C in IBC (2000).

The design of the hybrid connections in HFB1 and HFB2 followed the recommendations of Stanton and Nakaki (2002) and Celik and Sritharan (2004), which include a requirement that the design moment contribution ratio between those provided by the mild steel reinforcement and post-tensioning steel should be taken as 0.45:0.55. This requirement ensures a certain level of restoring force in the connection, thereby enabling re-centering of the hybrid buildings after undergoing an earthquake excitation.

6.4 ANALYTICAL MODEL

2-D analytical models were developed using the non-linear finite element computer program RAUMOKO (Carr 2003) for the analysis of the ten, seven and five story hybrid frame buildings by following the .methodology introduced by Rahman and Sritharan (2007) for the five story PRESSS (PREcast Seismic Structural System) test building at 60% scale (Nakaki et al. 1999; Priestley et al. 1999; Sritharan 2002) where the prototype building was identical to the five story building reported in this paper. Figure 6.3(a) shows the analytical model of the 60% scale hybrid frame building (Rahman and Sritharan 2007). In series with the seismic frame, a pin-based fictitious column was modeled. By lumping the seismic mass at the floor levels of the fictitious column and modeling the floor connections (X-plates) with bi-linear inelastic axial springs between the column and seismic frame, the influence of the floor connections was included in the analyses. For the validation study, two rotational springs connected in parallel were used at the base of the fictitious column to model the moment-response of a gravity column and the wall system subjected to out-of-plane bending. The lateral load resistance from the gravity columns and out-of-plane bending of the precast wall system was neglected in the analytical models, except for the validation portion of the study.

Figure 6.3(b) illustrates that the beams and columns in the RUAUMOKO models were represented by beam-column elements while two rotational springs per nodal location modeled the hybrid connections at the beam-to-column and column-to-footing interfaces (Rahman and Sritharan 2007; Pampanin et al. 2001). The use of two springs to model each hybrid connection was to represent the moment contributions of the mild steel reinforcement and prestressing steel separately. The moment-rotation response envelopes of the springs were derived using the procedure reported in (Celik and Sritharan 2004). In this procedure, the moment resistance of a hybrid connection is determined at a given interface rotation by accounting for the stress-strain behavior of the reinforcing steel, elongation of the post-tensioning tendon due to gap opening, and enhancement in concrete strength due to the confinement effect.

The modified Takeda hysteresis and bi-linear elastic models (Carr 2003) were used to define the cyclic behavior of the rotational springs representing the mild steel (MS) reinforcement and post-tensioning tendons (PT), respectively. The combination of using two cyclic models for the precast connections was to capture both the hysteretic energy dissipation and re-centering capability of the hybrid frames. To account for the influence of flexural cracking, the moment of inertia for the beam-column elements was taken as a fraction of that corresponded to the uncracked concrete gross section (I_g). Based on the test observations reported for the PRESSS building (Priestley et al. 1999) and recommendations by (Paulay and Priestley 1992), $0.6I_g$, I_g, and $0.5I_g$ were used for the columns in the first story, all other columns, and beams, respectively. Figure 6.4(a) shows the monotonic moment-rotation envelopes at the beam ends as modeled in the first floor of the ten story hybrid frame

buildings, while Fig. 6.4(b) illustrates the idealized responses for the aforementioned two types of rotational springs.

In the seismic frame direction, the PRESSS test building (Priestley et al. 1999; Sritharan 2002) was subjected to four levels of short-duration ground motions referred as 0.75EQ-I, 1.5EQ-I, EQ-II and EQ-III represent four levels of seismic hazard expressed in terms of spectral accelerations (see Fig. 6.5) established by the Performance-Based Seismic Engineering Ad Hoc Subcommittee (2003) of the Structural Engineers Association of California (SEAOC). Of these different seismic hazard levels, EQ-III represents the design-level earthquake ground motions, while EQ-IV, which is equivalent to 1.5 times EQ-III, correspond to the maximum considered earthquakes. The analytical model of the PRESSS building with the hybrid frame was also subjected to the aforementioned four levels of short-duration ground motions in (Rahman and Sritharan 2007). Comparison between the experiment and analytical results exhibited good agreement for the floor displacement and base moment as a function of time. All of these validations suggest that the hybrid frame model illustrated in Figs. 6.3(a) and (b) may be used to satisfactorily evaluate the seismic performance of hybrid frame systems for the ten, seven and five story buildings.

6.5 PERFORMANCE-BASED SEISMIC EVALUATION

Seismic performance of the five, seven and ten-story hybrid buildings designed using DDBD method was evaluated at EQ-1, EQ-II, EQ-III and EQ-IV using the maximum transient interstory drift, maximum residual interstory drift, and the maximum floor acceleration, where the interstory drift is defined as the relative floor displacement divided by story height. According to the performance-based seismic design concept presented by the SEAOC

Seismology Committee (1999), ordinary buildings with conventional structural systems when subjected to ground motions compatible with EQ-I, EQ-II, EQ-III and EQ-IV may be expected to produce operational, occupiable, life safety and near collapse performances for both structural and non-structural components. The precast hybrid frame buildings were expected to meet the aforementioned performance levels under the four earthquake levels EQ-I through EQ-IV.

Comparison of the maximum values of the transient interstory drift, residual interstory drift and floor acceleration against the limiting values was conducted to arbitrate the acceptable performance of the ten, seven and five story hybrid frame buildings. The limiting values for the transient interstory drifts and residual interstory drifts were defined in accordance with the recommendations of Seismology Committee (1999). However, the acceptable floor accelerations were defined using an IBC (2000) recommendation for the design of non-structural components. Multiple levels input ground motions and the limiting values for the inter-story drifts and floor acceleration are described in the subsequent sections.

6.6 INPUT GROUND MOTIONS

The five, seven and ten story hybrid frame buildings were evaluated by using two sets of earthquake input motions. Eight long-duration scaled input ground motions recorded in past earthquakes consisted one set of ground motions, and the other set of ground motions was consisted of four combinations of short-duration spectrum compatible earthquake motions. The reason for using the short-duration input ground motions was that it followed the procedure adopted for the pseudodynamic testing of the PRESSS building (Sritharan et al.

1999) and provided an opportunity to examine the validity of using short-duration input motions in performance-based seismic testing of structural systems for further research.

Table 6.1 lists the eight scaled long-duration input motions used for evaluating the performance of the jointed wall systems. The original records of these input motions were obtained typically from stations with soil profile type S_C as defined in (UBC 1997). As detailed in Table 6.1, the original recorded motions were scaled such that their spectra would be comparable to the target spectra within a dominant period range, following the procedure developed in (Rahman and Sritharan 2007). Additional information about these ground motions along with the graphical representation of the acceleration response spectra for all modified long-duration ground motions was reported elsewhere (Rahman and Sritharan 2007).

Table 6.2 shows different combinations of the short-duration ground motions used in the seismic evaluation of the three hybrid frame buildings, which were performed using each combination of records as one sequence with zero acceleration for twenty five seconds of duration between the records. This procedure enabled the free vibration response of the hybrid frame buildings to be examined after subjecting them to each earthquake segment. The original motions used to create the short-duration ground motions of 1.5EQ-I, EQ-II, EQ-III, EQ-IVa and EQ-IVb were recorded at stations with soil profile type S_C in the 1974 Hollister, 1971 San Fernando, 1940 Imperial Valley, 1993 Northridge and 1978 Tabas earthquakes, respectively. Additional descriptions of the input records and the process used for creating the short-duration input motions may be found in refs. (Sritharan et al. 1999; Sritharan et al. 2002; Rahman and Sritharan 2007).

6.7 INTER STORY DRIFT LIMITS

To evaluate the seismic performance of the ten, seven and five story hybrid frame buildings at the four earthquake intensity levels, the following inter story drift limits were used as acceptable limits: maximum transient interstory drifts of 0.5% (EQ-I), 1.5% (EQ-II), 2.5% (EQ-III) and 3.8% (EQ-IV); and maximum residual interstory drifts of 0.1% (EQ-I), 0.3% (EQ-II), 0.5% (EQ-III) and 0.75% (EQ-IV). These limits were chosen based on the guidance given in the SEAOC Blue Book (Seismology Committee 1999), and considering the re-centering nature of hybrid frames.

6.8 FLOOR ACCELERATION LIMITS

Floor acceleration limits were imposed to limit the damage to non-structural elements those may be anchored to the floors during seismic response of the precast buildings. These limits were derived in Rahman and Sritharan (2007) utilizing the recommendations of Tong et al. (2004) and the IBC (2000) provision for estimating design forces required to anchor different types of non-structural elements to building floors under seismic condition. A controlling parameter of these floor acceleration limits is the spectral acceleration corresponding to a short period that is used to define the design response acceleration spectrum (IBC 2000). For the design spectra recommended by the SEAOC Performance-Based Seismic Engineering Ad Hoc Subcommittee (2003), the values of the short-period spectral acceleration ordinates are 2.16 m/s^2, 4.80 m/s^2, 9.81 m/s^2 and 14.72 m/s^2 for EQ-I, EQ-II, EQ-III and EQ-IV, respectively (Rahman and Sritharan 2007). The corresponding limiting floor accelerations are 2.60 m/s^2 (EQ-I), 5.77 m/s^2 (EQ-II), 11.79 m/s^2 (EQ-III) and 17.68 m/s^2 (EQ-IV). The detail methodology of calculating these floor acceleration limits are shown in (Rahman and Sritharan 2007).

6.9 ANALYSIS RESULTS

Figures 6.6(a), (b) and (c) depict deflected shapes of the five, seven and ten story buildings when achieving the maximum interstory drift imposed by the four levels of long-duration ground motions EQ-I through EQ-IV. The increase of deflection at higher floor levels was observed for the three buildings except for EQ-IV level motion in the seven and ten story buildings. It seems that the deflection of the five story building for all levels of ground motions and the deflection of the seven and ten story building for EQ-I through EQ-III were predominantly controlled by the fundamental mode. It is to be noted that generally the rate of increase of deflection at higher floor levels for all of the hybrid frame buildings increased non-linearly, whereas this rate of increase was linear for the buildings with jointed precast post-tensioned shear wall system as primary lateral load resisting system as reported in (Rahman and Sritharan 2008).

Roof displacements were amplified by 234%, 93% and 156% in the five story building, by 358%, 73% and 17% in the seven story building, and by 329%, 97% and 38% in the ten story building due to elevation of ground motion from EQ-I to EQ-II, from EQ-II to EQ-III, from EQ-III to EQ-IV, respectively (see Figs. 6.6(a)-(c)). It shows that the maximum amplification of roof displacement for the three buildings occurred when ground motion was elevated from EQ-I to EQ-II compared to increase of ground motion intensity in the range of EQ-II - EQ-III and EQ-III - EQ-IV. The five story building experienced higher rate of amplification in roof displacement when ground motion was elevated from EQ-III to EQ-IV compared to the seven and ten story buildings. It suggests that the taller hybrid frame buildings (seven and ten story) became less sensitive in terms of roof displacement compared to low rise (five story) building when ground motion was elevated from EQ-III to EQ-IV. In contrast, the low rise

building demonstrated less responsiveness in roof displacement compared to taller buildings when the ground motion intensity was raised from EQ-I to EQ-II. In addition, for a common floor level in all three buildings, the low rise building (five story) demonstrated lower floor displacement consistently compared to both the seven and ten story buildings for the four levels of ground motion. It seems that the design procedure imposed higher displacement stiffness to the low rise building. It is to be noted that an opposite trend was observed in buildings with jointed precast post-tensioned shear wall system as primary lateral load resisting system as reported in (Rahman and Sritharan 2008).

Figure 6.7 shows correlations between average drift and the maximum interstory drift for the five, seven, and ten story hybrid frame buildings. These correlations were drawn based on the displacement performance of the three buildings imposed under eight long-duration ground motions reported in Table 6.1. After examining the correlations, it was found that the rate of increase of average drift with the elevation of the maximum interstory drift was reduced for taller buildings. It suggests that sensitivity of average drift toward the maximum interstory drift depletes if the height of hybrid frame buildings are raised. In addition, for a given value of the maximum interstory drift higher than 1.75%, buildings with lower heights exhibited higher values of average drift. The seven story building showed higher average drift compared to the ten and five story buildings for a chosen value of the maximum interstory drift lower than 1.75%. When the maximum interstory drift was less than 1.15%, the five story building had lower average drift compared to the ten story building, and an opposite trend was observed for the maximum interstory drift more than 1.15%. The aforementioned

information may be helpful for designing hybrid frame buildings based on extrapolated maximum interstory drift coming from average drift.

Figure 6.8 illustrates the pushover analyses responses of the five, seven and ten story hybrid frame buildings. Base shear normalized by building weight (normalized base shear) and the roof displacement normalized by the building height (called roof drift or average interstory drift) were introduced to compare the pushover analyses responses of the three buildings. Up to 2.5% average interstory drift, base shear normalized by building weight increased with the reduction of building height. Base shears normalized by building weight were 0.073, 0.105 and 0.126 for the ten story hybrid frame building; 0.089, 0.155 and 0.196 for the seven story hybrid frame building; 0.137, 0.170 and 0.197 for the five story hybrid frame building for average interstory drift of 0.50%, 1.50% and 2.50%, respectively. It suggests that taller hybrid frame buildings attracted smaller percentage of building weight as base shear compared to the low-rise buildings.

Figures 6.9(a), (b) and (c) represent the maximum interstory drift in the five, seven and ten story hybrid frame buildings when subjected to long-duration ground motions listed in Table 6.1. Generally, the three buildings demonstrated the maximum interstory drift less than the acceptable limits. It suggests that the modified approach of DDBD method recommended in this paper was successful to calculate the appropriate base shear for the hybrid frame buildings to ensure acceptable multiple levels seismic performance in terms of interstory drift encompassing buildings heights from low (five story) to mid-rise (ten story). The maximum interstory drift increased with the reduction of building height for ground motions up to EQ-II level. Similar trend was observed for IM-c (EQ-III), IM-g (EQ-IV) and IM-h (EQ-IV).

When building height was increased from the five story to the seven story, the maximum interstory drift decresed for all ground motions except the case of ground motion IM-f. Such generalized consistency of increase in the maximum interstory drift due to increase of building height does not hold true if the performance of the ten story building is taken into consideration along with the seven and five story buildings. It is to be noted that both the seven and five story buildings were designed based on the base shear coming from inelastic displacement spectrum option but the ten story building was designed using the base shear coming from elastic displacement spectrum as per the methodology recommended in this paper. The aforementioned variation of source of calculated base shear seems to be the reason of higher level of the maximum interstory drift in the ten story building compared to the seven and five story buildings for some of the ground motions. While investigating the seismic performance of the ten, seven and five story jointed post-tensioned wall system, it was found that the difference in capacity to resist interstory drift between the low (five story) and mid-rise (ten story) building increased with the elevation of ground motion intensity (Rahman and Sritharan 2008), but no such solid trend was observed for the hybrid frame buildings.

Tables 6.3 shows the maximum residual interstory drifts demonstrated by the five, seven and ten story hybrid frame buildings. The re-centering capacity of the post-tensioning tendons enabled the buildings to produce very insignificant amount of residual interstory drift compared to the acceptable limits. For all of the three buildings, it was observed that the increase of intensity of ground motions could not dictate to elevate the maximum residual interstory drift consistently. Similar trend was observed in seismic performance evaluation of

jointed post-tensioned wall system (Rahman and Sritharan 2008). In addition, there was no trend showing the influence of height of buildings in controlling the value of the maximum residual interstory drift for the hybrid frame buildings. But according to (Rahman and Sritharan 2008), in buildings with jointed post-tensioning wall system, higher level of the maximum residual interstory drift was exhibited by taller buildings.

Figures 6.10(a), (b) and (c) depict the maximum floor acceleration attained by the five, seven and ten story hybrid frame buildings when subjected to long-duration ground motions. All of the three buildings showed satisfactory performance in terms of the maximum allowable floor acceleration under four levels of ground motions. Generally, the values of the maximum floor acceleration decreased for taller buildings. This trend is opposite to that observed in seismic performance evaluation for jointed post-tensioning wall system (Rahman and Sritharan 2008).

Due to the design level ground motions of earthquake intensity EQ-III, the five story hybrid frame building showed the maximum floor acceleration in the range of 7.78 m/s^2 - 11.72 m/s^2, whereas the ten story hybrid frame building exhibited the maximum floor acceleration in the range of 5.86 m/s^2 - 8.70 m/s^2 (see Figs.6.10(a) and (c)). The low-rise building comprised of five stories, experienced 17.24% - 48.17% higher level of the maximum floor acceleration compared to the mid-rise building comprised of ten stories when imposed by the ground motions of intensity EQ-III. However, for EQ-I and EQ-IV level ground motions, the mid-rise (ten story) building showed the maximum floor acceleration of 1.59 m/s^2 and 9.79 - 15.02 m/s^2 and the low rise building (five story) demonstrated floor acceleration of 1.98 m/s^2 and 11.91 m/s^2 - 17.65 m/s^2 , respectively. The low-rise building comprised of five stories,

experienced 17.24% - 48.17% higher level of the maximum floor acceleration compared to the mid-rise building comprised of ten stories. This low-rise building attained 24.52% and 0.45% - 71% higher level of the maximum floor acceleration compared to the mid-rise building when subjected to ground motions of earthquake levels EQ-I and EQ-IV, respectively.

The dependency of the building responses in terms of floor acceleration on frequency contents of the input earthquake was also emphasized by the analyses results as shown in Figs. 6.10(a), (b) and (c). For example, at EQ-III level, the difference in responses of the ten and five story hybrid frame buildings for the maximum floor acceleration subjected by IM-c was 17.24%, whereas for IM-d the corresponding difference was 48.17%, although both of these ground motions were chosen to represent EQ-III level earthquake. Similar trend of frequency content dependency of the maximum floor acceleration was found for the ground motions representing EQ-IV level earthquake.

Traditionally, for research and testing purpose, short-duration ground motions are chosen. Therefore, the present study gave effort to investigate the performance of the hybrid frame buildings subjected by short-duration ground motions of four levels EQ-I through EQ-IV. Figures 6.11(a), (b) and (c) depict the maximum transient interstory drift of the five, seven and ten story hybrid frame buildings when subjected by four combinations of short-duration ground motions listed in Table 6.2. All of the three buildings showed satisfactory performance in terms of the maximum transient interstory drift with sufficient margin of safety. Short-durations ground motions from combination-2 were chosen to compare the maximum transient interstory drift and floor acceleration performance of the buildings under

short and long-duration ground motions. Generally, short-duration ground motions resulted lower levels of the maximum transient interstory drift compared to long-duration motions for all of the three hybrid frame buildings for EQ-II through EQ-IV. Similar trend was observed in the five story building, and the ten and seven story building showed an opposite trend under ground motion of EQ-I level intensity. It seems that the influence of duration of ground motions on the maximum transient interstory drift may be affected by intensity level of the ground motion and the height of the building. The long-duration ground motions induced as much as 0.26% and 36.00% and 43.81% higher values of the maximum transient interstory drift compared to the short-duration ground motions in the ten story building when subjected by EQ-II, EQ-III and EQ-IV level ground motions, respectively. For identical sequence of elevation in ground motion intensity on the five story building, the long-duration ground motions resulted as much as 63.81% and 55.33% and 107.43% higher values of the maximum transient interstory drift compared to the short-duration ground motions. It suggests that the difference of interstory drift performance due to short and long-duration ground motions depleted when the building height was increased from low-rise (five story) to mid-rise (ten story) in the range from EQ-I to EQ-IV.

Figures 6.12(a), (b) and (c) show the maximum floor acceleration resulted from short-duration ground motions in the five, seven and ten story hybrid frame buildings. All of the three buildings demonstrated satisfactory performance in terms of the maximum floor acceleration. As mentioned earlier, combination-2 of short-duration ground motions was chosen to compare the maximum floor acceleration of the three buildings under short and long- duration ground motions. In general, long-duration ground motions created higher

values of the maximum floor acceleration compared to short-duration ground motions for earthquake intensity levels from EQ-II to EQ-IV. An opposite trend was exhibited by the three buildings for EQ-I level ground motion (see Figs. 6.12(a)-(c) and-Figs. 6.10(a)-(c)). It is to be noted that for the jointed post-tensioning wall system buildings of low-to-mid-rise, long-duration ground motions created higher values of the maximum floor acceleration compared to short-duration ground motions for earthquake intensity levels from EQ-I to EQ-IV (Rahman and Sritharan 2006). It suggests that the trend of impact on the maximum floor acceleration due to the variation in duration ground motion may be affected based on the lateral load resisting system for low intensity ground motion i.e. EQ-I.

The largest differences between the maximum floor acceleration due to long and short-duration ground motions considering the aforementioned short-duration ground motion combination were 153.60% and 70.12 % for the ten story hybrid frame building; 230.54% and 113.11% for the seven story hybrid frame building; 88.42% and 1.45% for the five story hybrid frame building when subjected by EQ-III and EQ-IV level ground motions, respectively (see Figs. 6.12(a)-(c) and-Figs. 6.10(a)-(c)). It shows that the largest impact on amplifying the floor acceleration due to increase of duration of ground motion was demonstrated by the three hybrid frame buildings when they were subjected to ground motions representing EQ-III level earthquake. It seems that real hybrid frame buildings may face the challenge of significantly higher levels of transient interstory drift and floor acceleration due to long-duration ground motion than those derived from the laboratory testing under short-duration ground motions.

Figure 6.13 shows the maximum transient interstory drift at four levels of long-duration ground motions normalized by the respective allowable limits of interstory drift, in the five, seven and ten story hybrid frame buildings. The largest achievement in transient interstory drifts were 86.88%, 70.00%, 93.20% and 96.23% of the associated acceptable limit for the five story hybrid frame building when subjected by EQ-I, EQ-II, EQ-III and EQ-IV level ground motions, respectively. These achievements were 43.06%, 63.53%, 74.56% and 96.18% for the seven story building, and 32.76%, 36.41% 70.80% and 93.84% for the ten story building ignoring the response of one event IM-f. It suggests that low rise buildings tend to attain the maximum transient interstory drifts closer to the acceptable limits compared to the taller buildings for four levels of ground motions from EQ-I to EQ-IV. In addition, for a given building height, the achievement of the maximum transient interstory drift became closer to the respective acceptable limit with the increase of intensity of ground motions.

Figure 6.14 shows the maximum floor acceleration at four levels of long-duration ground motions normalized by the respective allowable limits of floor acceleration, in the five, seven and ten story hybrid frame buildings. The largest attainments of floor acceleration were recorded as 76.08%, 60.11%, 99.54% and 99.90% of the associated acceptable limit for the five story hybrid frame building when subjected by EQ-I, EQ-II, EQ-III and EQ-IV level ground motions, respectively. However, these attainments of floor acceleration were 72.05%, 89.21%, 96.32% and 97.40% for the seven story building, and 61.31%, 76.60%, 73.90% and 85.04% for the ten story building. Thus, the low-rise hybrid frame building has stronger tendency to approach unity of normalized floor acceleration compared to the taller building for EQ-I, EQ-III and EQ-IV level ground motions. An opposite trend was observed for EQ-II

level ground motion. It is to be notated that the closeness of the normalized floor acceleration and normalized interstory drift to unity indicates optimized use of construction materials to control interstory drift and floor acceleration.

Tables 6.4(a) and (b) show the maximum plastic rotations experienced by the five and ten story hybrid frames under the long-duration ground motions at the first floor level beam ends as well as at the column bases (i.e., at locations A through G identified in Fig. 6.2). When a connection responded only in linear range at a particular location, the corresponding plastic rotation was recorded as zero. The ten story hybrid frame building was free from plastic rotations when subjected by EQ-I and EQ-II level ground motions. No such trend was observed in the five story building. Overall, the maximum plastic rotations recorded at column bases were greater than those obtained at the beam ends. The maximum plastic rotations in mid-rise building (ten story) were less than those recorded in low-rise (five-story) building. It suggests that in the lower floor beam ends and column bases, the susceptibility for higher levels of plastic rotation increases with the reduction of building height.

6.10 CONCLUSIONS

Seismic performances of low to mid-rise hybrid frame buildings designed by the proposed improved direct displacement-based design approach were analytically investigated in this paper. Using a validated analytical modeling procedure, the five, seven and ten story hybrid frame buildings with identical plan view were subjected to long and short-duration earthquake input motions having acceleration response spectra comparable with those designated to represent four levels of earthquake intensities. Using the analysis results the following conclusions were drawn:

(1)   The low-rise hybrid frame building deflected predominantly by the fundamental mode. This trend diminished with the increase of height of building. For four levels of ground motions, in a common floor level, hybrid frame buildings having higher number of floors exhibited higher level of floor displacement compared to those with fewer floors at the moment of achieving the maximum transient interstory drift.

(2)   The sensitivity of average drift toward the maximum interstory drift depleted when the heights of hybrid frame buildings were raised. Hybrid frame buildings with lower heights exhibited higher values of average drift for a given value of the maximum interstory drift higher than 1.75%.

(3)   Pushover analysis results suggested that taller hybrid frame buildings attracted smaller percentage of building weight as base shear compared to the low-rise buildings.

(4)   In general, hybrid frame systems embedded in low to mid-rise buildings demonstrated satisfactory seismic performance in terms of the maximum transient interstory drift when subjected by both short and long-duration ground motions of four levels of ground motions.

(5)   The maximum transient interstory drift increased with the reduction of building height for ground motions up to EQ-II level.

(6)   The re-centering capacity of the hybrid frame systems enabled the buildings to produce negligible amount of residual interstory drift.

(7)   Hybrid frame buildings from low to mid-rise demonstrated satisfactory seismic performance in terms of the maximum floor acceleration when subjected by both short and long-duration ground motions of four levels of ground motions.

(8)   Generally, short-duration ground motions resulted lower levels of the maximum transient interstory drift and floor acceleration compared to long-duration ground motions for all of the three hybrid frame buildings for EQ-II through EQ-IV. It seems that a real life full scale hybrid frame building may experience the challenge of standing against higher transient interstory drift and floor acceleration arising from long-duration ground motions compared those resulting from short-duartion ground motions derived in the laboratory tests.

(9)   The low-rise hybrid frame building has stronger tendency to approach unity of normalized floor acceleration compared to taller hybrid frame building.

(10) The susceptibility of occurring higher level of plastic rotation increases with increase of building height.

(11) Based on the aforementioned concluding remarks in terms of seismic evaluation indicating satisfactory multiple-level seismic performance of the hybrid frame buildings designed by the proposed improved direct displacement-based design methodology, it may be recommended to use

hybrid frame system as lateral load resisting system for low to mid-rise buildings.

6.11 ACKNOWLEDGEMENTS

6.12 REFERENCES

Carr, A. J., 2003. *RUAUMOKO - Inelastic Dynamic Analysis Program*. University of Canterbury, Christchurch, New Zealand.

Celik, O., and Sritharan, S. (2004). An Evaluation of Seismic Design Guidelines Proposed for Precast Concrete Hybrid Frame Systems. ISU-ERI-Ames Report ERI-04425, Iowa State University, Ames, Iowa, USA, 83-198.

Englekirk, R. E. (2002). "Design-Construction of The Paramount – A 39-story Precast Prestressed Concrete Apartment Building." *PCI Journal,* **47(4),** 56-71.

International Building Code (IBC), 2000. *International Code Council*, Virginia, USA, 331-377.

Pampanin, S., Priestley, M. J. N., and Sritharan, S. (2001). "Analytical Modeling of Seismic Behavior of Precast Concrete Ductile Frame Connection." *Journal of Earthquake Engineering*, **5(3),** 329-367.

Paulay, T., and Priestly, M. J. N. (1992). Seismic Design of Reinforced Concrete and Masonry Buildings, John Wiley and Sons, Inc., New York, USA, 142, 163.

Nakaki, S. D., Stanton, J. F., and Sritharan, S., 1999. An overview of the PRESSS five-story precast test building, *PCI Journal*, **44(2),** 26-39.

Performance-Based Seismic Engineering Ad Hoc Subcommittee, 2003. Revised Interim Guidelines: Performance-Based Seismic Engineering for the SEAOC Blue Book, Structural Engineers Association of California, California, USA, 128-132.

Priestley, M. J. N., 2002. Direct displacement-based design of precast/prestressed concrete buildings, PCI Journal, 47 (6), 67-79.

Priestley, M. J. N., Sritharan, S., Conley, J., R., and Pampanin, S., 1999. Preliminary results and conclusions from the PRESSS five-story precast concrete test building, PCI Journal, 44 (6), 42-67.

Priestley, M. J. N., Tao, J. R, 1993. Seismic response of prestressed concrete frames with partially debonded tendons, *PCI Journal*, Jan-Feb.

Rahman, M., A., and Sritharan, S., 2008, Performance-Based Seismic Evaluation of Jointed Precast Post-Tensioned Wall Systems for Low to Mid-Rise Buildings Designed by Direct Displacement-Based Approach, to be submitted in *Earthquake Spectra*.

Rahman, M., A., and Sritharan, S., 2007, A performance-based seismic evaluation of two five-story precast concrete hybrid frame buildings, accepted in *ASCE Structural Journal* (in print).

Rahman, M., A., and Sritharan, S., 2006, An evaluation of force-based design vs. direct displacement-based design of jointed precast pot-tensioned wall systems, *Earthquake Engineering and Engineering Vibration* **5(2)**, 285-296.

Seismology Committee, 1999. Recommended Lateral Force Requirements and Commentary (Blue Book). Structural Engineers Association of California (SEAOC), California, USA, 327-421.

Sritharan, S., 2002. Performance of four jointed precast frame systems under simulated

seismic loading, *Proceedings of the Seventh National Conference on Earthquake Engineering,* Paper No. 264, Boston, USA.

Sritharan, S., and Ingham J. M. (2003). "Application of Strut-And-Tie Concepts to Concrete Bridge Joints in Seismic Regions." PCI Journal, 48 (4), 66–89.

Sritharan, S., Igarashi, A., Priestley, M. J. N., and Seible, F. (1999). "Test Design of the PRESSS Five-Story Precast Concrete Building." Proceedings of the 68th SEAOC Annual Convention, Santa Barbara, California, USA, 255-261.

Sritharan, S., Pampanin, S., and Conley, J., 2002. Design Verification, Instrumentation and Test Procedures, PRESSS-3: The Five-Story Precast Test Building, Vol. 3-3. ISU-ERI-Ames Report ERI-03325, Iowa State University, Ames, Iowa, USA.

Stanton, J. F., Stone, W. C., and Cheok, G. S. (1997). "A Hybrid Reinforced Precast Frame for Seismic Regions." PCI Journl, 42(2), 20-32.

Stanton, J. F., and Nakaki, S. D. (2002). Design Guidelines for Precast Concrete Seismic Structural Systems, PRESSS Report Number-01/03-09, University of Washington Report Number-SM 02-02, University of Washington, Seattle, USA.

Stone, W. C., Cheok, G. S., and Stanton, J. F. (1995). "Performance of Hybrid Moment-Resisting Precast Beam-Column Concrete Connections Subjected to Cyclic Loading." ACI Structural Journal, 91(2), 229-249.

Uniform Building Code (UBC), 1997. International Conference of Building Officials, Whittier, California, USA, 2, 13-38.

Table 6.1.   List of ground motions selected for the analysis

Identification of the Input Motion	Earthquake Intensity	Earthquake Name (Year)	Magnitude	Scale Factor	PGA after multiplying by the Scale Factor (g)
IM-a	EQ-I	Morgan Hill (1984)	6.1 (M_s)	0.65	0.19
IM-b	EQ-II	Loma Prieta (1989)	7.1 (M_s)	0.64	0.32
IM-c	EQ-III	Northridge (1994)	6.8 (M_s)	1.68	0.67
IM-d	EQ-III	Imperial valley (1940)	7.2 (M_s)	1.50	0.48
IM-e	EQ-III	Kobe-Japan (1995)	6.9 (M_w)	1.10	0.66
IM-f	EQ-IV	Tabas-Iran (1978)	7.4 (M_s)	1.00	0.93
IM-g	EQ-IV	Chi-Chi-Taiwan (1999)	7.6 (M_s)	1.47	0.86
IM-h	EQ-IV	Kobe-Japan (1995)	6.9 (M_w)	1.77	0.97

PGA = Peak Ground Acceleration, M_s = Surface Wave Magnitude,

M_w = Moment Magnitude

Table 6.2.   Different combinations of short-duration ground motions used in the analysis

Idendification of Combinations	Earthquake Intensity			
	Earthquake Level-I	Earthquake Level-II	Earthquake Level-III	Earthquake Level-IV
Combination-1	EQ-I	EQ-II	EQ-III	EQ-IVa
Combination-2	EQ-I	EQ-II	EQ-III	EQ-IVb
Combination-3	0.22EQ-III	(-) 0.50EQ-III	EQ-III	(-) 1.5EQ-III
Combination-4	0.15EQ-IVb	(-) 0.33EQ-IVb	0.67EQ-IVb	EQ-IVb

Table 6.3.   Maximum residual interstory drift in the five, seven and ten story hybrid frame buildings

Identification of the Input Motion	Earthquake Intensity	Maximum resedual interstory drift (%)			Acceptable resedual interstory drift (%)
		Five story	Seven story	Ten story	
IM-a	EQ-I	0.000114	3.91×10^{-7}	6.21×10^{-6}	0.10
IM-b	EQ-II	0.000115	0.002770	0.001477	0.30
IM-c	EQ-III	0.00848	0.000666	0.001304	0.50
IM-d	EQ-III	0.000872	0.005652	0.001856	0.50
IM-e	EQ-III	0.004898	0.003629	0.003163	0.50
IM-f	EQ-IV	0.001038	0.001732	0.001578	0.75
IM-g	EQ-IV	0.01504	0.004790	0.003410	0.75
IM-h	EQ-IV	0.004704	0.001877	0.005300	0.75

Table 6.4(a).　　Maximum plastic rotation at the first floor level of beam-to-column connections, and at column-to-base connections at locations A, B, C, D, E, F and G as shown in Fig. 6.2(a) for the five story hybrid frame building

Input motion	Location A	Location B	Location C	Location D	Loaction E	Location F	Location G
IM-a	0.00258	0.00000	0.00175	0.00000	0.00000	0.00257	0.00000
IM-b	0.00829	0.00587	0.00801	0.00525	0.00526	0.00826	0.00589
IM-c	0.02084	0.01817	0.02123	0.01722	0.01723	0.02079	0.01823
IM-d	0.01121	0.00829	0.01114	0.00761	0.00762	0.01121	0.00833
IM-e	0.01320	0.01132	0.01320	0.01059	0.01059	0.01316	0.01134
IM-f	0.01518	0.01348	0.01548	0.01269	0.01269	0.01516	0.01352
IM-g	0.03308	0.03468	0.03346	0.03361	0.03361	0.03303	0.03469
IM-h	0.03293	0.03267	0.03328	0.03159	0.03159	0.03287	0.03270

Table 6.4(b).   Maximum plastic rotation at the first floor level of beam-to-column connections, and at column-to-base connections at locations A, B, C, D, E, F and G as shown in Fig. 2(b) for the ten story hybrid frame building

Input motion	Location A	Location B	Location C	Location D	Location E	Location F	Location G
IM-a	0.00000	0.00000	0.00000	0.00000	0.00000	0.00000	0.00000
IM-b	0.00000	0.00000	0.00000	0.00000	0.00000	0.00000	0.00000
IM-c	0.01119	0.01110	0.01199	0.00987	0.00988	0.01104	0.01121
IM-d	0.00812	0.00805	0.00884	0.00708	0.00709	0.00817	0.00822
IM-e	0.01103	0.01090	0.01178	0.00963	0.00962	0.01077	0.01100
IM-f	0.03964	0.03842	0.04089	0.03661	0.03662	0.03976	0.03855
IM-g	0.02823	0.02796	0.02934	0.02611	0.02610	0.02770	0.02808
IM-h	0.01643	0.01585	0.01735	0.01430	0.01429	0.01601	0.01600
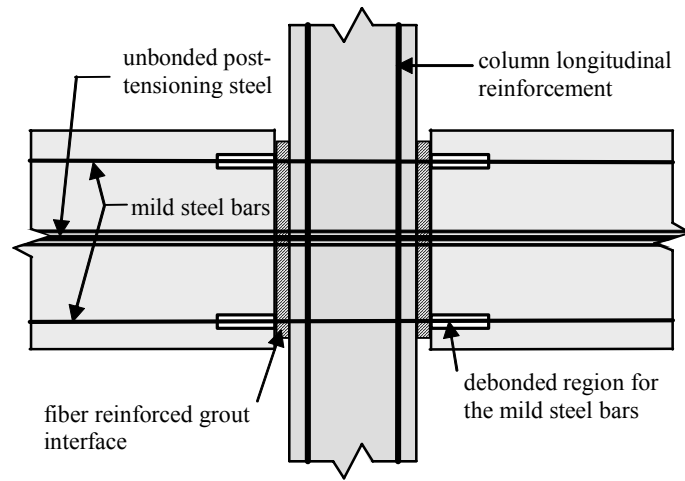
Figure 6.1(a).   The typical connection details of a precast hybrid frame (transverse reinforcements are omitted for clarity)
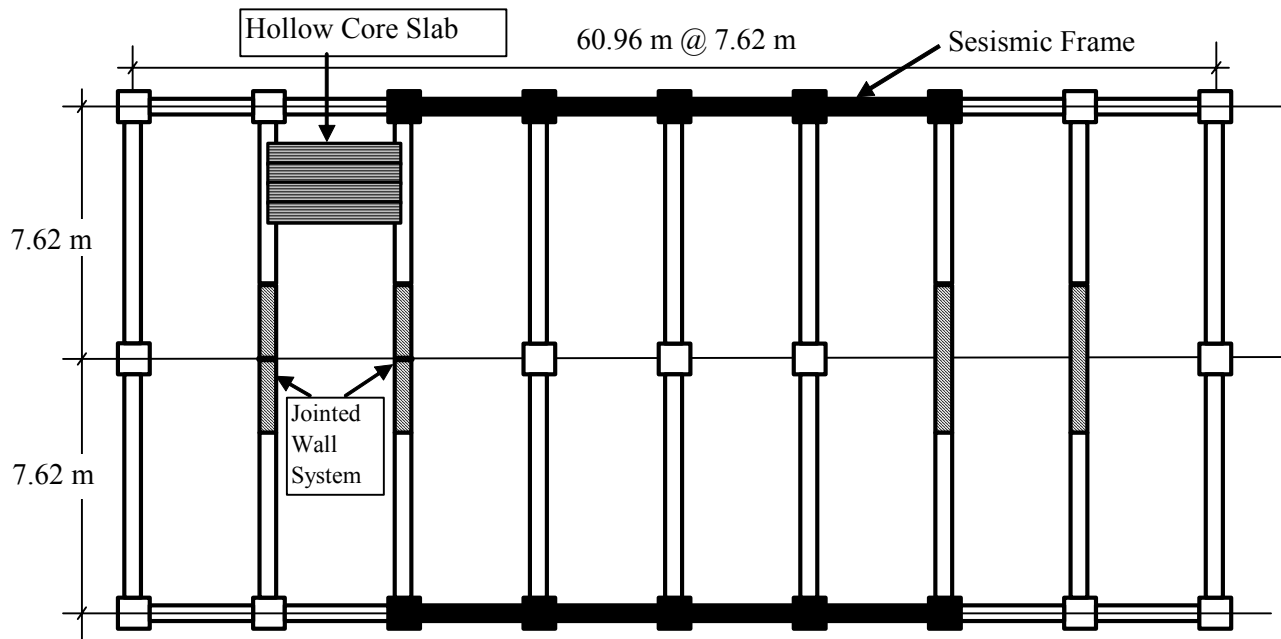
Figure 6.1(b).   Plan view of the five, seven and ten story prototype buildings
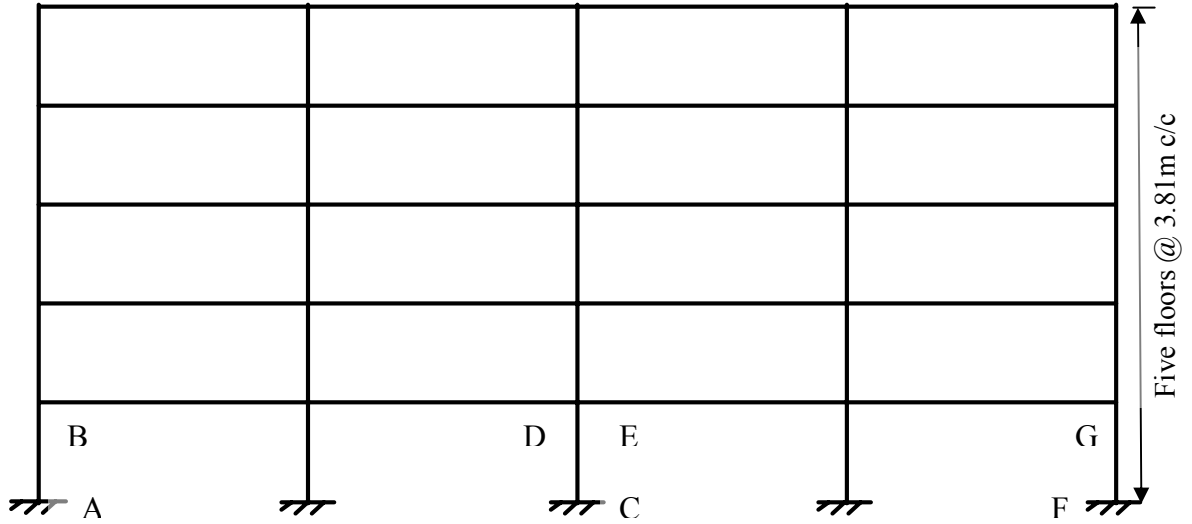
Figure 6.2(a).   Elevation of the ten story hybrid frame
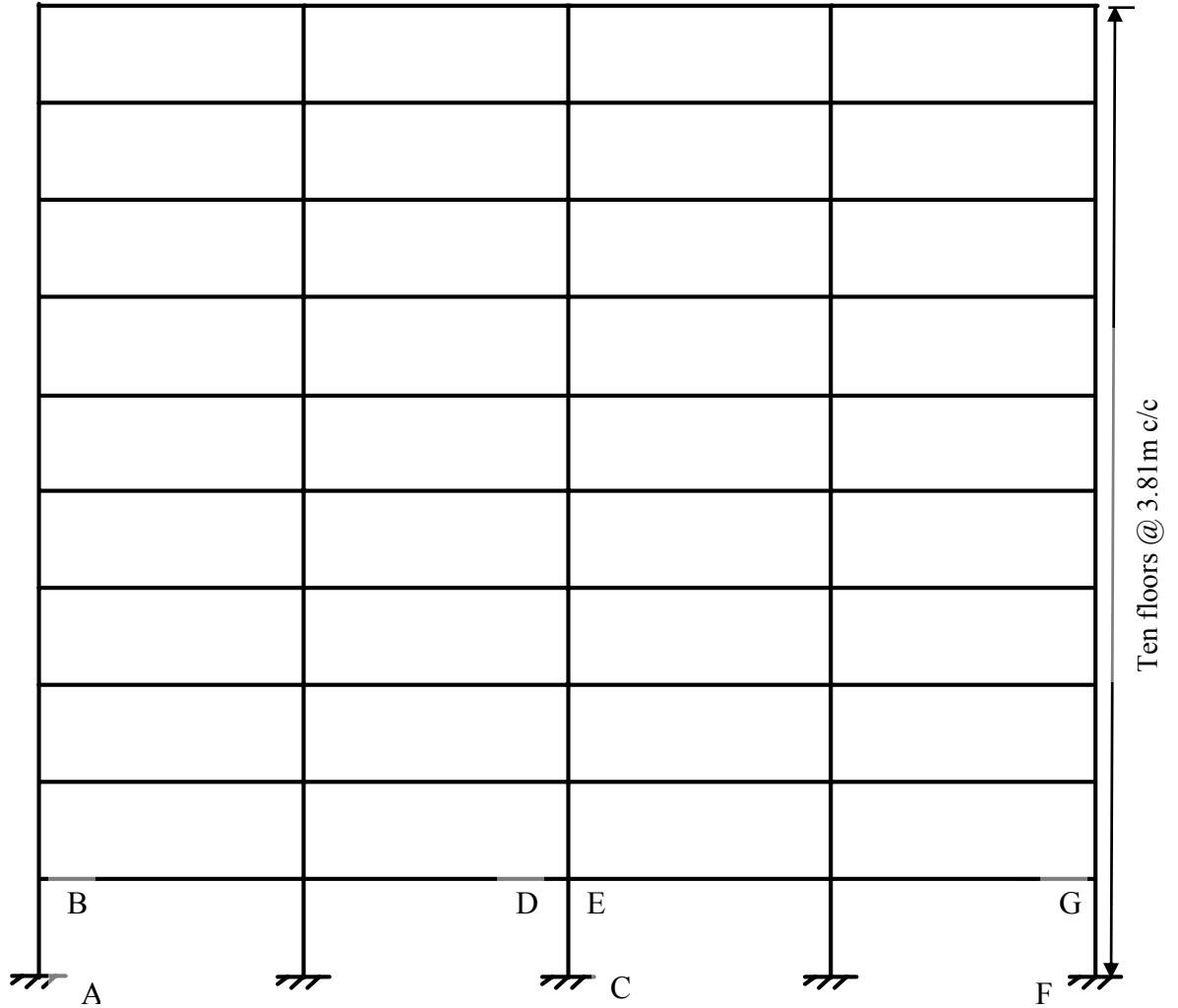
Figure 6.2(b).   Elevation of the ten story hybrid frame
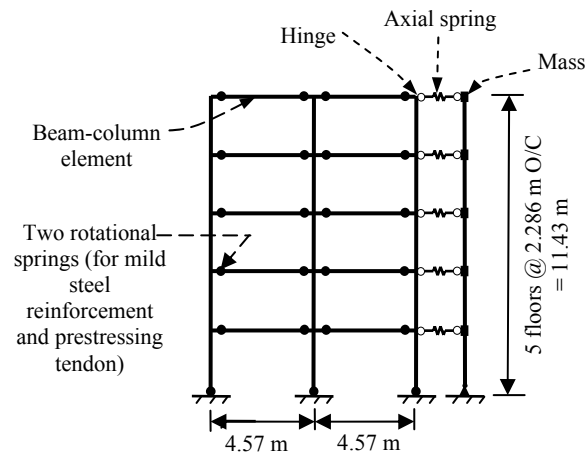
Figure 6.3(a).   A schematic view of the 2-D model used for the analysis of hybrid frame building at

60% scale (Rahman and Sritharan 2007)
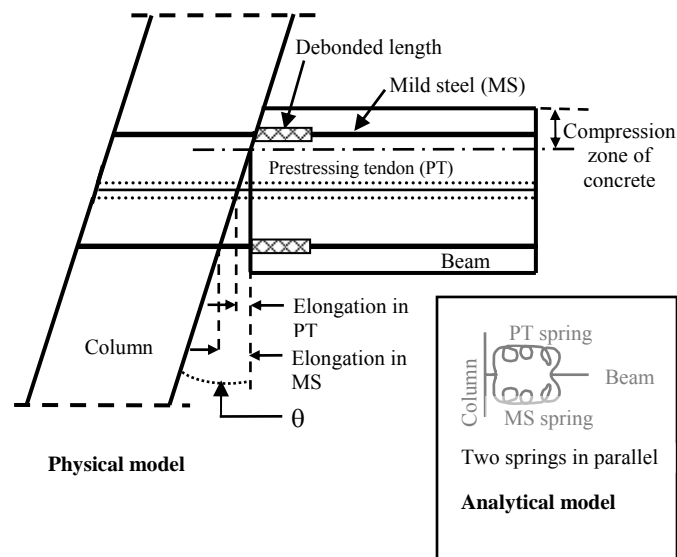
Figure 6.3(b).   Details of a typical hybrid connection are shown at interface rotation θ
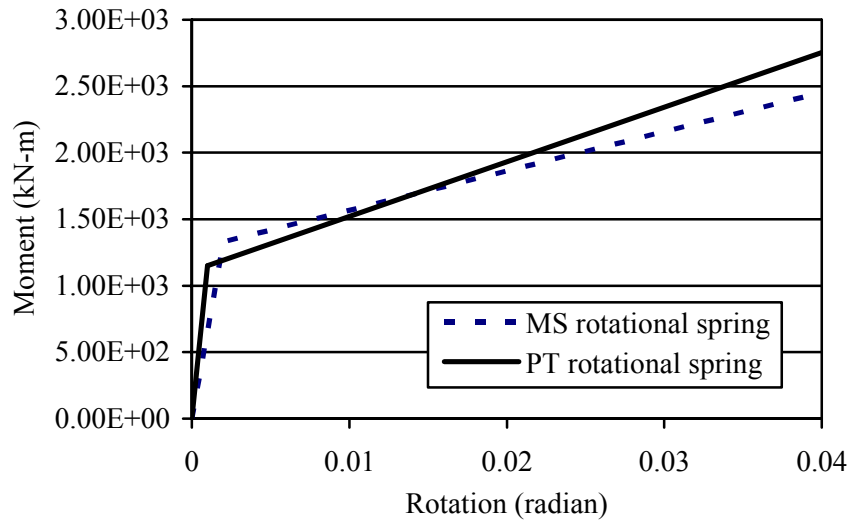
Figure 6.4(a). Monotonic moment-rotation envelopes of PT and MS rotational springs at the first

floor beam ends of the ten story hybrid frame building
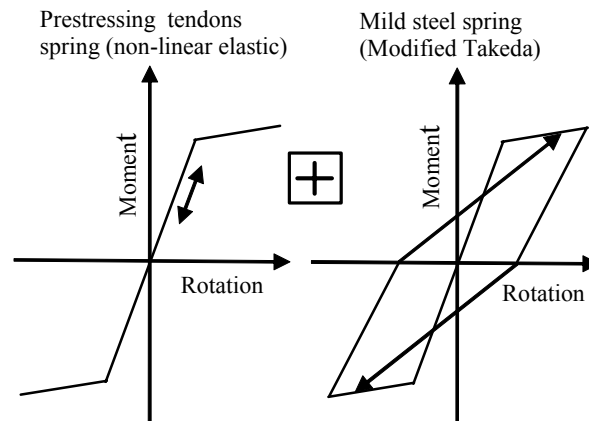
Figure 6.4(b). Illustration of typical moment rotation responses of PT and MS rotational springs
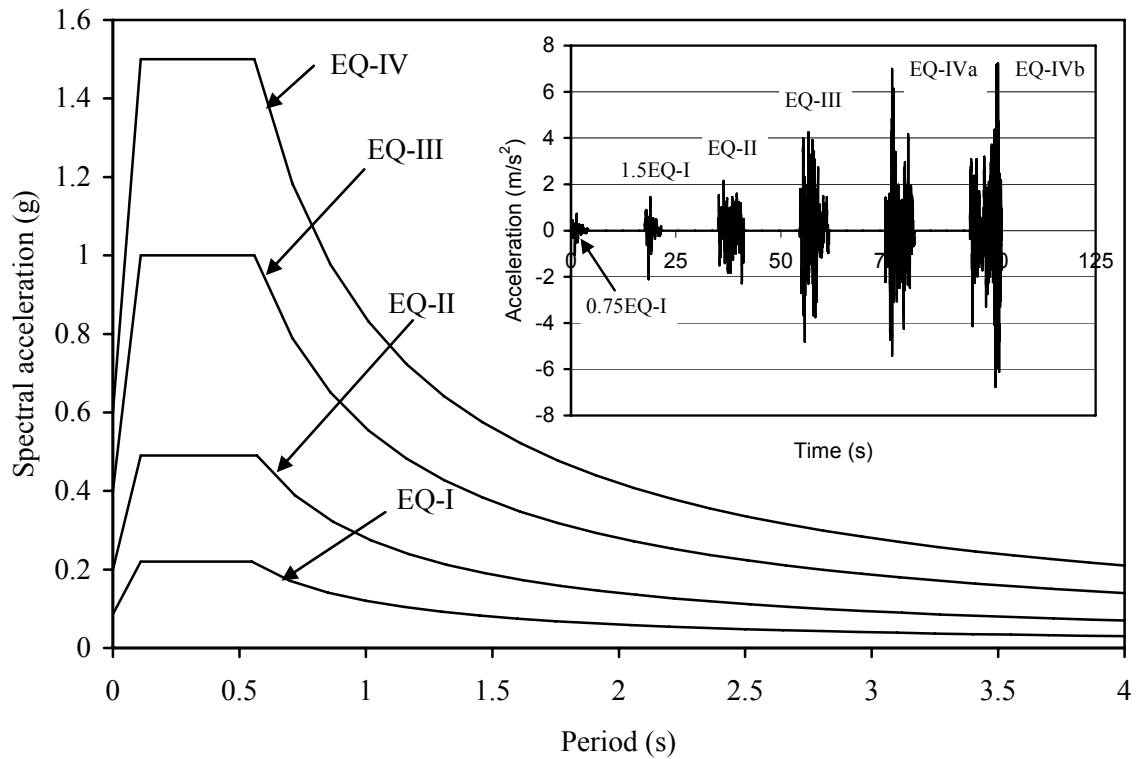
Figure 6.5.   The 5% damped multiple-level acceleration response spectra suggested for soil type S_c in high seismic zone as per the Performance-Based Seismic Engineering Ad Hoc Subcommittee (2003) of SEAOC. (The inserted in the figure shows short-duration earthquake ground motions used for testing of the PRESSS building in the seismic frame direction)
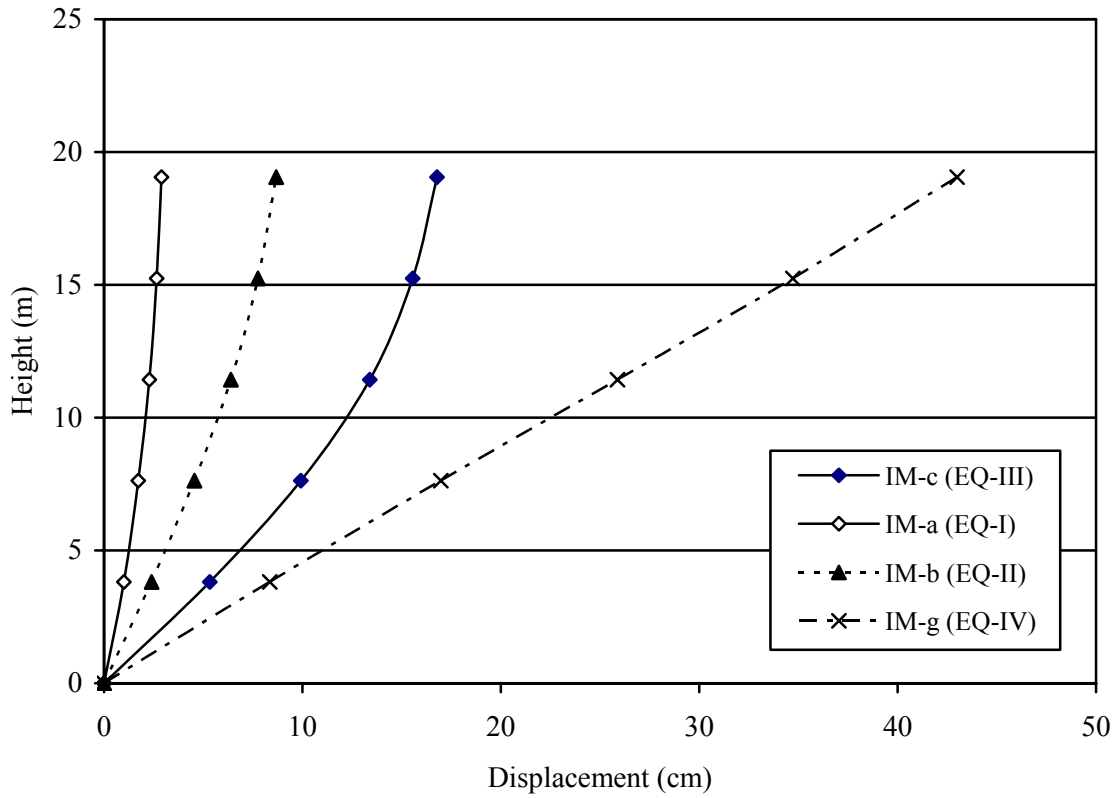
Figure 6.6(a).   Deflected shape of the five story building when achieving at the maximum

interstory drifts imposed by the four levels of ground motions
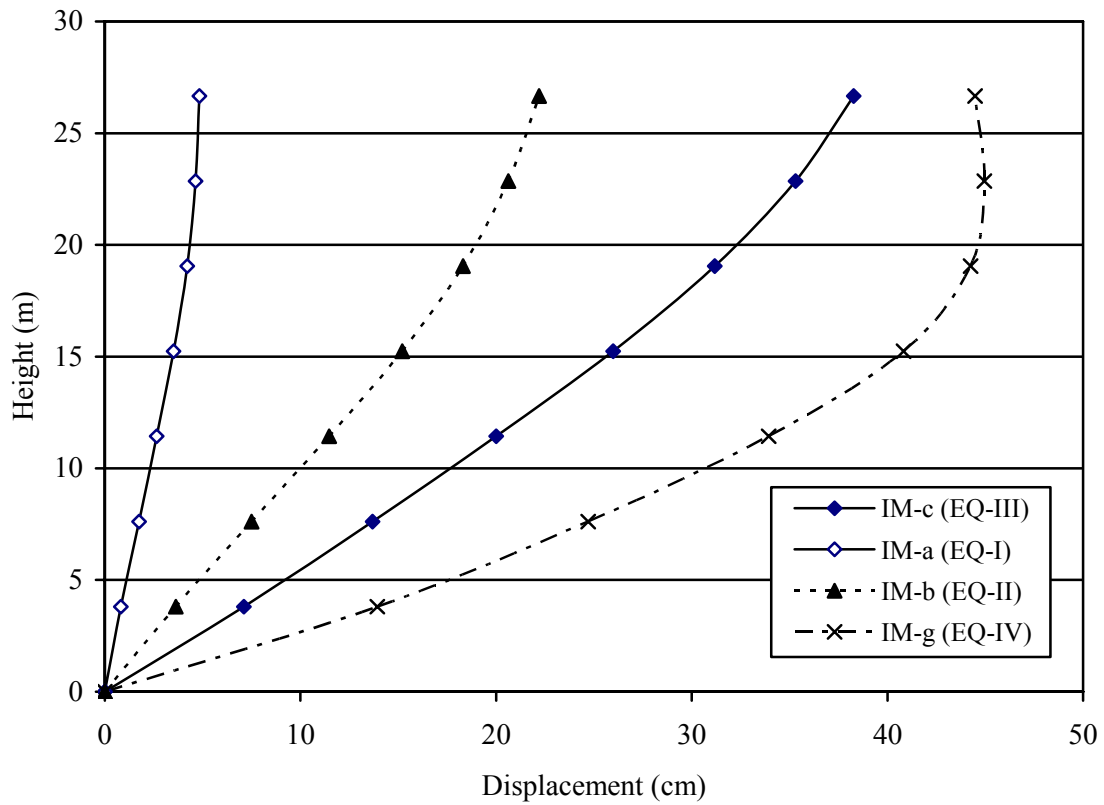
Figure 6.6(b).   Deflected shape of the seven story building when achieving at the maximum

interstory drifts imposed by the four levels of ground motions
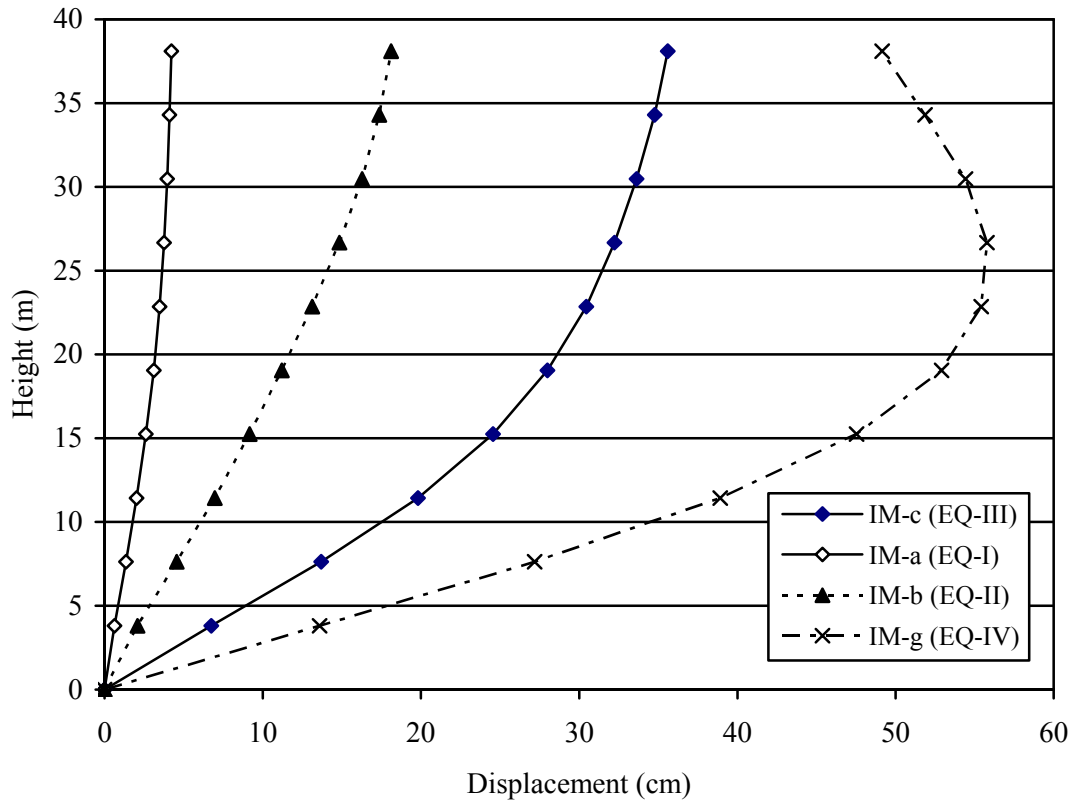
Figure 6.6(c).   Deflected shape of the ten story building when achieving at the maximum
                    interstory drifts imposed by the four levels of ground motions
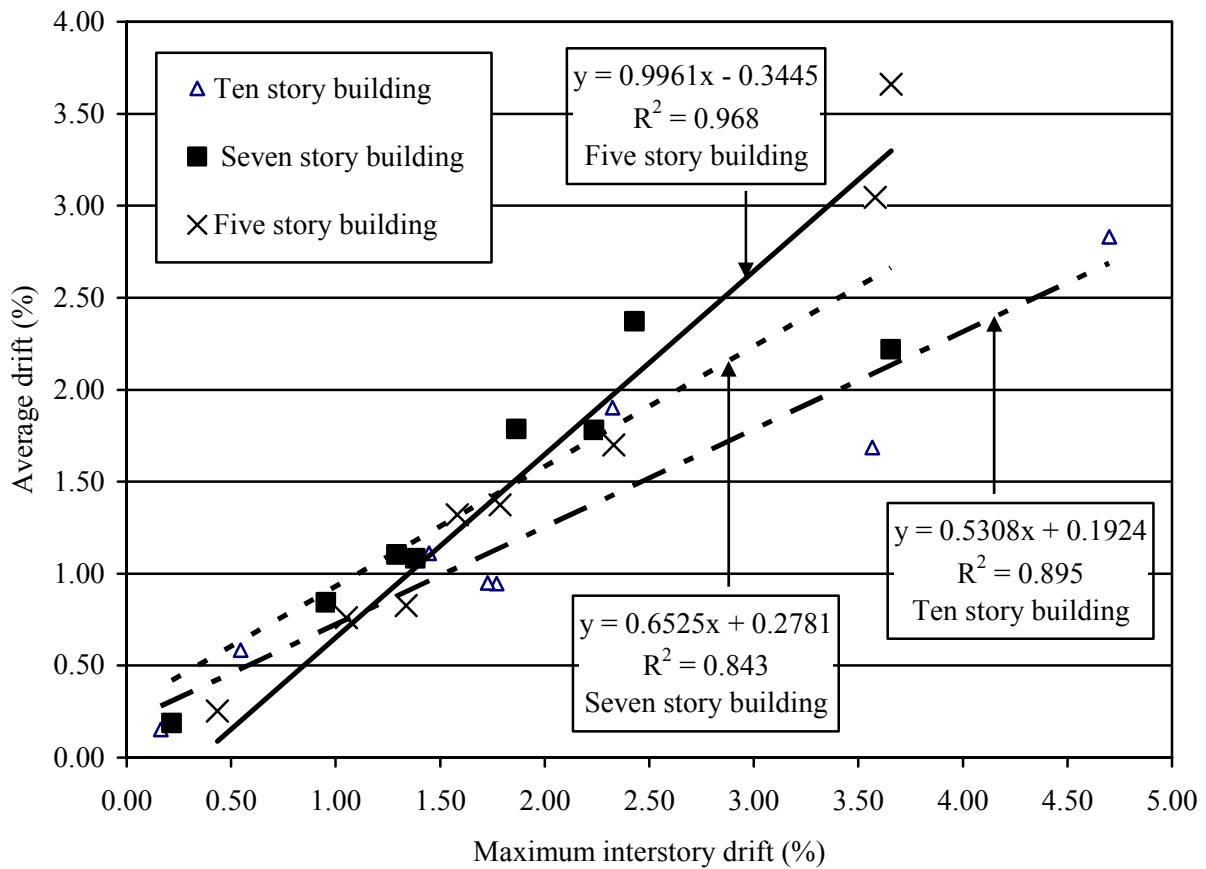
Figure 6.7.   Correlation between the average and maximum interstory drifts obtained for the five, seven and ten story hybrid frame buildings based on the responses to long-duration ground motions
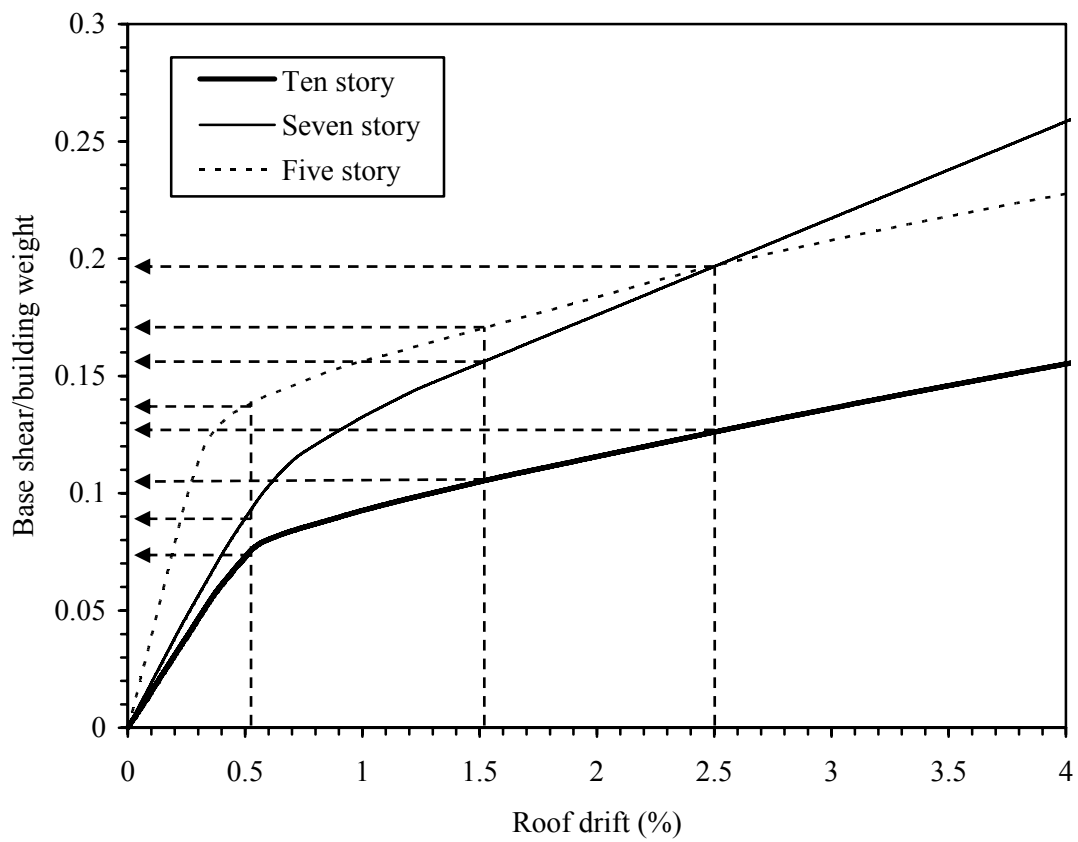
Figure 6.8.   Pushover analysis results for the five, seven and ten story hybrid frame buildings
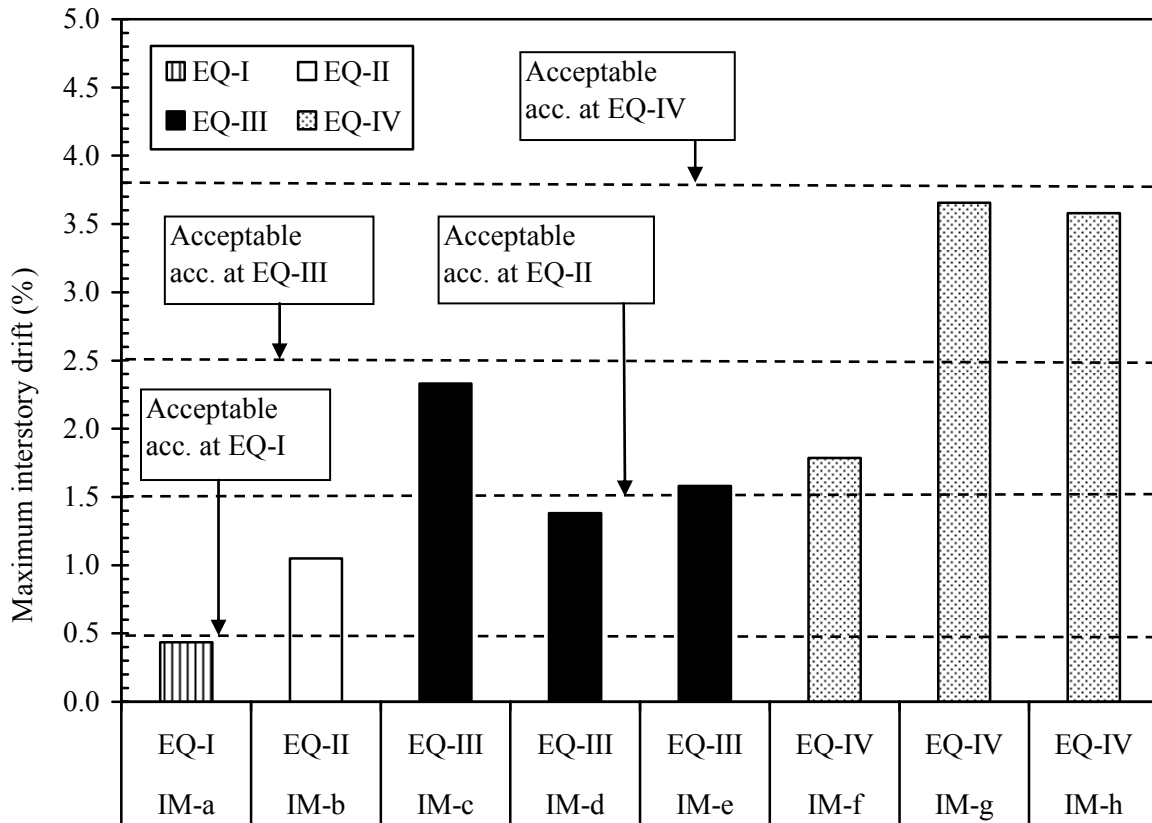
Figure 6.9(a).   Maximum transient interstory drift obtained for the five story hybrid frame

system building subjected to the long-duration ground motions
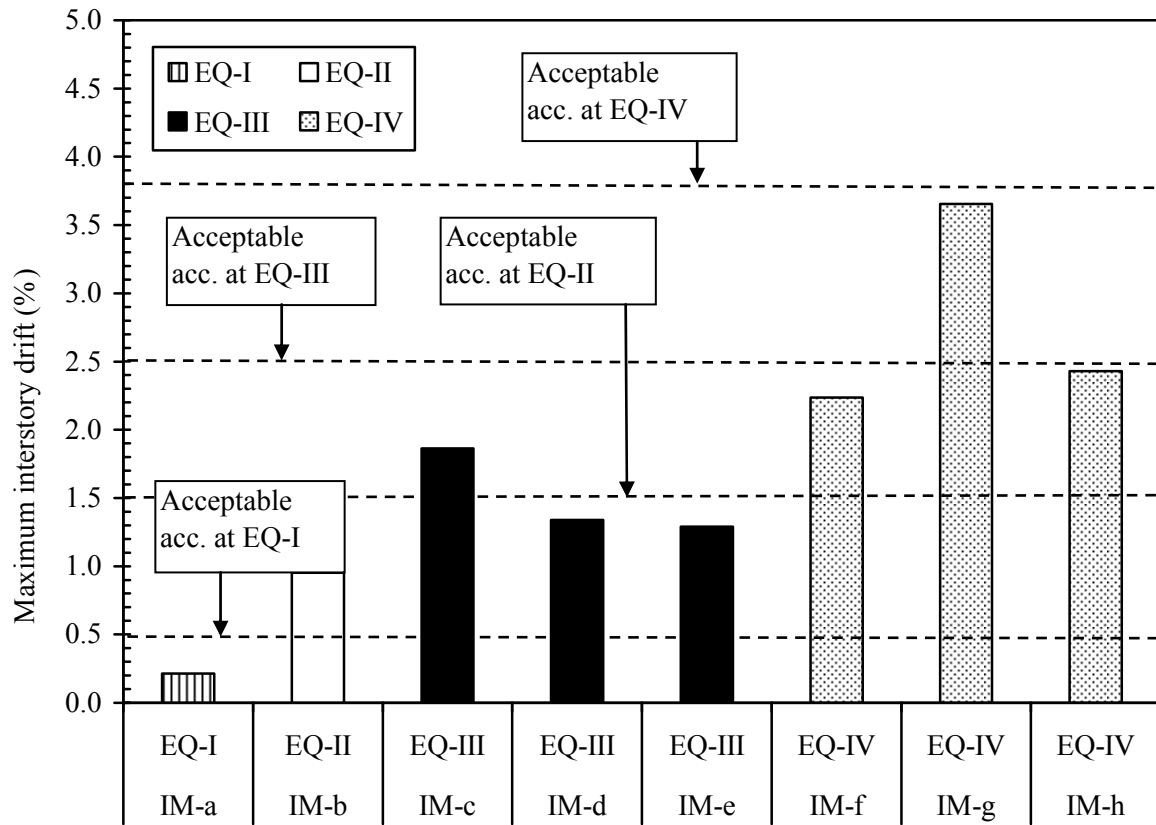
Figure 6.9(b).   Maximum transient interstory drift obtained for the seven story hybrid frame

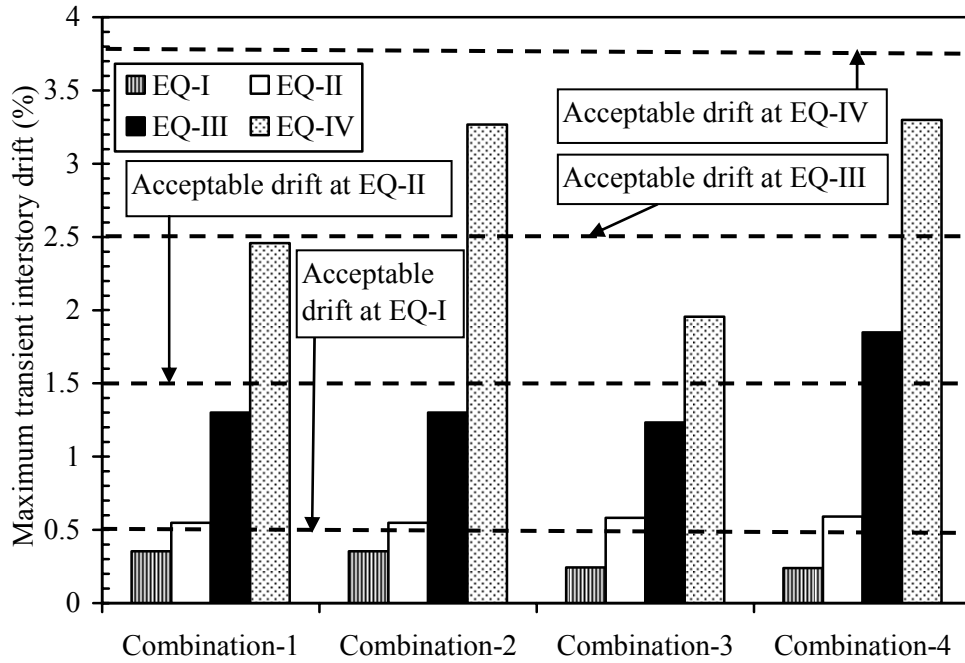system building subjected to the long-duration ground motions
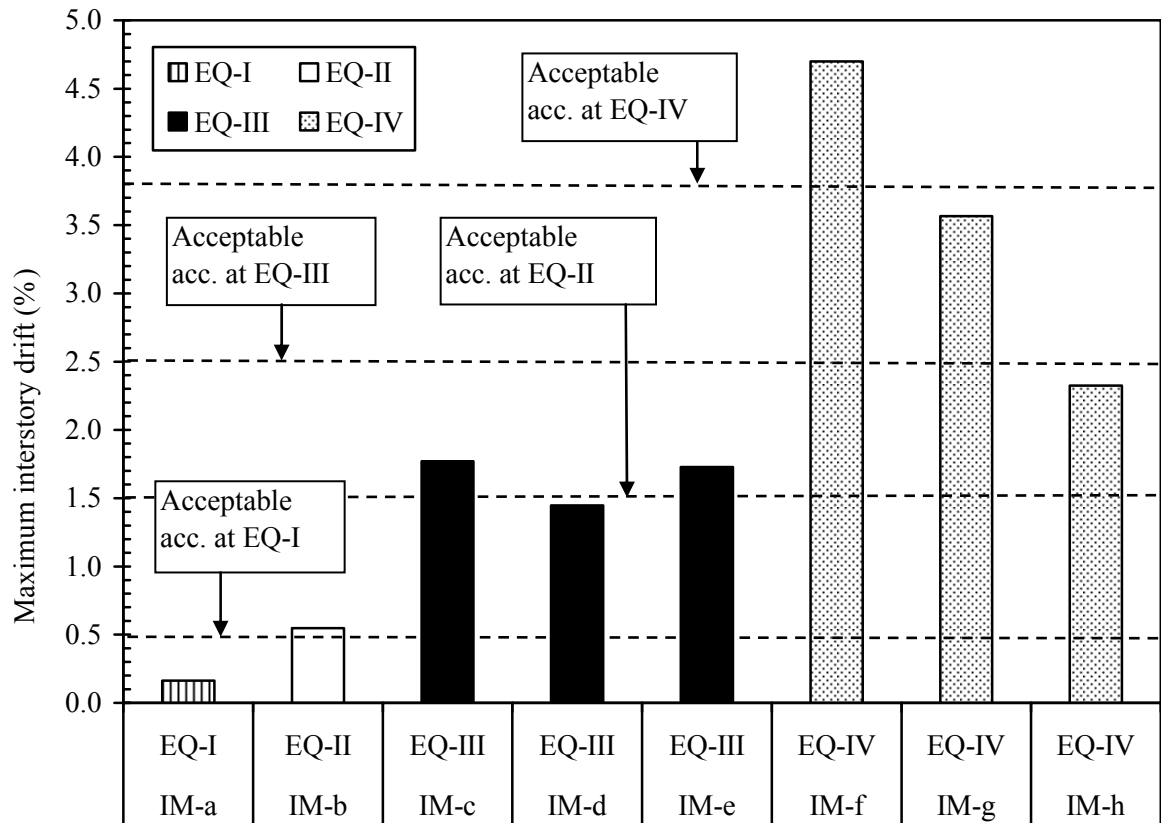
Figure 6.9(c).   Maximum transient interstory drift obtained for the ten story hybrid frame system
building subjected to the long-duration ground motions
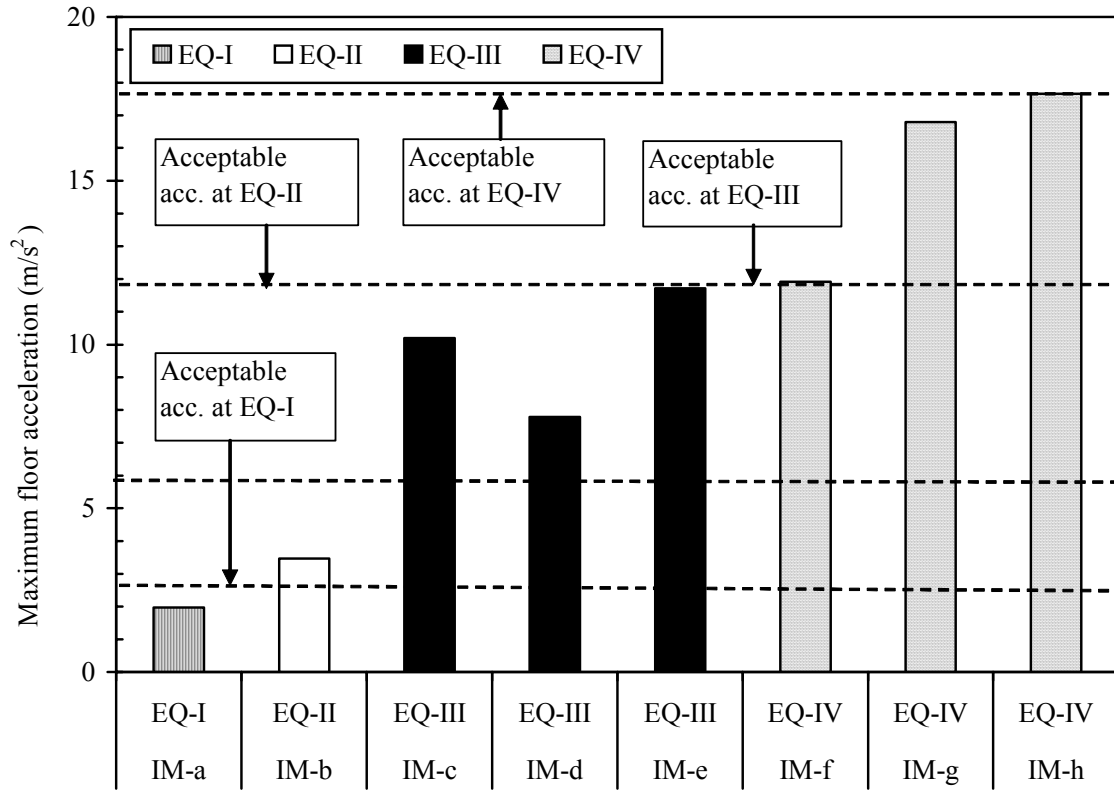
Figure 6.10(a).   Maximum floor acceleration obtained for the five story hybrid frame system building subjected to the long-duration ground motions
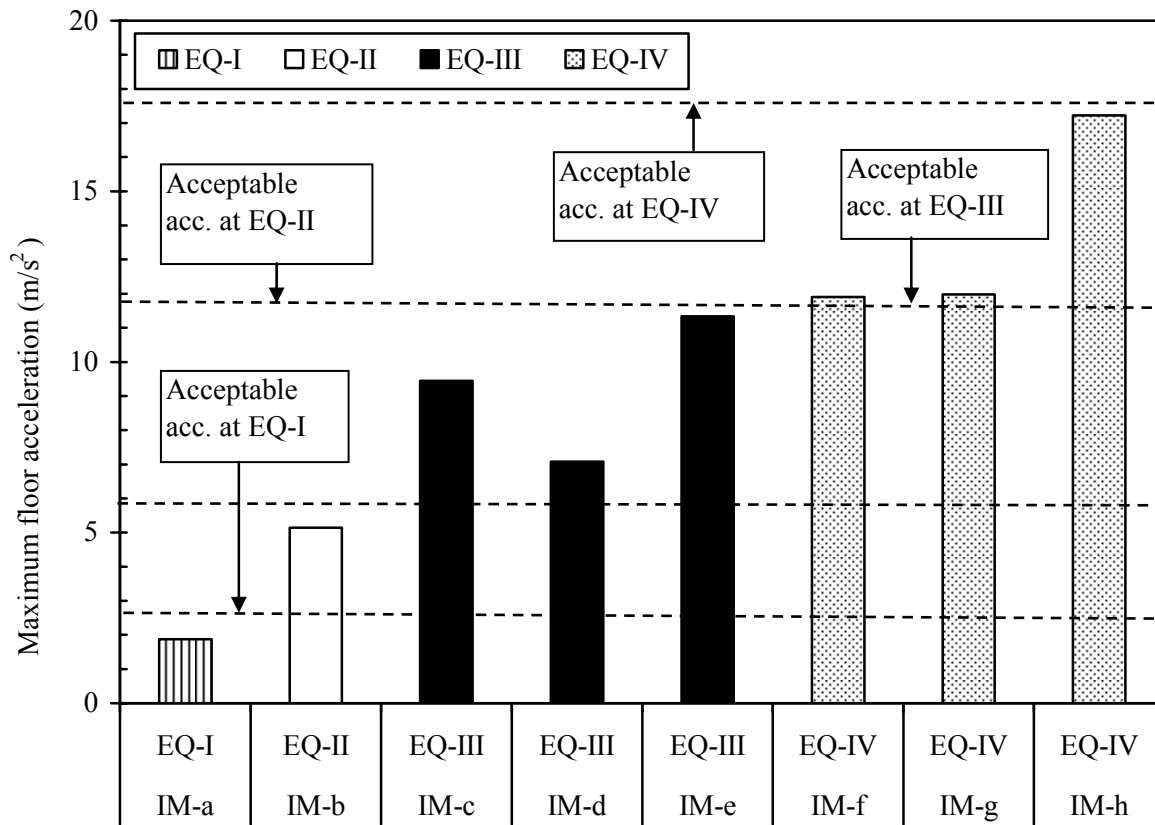
Figure 6.10(b).   Maximum floor acceleration obtained for the seven story hybrid frame system

building subjected to the long-duration ground motions
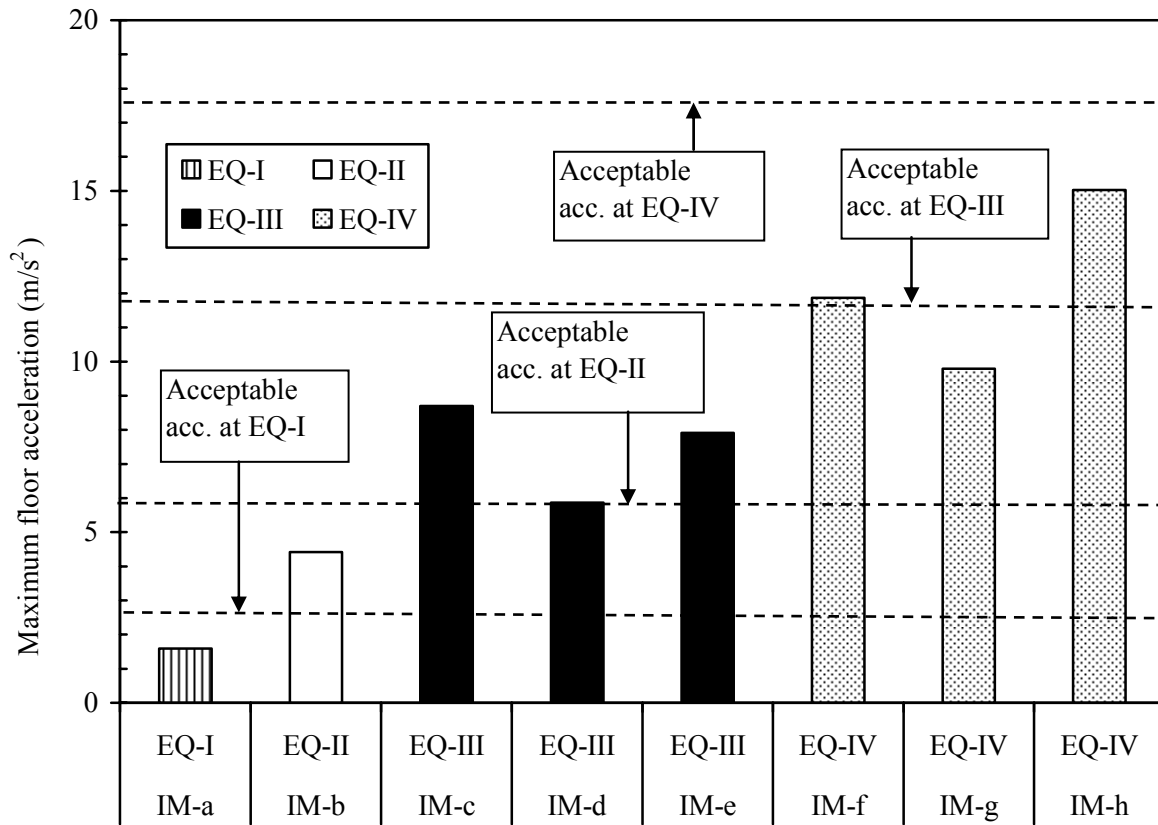
Figure 6.10(c).   Maximum floor acceleration obtained for the ten story hybrid frame system

building subjected to the long-duration ground motions
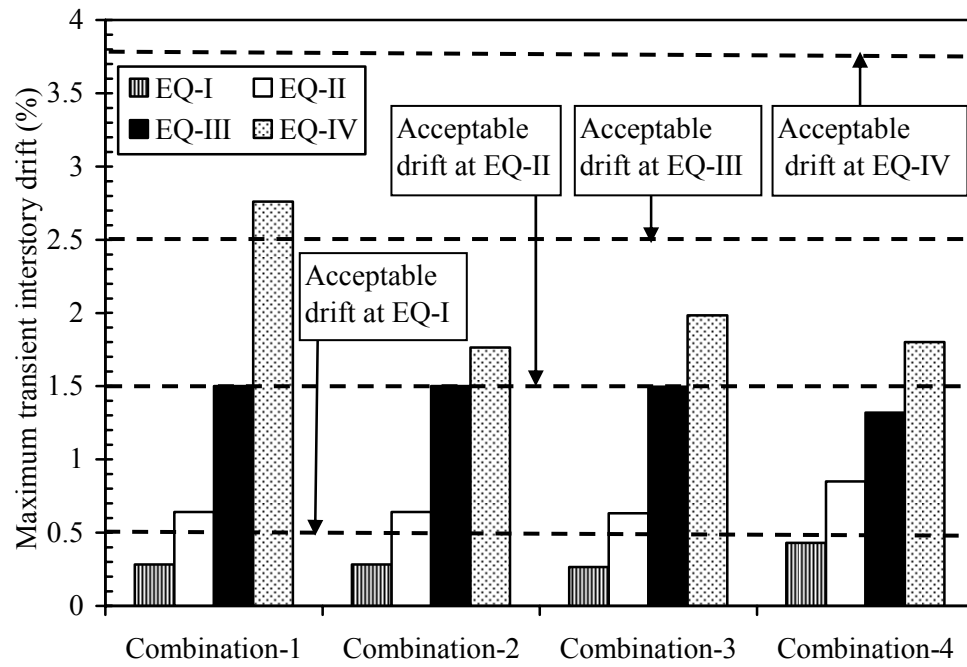
Figure 6.11(a).   Maximum transient interstory drift obtained for the five story building when subjected to short-duration ground motions
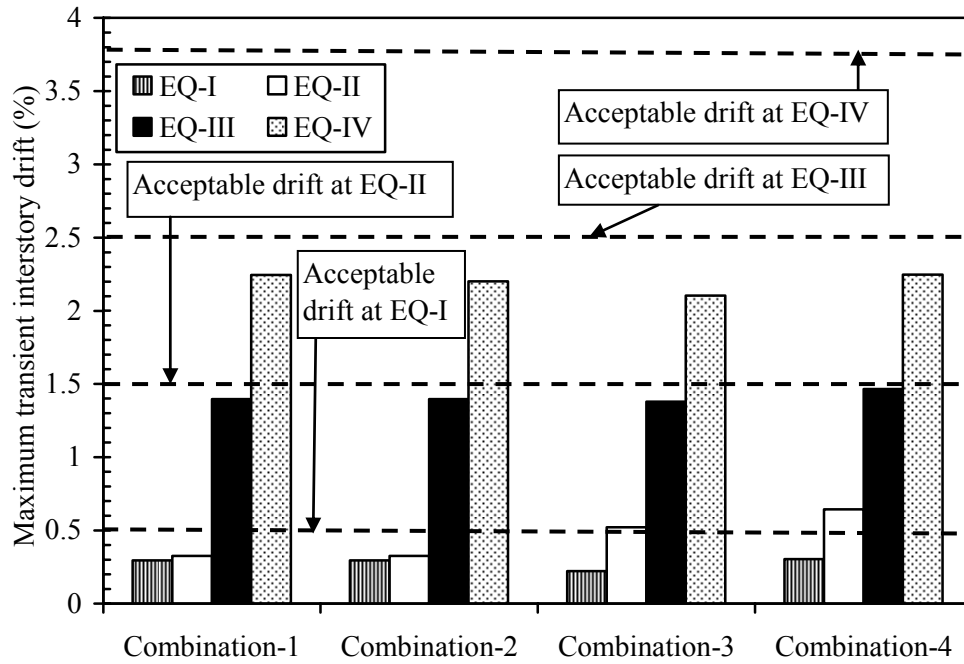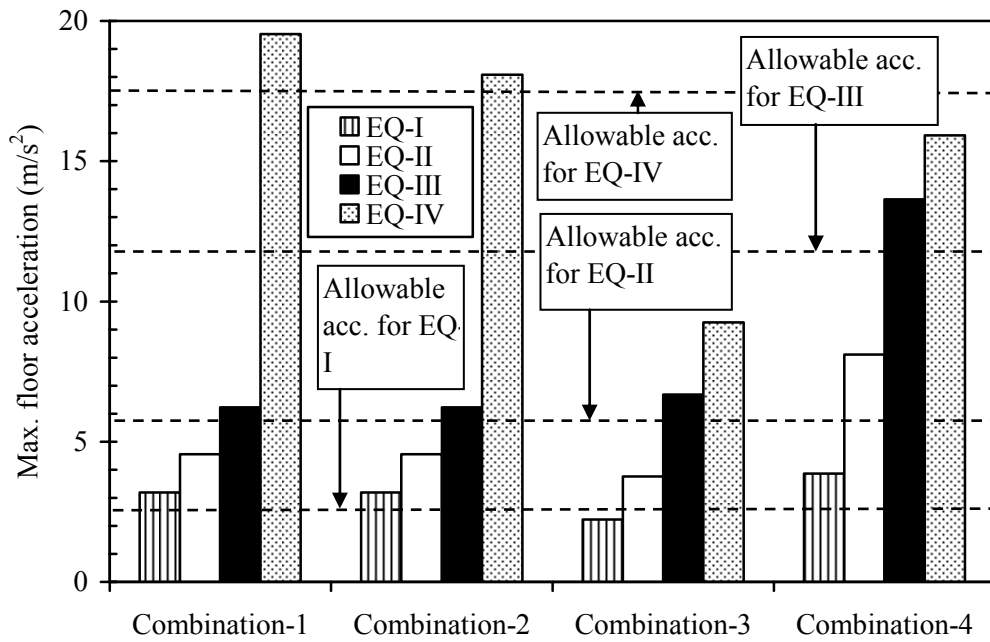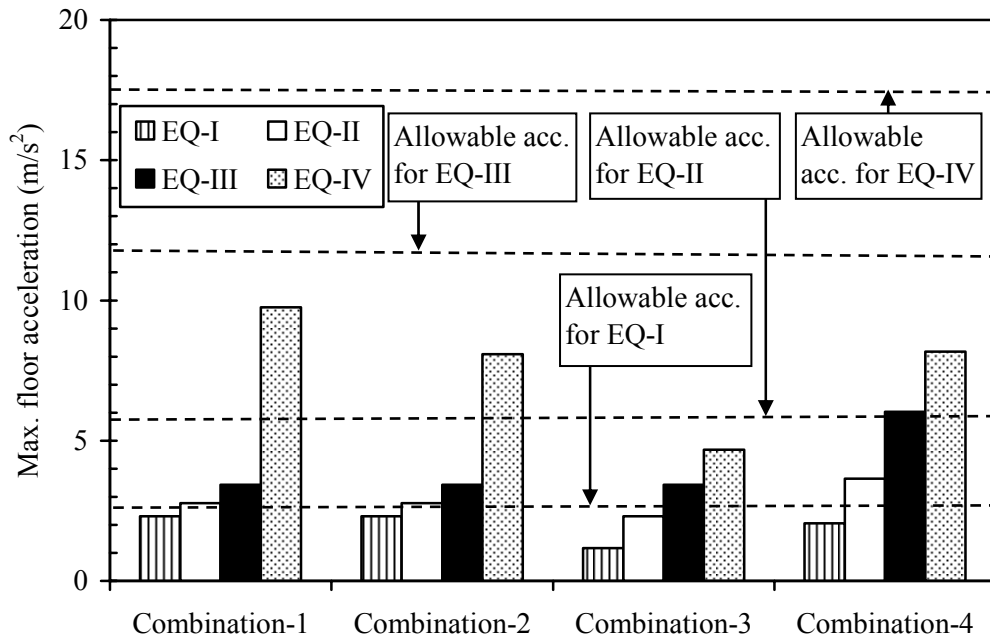
Figure 6.11(b).   Maximum transient interstory drift obtained for the seven story building when subjected to short-duration ground motions

Figure 6.11(c). Maximum transient interstory drift obtained for the ten story hybrid frame building when subjected to short-duration ground motions

Figure 6.12(a).　　Maximum floor acceleration obtained for the five story hybrid frame building when subjected to short-duration ground motions

Figure 6.12(b).   Maximum floor acceleration obtained for the seven story hybrid frame building when subjected to short-duration ground motions
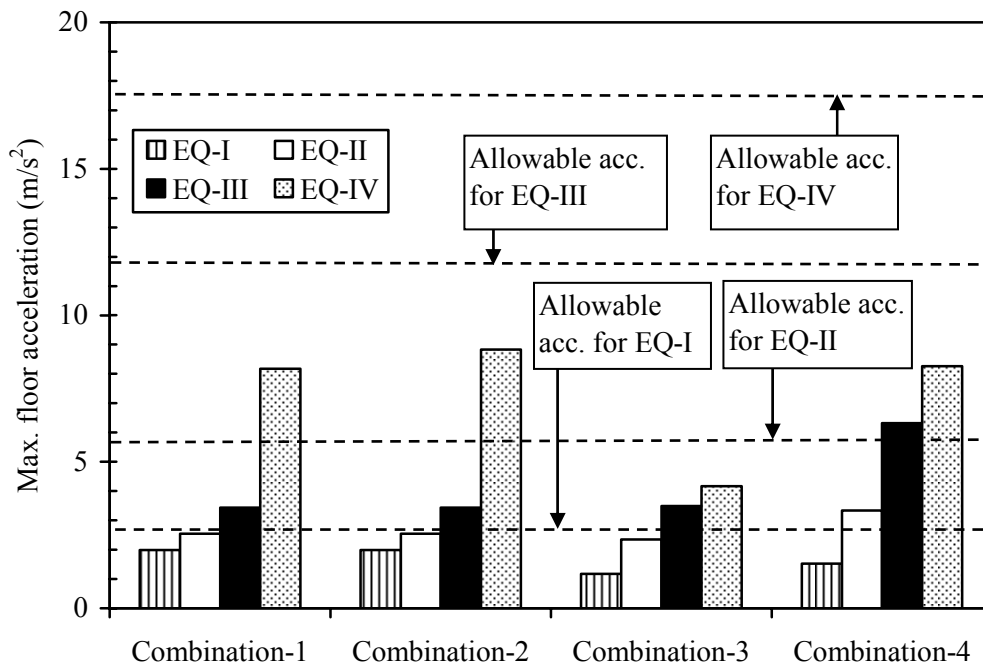
Figure 6.12(c).   Maximum floor acceleration obtained for the ten story hybrid frame building
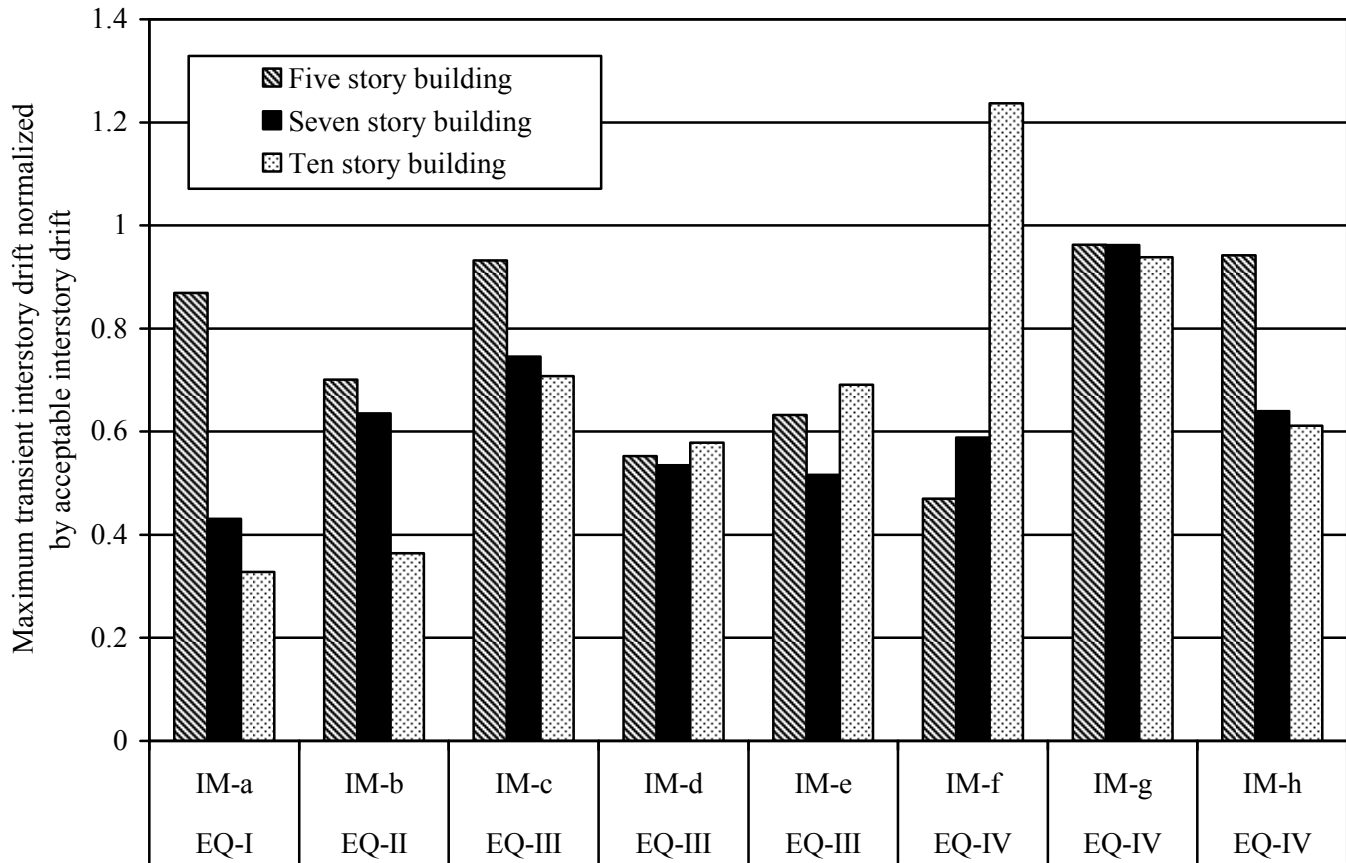when subjected to short-duration ground motions

Figure 6.13.   Maximum transient interstory drift normalized by the acceptable interstory drift
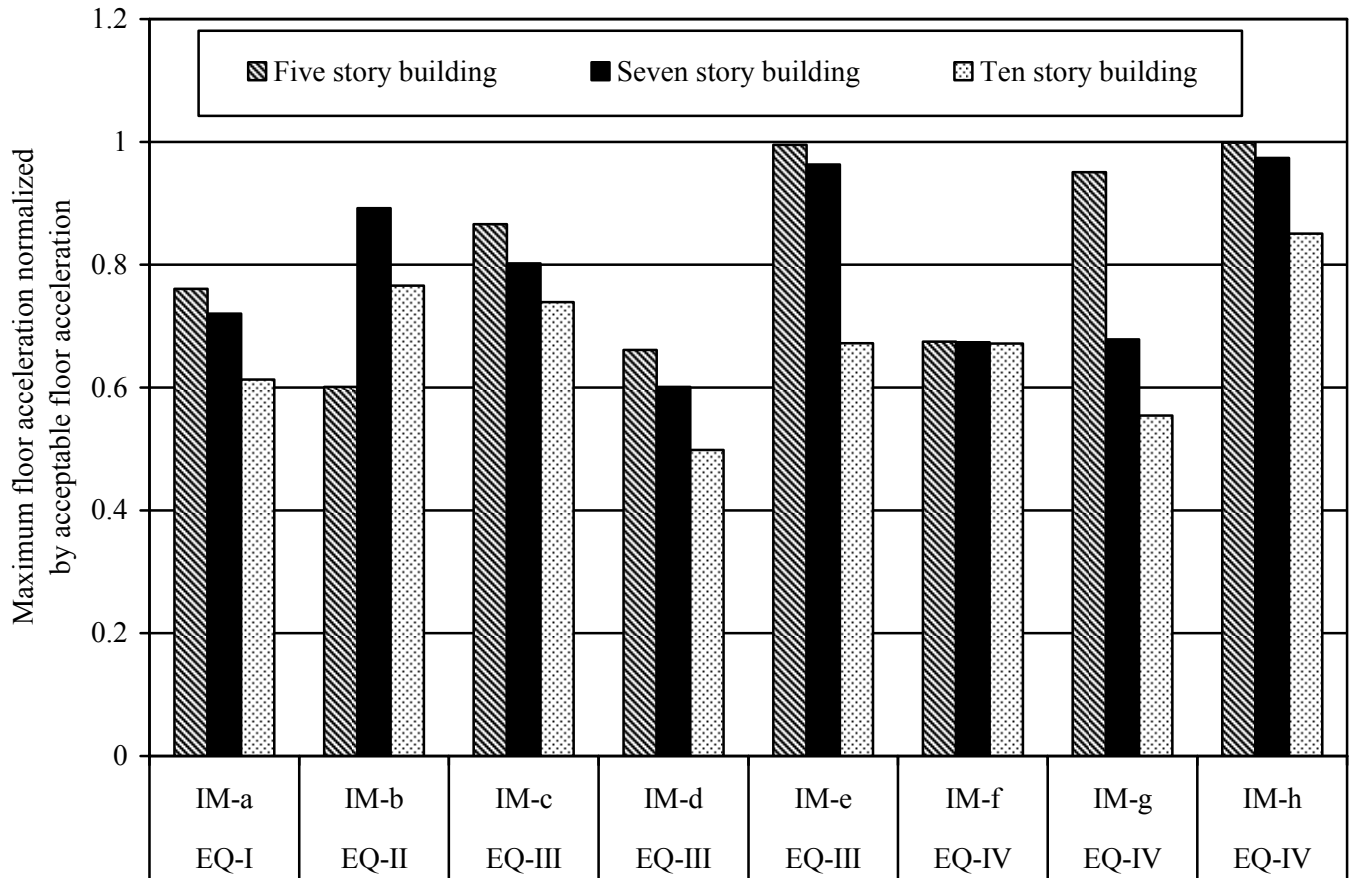
Figure 6.14.   Maximum floor acceleration normalized by the acceptable floor acceleration

CHAPTER 7. GENERAL CONCLUSION

7.1 OVERVIEW

Precast concrete structural systems have several advantages including high quality, efficient use of materials, reduced construction time, and cost efficiency. Lack of enough knowledge about the intrinsic structural capacity of precast prestressed concrete structural systems kept the structural design professionals away from using these structural systems in seismic zones. The traditional design codes have also imposed penalty on use of precast concrete due to unknown fear and lower level of performance of precast structures in past earthquakes, although such lower level of performance resulted from using poor connection details between precast elements and lack of sufficient number of lateral load resistance systems in the structures. Recent research shows that hybrid frames and unbonded jointed postensioned walls have the capacity of showing acceptable seismic performance.

The present study introduced analytical models for hybrid frames and jointed precast post-tensioned wall systems with validation. This study investigated the viability of use of hybrid frames and unbonded jointed post-tensioned walls in buildings from low to mid-rise in most intensive seismic region of the United States zone-4 considering the performance parameters of the maximum transition interstory drift, maximum floor acceleration and residual interstory drift. Both systems contained unique properties of re-centering and energy dissipation capacity. It was found that the use of hybrid frames and jointed wall systems are economical solution for resisting seismic loads if direct displacement-based design method is used instead of traditional force-based design method for designing these structural systems. In addition, direct displacement-based design method has better tie with the actual

performance of the structure compared to force-based design method. The specific conclusion derived through this study is presented below.

7.2 CONCLUSIONS

Two five story hybrid frame buildings designed by direct displacement-based and force-based approaches at 60% scale were studied analytically. The design base shear of the first building was 40% lower than that of the second building. Up to design level ground motion, the seismic performance of the two buildings satisfied the performance limits when subjected by short-and long-duration ground motions having comparable acceleration response spectra corresponding to four levels of earthquake intensities. Thus, direct displacement-based design method appeared to be acceptable to design hybrid frames to produce acceptable performance at design level earthquakes. The building designed according to the displacement-based method produced the maximum transient interstory drift higher than the acceptable limit of 3.8% when subjected by EQ-IV level ground motions. It seemed that the performance of this building could be enhanced by improving the direct displacement-based design.

For all of four levels of ground motions, the combination of hysteretic energy dissipation and re-centering capabilities of the hybrid connections produced negligible residual drifts, and thus satisfied the maximum residual inter-story drift limits. The maximum floor accelerations determined for both buildings were below the acceptable limits for all input motions. Generally, the building designed by force-based approach demonstrated lower level of the maximum transient interstory drift and plastic rotation in beam-column connection compared

to those of the building designed by direct displacement-based approach. An opposite trend was observed for the floor acceleration.

Two five story jointed precast post-tensioned wall systems designed by direct displacement-based and force-based approaches at 60% scale were studied analytically. In this case, direct displacement-based design approach resulted in base shear 50% less than that of force-based design method. Both wall systems performed satisfactorily in terms of the maximum interstory drift, maximum floor acceleration and residual interstory drift. The transient interstory drift of the jointed wall system reduced with higher number of energy dissipating shear connector without exceeding the limits of residual interstory drift.

Following the study of the five story jointed wall system at 60% scale, performance-based seismic evaluation of jointed precast post-tensioned wall systems for low to mid-rise buildings designed by direct displacement-based approach was conducted using analytical models of the five, seven and ten story full scale buildings. For four levels of ground motions, the three buildings performed satisfactorily in terms of the maximum transient interstory drift and residual interstory drift. Few violations in the maximum floor acceleration of the ten and seven story building were observed which could be mitigated by modifying the wall dimension. It was observed that the sensitivity of the average drift to the increase of the maximum transient interstory drift reduced in jointed wall systems with the increase of the height of the building. Taller building demonstrated stronger tendency to approach and exceed unity of normalized floor acceleration compared to low-rise building. Low-rise building achieved the maximum transient interstory drifts closer to the acceptable limits compared to the taller building.

Similarly, performance-based seismic evaluation of precast concrete hybrid systems for low to mid-rise buildings designed by the proposed improved direct displacement-based design approach was conducted using analytical models of the five, seven and ten story full scale buildings. The three buildings performed satisfactorily in terms of the maximum transient interstory drift, maximum floor acceleration and residual interstory drift for four levels of ground motions. The sensitivity of average drift toward the maximum transient interstory drift depleted when the height of the hybrid frame buildings were raised. Pushover analysis examination suggested that taller hybrid frame buildings attract smaller percentage of building weight as base shear compared to low-rise building. The maximum transient interstory drift increased with the reduction of building height up to EQ-II level ground motion. It seemed that low-rise hybrid frame system had higher tendency to approach the maximum acceptable floor acceleration compared to taller system. In addition, the susceptibility of occurring higher level of plastic rotation increased with reduction of building height.

In summary, this study suggests that precast hybrid frames and post-tensioned jointed walls are effective lateral load resistance systems and they can be used to adequately protect low to mid-rise buildings experiencing seismic damages of structural and non-structural elements. These two systems have the capability to show satisfactory seismic performance not only under design level earthquakes but also under multiple levels of earthquakes, which is a high priority for keeping the buildings serviceable. In addition, the direct displacement-based design approach appears to be the preferred design methodology compared to traditional force-based approach for designing precast hybrid frame and post-tensioned jointed wall systems because of its coherent tie with the performance of buildings and economy of

construction as well. In addition, improvement in direct displacement-based design method presented in this study should be considered in designing the two precast systems.

7.3 FUTURE RESEARCH

In future research, combined use of hybrid frame and jointed precast post-tensioned wall systems in the same direction of building may be considered. By observing the trend of results of the present research, it seems combined use of hybrid frame and jointed precast post-tensioned wall systems in the same direction may lead to improved performance by producing optimized values of the maximum transient interstory drift and maximum floor acceleration leading to economical structural solution. In addition, similar research may be conducted for seismic zones other than zone-4 and soil class C. Reconciliation of such recommended research may help the structural design professionals by providing them a comprehensive direction to take technological advantage of precast concrete hybrid frame and jointed precast post-tensioned wall systems as primary seismic load resistance systems.

ACKNOWLEDGEMENTS